

D10.9 Products derived from GNSS data analysis

Document information Summary

Date	27 September 2017
Document title:	D10.9 Products derived from GNSS data analysis
WP name and no	WP10 TCS GNSS Data and Products
Lead Partner	CNRS-UGA
Main Author(s)	Aline Deprez
Contributing author(s)	Anne Socquet, Nicola d'Agostino, Antonio Avallone, Ambrus Kenyeres, Martin Lidberg, Athanassios Ganas, Rui Fernandes and Machiel Bos
Reviewer(s)	
Approved by	
Target audiences	
Keywords	Products
Deliverable nature	
Dissemination level	
Delivery date	27 September 2017
Version/Date	1.0

Table of Contents

Table of Contents

1. INTRODUCTION	3
2. PRODUCTS LEVEL 1 (COORDINATE TIME SERIES)	4
2.0 GUIDELINES	4
2.1 CNRS-UGA	4
2.2 INGV	7
2.3 BFKH	8
2.4 WUT	9
2.5 CURRENT OVERVIEW	9
2.6 COMPARISON	10
2.7 VALIDATION OF TIME SERIES	12
3. PRODUCTS LEVEL 2 (VELOCITIES)	12
3.0 GUIDELINES	12
3.1 CNRS-UGA	12
3.2 INGV	15
3.3 BFKH	15
3.5 CURRENT OVERVIEW	18
3.6 COMPARISON	18
4. PRODUCTS LEVEL 3 (STRAIN RATES).....	20
4.0 GUIDELINES	20
4.1 LM	21
4.2 CNRS-UGA	21
4.3 INGV	22
4.4 CURRENT OVERVIEW	22
REFERENCES	23
ANNEX 1 – GUIDELINES DOCUMENTS	24
ANNEX 2 – PRESENTATIONS/POSTERS/PUBLICATIONS	25

1. Introduction

Within WP10 the task 'Products' is responsible for:

1. development of Guidelines for processing, implementing massive processing at two EPOS processing centers to obtain European-scale solution, and harmonized distributed processing at National Analysis Centers;
2. combination of weekly solutions to obtain homogeneous velocities and combination of solutions at the velocity level (large-scale European solutions, EPN densification product, and solutions from National processing centers);
3. collection of daily and weekly GNSS position time series and velocity fields in standardized formats;
4. derivation of strain rate maps;
5. testing and validation of the products.

This report describes the progress of each of these points made in the last 2 years.

2. Products level 1 (coordinate time series)

2.0 GUIDELINES

In the framework of the EPOS implementation phase, it was decided within the GNSS work package (WP10) to implement 2 massive processing in order to produce 2 internally consistent prototype solutions and generate the associated products by two independent ways on a large subset of chosen stations.

The 2 EPOS processing centers are:

- CNRS-UGA, in which the data was processed using the double differences (DD) method using GAMIT (developed at MIT) software.
- INGV, in which the data was processed using the precise point positioning (PPP) method using GIPSY (developed at JPL) software

These 2 prototype solutions include several hundreds of stations (about 600) constituting a widespread pan-European network, over a 11-years time span [2000-2016]. In this context, the processing centers have to take up the upscaling challenge and to generate from a big data set the usual GNSS products: position time series, in a first instance.

Between the end of 2015 and the beginning of 2016, it was also decided to include in the EPOS-GNSS processing 2 other contributions

- another solution processed at KOERI, with Turkish sites (22 sites from MAGNET network) and some EPN sites, using GAMIT software (see annex 2.7).
- an analysis of a densified solution conducted at BFKH by A. Kenyeres. In a first instance, this analysis is based on a combination of EPOS solutions and regional solutions (in particular KOERI GAMIT solution), using CATREF software and daily SINEX solutions as input, giving access to time series of all stations.

2.1 CNRS-UGA

Due to limitations inherent to the software, the huge amount of data prevented the DD processing from being implemented using a usual way. For each day of the period to be processed, the massive data set was split into sub-networks and the GAMIT software launched for each sub-network.

Then a daily combination allowed to obtain a daily Sinex file which was followed by a global combination over the whole period, giving access to the position time series.

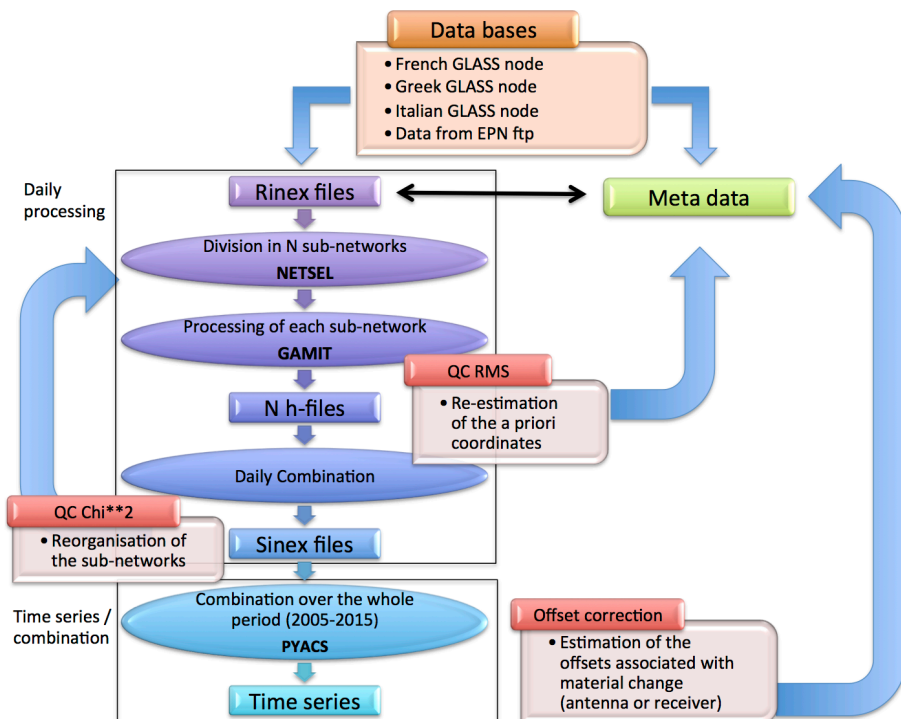


Figure 1. Processing chart at CNRS-UGA to produce time series

The computing and post-processing of time series were conducted using PYACS software (set of tools written in python language developed at Observatoire de Côte d’Azur, Nice, France by J.M. Nocquet). This package allowed the visualisation of the position time series and the post-processing, consisted in removing a linear trend, removing the outliers, estimating and correcting the jumps associated with equipment changes.

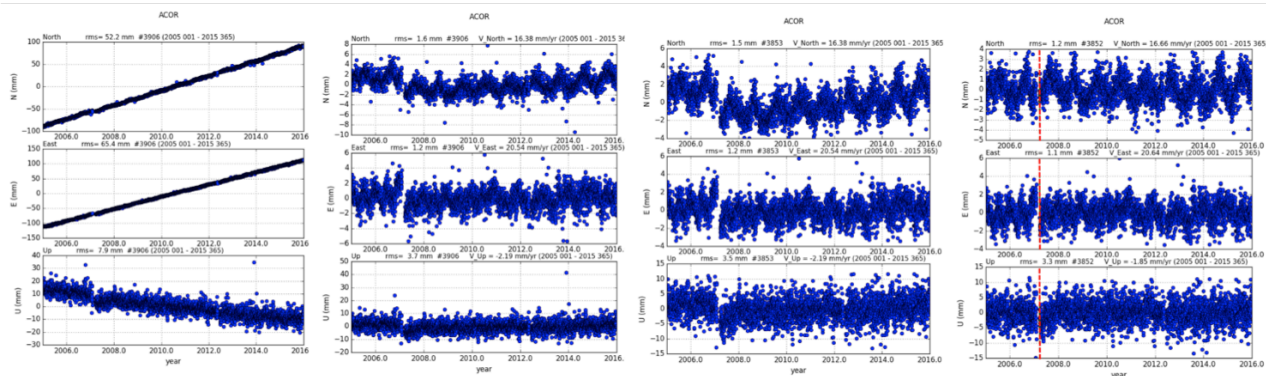


Figure 2. Example of time series processing for the station A Coruna (ACOR) in Spain

Given the fact that the processing was divided into a large number of small processes which should run independently, the use of high performance computing platform (CIMENT) hosted at CNRS-UGA became necessary. This platform consists in a set of computing nodes allocated between a few computing clusters. Theoretically, for this prototype solution $\sim 56\,400$ processes

had to be launched during the sub-network processing phase and ~ 4000 during the daily combination phase. Each process with their own parameters was associated with a job launched on a cluster node.

Thanks to an optimal use of this platform, the parallelized processing itself lasted ~ 1 week instead of the many years (~ 4 years) required by a linear processing.

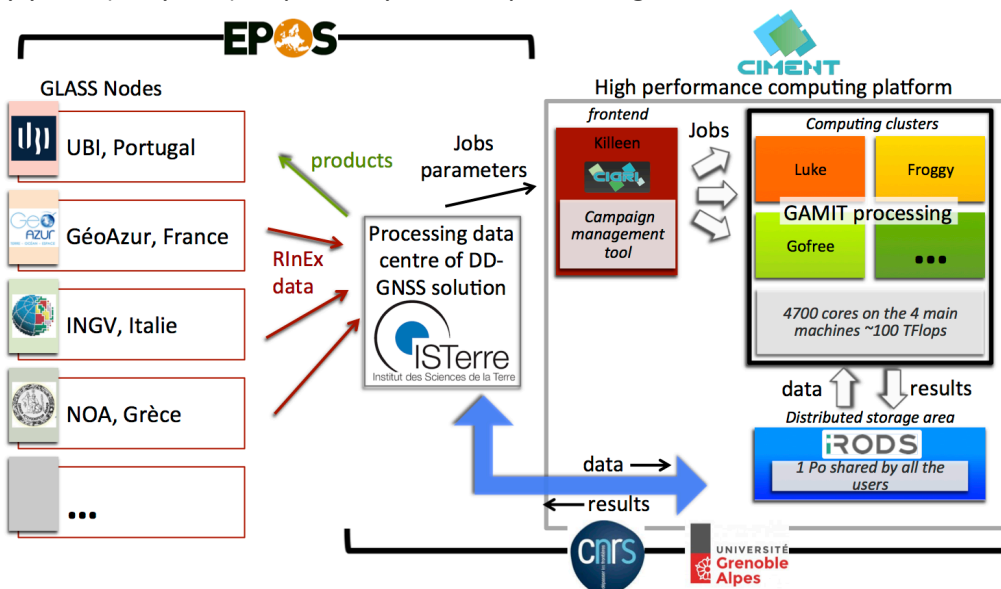


Figure 3. Computing resources at CNRS-UGA using for the massive processing implementation.

In order to facilitate the visualisation of the time series, an interactive map was designed (<https://www.isterre.fr/recherche/projets-de-recherche/projets-en-cours/projets-europeens/article/epos-ip-gnss-products>).

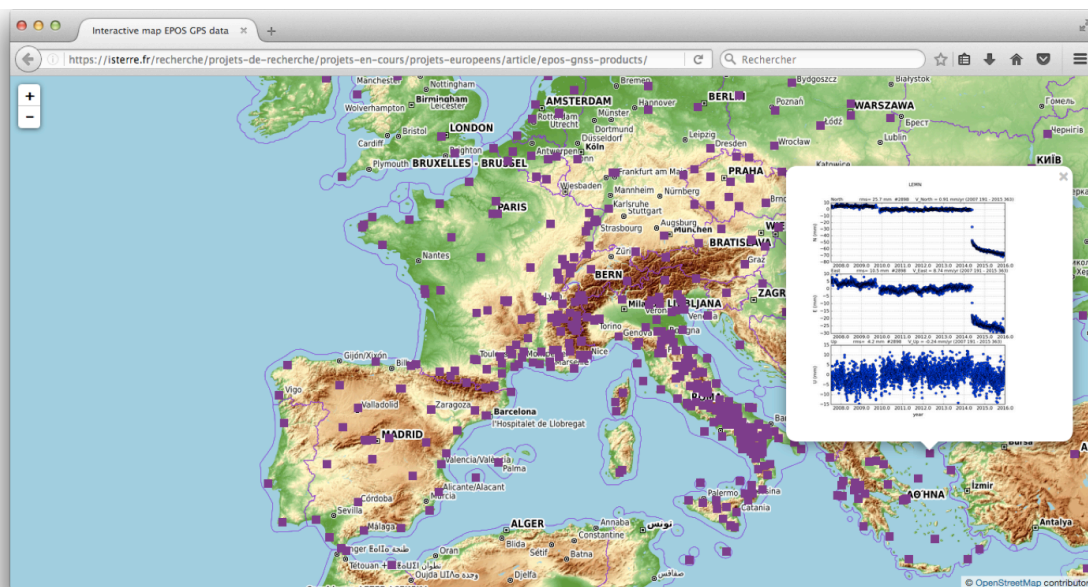


Figure 4. Interactive map designed at CNRS-UGA allowing to visualise position time series by clicking on the station location point.

2.2 INGV

The processing implemented at INGV was based on the PPP software, GIPSY OASIS 6.4 and followed a 3 steps strategy:

- The **PPP solution** was computed (IGS08 with JPL x-files). The ocean loading was modeled using the FES2004 tidal model and no atmospheric loading was applied. The IGS08 absolute antenna phase center variations was used to model the azimuthal and elevation dependence.
- The orbit and clock products provided by JPL include now a record of the **wide-lane and phase bias estimates** (Bertiger et al. 2010). This use of such products allowed to perform single receiver ambiguity resolution
- In order to reduce the common mode signal, a **final alignment to EU16** was applied (Blewitt et al. 2013). EU16 is a terrestrial frame for geodetic studies near Eurasian plate. This frame is defined by 6 Cartesian coordinates and velocities of each of 132 GPS stations spanning the 2000-2016.37 period and selected by specific quality criteria. The EU16 frame is aligned in origin and scale with IGS08.

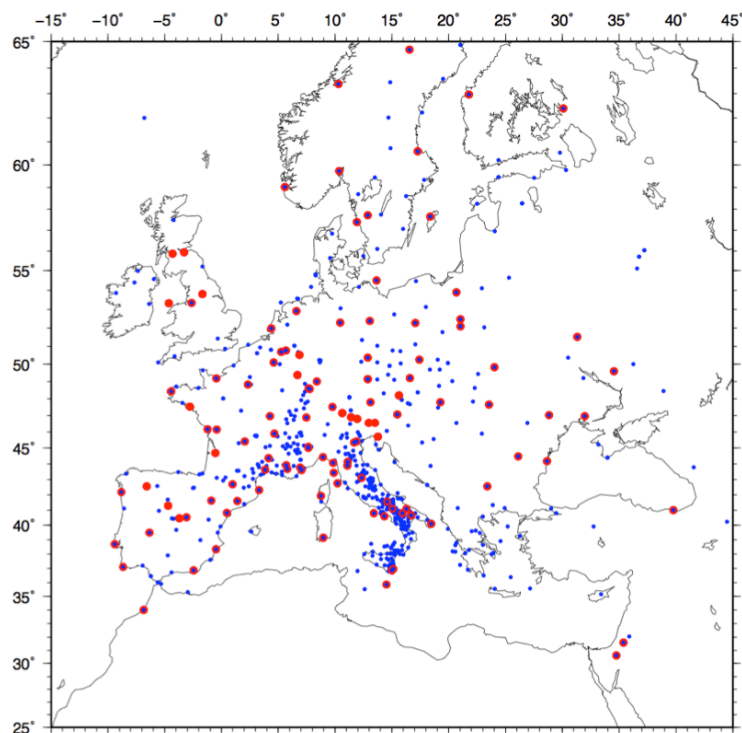


Figure 5. EU16: a terrestrial frame for geodetic studies of crustal deformation near Eurasian plate. Stations in red was used to defined EU16 (plus others out of the map).

Each step of the GIPSY processing allowed to increase the time series precision in term of RMS as it can be observed on an example figure 6.

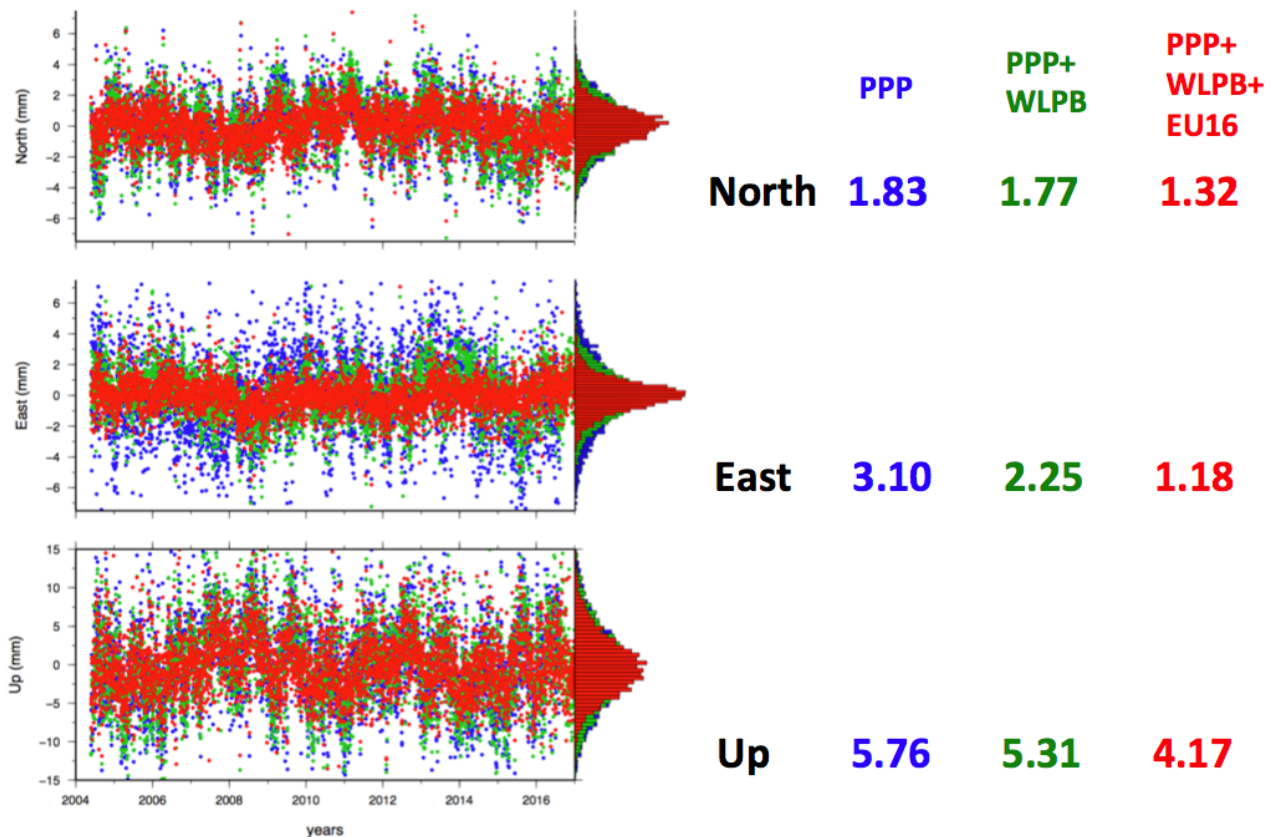


Figure 6. Effects of GIPSY processing steps in time series precision RMS of GROT (Grottaminarda RING station) time series (mm).

2.3 BFKH

BFKH did not perform any EPOS GNSS data processing, it's primary role is the different level combination of the daily SINEX product series stemming from the above described pan-European processing services.

Due to the high IT demand of the complete daily SINEX combination the work and the product is separated into two parts:

- The individual daily SINEX files of the EPOS processing centres are merged together into one combined daily SINEX series. This will be the basis of the combined daily position time series product, in which all individual contributions are integrated.
- On the individual analysis center level, based on the daily SINEX solutions, weekly combined SINEX files are generated. These weekly solutions are then used to derive the multi-year position and velocity solution, this step is described in section 3.3.

2.4 WUT

WUT is the EPN Analysis Combination Centre. WUT regularly combines and analyses GNSS weekly and daily coordinate solutions provided in SINEX files by the 16 EPN Analysis Centers (AC). The combined solutions are the official EPN daily and weekly coordinate solutions. These combined solutions are also the input for EPN cumulative solutions.

In 2016, a methodology for creating weekly combined EPN solutions was changed. Since November 27, 2016 the daily AC solutions are combined for each day of the week, and then the seven daily combined solutions are stacked into a weekly solution. The new approach allows to more consistently handle position outliers on a daily level, and it helps to mitigate possible inconsistencies between AC solutions. Before the change, the weekly combined solutions were created directly from the AC weekly solutions.

Starting with January 29, 2017 (GPS week 1934), the new IGS14/igs14.atx framework has been used by ACs to generate GNSS solutions, which replaced the IGB08/igs08.atx framework. Since week 1934 all EPN combined solutions are aligned to the new IGS14 reference frame.

2.5 CURRENT OVERVIEW

DDSS	Agency	ready or not	station number	time span
Products.EPOS.PPPsolution WP10-DDSS-007	INGV	yes	667	2000-2016
Products.EPOS.DDsolution WP10-DDSS-008	CNRS-UGA	yes	581	2000-2016
Products.EPOS.PPPsolution.TS WP10-DDSS-009	INGV	yes	667	2000-2016
Products.EPOS.DDsolution.TS WP10-DDSS-010	CNRS-UGA	yes	581	2000-2016
Products.EPOS.weekly-comb.TS WP10-DDSS-018	BFHK/ROB	yes	729	2004-2016
Products.EUREF.weekly-comb WP10-DDSS-016	WUT	yes	320	1996-2017

2.6 COMPARISON

At CNRS-UGA, a time series comparison was done. From the SINEX files provided by the processing centers, the time series were generated with PYACS using the protocol described before (section 2.1) for both DD (CNRS-UGA) and PPP (INGV) solutions.

A superposition was done for an example (station BORJ, NL in figure 7) followed by a statistical approach based on 524 time series spanning the 2000-2015 period. First, the difference to a sliding mean value was calculated. The average was computed within a sliding window encompassing 15 values before and after the observed point, and this for the 3 components independently. The histograms of the differences in daily positions were also plotted (figure 8).

If the scatter is very similar for the 2 software types (DD at CNRS-UGA and PPP at INGV) for the East component, it is more significant for the North and Up component in the time series resulting from the PPP processing.

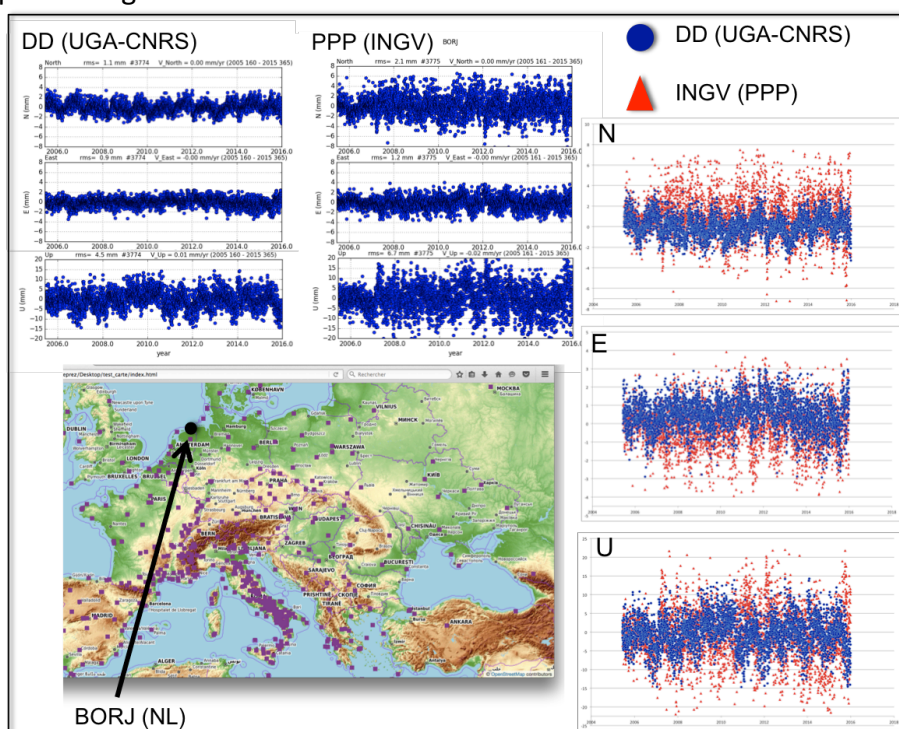


Figure 7. Time series comparison between DD (at CNRS-UGA) and PPP (at INGV) for the example of the station BORJ, NL.

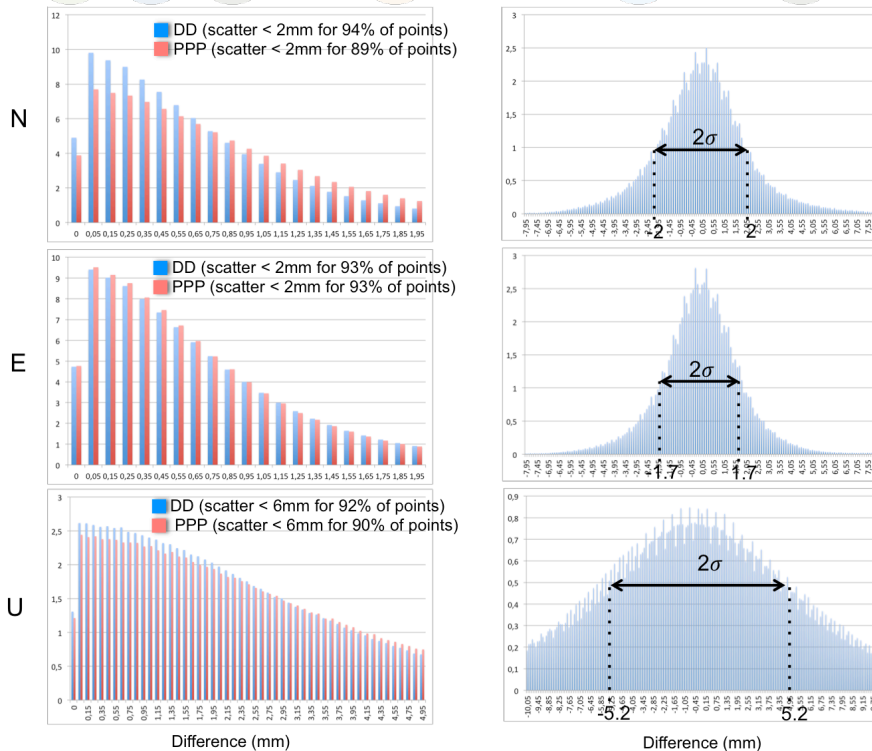


Figure 8. Statistical approach for time series comparison (DD vs PPP), for the 3 components independently (North, East, Up), based on 524 time series spanning the 2000-2005 period. On the left: difference to a sliding mean value in %. On the right: differences in daily positions in %.

Following this comparison at CNRS-UGA, pointing out a larger scatter for the PPP processing, in particular for some EUREF sites, a problem was detected and resolved at INGV. The corrected PPP-GIPSY time series seems to be more consistent with the DD-GAMIT time series (Figure 9).

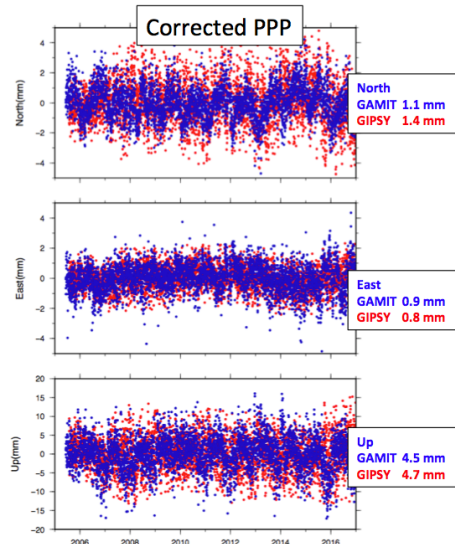


Figure 9. Discrepancy between GAMIT and GIPSY after the problem resolution (GIPSY processing was pointing to wrong ocld tables for some sites).

2.7 VALIDATION OF TIME SERIES

The previous section showed a comparison of the time series. In addition, the noise parameters of the time series will be estimated at UBI using the Hector software. These estimated values will provide additional information about the quality of the time series and will be provided at the product portal.

Another quality check will be the automatic search for outliers in the time series. This has been implemented but no outliers have been found so far, showing the quality of the processing of the EPOS analysis centres.

In addition, all time series will be investigated for undetected jumps. These are sudden displacements in the position found in the time series which are not identified as being due to known causes such as earthquakes. If such a potential jump is detected, the corresponding EPOS analysis centre will be contacted in order to investigate the cause of this event.

3. Products level 2 (velocities)

3.0 GUIDELINES

In a second instance, the massive processing implementation requires innovative strategies in order to satisfy the efficiency, robustness and automatization criteria for the computation of another usual GNSS product: the velocity field. A key issue is the time computation but the outlier and offset detection is also of crucial importance.

The software MIDAS was proposed to be tested at CNRS-UGA and INGV. This software was developed at Nevada Geodetic Laboratory, USA by G. Blewitt and allows to obtain GNSS velocities robust to outliers, steps and seasonality by estimating automatically the time series trend. If the Globk (developed at MIT) software based on Kalman filter can also be tested for this prototype solution, the limitations of such a software with regard to the amount of data (stations number and time span) must be evaluated.

In addition to the generation of velocity fields at both EPOS processing centers, a multiyear combined velocity field is computed including all weekly combined SINEX.

In section 2.7 it was mentioned that the noise parameters were estimated using the Hector software package. During this process also the velocities are estimated and these can also be used to compare the estimated velocities by the EPOS analysis centres to detect any anomalies. If velocities are above a certain threshold, then the corresponding EPOS analysis centre will be contacted in order to find an explanation for this discrepancy.

All scripts to convert the SINEX time series to the format readable by Hector are in place and velocities have been estimated with Hector.

3.1 CNRS-UGA

In order to test and validate the generation of a velocity field with MIDAS, two independent velocity fields have been generated and compared: one using GLOBK (a well established method based on a Kalman Filter) and one using MIDAS software. Indeed, the 2005-2015 velocity field

computation using GLOBK is very time consuming (more than 100h for 581 station over a 11-years time span), this no splittable step was exposed to computer instability and MIDAS software seemed to be a good and faster (a few minutes for the same data set) alternative. If the velocity field computation was manageable for this prototype solution, it can be considered that the limits of the Kalman filter method are reached here in terms of data amount.

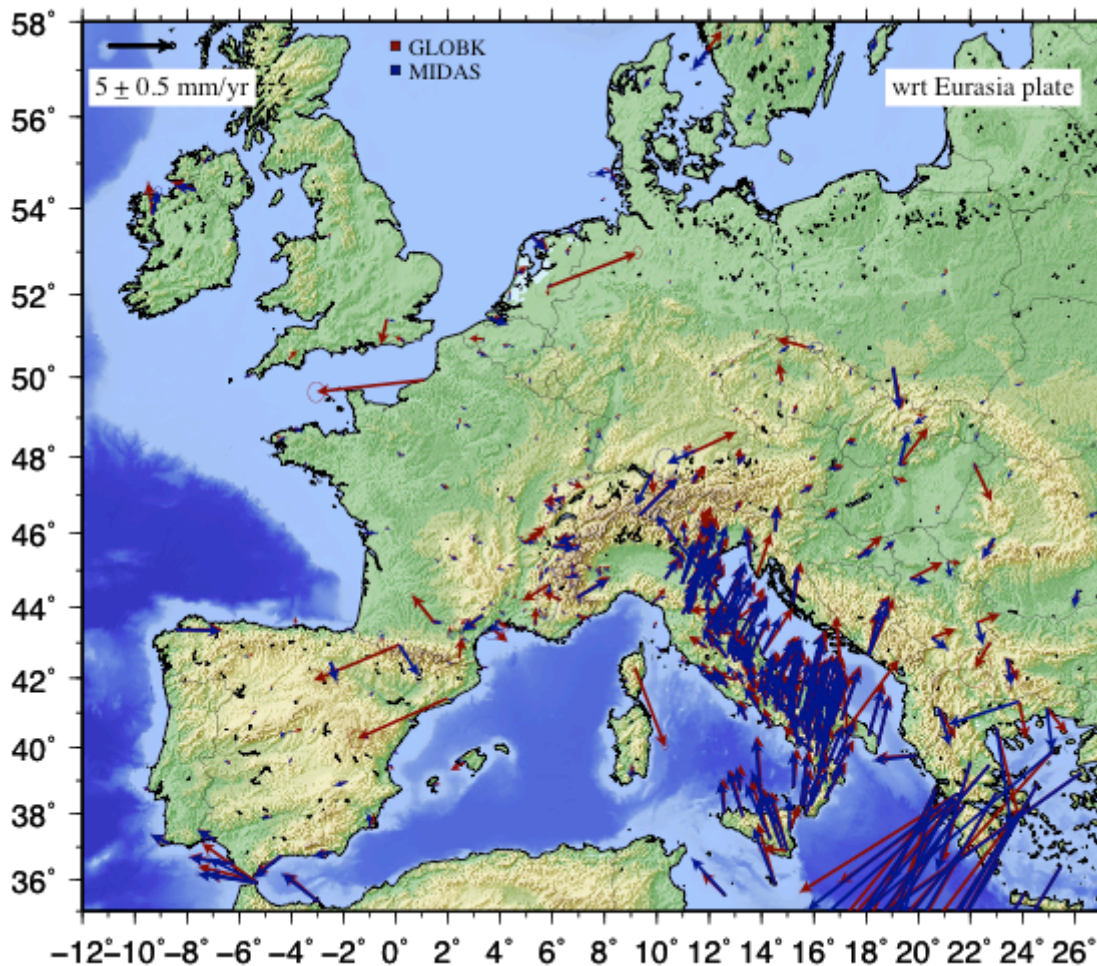


Figure 10. Comparison of the 2005-2015 velocity fields obtained with either GLOBK or MIDAS softwares.

The comparison between the 2005-2015 velocity field obtained with either GLOBK or MIDAS software showed significant differences for some sites (see figures 11 & 12), which can be easily explained by:

- either a too short time series (see the example of DIPP), in this case MIDAS is not able to provide a result.
- or a noisy or affected by seasonal signal time series. In the example of PESA the difference value is 7.8mm/yr for the horizontal component and 2.1mm/yr for the vertical one.
- or a time series offset by geophysical signal. In the example of AQUA, the station was affected by the Mw6.3 l'Aquila earthquake that occurred on 6/04/2009. The difference value is 4.7mm/yr for the horizontal component and 8.7mm/yr for the vertical one.

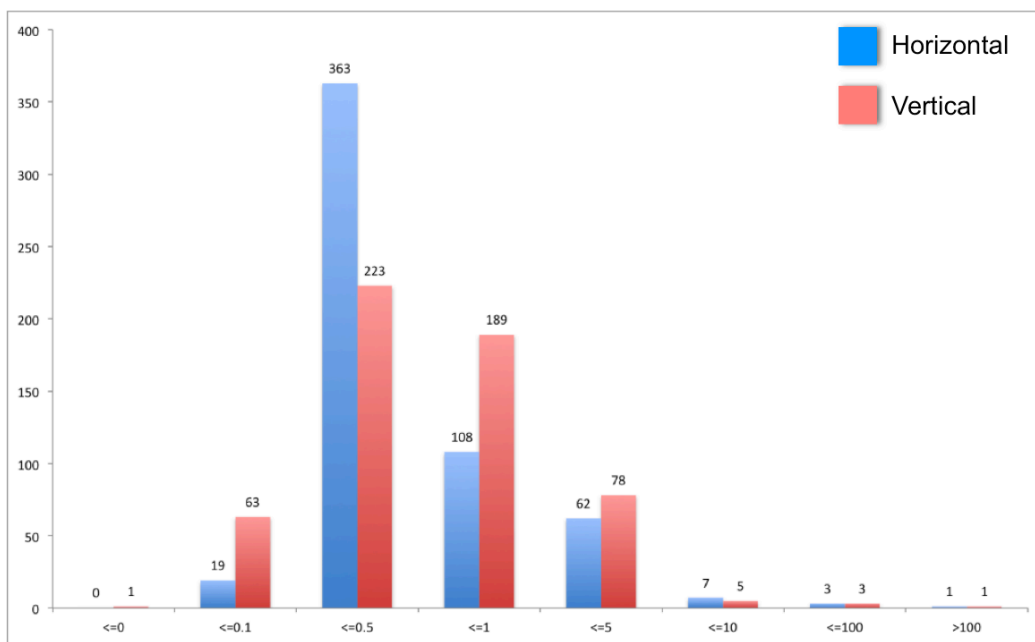


Figure 11. Histogram showing the repartition of the velocity difference between the 2 processing strategies with GLOBK and MIDAS.

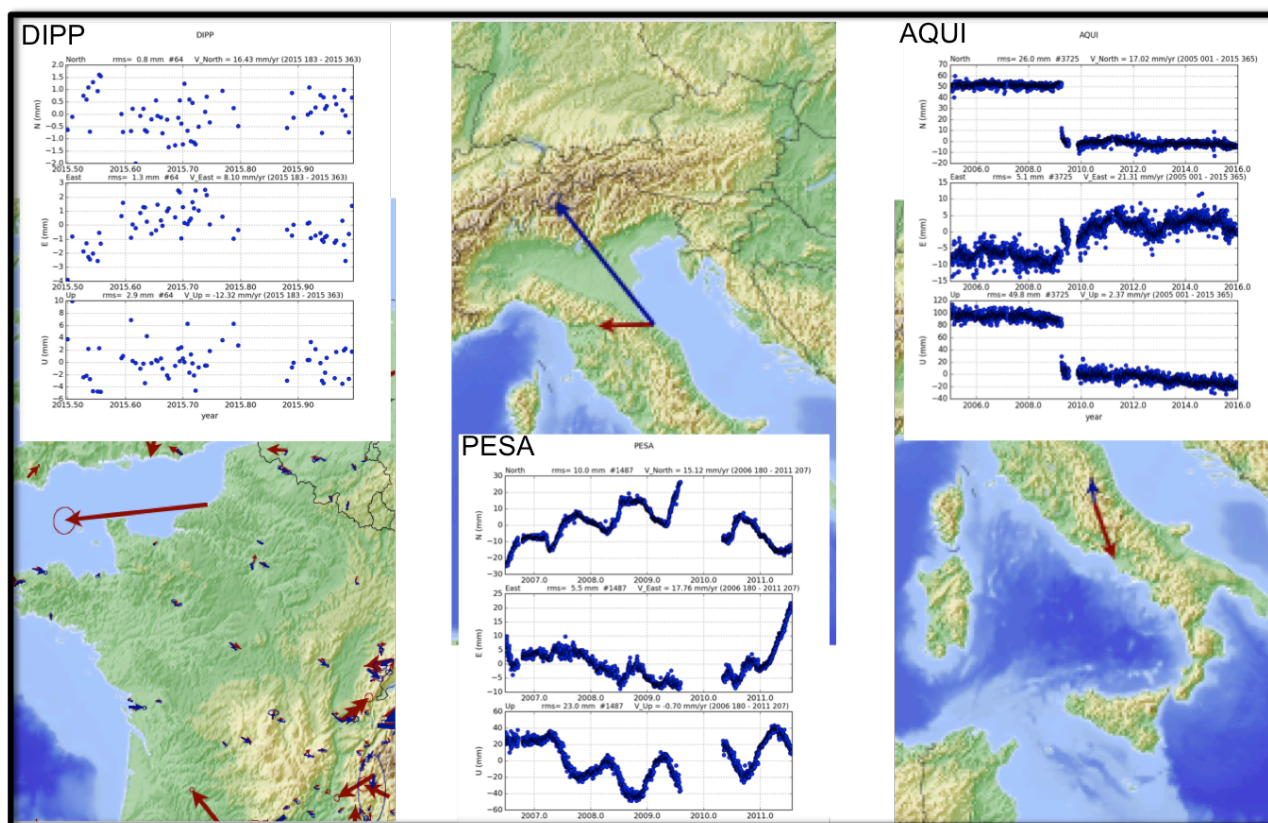


Figure 12. Explanations for the velocity differences by looking at the time series specificities.

3.2 INGV

At INGV, a MIDAS velocity field including 537 stations was computed and following by a comparison with the one computed at CNRS-UGA (see annex 2.4). The resulting mean uncertainty is 0.32 mm/yr for the horizontal component and 0.69 mm/yr for the vertical component.

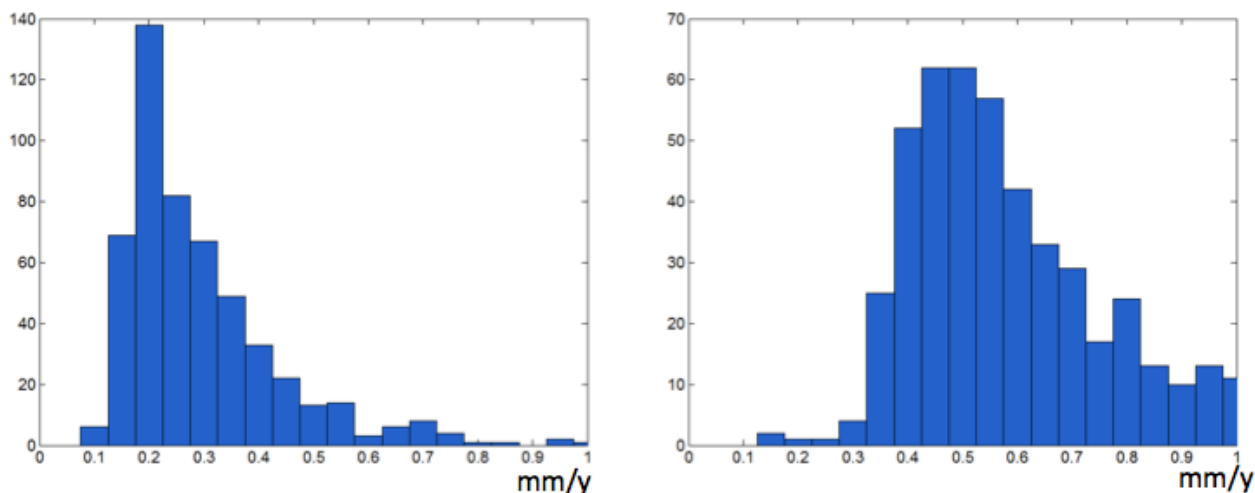


Figure 13. Uncertainties of the MIDAS-INGV velocity field. On the left: horizontal uncertainties. On the right: vertical uncertainties.

3.3 BFHK

The combined EPOS multi-year position and velocity solution is based on the weekly sinex combination from all available qualified/approved sources - as the pan-European daily SINEX series of CNRS-UGA and INGV - as described in sections 2.1- 2.2 - and a regional solution series of the Marmara region provided by the Kandili University (KAN).

The combination was performed according to the following steps:

- checking and correction of metadata (station naming, DOMES numbers) of the individual solutions,
- individual combination of the three SINEX series for outlier identification/rejection and identification of offsets in the position time series,
- set up database for outliers and offsets in a standard format (soln.snx),
- creation of individual (UGA-CNRS, INGV, KAN) weekly SINEX solution series using the daily SINEX series,
- combination of the individual weekly SINEX solutions into a unique combined weekly SINEX solution series. The EPN weekly SINEX series is involved as well and used as reference. At this step a final check of the station metadata is performed looking for naming overlaps and creating the final meta data of the complete network.
- creation of the final multi-year position and velocity solution based on the weekly combined SINEX solution series. The reference frame is defined by the same set of IGB08 stations as for the EPN multi year solution (see section 3.4). The reference frame is realized by the Minimal Constraint

approach, where the constraints are put on the reference frame parameters instead of any positions and velocities.

At all computation steps the CATREF software (Altamimi et al, IGN, FR) was used.

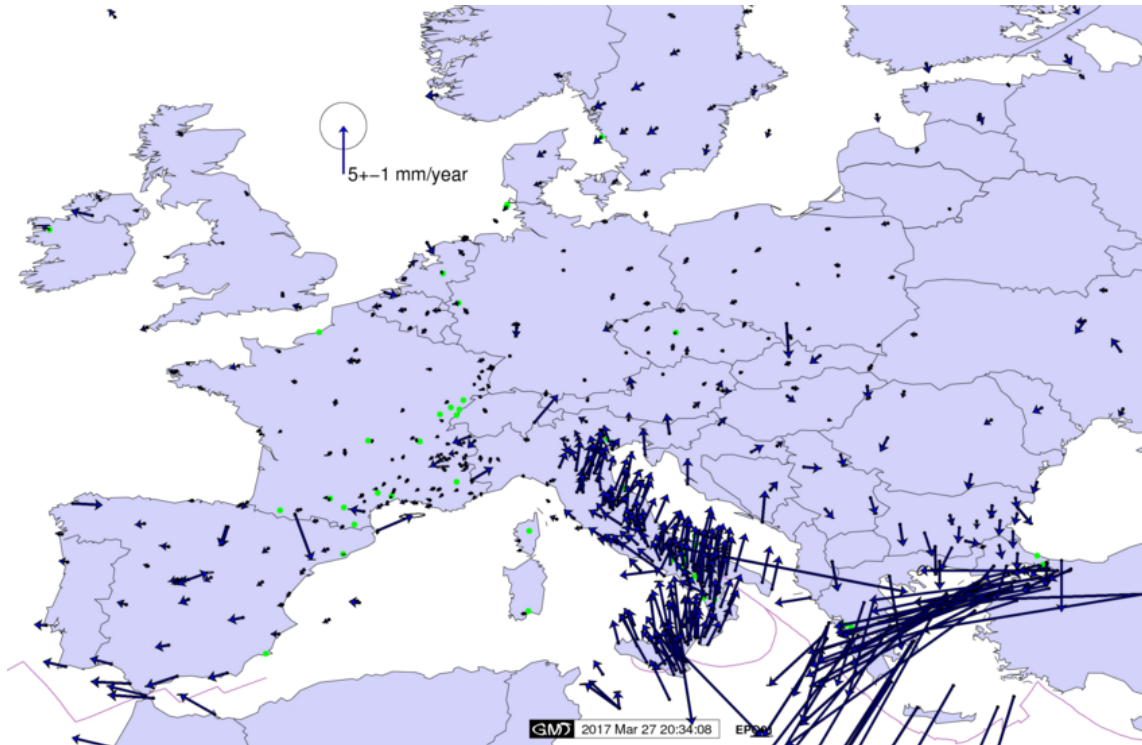


Figure 14. 2D velocities, referring to the EURA plate derived from the combination of EPN, INGV, UGA-CNRS and KAN solutions. The green dots are stations with short data availability. Few velocity outliers with longer history were kept on the map – those may reflect very local issues.

The involvement of the EPN Densification solution in the product level is also considered following the clarification of the technical and legal conditions.

3.4 EUREF

Within EPOS, EUREF is providing the EPN multi-year reference position and velocity solution, which is in each 15 weeks updated. The multi-year solution integrates all weekly combined EPN SINEX files from GPS week 834 (1986) to present. This cumulative solution is aligned to the IGS reference frame realization: up to GPS week 1933 (weekly SINEX files up to 28 January, 2017) it was IGB08, then we change to IGS14. The alignment is being done using the Minimal Constraint approach as implemented in the CATREF software. The solution is provided in SINEX format and in the internationally recognized SSC format, where the latter includes only the position and velocity estimates with their uncertainties. We also provide positions and velocities expressed in ETRS89 and realized by ETRF2000. All related information, which is available at the EPN CB website (station discontinuities, Helmert-transformation parameters, weekly WRMS) are also provided for EPOS.

We also developed a station categorization tool, which tests the quality of the time series and the convergence of the velocity estimates and make distinctions between stations and offer selection (category A) for national reference frame definition.

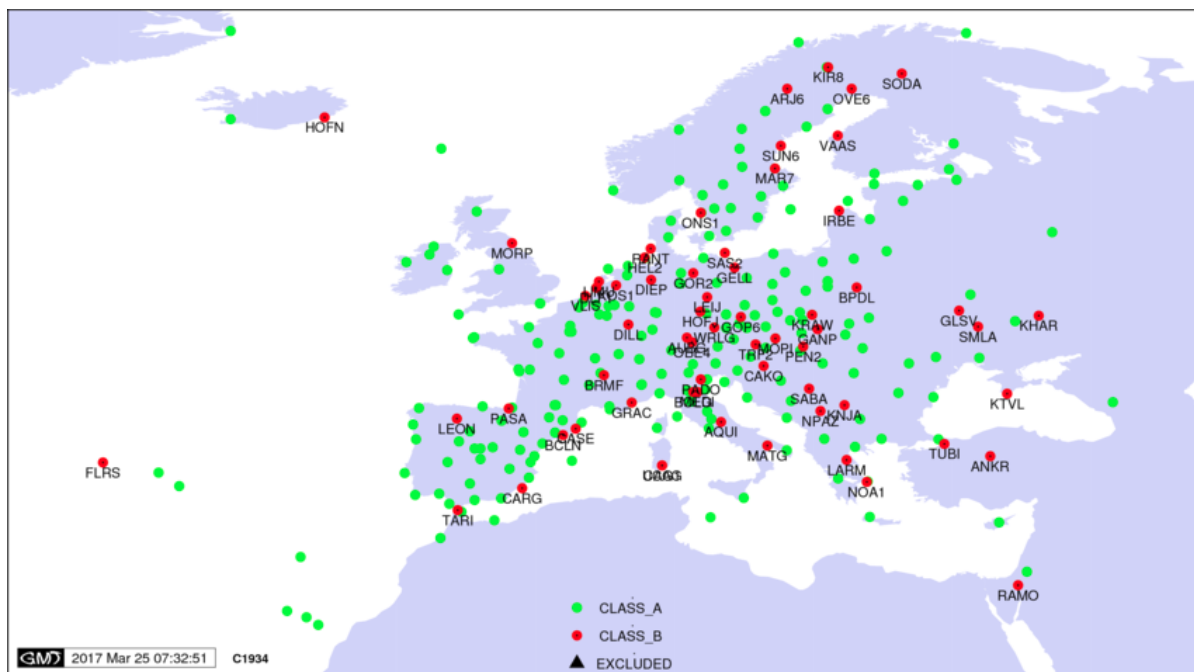


Figure 15. EPN station categories. The red stations are not offered for reference frame realization due to the noisy time series or the short lifetime with less realistic velocity estimate.

3.5 CURRENT OVERVIEW

DDSS	Agency	ready or not	station number	time span
Products.EPOS.DDsolution.velocity WP10-DDSS-012	CNRS-UGA	yes	581	2000-2016
Products.EPOS.PPPsolution.velocity WP10-DDSS-013	INGV	yes	667	2000-2016
Products.EPOS.Combined.velocity WP10-DDSS-014	BFHK	yes	729	2004-2016
Products.EPOS.validation.pos_vel <i>(only validates time series and estimated velocities)</i> WP10-DDSS-015	UBI	yes	-	-
Products.EUREF.reference.pos-vel WP10-DDSS-018	BFHK/ROB	yes	320	1996-2017

3.6 COMPARISON

At CNRS-UGA, a comparison was done between 2 velocity fields generated within both EPOS processing centers with MIDAS software from DD and PPP raw time series. Even if some sites present large differences, the 2 velocity fields are generally in accordance. Large differences (9 stations with a difference > 1mm/yr, see figures 14 & 15) are most of the time associated with very low amount of data.

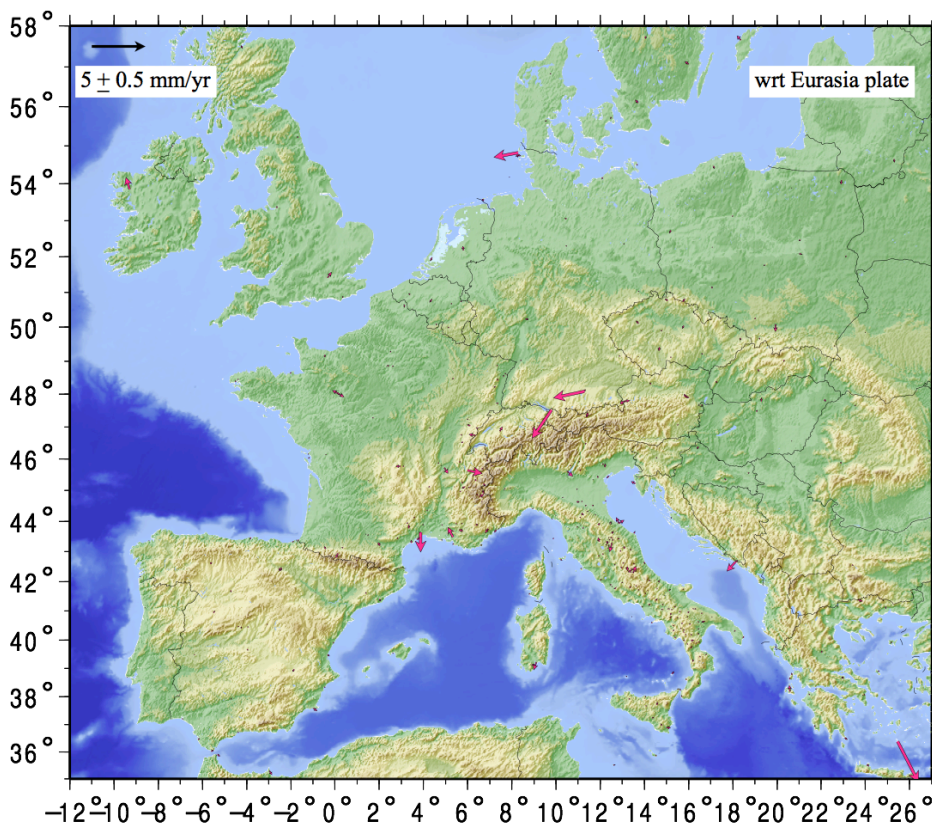


Figure 16. Velocity field of the differences between velocities computed with MIDAS using as input either DD raw time series computed at CNRS-UGA or PPP raw time series computed at INGV .

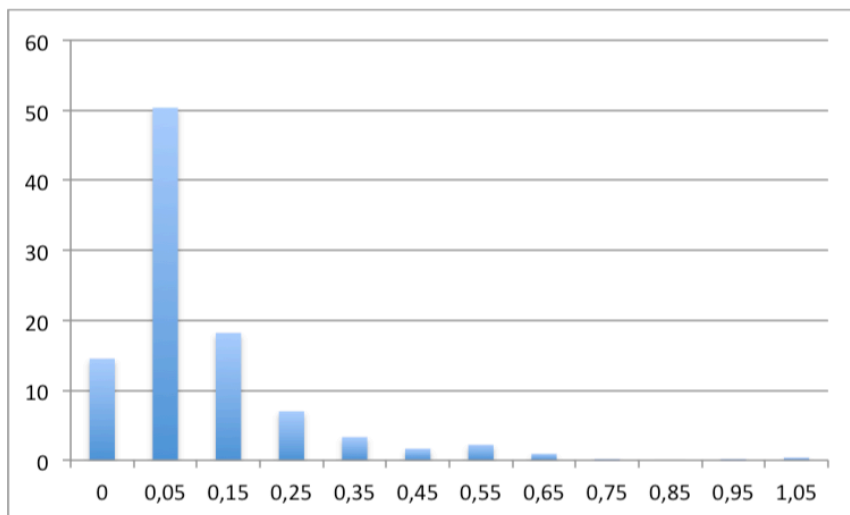


Figure 16. Histogram of the velocity difference distribution in %.

The comparison conducted at INGV between the MIDAS velocity fields computed either at CNRS or INGV pointed out no detectable systematics and velocity differences lower than the mean uncertainties, showing the good accordance between the 2 processing centers.

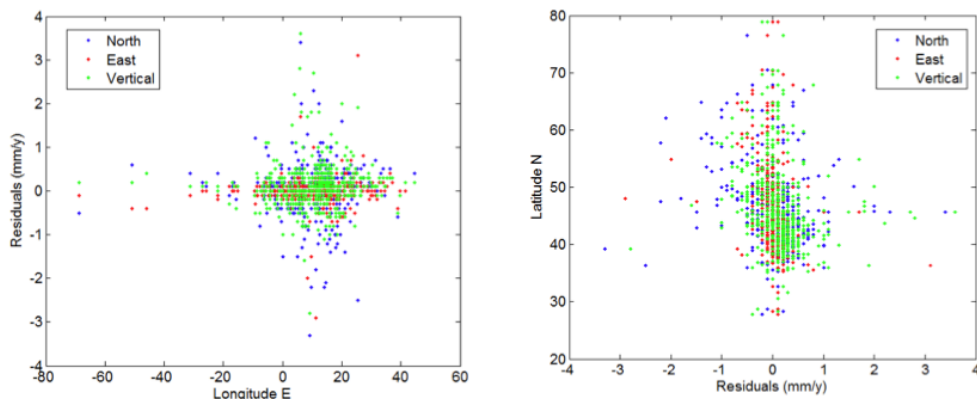


Figure 18. Geographical distribution of the velocity differences between CNRS and INGV MIDAS velocity fields.

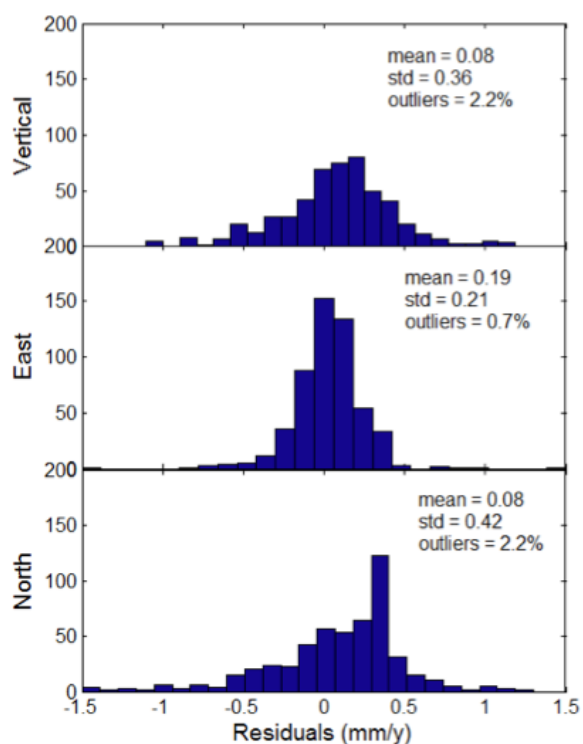


Figure 19. Statistics of the velocity differences between CNRS and INGV MIDAS velocity fields. The rotation parameters between INGV and CNRS are $R_x = -0.09^\circ \pm 0.1^\circ$, $R_y = -0.14^\circ \pm 0.1^\circ$, $R_z = 0.09^\circ \pm 0.1^\circ$.

4. Products level 3 (strain rates)

4.0 GUIDELINES

This is the most difficult product to catalogue since there is still no clear format adopted by the scientific community. In December 2016, guidelines for the strain rate map computation were

defined at NOA by A. Ganas. The strain rate DDSS product requires a method using only geodetic data. The main principle of the method would be to calculate on a regular grid the components of the strain rate tensor from a table of tectonic velocity recorded at GNSS sites. A major drawback that we have to face is the variable site density and tectonic strain from one region to the other, that would allow a variable resolution in the strain rate maps.

4.1 LM

LM is currently evaluating the methodology proposed by NOA in order to adopt it for the production of strain rates based on the combined velocity solution produced by BFHK.

This is planned to start this next fall (October/November) in order to be able to have some first product available at middle 2018.

During this period, solutions will be found regarding data formats, how to publish the results, and how to estimate the uncertainty in the products. This will be done in coordination with the other partners making the velocities available and also with the products portal.

4.2 CNRS-UGA

A processing chain called STIB (strain tensor inversion of baselines, Masson et al., GJI, 2015) was tested at CNRS-UGA. This set of tools, written in Python language, takes as input the temporal variation of the baseline components. Thus, the deformation is supposed to be steady state. The deformation observed between each pair of stations is distributed along the baseline. The full set of baselines, associated with the station network is used and allows to obtain a deformation map on the surface covered by the whole set of baselines.

Preliminary results obtained after a selection of reliable sites in Italy and surrounding areas are presented on the following figures, showing the extensional pattern in the Apennines. Some works remains to extend this procedure on the whole European territory, in particular in term of smoothing and to allow to take into account the inhomogeneous station density.

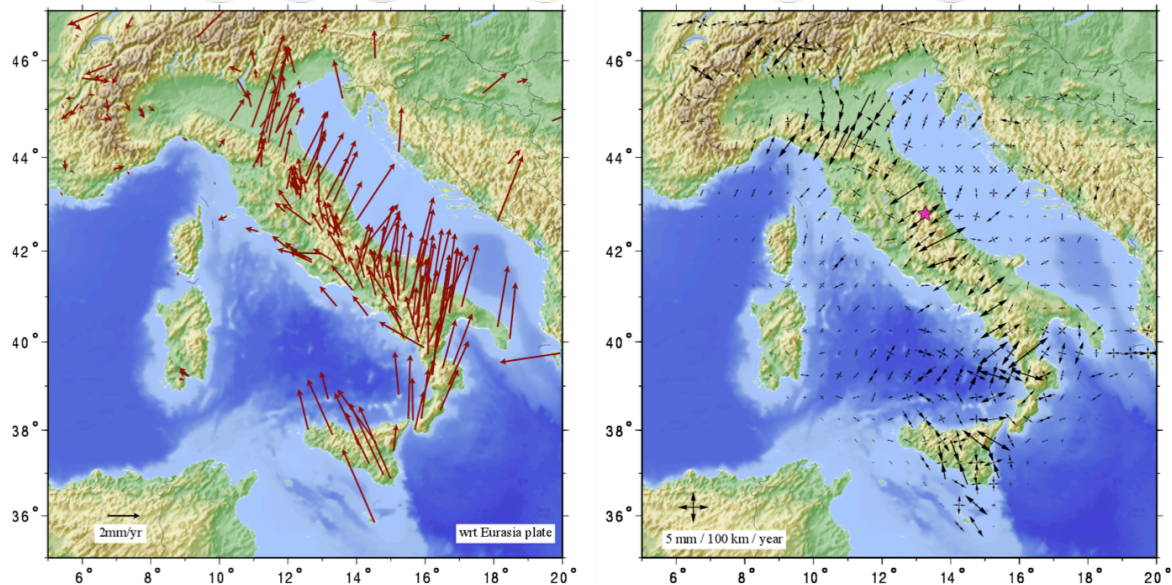


Figure 20. Strain rate computation. On the left: 2005-2015 velocity field computed with Globk software (CNRS-UGA). On the right: strain rate map deduced from the velocity field on the left. The pink star shows the Mw6.2 Amatrice earthquake that occurred on 25/08/2016

4.3 INGV

Starting from the EPOS PPP velocity field, a processing is in progress to obtain a strain rate map. In order to relate the geodetic velocities to crustal deformation rates we are modeling the crustal horizontal velocity field under the assumption that the crust deforms as a continuum (Haines and Holt, 1993; England and Molnar, 1997) and a smooth estimate of the deformation field will be provided. To derive continuous velocity gradient tensor field we will apply a spline interpolation technique modified from the approach of Haines and Holt (1993).

4.4 CURRENT OVERVIEW

DDSS	Agency	ready or not	input velocity field	software / method
Products.EPOS.strainrates WP10-DDSS-017	LM	in progress	EPOS combined	tbd
Products.EPOS.strainrates WP10-DDSS-012	CNRS-UGA	in progress	DD CNRS-UGA	STIB / inversion of baseline length variation
Products.EPOS.strainrates WP10-DDSS-013	INGV	in progress	PPP INGV	SPARSE

References

- Bertiger W, Desai SD, Haines B, Harvey N, Moore AW, Owen S, Weiss JP (2010) Single receiver phase ambiguity resolution with GPS data. *J Geod* 84(5):327–337
- Blewitt, G., C. Kreemer, W.C. Hammond, J. Gazeaux, 2016, MIDAS robust trend estimator for accurate GPS station velocities without step detection, accepted for publication in the *Journal of Geophysical Research*, doi: 10.1002/2015JB012552
- Blewitt, G., C. Kreemer, W.C. Hammond, and J.M. Goldfarb, (2013). Terrestrial reference frame NA12 for crustal deformation studies in North America. *J. of Geodynamics*, 72, pp. 11-24, doi:10.1016/j. jog.2013.08.004.
- England, P., Molnar, P., 1997. The field of crustal velocity in Asia calculated from Quaternary rates of slip on faults. *Geophys. J. Int.* 130, 551–582.
- Haines, A.J., Holt, W.E., 1993. A procedure for obtaining the complete horizontal motions within zones of distributed deformation from the inversion of strain rate data. *J. Geophys. Res.* 98, 12057–12082
- King, R. W. et Bock, Y. (2015). Documentation for the GAMIT/GLOBK GPS software analysis, release 10.06. Massachusetts Institute of Technology, Cambridge.
- PYACS: PhD thesis Dinh Trong Tran supervised by J. M. Nocquet. Analyse rapide et robuste des solutions GPS pour la tectonique. Autre. Université Nice Sophia Antipolis, 2013. Français.
- Masson, F., Lehujeur, M., Ziegler, Y., and Doubre, C. (2014). Strain rate tensor in Iran from a new GPS velocity field. *Geophys. J. Int.*, 197(1):10–21.
- Gipsy-Oasis, JPL: <https://gipsy-oasis.jpl.nasa.gov>

Annex 1 – Guidelines documents

Annex 1.1: Guidelines for the processing of the prototype solution

[EPOS processing guidelines for prototype solution](#)

Annex 1.2: Guidelines for the strain rates computation

[EPOS strain product format](#)

Annex 2 – Presentations/Posters/Publications

Annex 2.1: Depez et al. poster presented at wegener 2016 congress

[depez_et_al_2016](#)

Annex 2.2: Presentation of CNRS-UGA done for the EPOS meeting in Madrid, Oct. 2016

[CNRS-UGA October 2016](#)

Annex 2.3: INGV PPP solution for EPOS-IP

[PPP-GIPSY INGV solution](#)

Annex 2.4: INGV combination process

[INGV combination velocities](#)

Annex 2.5: Annals of Geophysics, Devoti et al. 2017 (INGV)

[A Combined Velocity Field of the Mediterranean Region](#)

Annex 2.6: Presentation of BFHK done for EPOS meeting in Prague, Feb. 2017

[EPOS combination status report](#)

Annex 2.7: KOERI GAMIT Processing

[Marmara continuous GPS network \(MAGNET\)](#)

Annex 1.1 : Guidelines for the processing of the prototype solution

EPOS-IP GNSS Processing

On the 20th of November 2015, we agreed that the objective for 2016 is to run, and generate products on a subset of stations. Test solutions will be processed in the 2 EPOS processing centers (CNRS with GAMIT, INGV with GIPSY), and another one will be processed in KOERI with Turkish sites + some EPN sites

NB: the contribution of other processing centers to the densified solution will be discussed later (in January or Feb. 2016), and coordinated by A. Kenyeres.

1. Contours of the prototype solutions

a- for CNRS and INGV processing centers

- + RENAG: 73 stations
- + RING (191 = 186 sites -1 site [KLOK] delivered by NOA + 6 sites [CARO; INGP, MESS, MMME, MURB and PESA] now out of service but with data spanning more than 3 years)
- + NOA sites (around 22 sites)
- + EPN: 265 stations
- + local IGS sites (10 in Italy + 11 in France + 1 in Greece)

= 573 stations, Time span = 2005-2015

b- for KOERI

- + MAGNET: 22 stations
- + a subset of EPN (to be discussed with A. Kenyeres → ~15 stations) over a minimum time period spanning = 2011-2015

2. General processing Instructions

a- Preparation

1. Download the RINEX observation files of the network for the period to be processed through existing GSAC nodes :
 - RENAG: <http://epos.unice.fr:8080/renagbgsac/>
 - INGV: <http://ring.gm.ingv.it>
 - NOA: <http://194.177.194.238:8080/noanetgsac>
 - The data of EPN stations are available at the EPN data centres (see http://www.epncb.oma.be/_dataproducs/data_access/dailyandhourly/).
2. Download the satellites orbits, clocks (if necessary) and Earth Rotation Parameter (ERP) files from the IGS/JPL/MIT. Final products have to be used. For information about access to IGS products see <http://igs.org/>.
3. Download the coordinates and velocities of the actual IGS realisation of the ITRF (e.g. IGB08) from the IGS CB at <ftp://igsb.jpl.nasa.gov/>.

4. Prepare a table of ocean loading displacements for involved sites (or convert into a grid) through the online computation service of OSO at <http://holt.oso.chalmers.se/loading/index.html> using FES2004 model.
5. Prepare the receiver and satellite antennae calibration table using IGS antenna calibrations ANTEX files.
6. Make sure the correct meta-data (provided through GSAC servers and in <ftp://epncb.oma.be/pub/station/general/euref.snx>) is used during all steps of the data analysis, independent of the information in the RINEX header.

b- Processing options

During 2015/12/09 visioconference, we agreed that for the prototype solution at least we will perform the best solution possible, making the best use of each processing softwares (GAMIT & GIPSY). For this reason, we do not always use the same processing option for both solutions. The processing options of each center will be fully detailed and should be available to the products users (A. Socquet & N. d'Agostino are the contact persons).

1. Use IGS/JPL/MIT final products (satellite orbits, satellite clocks and Earth orientation parameters). Take in particular care on the usability of orbits for unhealthy satellites. Orbits can either be fixed or re-estimated.
2. Introduce ocean-loading corrections for the stations, using FES2004 Ocean tidal loading.
3. Use the 0° elevation cut-off angle. Apply elevation dependent weighting of observations.
4. Use the tropospheric mapping function with a priori ZHD model using the Vienna Mapping Function (VMF1) to map the tropospheric delay in zenith direction.
5. Don't implement atmospheric loading (tidal and non-tidal) for the prototype solution. The results will be compared to the current RENAG solution that implements atmospheric loading. Depending on this comparison, atmospheric loading might be introduced in the next solution.
6. Estimate station specific troposphere parameters every 2 hours. Estimate one couple of horizontal tropospheric gradients per 24h session.
7. Fix the initial phase ambiguities to integer numbers for GPS data processing.
8. Distribute the loosely constrained solution.
9. Align the solution to the IGB08 at the current epoch, e.g., through applying "minimum-constraint-conditions" to the reference sites (do NOT "fix" any reference coordinates).

3. Details of processing options for GIPSY solution at INGV

INGV-CNT-GIPSY Analysis Center Strategy Summary	
ANALYSIS CENTER	Centro Nazionale Terremoti Istituto Nazionale Geofisica e Vulcanologia Via Vigna Murata 605 00143 Roma ITALY Fax: +39 06 51860541 Data Archive: http://ring.gm.ingv.it ftp://gpsfree.gm.ingv.it
CONTACT PERSON(S)	Dr. Nicola D'Agostino E-mail: nicola.dagostino (at) ingv.it Phone: +39-06-51860537
SOFTWARE USED	GIPSY/OASIS-II Version 6.3 developed at JPL
PRODUCTS USED	Final, non-fiducial daily products from JPL archive: ftp://sideshow.jpl.nasa.gov/pub/JPL_GPS_Products/Final Including: GPS satellite orbit estimates GPS satellite clock estimates WLPB estimates (wideline & phase biases) Name of TRF (terrestrial reference frame) Transformation parameter estimates to named TRF Time-pole parameter estimates GPS satellite eclipse times Name of IGS ANTEX antenna calibration file Auxiliary data updated periodically from JPL: IGS ANTEX antenna calibration file JPL planetary ephemeris CODE CA-P DCB (differential code biases) GPS receiver type codes GPS constellation configuration history IERS/BIH leap seconds history IERS earth orientation parameters Auxiliary data updated from IGS Central Bureau: http://igsb.jpl.nasa.gov/ IGS station receiver/antenna configuration history Auxiliary data from Chalmers University, Sweden: http://holt.oso.chalmers.se/loading/ Ocean tidal loading coefficients for all stations
PREPARATION DATE	January 21, 2016
MODIFICATION DATES	January 21, 2016 Creation
EFFECTIVE DATE FOR DATA ANALYSIS	2000-01-01 onward using JPL version 2 reprocessing with IERS2010/IGS08 conventions

MEASUREMENT MODELS	
Preprocessing	<p>RINEX header must be interpretable</p> <ul style="list-style-type: none"> - alias table replaces antenna type with IGS standard - fix obvious formatting errors - require antenna type has IGS ANTEX calibrations - non-calibrated radome set to "NONE" (IGS standard) <p>Require minimum file size, typically ~18 hr/day Apply CA-P1 biases Fix non-compliant time-tags for older receiver types Remove non-GPS GNSS data (e.g., GLONASS) Remove L2C and C2 data Cycle slip detection Delete phase connected arcs < 20 minutes Carrier Phase: Decimated to 5 minutes Pseudorange: Carrier aided smoothing to 5 minutes</p>
Basic Observable	<p>Undifferenced ionosphere-free carrier phase, LC Undifferenced ionosphere-free pseudorange, PC</p> <hr/> <p>Elevation angle cutoff: 0 degrees Sampling rate: 5 minutes Data weight, LC: 1 cm Data weight, PC: 1 m Weighting: $\text{Sigma}^2=1/\sin(e)$</p>
Modeled observable	<p>Undifferenced LC and PC combinations CA-P1 biases from CODE applied</p>
RHC phase rotation corr.	Applied
Marker -> antenna ARP eccentricity	dN, dE, dU eccentricities from IGS sinex file applied to compute station marker coordinates
Ground antenna phase center cal.	PCV model from igs08_www.atx applied Receiver antenna and radome types from IGS sinex file
Troposphere	<p>A priori model: Wet and Dry from VMF1 model (Boehm et al, 2006) Mapping Function: VMF1 grid Estimation: Zenith delay and horizontal gradients</p>
Ionosphere	<p>1st order effect: Removed by LC and PC combinations 2nd order effect: Modeled</p>
Plate motions	Not applied to a priori positions
Tidal	<p>Solid earth tide: IERS 2010 Conventions</p> <hr/> <p>Permanent tide: NOT removed from model, so NOT in estimated site coordinates</p> <hr/> <p>Pole tide: IERS 2010 Conventions</p>

	<p>Ocean Tide Loading: Diurnal, Semidiurnal, MF, and MM Model: GOT4.8ac Semiannual: Self-consistent equilibrium model hardisp.f from IERS2010</p> <p>Surface deformations computed at JPL with respect to instantaneous center of mass</p> <hr/> <p>Ocean Pole Tide Loading: Applied</p>
Non-tidal loading	<p>Atmospheric Pressure: Not applied</p> <hr/> <p>Ocean Bottom Pressure: Not applied</p> <hr/> <p>Surface Hydrology: Not applied</p> <hr/> <p>Other Effects: None applied</p>
Earth Orientation Parameter (EOP) Model	IERS 2010 Conventions for diurnal, semidiurnal, and long period tidal effects on polar motion and UT1
Satellite center of mass correction	Phase centers offsets from igs08_www.atx applied
Satellite antenna phase variations	PCV model w.r.t. phase center from igs08_www.atx applied
Relativistic corrections	Periodic Clock Corrections, $(-2*R*V/c)$: Applied Gravity Bending: Applied
GPS Attitude model	GYM95 nominal yaw rate model from Bar-Sever (1996) and yaw rates estimated for Block II satellites

ORBIT MODELS	
Geopotential	<p>EGM2008 12x12 C20, C30, C40, C21, S21 from IERS2010 standards</p> <hr/> <p>GM = 398600.4415 km**3/sec**2</p> <hr/> <p>AE = 6378.1363 km</p>
Third-body	<p>Sun, Moon, and All Planets</p> <hr/> <p>Ephemeris: JPL DE421</p>
Solar radiation pressure	<p>Block II/IIA/IIR: JPL empirical SRP model, GSPM-13, Bar-Sever and Kuang, (2004) Sibois et al, 2014</p> <hr/> <p>Estimate GPS "Y-Bias" and solar radiation pressure(SRP) coefficient as constant with no a-priori constraint. Make small time-varying (stochastic) adjustments to SRP coefficients in spacecraft body-fixed X and Z</p>

	<p>directions (1% process noise sigma with 1 hr 11 sec updates and 4-hour correlation time.) Estimate tightly constrained time-varying empirical acceleration in spacecraft Y direction (0.01 nm/s² process noise sigma with 1 hr 11 sec updates and 4-hour correlation time.)</p> <p>Earth shadow model: conic model with oblate Earth, umbra and penumbra</p> <p>Earth albedo: applied</p> <p>Attitude Model: GYM95 yaw model from Bar-Sever (1996)</p>
Tidal forces	<p>Solid earth tides: IERS 2010 Conventions</p> <p>Ocean tides: FES2004 to degree and order 30 with convolution formalism of Desai and Yuan (2006)</p> <p>Solid Earth Pole tide: IERS 2010 conventions</p> <p>Ocean Pole tide: IERS 2010 conventions</p>
Relativity	<p>Applied</p> <p>Acceleration due to point mass of Earth</p> <p>Acceleration due to geodesic precession</p> <p>Acceleration due to Lense-Thirring precession</p>
Numerical Integration	<p>Variable high order Adams predictor-corrector with direct integration of second-order equations</p> <p>Integration step: variable</p> <p>Starter procedure: RKF</p> <p>Arc length: 30 hours centered at 12:00 of each day</p>

ESTIMATED PARAMETERS (APRIORI VALUES & SIGMAS)	
Adjustment	Stochastic Kalman filter/smoothen implemented as square root information filter with smoothen
Station coordinates	Daily free-network estimates for all sites Combine free-network estimates to get daily solution Apply three rotations to daily solution
Satellite clock	Estimate every 5 minutes relative to reference clock Recompute every 30 seconds relative to reference clock
Receiver clock	Estimate every 5 minutes relative to reference clock Reference clock usually USN3 or AMC2
Orbital parameters	Epoch state, solar pressure parameters, Y-bias Solar scale X and Z, Y acceleration

GPS Attitude parameters	Estimate yaw rates for eclipsing spacecraft Yaw rates used for measurement but not dynamic models
Troposphere	Zenith delay: random walk 5.0d-8 km/sqrt(sec) Horizontal delay gradients: random walk 5.0e-9 km/sqrt(sec) Mapping function: VMF1
Ionosphere	1st order effects removed by LC and PC combinations and 2nd order effects modeled
Ambiguity	Global ambiguities resolved
Earth Orientation Parameters	Estimate polar motion, polar motion rate, and LOD UT1 integrated from estimated LOD

REFERENCE FRAMES

Inertial	J2000 Geocentric
Terrestrial	IGS08 station coordinates and velocities
Interconnection	Precession: IAU 2006 Precession Theory Nutation: IAU 2006 Nutation Theory A priori EOPS: Bula updated daily, with polar motion and length of day estimated daily

REFERENCES

- Bar-Sever, Y. E. (1996), "A new model for GPS yaw attitude", *Journal of Geodesy*, 70:714-723
- Bar-Sever, Y. E., and D. Kuang (2004), New empirically-derived solar radiation pressure model for GPS satellites, IPN Progress Reports 42-159, JPL. Available online: http://ipnpr.jpl.nasa.gov/progress_report/42-160/title.htm
- Bassiri, S., and G. A. Hajj, (1993), Higher-order ionospheric effects on the global positioning systems observables and means of modeling them, *Manuscripta Geodtica*, 18, 280-289, 1993
- Blewitt, G., (1990), An automatic editing algorithm for GPS data. *Geophysical Research Letters*, Vol. 17, No. 3, p. 199-202
- Boehm, J., A.E. Niell, P. Tregoning, H. Schuh (2006), "Global Mapping Functions (GMF): A new empirical mapping function based on numerical weather model data", *Geophysical Research Letters*, Vol. 33, L07304, DOI:10.1029/2005GL025545.
- Boehm J, Werl B, Schuh H (2006a), "Troposphere mapping functions for GPS and very long baseline interferometry from European Centre for

Medium-Range Weather Forecasts operational analysis data", " Journal
Geophys Res 111:B02406. doi:10.1029/2005JB003629

Boehm, J., R. Heinkelmann and H. Schuh (2007), "Short Note: A global
model of pressure and temperature for geodetic applications", Journal
of Geodesy, DOI: 10.1007/s00190-007-0135-3

IERS Conventions 2003, D.D. McCarthy & G. Petit (editors), IERS Technical
Note 32, Frankfurt am Main: Verlag des Bundesamts fuer Kartographie und
Geodaesie, 2004.

Kedar, S., G. Hajj, B. Wilson, and M. Heflin (2003), The effect of the
second order GPS ionospheric correction on receiver positions, Geophys.
Res. Lett., 30(16), 1829, doi:10.1029/2003GL017639

Moyer, T.D., (2000) Formulation of observed and computed values of deep
space network data types for navigation, Deep Space Communications and
Navigation Series, Jet Propulsion Laboratory, California Institute of
Technology, Pasadena, CA, Chapter 4, pp, 19-28.

Sibois, A., C. Selle, S. Desai, A. Sibthorpe, and J. Weiss, GSPM13: An
updated empirical model for solar radiation pressure forces acting on
GPS satellites, IGS Workshop 2014, Pasadena, CA, 2014.

Sibthorpe, A., J. Weiss, N. Harvey, D. Kuang, and Y. Bar-Sever, Empirical
modeling of solar radiation pressure forces affecting GPS satellites,
AGU Fall Meeting, San Francisco, CA, 2010.

=====

3. Details of processing options for GAMIT solution at CNRS-ISTerre

EUROPEAN PLATE OBSERVING SYSTEM CNRS-OSUG-ISTERRE GAMIT Analysis Center Strategy Summary	
ANALYSIS CENTER	CNRS Observatoire des Sciences de l'Univers de Grenoble ISTerre Université Grenoble Alpes BP 53 38041 Grenoble CEDEX 9 FRANCE Fax: +33 (0)4 76 63 52 52 Data Archive: http://epos.unice.fr:8080/renagbgsac/
CONTACT PERSON(S)	Pr. Anne Socquet E-mail: anne.socquet (at) univ-grenoble-alpes.fr Phone: +33 (0)4 76 63 52 08
SOFTWARE USED	GAMIT v. 10.5, GLOBK v. 10.5, developed at MIT/SIO
PREPARATION DATE	January 29, 2016
MODIFICATION DATES	January 29, 2016 Creation
EFFECTIVE DATE FOR DATA ANALYSIS	

MEASUREMENT MODELS	
Observable	Doubly differenced, ionosphere-free combination of L1 and L2 carrier phases. Pseudorange are used only to obtain receiver clock offsets and in ambiguity resolution.
Data weighting	Sigma on doubly difference LC phase: Site and elevation dependent based on iterated Cleaning at 30-second rate. Sampling rate: 2 minutes Elevation angle cutoff : 0
Data Editing	Cycles slips detected and fixed. Unresolved cycle slips estimated in solution. Postfit editing using 4 times RMS deletion.
RHC phase rotation corr.	Phase polarization effects applied (Wu et al, 1993)
Ground antenna phase center cal.	Elevation- and azimuth-dependent phase center corrections are applied according to the model IGS08.

Troposphere	Atmospheric mapping functions and hydrostatic zenith delays from VMF1 numerical model (Boehm et al., 2006b) 2-hour piecewise linear function estimated, 1 NS and EW gradient per day.
	Met data input: VMF1 global numerical model (Boehm et al, 2006) Mapping Function: VMF1 grid Estimation: Zenith delay and horizontal gradients
Ionosphere	Not modeled (ionosphere eliminated by forming the ionosphere-free linear combination of L1 and L2).
Plate motions	ITRF2008 velocities
Tidal	Solid earth and tidal displacement: constant Love number tides frequency dependent radial tide (K1) Pole tide: Applied to Mean IERS pole position Ocean loading: FES2004 (Lyard et al., 2006)
Non-tidal loading	Atmospheric Pressure: Not applied Ocean Bottom Pressure: Not applied Surface Hydrology: Not applied Other Effects: None applied
Earth Orientation Parameter (EOP)	IERS Bulletin A plus diurnal and semidiurnal variations in x,y, and UT1 models (EOP) R. Ray [1995], IERS
Model	Tech. Note 21 [1996]
Satellite center of mass correction	Block I x,y,z: 0.2100, 0.0000, 0.8540 m Block II/IIA x,y,z: 0.2790, 0.0000, 0.9519 m Block IIRA/IIRB x,y,z: -0.0031, -0.0012, 0.0000 m Block IIRM x,y,z: 0.0000, 0.0000, 0.0000 m Block IIF x,y,z: 0.3940, 0.0000, 1.6000 m
Satellite phase center calibrat	Phase centers offsets from igs08_www.atx applied
Relativity corrections	Relativistic corrections applied
GPS attitude model	Yaw computed using model of Bar-Sever (1996), using nominal rates or estimates supplied by JPL

ORBIT MODELS

Geopotential	<p>EGM2008 12x12 and order 9 (Pavlis et al., 2012)</p> <hr/> <p>GM = 398600.4415 km**3/sec**2</p> <hr/> <p>AE = 6378.1363 km</p>
Third-body	<p>Sun and Moon as point masses</p> <hr/> <p>Ephemeris: CfA PEP NBODY 740</p> <hr/> <p>GMsun = 132712440000 km**3/sec**2</p> <hr/> <p>GMmoon = 4902.7989 km**3/sec**2</p>
Solar radiation pressure	<p>Block II/IIA/IIR: JPL empirical SRP model, GSPM-13, Bar-Sever and Kuang, (2004) Sibois et al, 2014</p> <hr/> <p>Estimate GPS "Y-Bias" and solar radiation pressure(SRP) coefficient as constant with no a-priori constraint. Make small time-varying (stochastic) adjustments to SRP coefficients in spacecraft body-fixed X and Z directions (1% process noise sigma with 1 hr 11 sec updates and 4-hour correlation time.) Estimate tightly constrained time-varying empirical acceleration in spacecraft Y direction (0.01 nm/s^2 process noise sigma with 1 hr 11 sec updates and 4-hour correlation time.)</p> <hr/> <p>Earth shadow model: umbra and penumbra</p> <hr/> <p>Earth albedo: not applied</p> <hr/> <p>Satellite attitude model not applied</p>
Tidal forces	<p>Solid earth tides: frequency independent Love number K2= 0.300</p> <hr/> <p>Ocean tides: None</p>
Relativity	<p>applied (IERS 1996, Chapter 11, Eqn.1)</p>
Numerical Integration	<p>Adams-Moulton fixed-step, 11-pt predictor-corrector with Nordsieck variable-step starting procedure (see Ash, 1972 and references therein)</p> <hr/> <p>Integration step-size: 75 s; tabular interval: 900 s</p> <hr/> <p>Arc length: 24 hours</p>

ESTIMATED PARAMETERS (APRIORI VALUES & SIGMAS)

Adjustment	Weighted least squares plus Kalman filter
Station coordinates	~15 networks of ~40 stations per network 2-3 common sites between networks Weak constrains applied to site coordinates
Satellite clocks bias Receiver clock bias	Initial values from linear fit to Broadcast ephemeris. Values estimated during data cleaning. Time estimated from pseudorange.
Orbital parameters	Initial Position and Velocity (IC) plus 9 radiation-pressure terms: constant and sin/cos once-per-rev terms for a direct, y-axis, and b-axis acceleration. ICs estimated each day. Radiation parameters treated as random walk with process noise based on independent daily estimates. ICs fixed to IGS Final orbit values.
Troposphere	Piece-wise linear function in zenith delay estimated once per 2-hr for each station constrained by a random-walk process to 20mm/sqrt(hr); 1 N-S & 1 E-W gradient parameter per day per station, constrained to 30 mm at 10 deg elevation angle Mapping function: VMF1
Ionosphere	1st order effects removed by linear combination of L1 and L2 phase
Ambiguity	Resolution attempted for all baselines but resolving Melbourne-Webena Widelines for L2-L1 using pseudo-ranges with differential code biases applied, and then L1 from geodetic solution using ionospheric free observable.
Earth Orientation Parameters (EOP)	Pole X/Y and their rates, and UT1 rate estimated once per day.
GPS attitude model	Not estimated

REFERENCE FRAMES

Inertial	J2000 Geocentric
Terrestrial	IGS08 station No constrained coordinates and velocities
Interconnection	Precession: IAU 1976 Precession Theory Nutation: IAU 2000 Nutation Theory

REFERENCES:

Ash, M. E., Determination of Earth satellite orbits, Tech. Note 1972-5, Lincoln Laboratory, MIT, 19 April 1972.

Bar-Sever, Y. E., A new module for GPS yaw attitude, in Proc. IGS Workshop: Special Topics and New Directions, edit. G. Gendt and G. Dick, pp. 128-140, GeoForschungsZentrum, Potsdam, 1996.

Beutler, G., E. Brockmann, W. Gurtner, U. Hugentobler, L. Mervart, and M. Rothacher, Extended Orbit Modeling Techniques at the CODE Processing Center of the International GPS Service for Geodynamics (IGS): Theory and Initial Results, Manuscripta Geodaetica, 19, 367-386, 1994.

Boehm, J., and H. Schuh, Global Pressure and Temperature (GPT): A spherical harmonic expansion of annual pressure and temperature variations for geodetic applications, J. Geod., 2006

Boehm, J., A. Niell, P. Tregoning, and H. Schuh, Global Mapping Function (GMF):
 A new empirical mapping function based on numerical weather model data, Geophys. Res. Lett., 33, L07304, doi:10.1029/2005/GL025546, 2006a.

Boehm J, Werl B, Schuh H, Troposphere mapping functions for GPS and very long baseline interferometry from European Centre for Medium-Range Weather Forecasts operational analysis data, J Geophys Res 111:B02406. doi:10.1029/2005JB003629, 2006b.

Dong, D., and Y. Bock, Global Positioning System network analysis with phase ambiguity resolution applied to crustal deformation studies in California, Journal of Geophysical Research, 94, 3949-3966, 1989.

Dong, D., T. A. Herring, and R. W. King, Estimating Regional Deformation from a Combination of Space and Terrestrial Geodetic Data, J. Geodesy, 72, 200-214, 1998.

Lyard, F., F. Lefèvre, T. Letellier and O. Francis. Modelling the global ocean tides: a modern insight from FES2004, Ocean Dynamics, 56, 394-415, 2006.

Niell, A. E., Global mapping functions for the atmospheric delay, J. Geophys. Res., 101, 3227-3246, 1996.

Pavlis, N.K., S.A. Holmes, S.C. Kenyon, J.K. Factor, The development and evaluation of the Earth Gravitational Model 2008 (EGM2008), J. Geop. Res., 117(B4), 2012.

Ray, R.D., ftp://maia.usno.navy.mil/conventions/chapter8/ray.f (IERS Standards), 1995

Schaffrin, B., and Y. Bock, A unified scheme for processing GPS phase observations, Bulletin Geodesique, 62, 142-160, 1988.

Springer, T. A., G. Beutler, and M. Rothacher, A new solar radiation pressure model for the GPS satellites, IGS Analysis Center Workshop, Darmstadt, 9-11 February 1998.

Wu, J. T., S. C. Wu, G. A. Hajj, W. I. Bertiger, S. M. Lichten, Effects of antenna orientation on GPS carrier phase. Manuscripta Geodaetica 18, 1993, 91-98, 1993.

Annex 1.2 : Guidelines for the strain rates computation

Contribution to EPOS-IP WP10 STRAIN PRODUCT

Task 10.6 GNSS Products - Guidelines for DDSS Strain-rate derivation maps

The report contains guidelines for information included in metadata + formats, and methods for strain rate computations.

Prepared by A. Ganas (NOA), K. Chousianitis (NOA)

with comments by N. D'Agostino (INGV), A. Deprez (CNRS), M. Bos (UBI), Andrzej Araszkiwicz (MUT).

Release of Version 1.0 : 7 December 2016

Release of final version: 20 December 2016

A. Preparation: Table of Tectonic VELOCITY INPUTS (ASCII Type)

1. Provide Eurasia-fixed velocity data.
 - i. Site: GPS station name
 - ii. LON: site longitude (with 3 decimal places – decimal degrees)
 - iii. LAT: site latitude (with 3 decimal places – decimal degrees)
 - iv. Ve: East component of velocity (in mm/yr with 2 decimal places)
 - v. Vn: North component of velocity (in mm/yr with 2 decimal places)
 - vi. Se: Uncertainty of East component (in mm/yr with 2 decimal places)
 - vii. Sn: Uncertainty of North component (in mm/yr with 2 decimal places)
 - viii. RHO: correlation coefficient between East and North components (optional)
 - ix. T(yrs): time span of observations (with 2 decimal degrees)
- b. Notes:
 - Any offset along with annual and semiannual signals in GPS time-series should have been estimated in the velocity determination.
 - Account for time-correlated noise content (note that a more recent approach, MIDAS – Blewitt et al., 2016 - does not explicitly accounts for time correlated noise but can produce realistic errors)
 - Station observation period more than 3 years to ensure reliable velocity estimation.
2. Provide Euler pole position and velocity (Lon, Lat, omega; this information is useful to users so they understand the strain rate product), e.g. Eurasia w.r.t ITRF so site velocities are computed with respect to stable Eurasia
 - i. Lon: longitude of pole (with 3 decimal places)
 - ii. Lat: latitude of pole (with 3 decimal places)
 - iii. Omega: angular velocity (deg/My; with 3 decimal places)

General Notes:

- All velocity results should be transformed into a single reference frame prior to the computation of the strain rates.
- Tectonic velocity explanation: the long-term site displacement due to tectonic motions

B. STRAIN RATE DDSS Product (Method)

The aim of the method is to obtain a continuous strain rate field using only geodetic data.

Method 1

The simplest method is based on the Delauney triangulation approach where the computation of the internal strain rates is performed within a network of triangles that comprise the study area (e.g. *Feigl et al., 1993*). The formation of these triangles is dependent on the station location.

Method 2

Similarly, a continuous strain rate field can be derived through a finite element model by calculating strain rates for each element of the model (see *Jimenez-Munt et al. 2003 JGR*). However, these approaches cannot detect and remove outliers and they are applicable for small areas with few observation points, which comprise a serious disadvantage within the EPOS concept. Furthermore, they produce a continuous displacement field, but the obtained strain rates are discontinuous.

Method 3

The most robust approaches use inversion techniques to map the continuous strain rate field. Among them, the most widely applied are the *Spakman and Nyst (2002 EPSL)* method, which is based on the seismic tomography concept, the *Beavan and Haines (2001 JGR)* method, the *Wdowinski et al. (2001 GRL)* method, the *Shen et al. (1996 JGR; 2015 BSSA)* approach and the STIB Python chain (strain tensor inversion of baselines; *Masson et al., 2014 GJI*). The first method is based on the strain rate assignment to a discretized region using different paths of relative displacement between pairs of observation points. *Beavan and Haines (2001)* evaluated strain using geologic and geophysical information like fault plane solutions and inverted for the Euler poles that locally minimizes the strain rate and velocity field residuals along a regional curvilinear reference system. Both methods are robust, but the “seismological” concept of the former method, as well as the supplementary information needed in the latter approach make these methods somewhat cumbersome within the EPOS concept. Alternatively, interpolation of geodetic data can produce continuous strain rate fields suitable to identify new structures without assuming anything about the deformation mechanisms that dominate a region. For this reason, the approaches of *Wdowinski et al. (2001)* and *Shen et al. (1996; 2015)* are the most appropriate for the strain rate maps of EPOS. *Wdowinski et al. (2001)* interpolated the GPS velocities along small circles, while *Shen et al. (1996; 2015)* devised a distance weighted method (the velocity interpolation for

strain rate; VISR) to get a continuous velocity field from which the strain rate pattern can be achieved. The so-called STIB method (Strain Tensor from Inversion of Baselines; *Masson et al., 2014*), uses the length variations of the baselines between each pair of the geodetic stations to provide a map of the deformation over the whole area covered by the network, reducing the impact of erroneous data and noise. The latter 3 methods are among the wider employed methods for strain rate calculation, but taking into account the huge European region in conjunction with the heterogeneous GPS station distribution, we recommend the *Shen et al. (1996; 2015)* method, but with a slight modification in terms of the alpha-parameter. In this context, the best results would be achieved if this parameter varies according to the GPS stations density. Of course, regardless of the final adopted method for the production of the strain rate field within Europe, it is crucial the removal of all insignificant cells.

Note:

It is recommended that tectonic strain rate maps are validated with geological data (active fault maps), seismological data (e.g. the global stress map project; <http://www.world-stress-map.org/data/>) or other geodetic data as it may be possible that strain rates are locally biased due to anthropogenic or other geophysical (glacio-isostasy or volcanism) signals.

c. STRAIN RATE DDSS Product (output format)

Output is proposed to comprise the following files:

- a. an ASCII file for principal strain axis (x / y / emax / trend / emin / trend).
X: LON (with 3 decimal places – decimal degrees)
Y: LAT (with 3 decimal places – decimal degrees)
Emax: magnitude of largest principal axis (1e-9/yr)
Emax 1-sigma uncertainty: in 1e-9/yr
Trend: azimuth more compressive principal axis (degrees clockwise from north; 3 decimal places, decimal degrees)
Emin: magnitude of smallest principal axis (1e-9/yr)
Emin 1-sigma uncertainty: in 1e-9/yr
Trend: azimuth smallest principal axis (degrees clockwise from north; 3 decimal places, decimal degrees)

Notes:

- a) The arguments to include in the header could be the region boundaries (LONmin / LONmax / LATmin / LATmax), the principal axis boundaries and the interpolation method used along with all important parameters of the method (e.g. cell size, alpha parameter, etc).
- b) four binary formats (.grd Global Mapping Tools file), one for Emax, one for Emin, one with the second invariant of the tensor and one with azimuth of one of the principal axes.
- c) Other components of the velocity gradient tensor that could be presented are: Shear Strain rates (1e-9/yr), rotation rates and dilatation rates (1e-09/yr).
- d) KML/KMZ files for each grid file for use in Google Earth.
- e) Grid and table files should include NaN flags where strain rate cannot be reliably resolved (i.e. insufficient station density)

References

- Beavan, J., and J. Haines (2001), Contemporary horizontal velocity and strain rate fields of the Pacific-Australian plate boundary zone through New Zealand, *J. Geophys. Res.*, 106(B1), 741–770, doi:10.1029/2000JB900302.
- Blewitt G., Kreemer C., Hammond W. C., and Gazeaux J. (2016), MIDAS robust trend estimator for accurate GPS station velocities without step detection, *J. Geophys. Res. Solid Earth*, 121, 2054–2068, doi:10.1002/2015JB012552.
- Feigl, K. L., et al. (1993), Space geodetic measurement of crustal deformation in central and southern California, 1984–1992, *J. Geophys. Res.*, 98, 21677–21712.
- Jiménez-Munt, I., R. Sabadini, and A. Gardi (2003), Active deformation in the Mediterranean from Gibraltar to Anatolia inferred from numerical modeling and geodetic and seismological data, *J. Geophys. Res.*, 108(B1), 2006, doi:10.1029/2001JB001544.
- Masson, F., Lehujeur, M., Ziegler, Y., and Doubre, C. (2014). Strain rate tensor in Iran from a new GPS velocity field. *Geophys. J. Int.*, 197(1), 10–21.
- Shen, Z.-K., D. D. Jackson, and B.-X. Ge (1996), Crustal deformation across and beyond the Los Angeles basin from geodetic measurements, *J. Geophys. Res.*, 101, 27957-27980.
- Shen, Z.-K., M. Wang, Y. Zeng, and F. Wang, (2015), Strain determination using spatially discrete geodetic data, *Bull. Seismol. Soc. Am.*, 105(4), 2117-2127, doi: 10.1785/0120140247.
- Spakman, W., and M.C.J. Nyst (2002), Inversion of relative motion data for fault slip and continuous deformation in crustal blocks, *Earth Planet. Sci. Lett.*, 203, 577- 591.
- Wdowinski, S, Sudman Y, Bock Y. (2001), Geodetic detection of active faults in S. California. *Geophysical Research Letters*, 28, 2321-2324.

Annex 2.1 : Deprez et al. poster presented at wegener 2016 congress

EPOS-GNSS: prototype solution in double difference from CNRS-UGA analysis center

A. Déprez⁽¹⁾ (a.deprez@univ-grenoble-alpes.fr), A. Socquet⁽¹⁾, N. Cotte⁽¹⁾, A. Walpersdorf⁽¹⁾ and M.G. Bato⁽²⁾

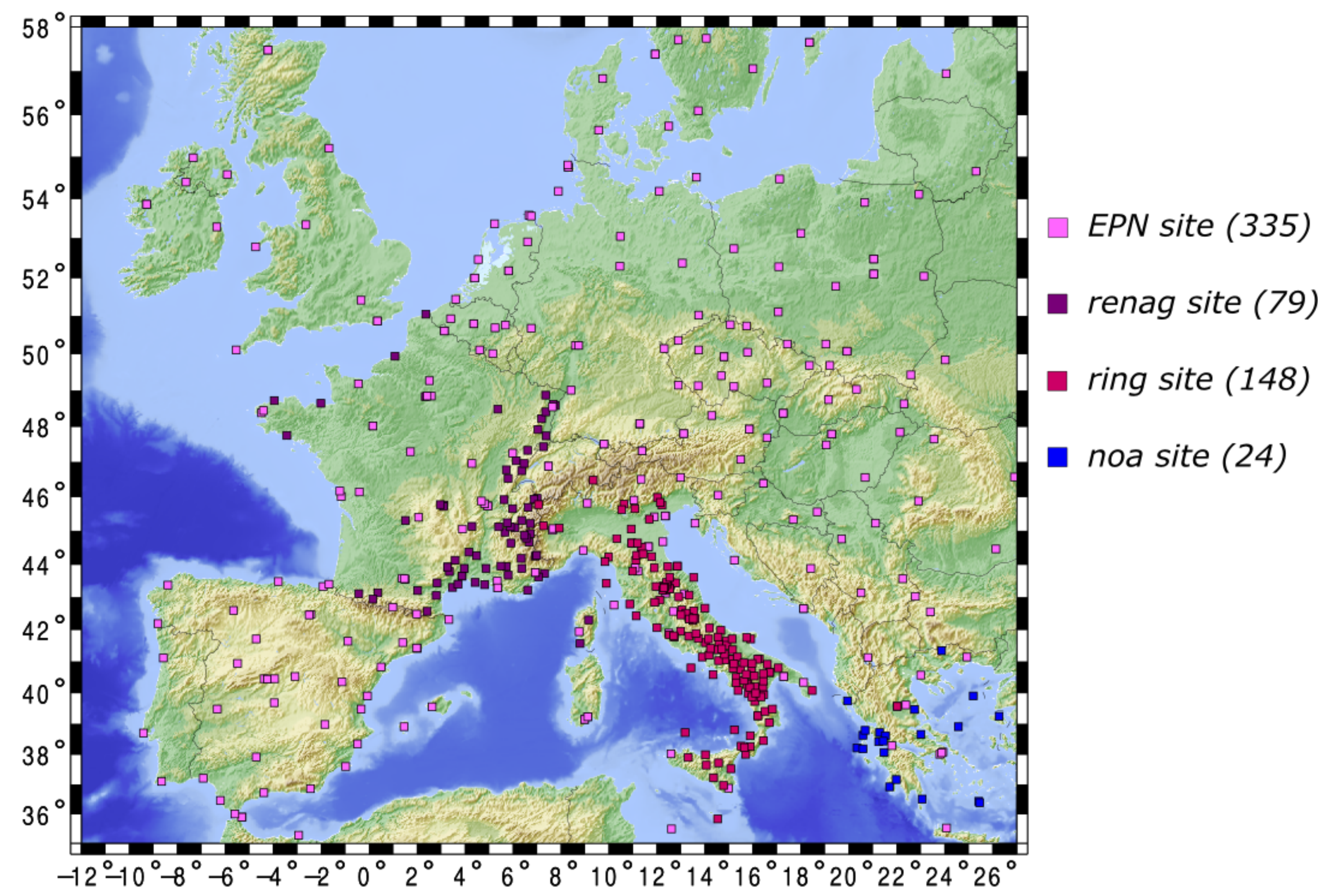
(1) ISTERre, CNRS-Université Grenoble Alpes, FRANCE
 (2) ISTERre, CNRS-Université Savoie Mont-Blanc, FRANCE



1. Data bases

The prototype EPOS solution spans the **2005-2015 period** and includes about **600 European permanent stations**.

Network of the European permanent stations used for the prototype EPOS solution



The RINEX data and metadata were downloaded from archive centres (GSAC nodes) maintained in:

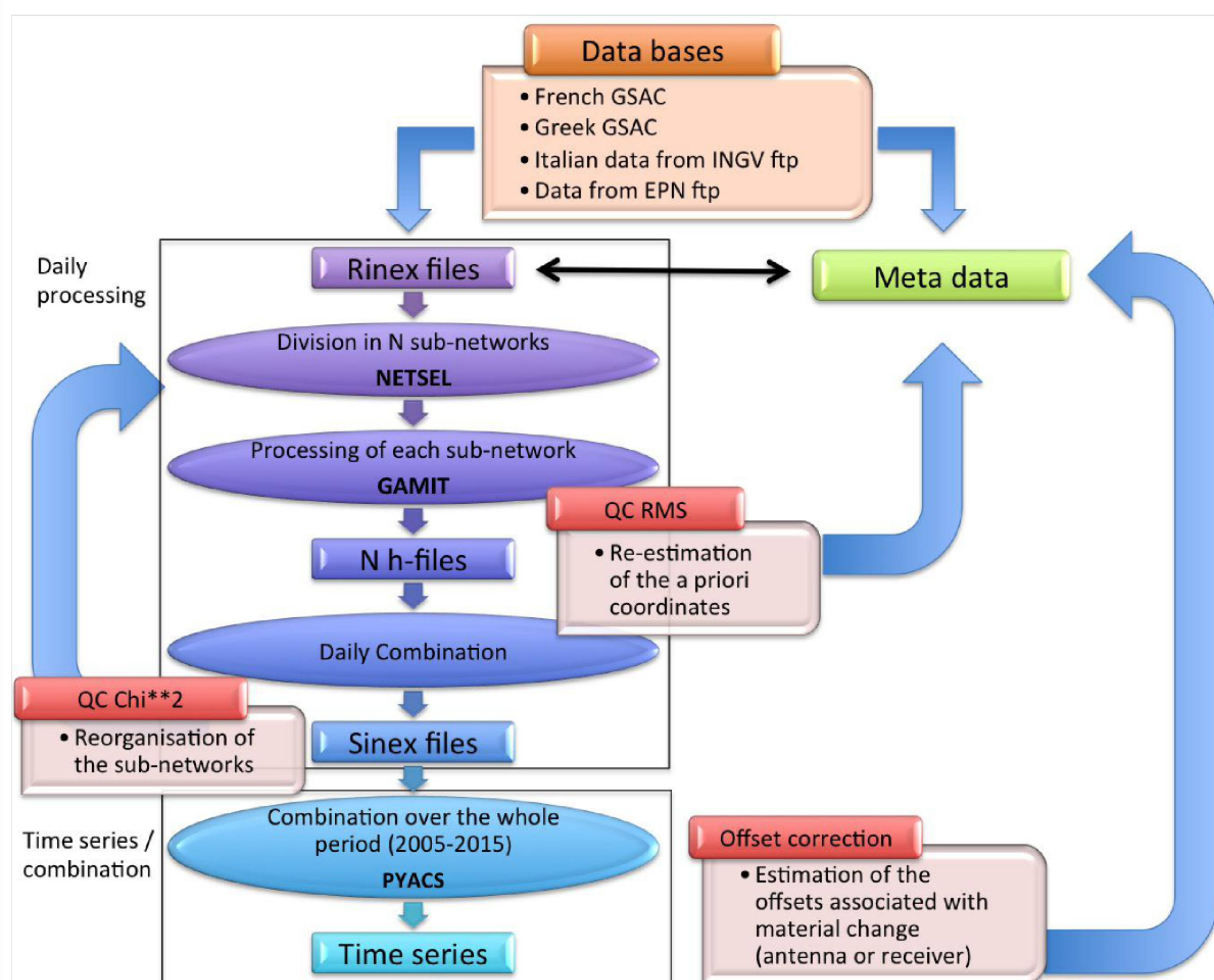
- France (CNRS-OCA): RENAG cGPS network
- Greece: NOA cGPS network
- Italy (INGV): RING cGPS network

Data from the European Permanent Network (EPN), downloaded from the EPN server, were also included.

Our data set is stored on a distributed data-management system called **IRODS**, maintained in the University Grenoble Alpes (UGA), France. It consists in about **1 850 000 rinex files** of about **3kb**, being an amount of data of about **750G**.

Data were processed in double difference with **GAMIT/GLOBK** software.

2. Processing chart

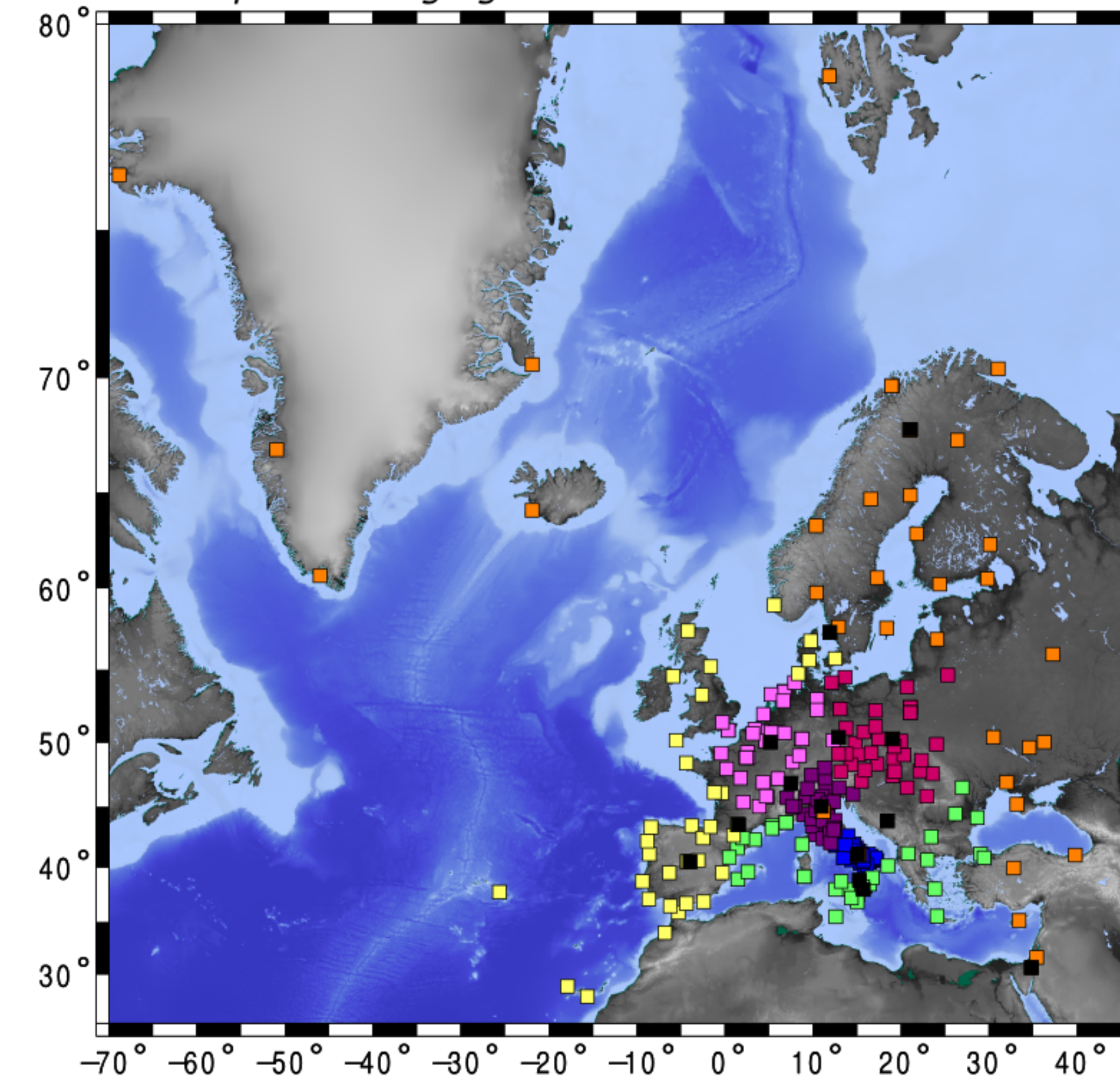


3. Daily processing

a. Division in N sub-networks

For each day independently, the network is first split into **sub-networks** (between 8 and 14 subnetworks) using **NETSEL** tool included in the GAMIT/GLOBK package. The sub-networks consist in about **40 stations**, with **2 overlapping** stations.

Example of division in 8 sub-networks for the day 100 in 2006. The tie sub-network, in black, consists in a set of station couples belonging to the 7 others sub-networks



It allowed us to define parameters of the jobs (GAMIT processing) to launch on a distributed system.

b. All sub-network processing

For each day and for each sub-network the GAMIT processing is **conducted independently** on the **high performance computing platform** CIMENT hosted at UGA. Theoretically, for the EPOS prototype solution, 56 400 jobs have to be launched. These jobs, launched in **best-effort** on 3 different clusters, present an identical format with a walltime of 2h. The mean duration of these jobs is **25 min**. At the end of this step, a GAMIT **h-file** is available for each couple day/sub-network.

c. Daily combination

An other set of about 4000 (in theory) very short jobs has to be launch to **combine the h-files** of the different sub-networks and obtain a daily solution for the whole network. These jobs last a **few minutes**.

The **daily solution** is obtained at that time in the form of a **SINEX file**. The whole SINEX file set consists in an amount of about **400G**.

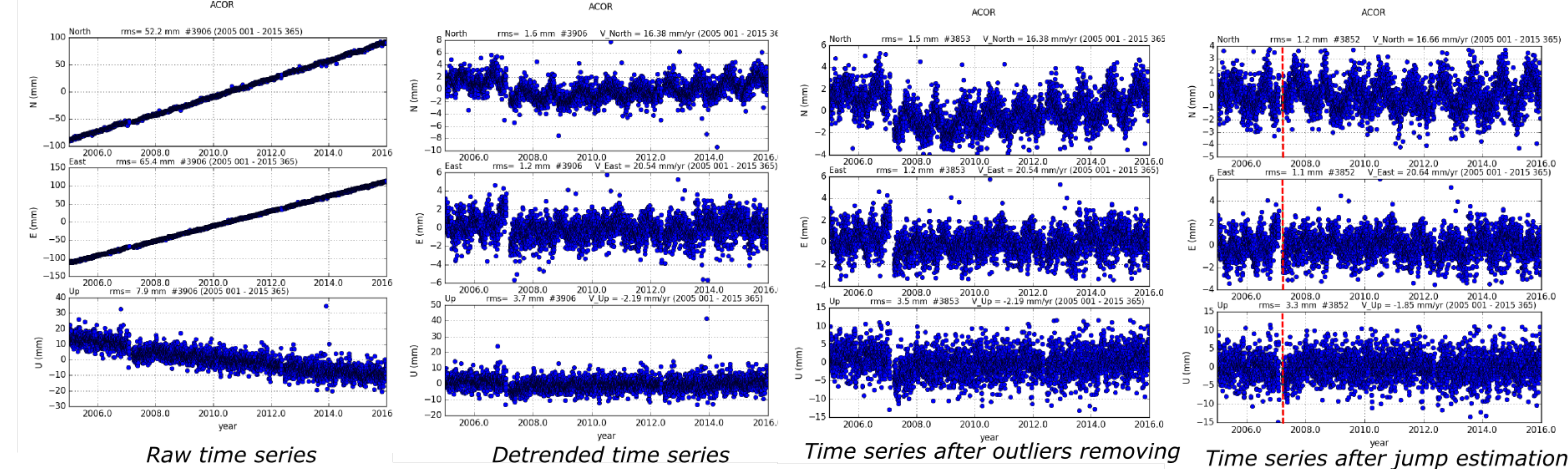
4. Quality check

Along our processing chain, we included **two quality checks**. After the GAMIT processing of the sub-networks, we checked the **RMS value**. The unexpected high RMS values were due to no accurate enough **a priori coordinates** for some sites. We re-estimated them and re-launched the processing of the sub-network. After the daily combination a few SINEX files were associated with high **CHI**2 value**. A **sub-networks reorganisation** allowed us to optimize the consistency within the daily sub-network set.

5. Products

a. Time series combination

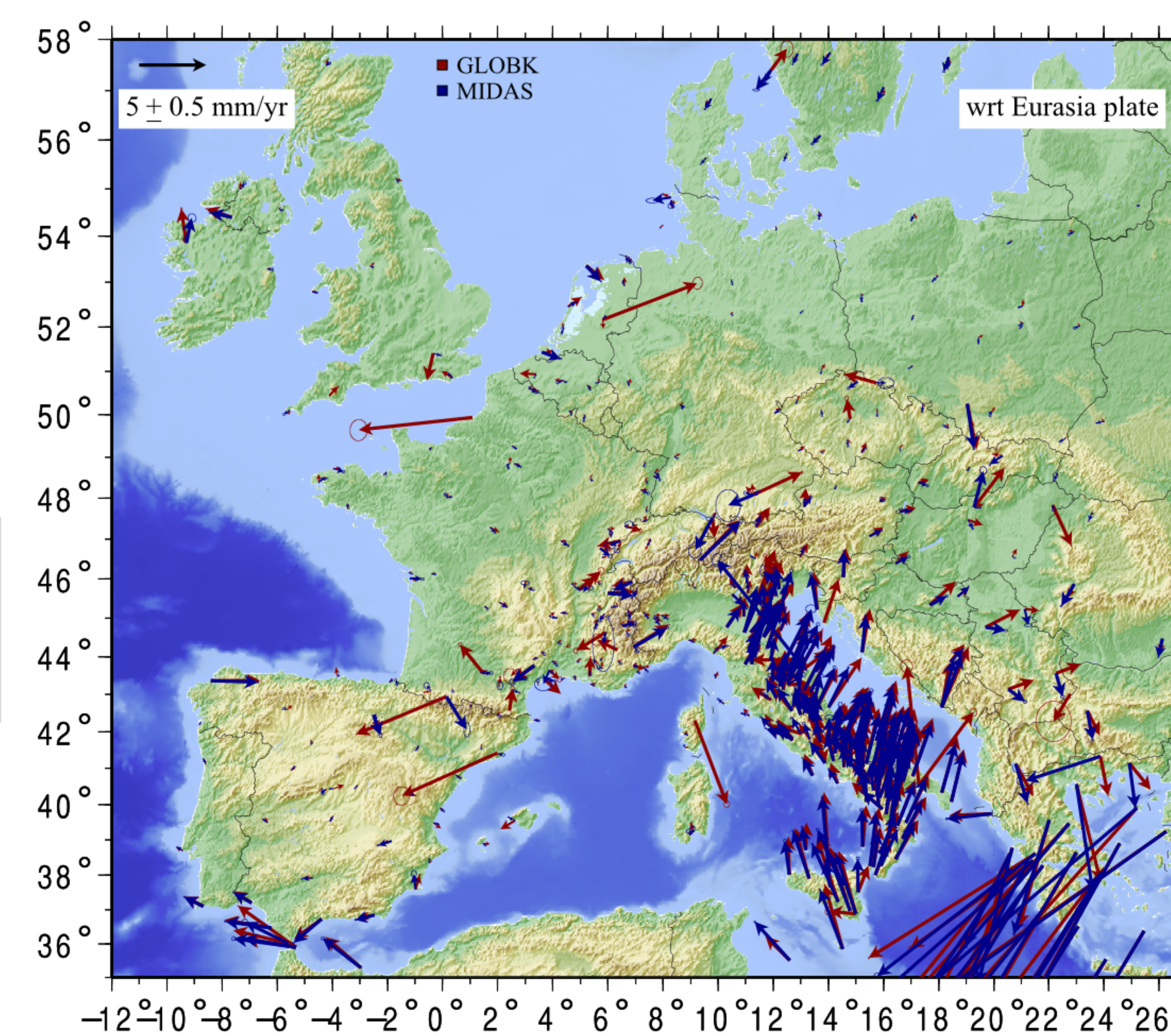
Example of time series processing for the station A Coruna (ACOR) in Spain



The **PYACS** software was used to **compute the time series**. PYACS consists in a set of tools, written in python language and dedicated to the analysis of geodetic data. It was developed in Observatoire de la Côte d'Azur in Nice (France) by J.M. Nocquet. This package allowed us to **visualize the position time series** for each station, to **detrend it**, to **remove potential outliers** and to **estimate and correct** for the **jumps** associated with **material changes** (antenna or receiver).

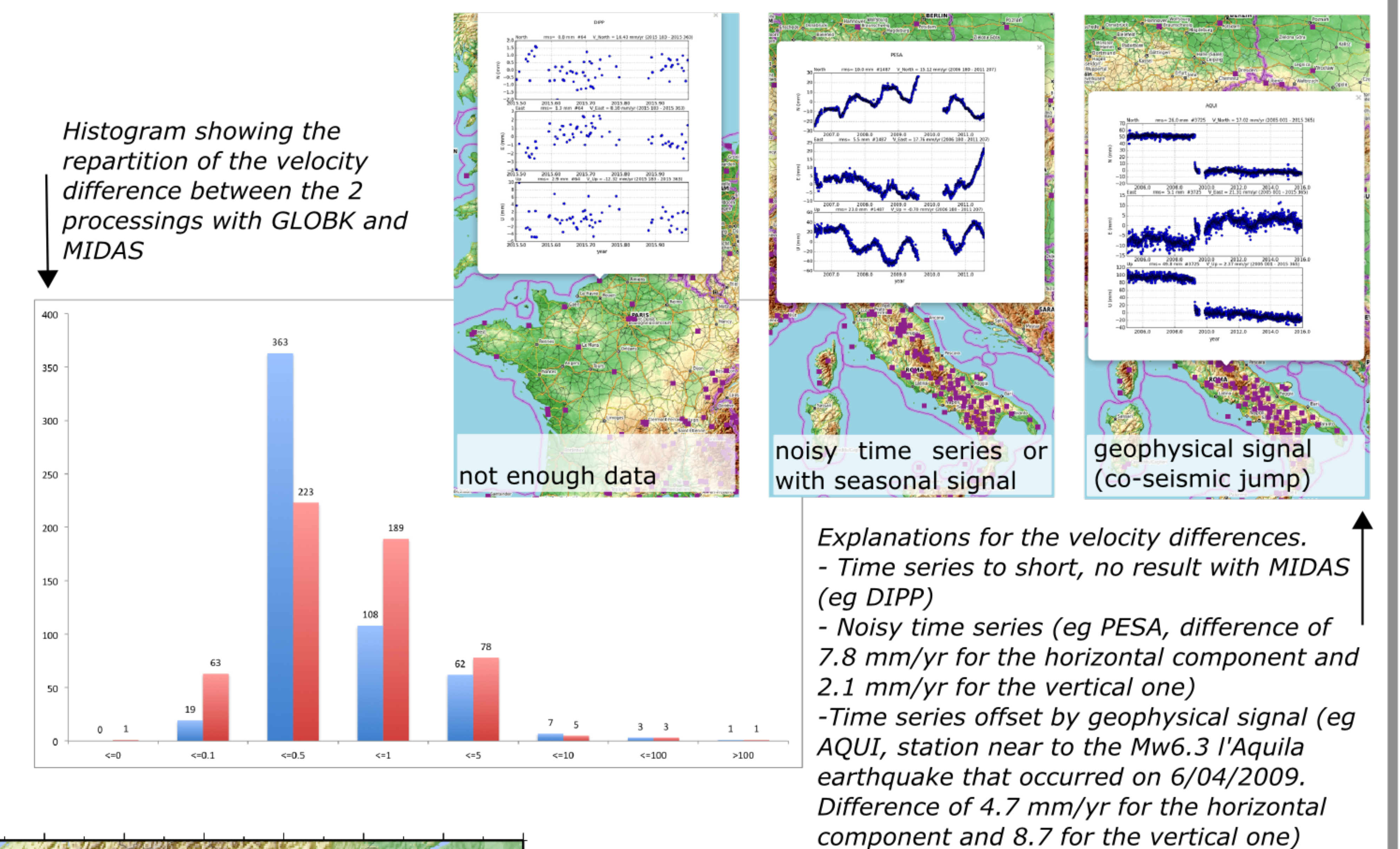
b. Velocity field computation

Comparison of 2005-2015 velocity field obtained with either GLOBK or MIDAS softwares



We computed the 2005-2015 **velocity field** by using GLOBK software. Such a combination on 11 years with about 600 stations is very **time consuming** (more than 100h). This no splittable step is exposed to computer instability that is why we are **looking for a faster method**.

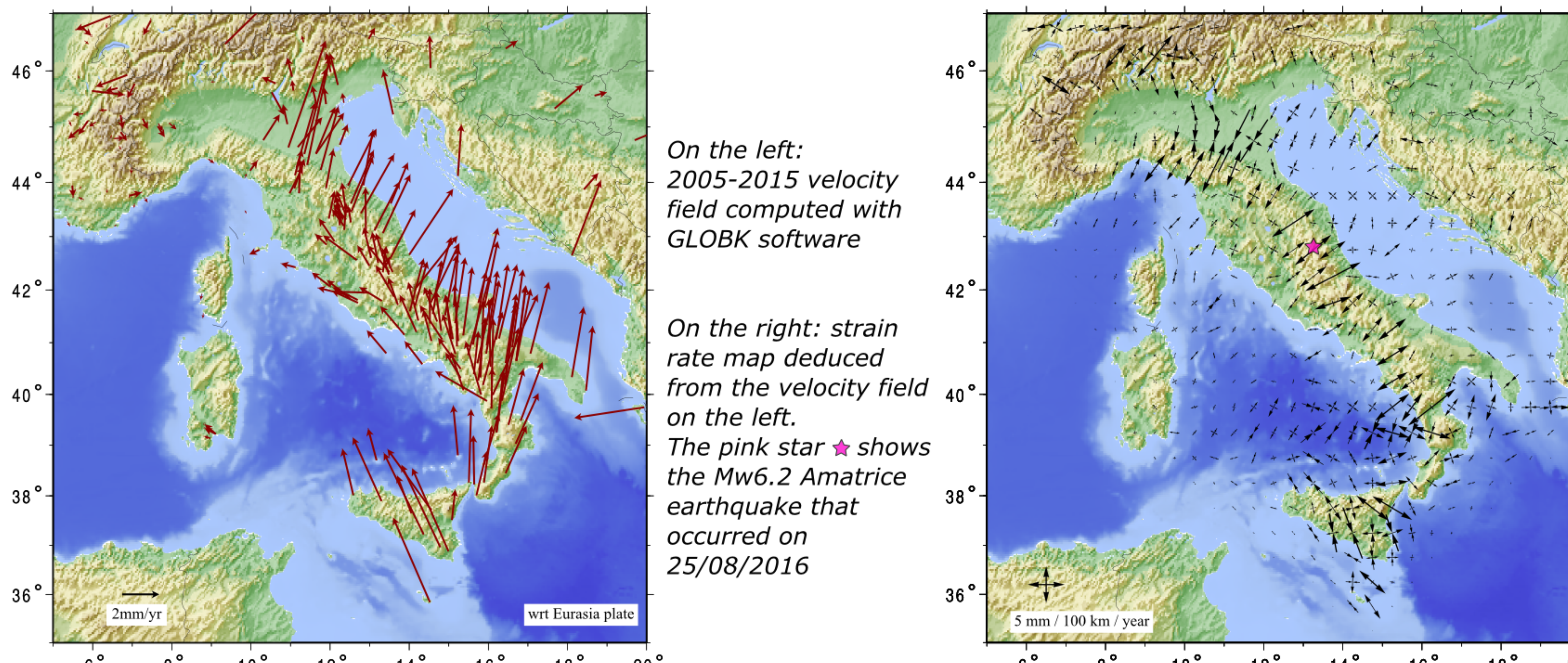
MIDAS software, developed by G. Blewitt in Nevada Geodetic Laboratory (USA), seems to be a good alternative, that we are actually testing. We compared the 2 velocity fields and highlighted significant differences for some site.



Explanations for the velocity differences.

- Time series too short, no result with MIDAS (eg DIPP)
- Noisy time series (eg PESA, difference of 7.8 mm/yr for the horizontal component and 2.1 mm/yr for the vertical one)
- Time series offset by geophysical signal (eg AQU1, station near to the Mw6.3 l'Aquila earthquake that occurred on 6/04/2009. Difference of 4.7 mm/yr for the horizontal component and 8.7 for the vertical one)

c. Strain rate computation



After a selection of reliable sites in Italy and surrounding areas, we made some tests for the **strain rate computation**, using a set of tools developed by Y. Ziegler in Ecole et Observatoire des Sciences de la Terre, Strasbourg (France).

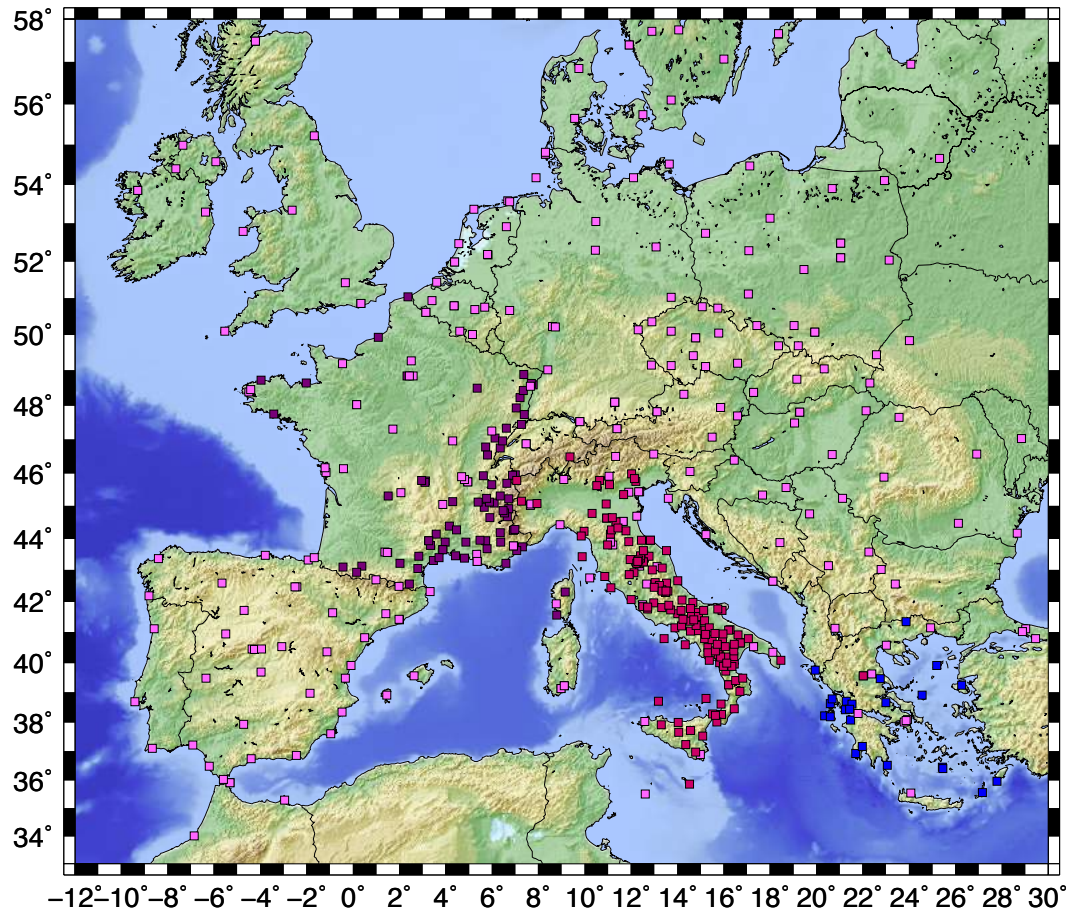
References:
 Blewitt, G., C. Kreemer, W.C. Hammond, J. Gazeaux, 2016, MIDAS robust trend estimator for accurate GPS station velocities without step detection, accepted for publication in the Journal of Geophysical Research, doi: 10.1002/2015JB012552
 Masson, F., Lehujeur, M., Ziegler, Y., and Doubre, C. (2014). Strain rate tensor in Iran from a new GPS velocity field. Geophys. J. Int., 197(1) :10-21.

**Annex 2.2 : Presentation of CNRS-UGA done for the EPOS meeting in Madrid,
Oct. 2016**

GNSS processing with GAMIT-GLOBK in CNRS-UGA, France

A. Déprez, A. Socquet, N. Cotte, A. Walpersdorf, M. Volat, Q. Sun, MG. Bato

cGPS network used or the prototype EPOS solution



- Data set stored on a distributed management system : IRODS (in UGA, France) :
 - **1 850 000 RInEx files**
 - **750 G**

- Download of the RInEx data (2000-2015) and metadata from GSAC nodes in:

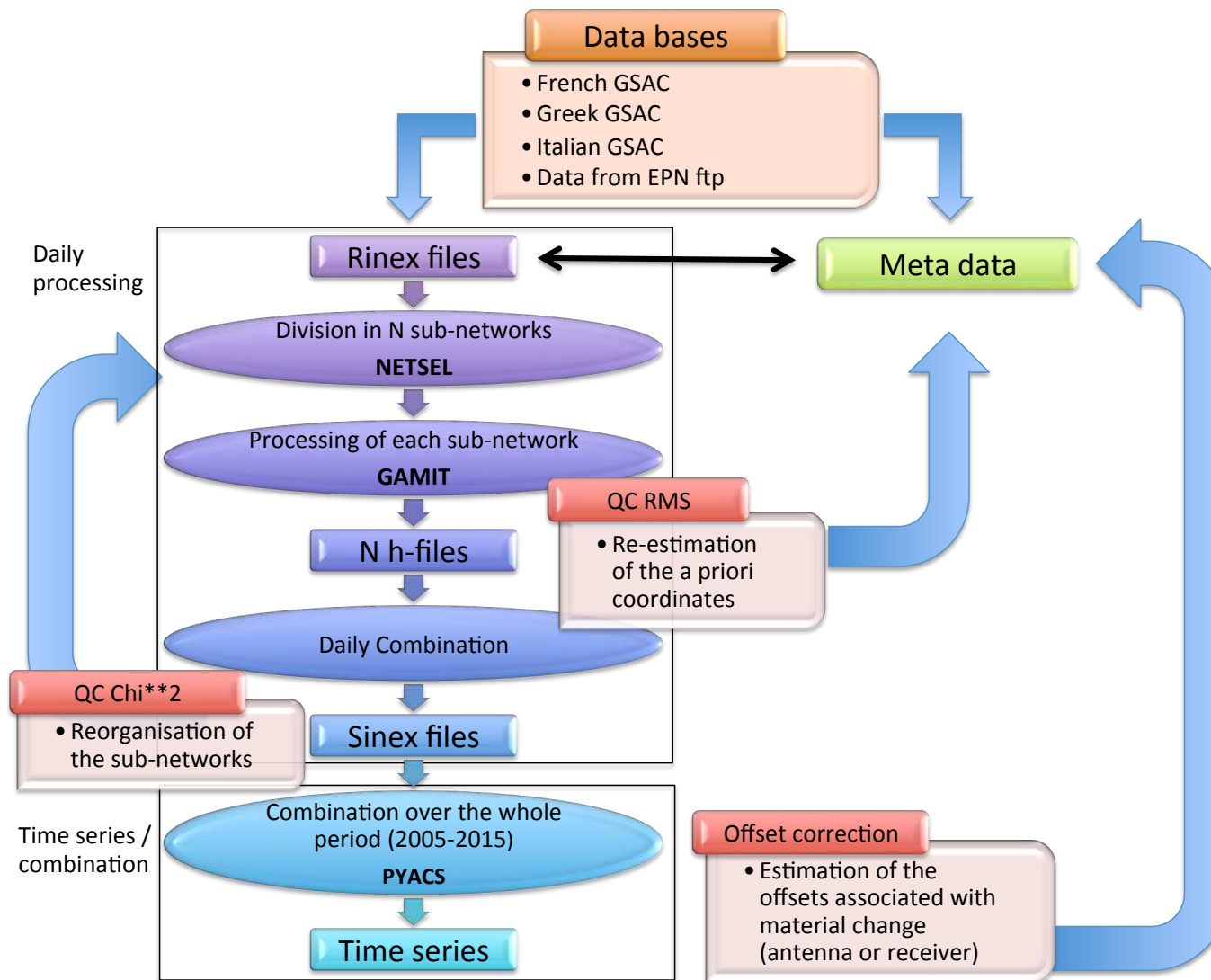
- 79** • **France (CNRS-OCA) :** RENAG cGPS network (<http://epos.unice.fr>)
- 24** • **Greece :** NOA cGPS network (<http://www.gein.noa.gr>)
- 148** • **Italy (INGV) :** RING cGPS network (<ftp://gpsfree.gm.ingv.it>)

- Test of these nodes
- Data from **EPN** included **335**

iRODS

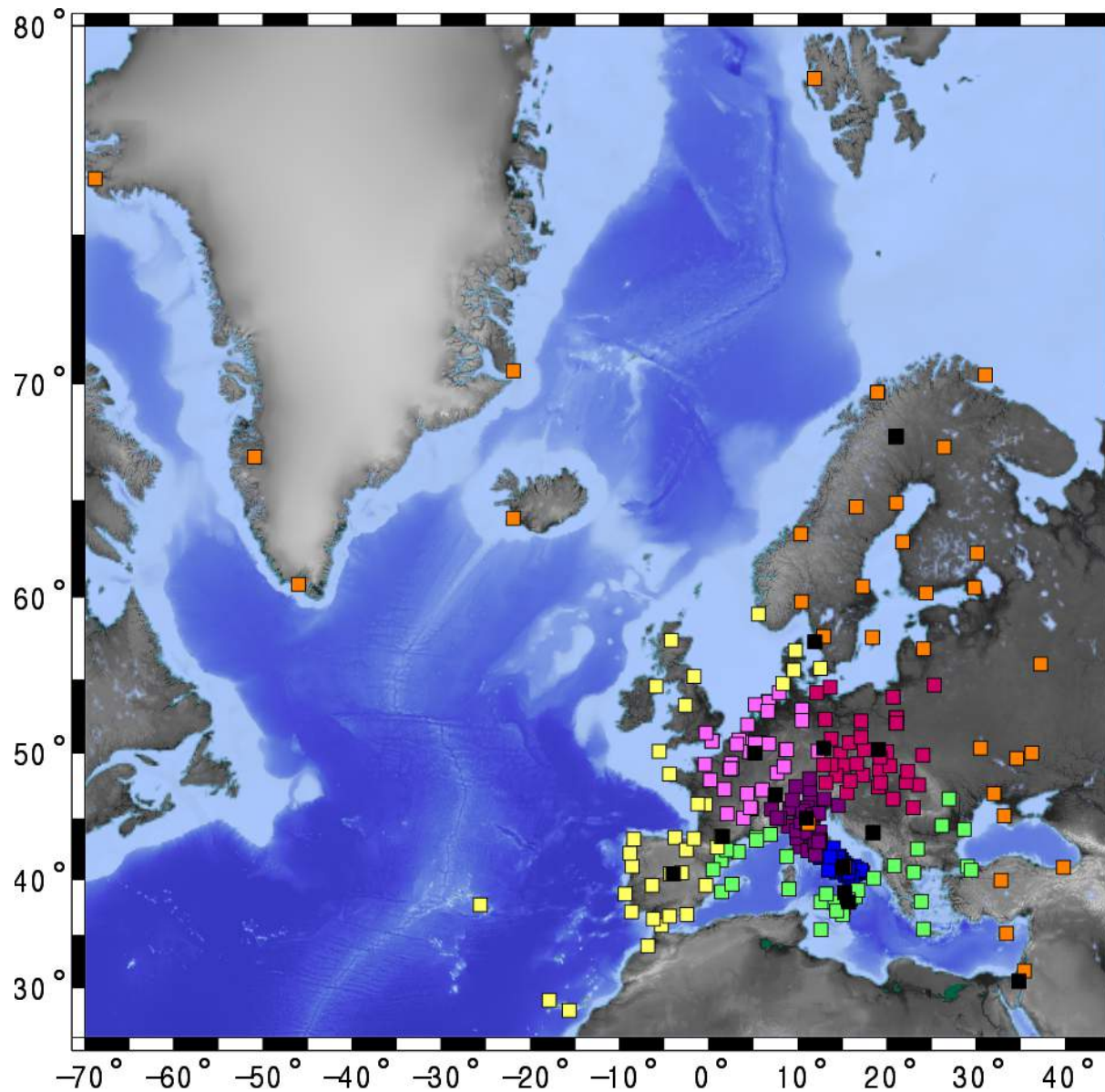


Processing chart



- Data set processed in double difference with GAMIT/GLOBK software

Daily processing: Division in N sub-networks



- For each day independantly, the network is split into **sub-networks (8-14)**
- Subnetworks consist in **~40 stations + 2 overlapping stations**
- ⇒ define parameters of the jobs to launch on a distributed system

Example of division in 8 sub-networks for the day 100 in 2006. The tying sub-network (in black) consists in a set of stations couples belonging to the 7 others sub-networks.

Daily processing:

All sub-network processing

- Processing **conducted independently** for each day and for each subnetwork
- Use of a **high computing platform** hosted at UGA
- ~ **56 400** jobs to launch
- **Best-effort** mode
- Identical format
 - ✓ Walltime = 2h
 - ✓ Mean job duration = 25min

⇒ **GAMIT h-file** for each couple day/sub-network

Daily combination

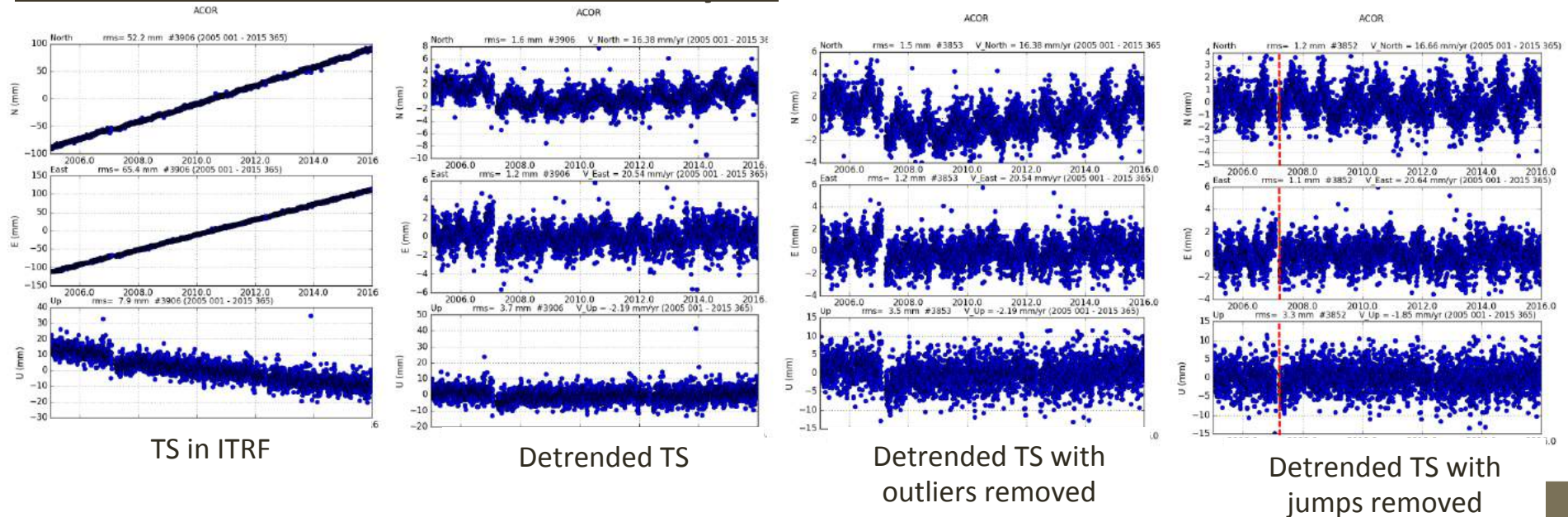
- ~ **4000** short jobs
- Job duration = a few minutes

⇒ Daily solution in the form of a SINEX file

The whole SINEX file set = **400G**



Products : Time series combination, Pyacs



PYACS

- developed in OCA, Nice by J.M. Nocquet
- A set of **tools** to analyse and model geodetic data
- Execution **time reduced** by neglecting the full variance associated with the solution
- **Visualizing** time series
- **Chaining** method
- Easy **automatic** analysis

The PYACS software was used to compute the time series
We successively :

- **Visualize** the time series
- **Detrend** it
- Remove the **outliers**
- Estimate and correct for the **jumps** associated with material changes using the information contained in the meta-data

Products : Velocity field computation, GLOBK vs MIDAS

We test 2 different ways to compute the velocity field for ~600 stations, over 11 year :



GLOBK:

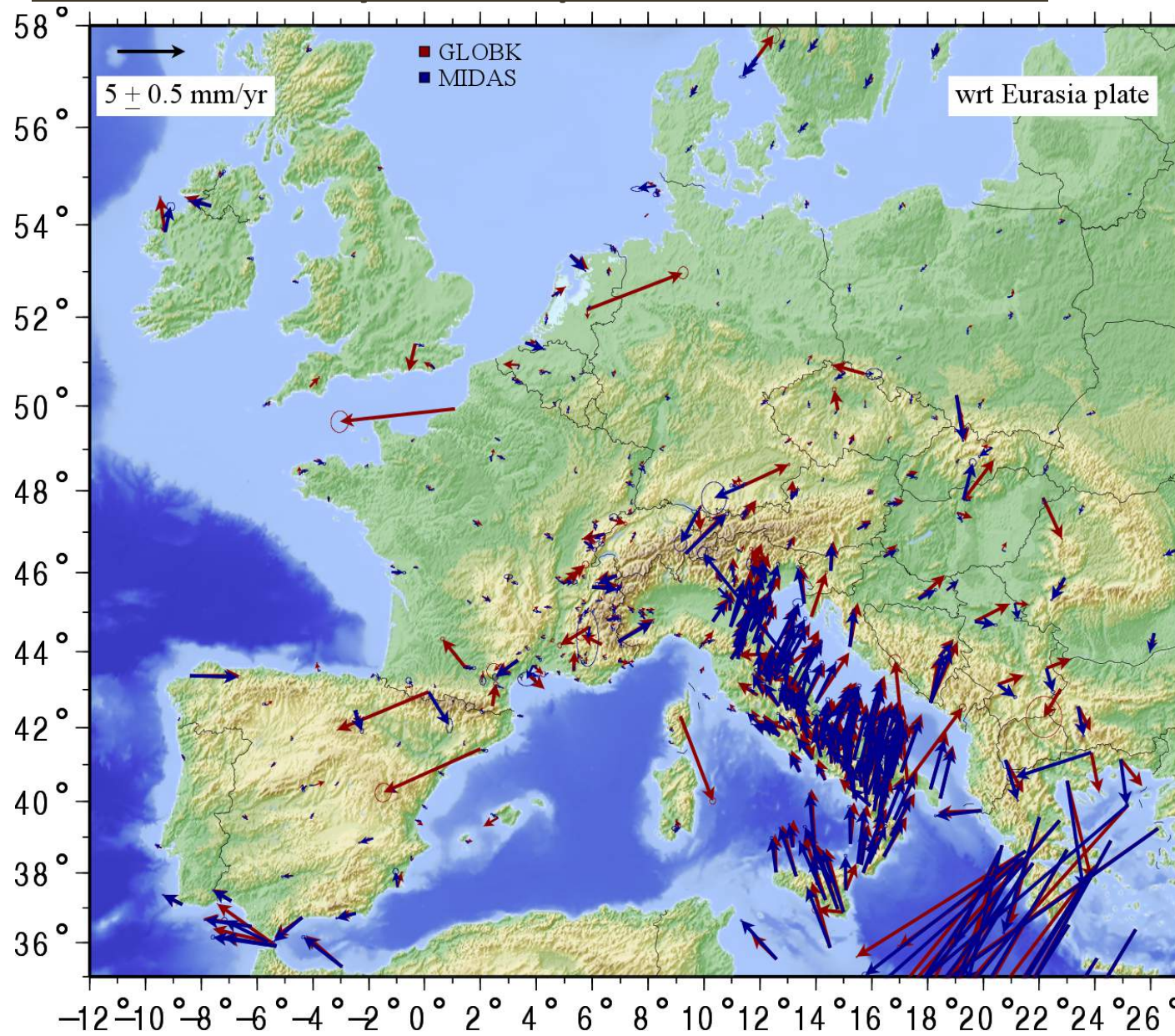
- Developed in the MIT by Herring, King, Floyd and McClusky
- Kalman filter
- Combine various geodetic solutions (GPS, VLBI, SLR) from the processing of primary data (space-geodetic or terrestrial observations)
- Input data : SINEX files
- Time consuming (more than 100h for our data set)
- No splittable

MIDAS:

- Developed in NGL by Blewitt, Kreemer, William, Hammond and Gazeaux
- Statistical method based on a set of position pairs separated by 1 year
- Automatic estimator of position time-series trend
- Input data : time series
- Robust to outliers, steps, seasonality
- Fast (less than 1min for our data set)

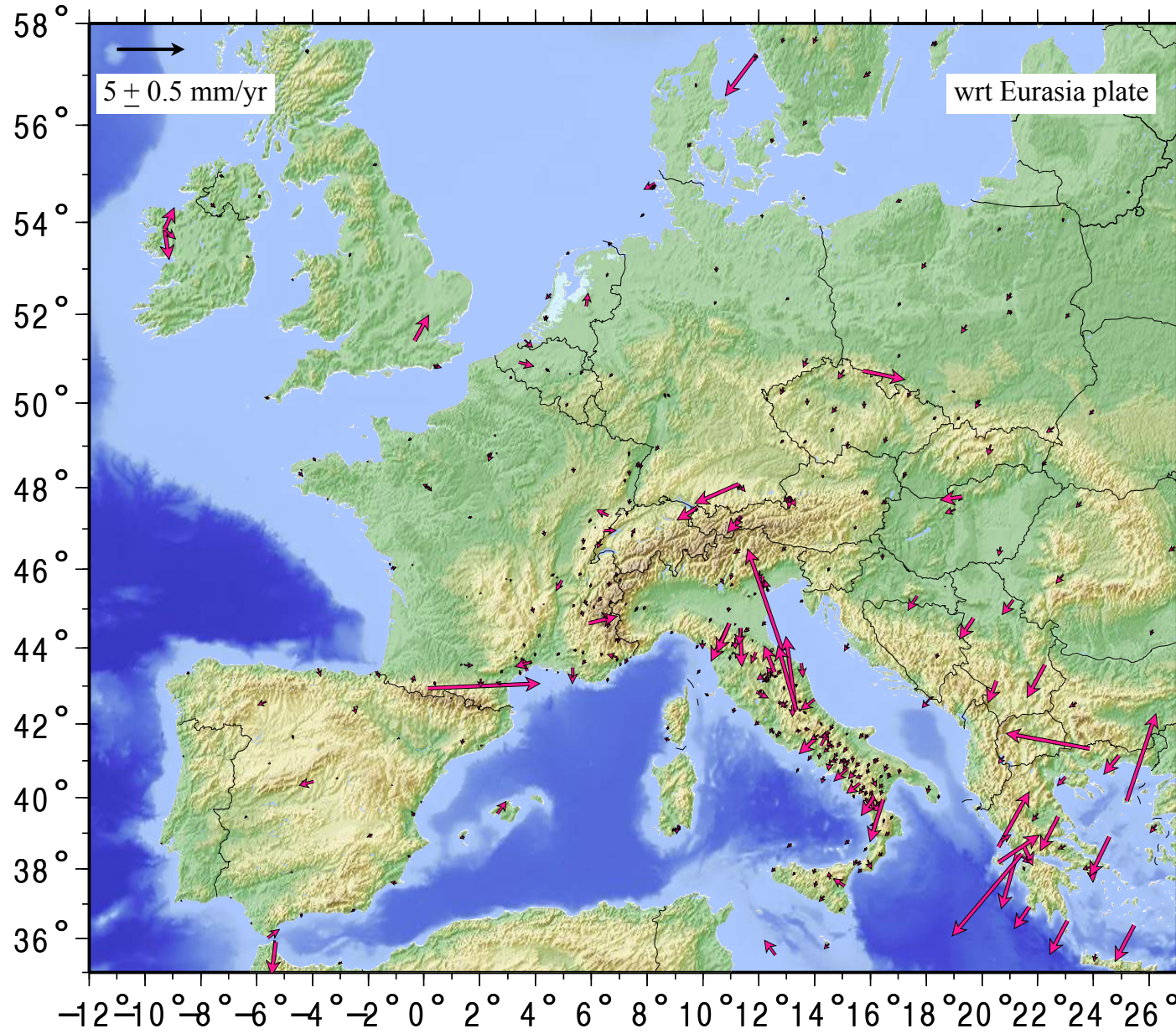


Products : Velocity field computation, GLOBK vs MIDAS : the 2 velocity fields



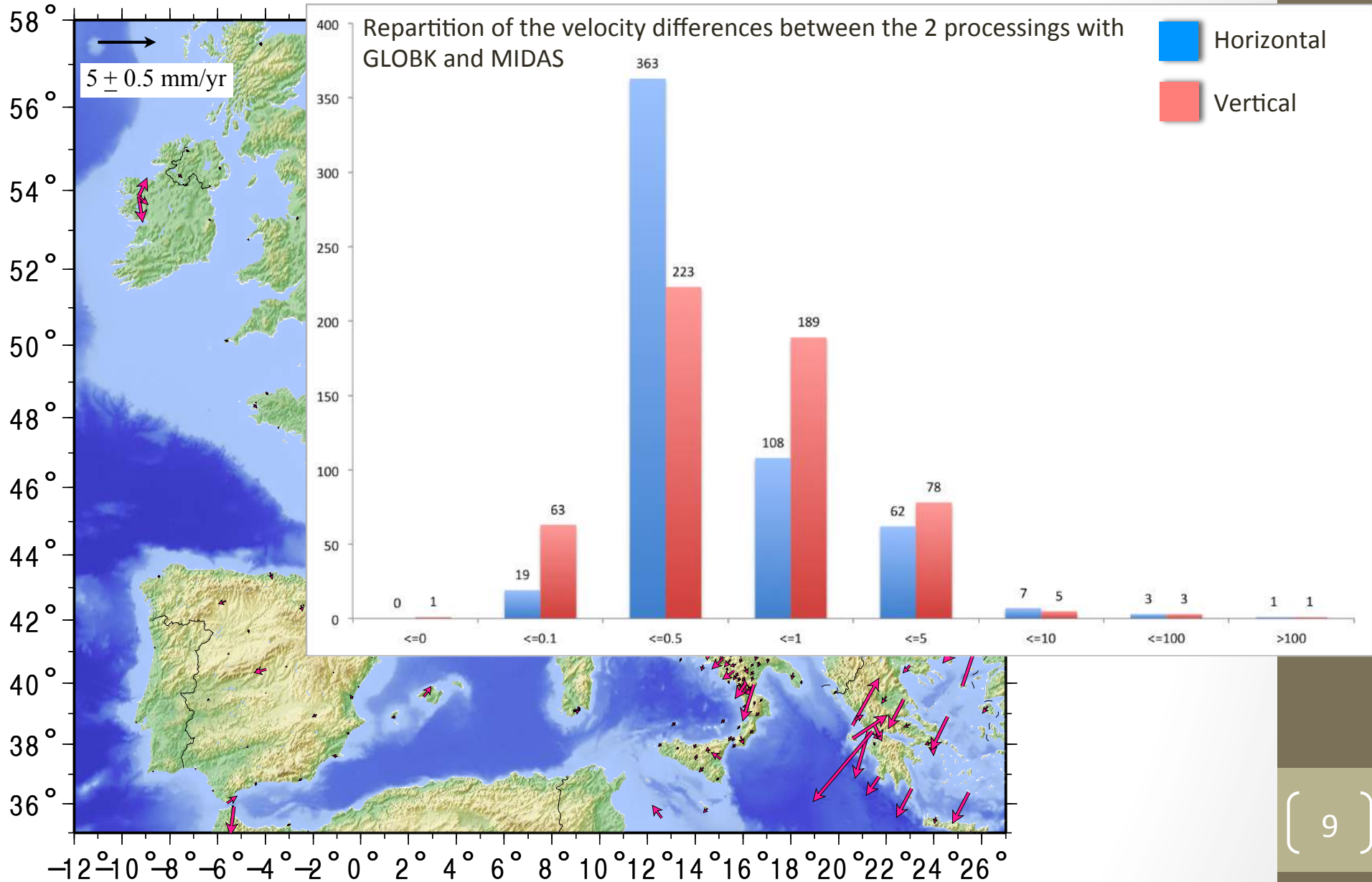
The velocity fields obtained with either **GLOBK** or **MIDAS** software are very similar in general for both methods ...

Products : Velocity field computation, GLOBK vs MIDAS: differences



... But **significant differences** are observed for some sites.

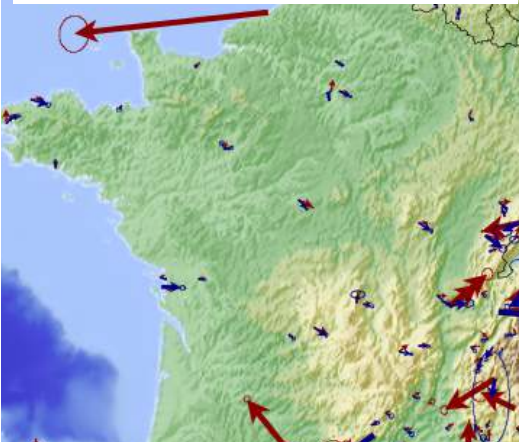
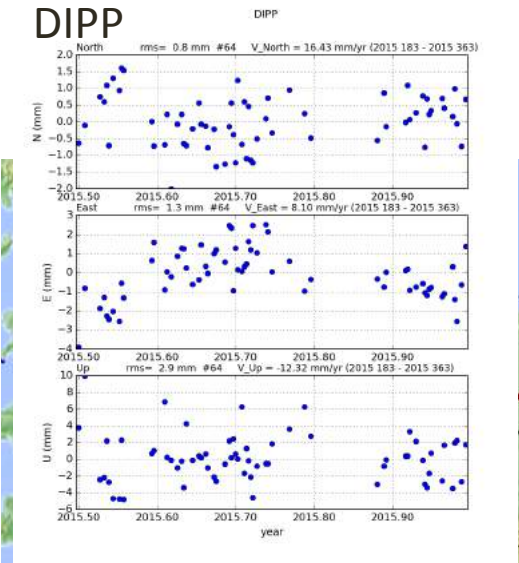
Products : Velocity field computation, GLOBK vs MIDAS



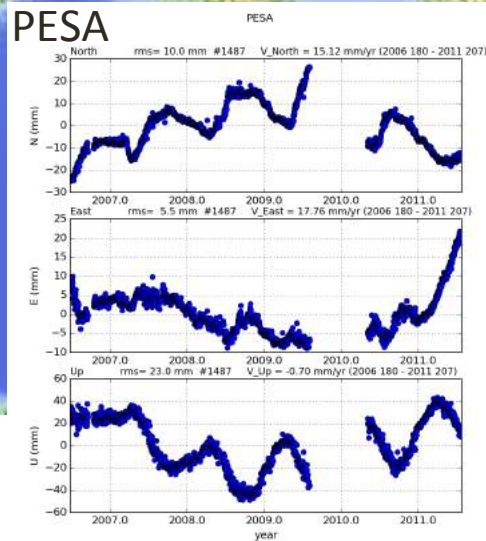
The comparison of the velocity field obtained with either **GLOBK** or **MIDAS** software showed **significant differences** for some sites.

Products : Velocity field computation, GLOBK vs MIDAS

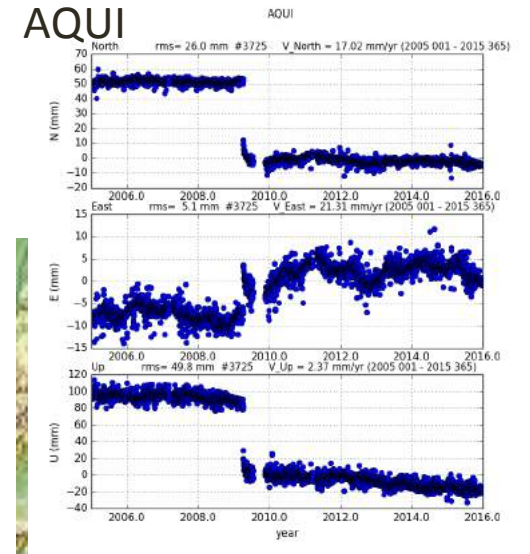
Explanation for the velocity differences:



Time series too short, no result with MIDAS or statistical velocity value not reliable



Noisy time series



Time series offset by geophysical signal (AQUI, station near to the Mw6.3 L'Aquila earthquake that occurred on 6/04/2009)

Products : Strain rate computation : example of Italy

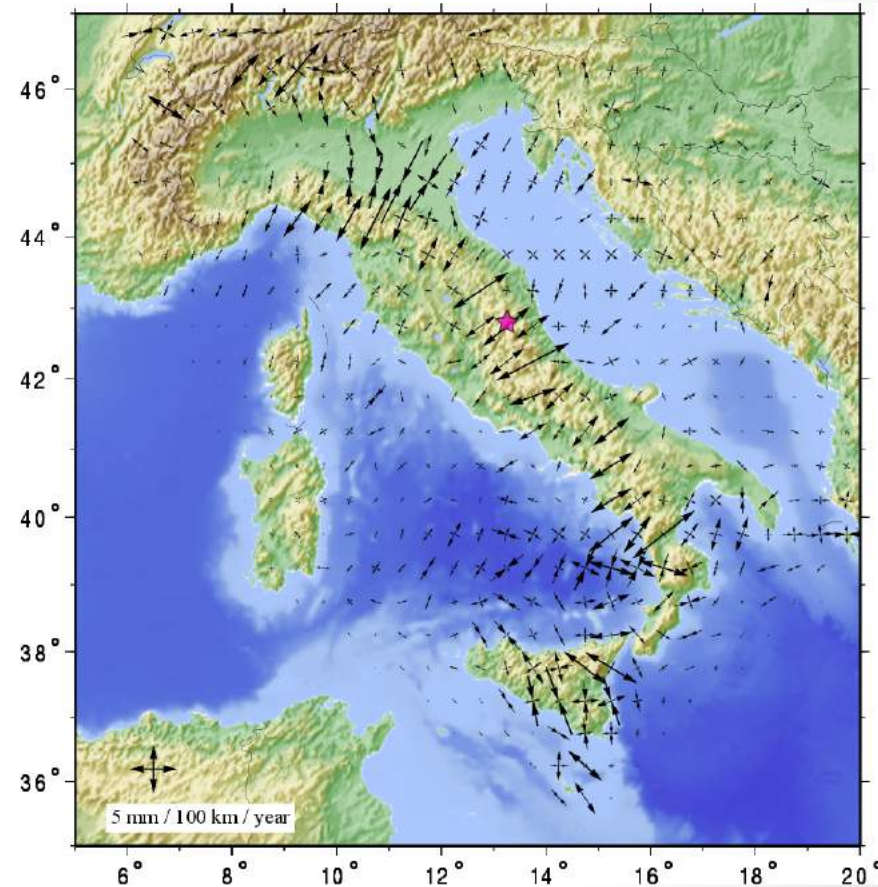
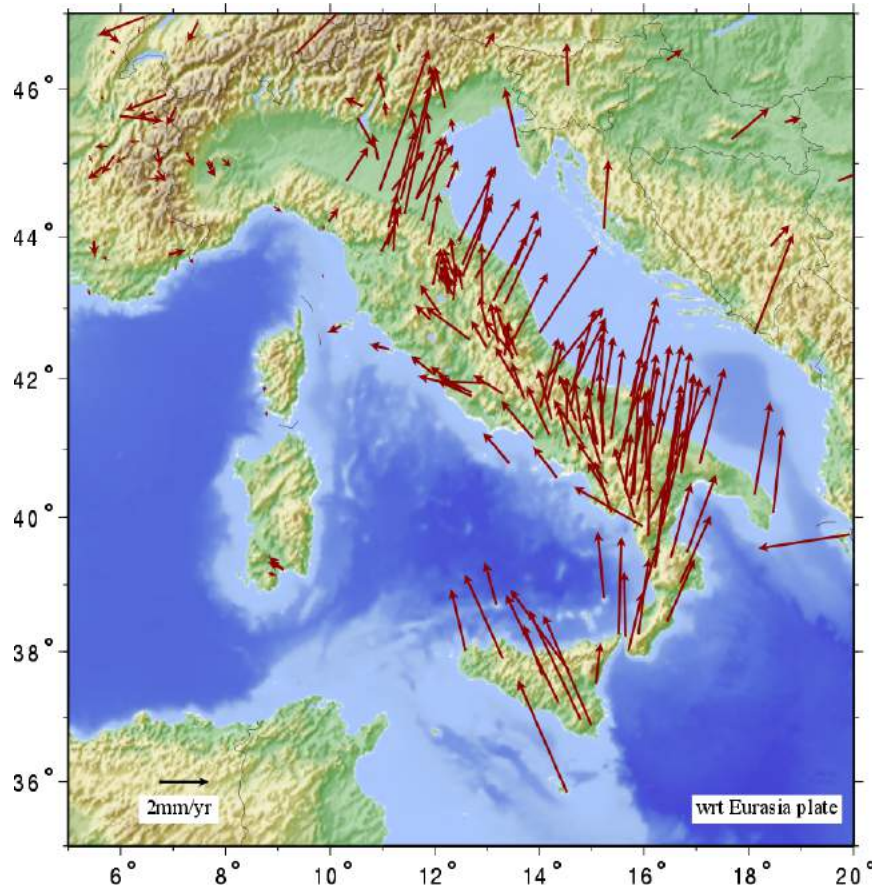
STIB

(strain tensor from inversion of baselines)

- Input data : temporal variation of baseline component
 - Hypothesis : steady state deformation

- deformation observed between each pair of stations distributed along the baseline
- Using a full set of baselines

⇒ deformation map on the surface covered by the whole set of baselines



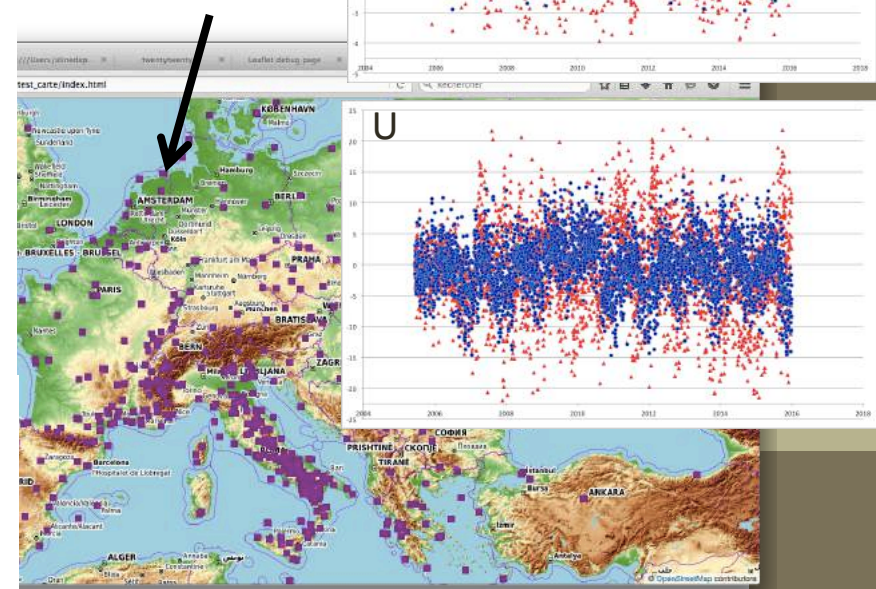
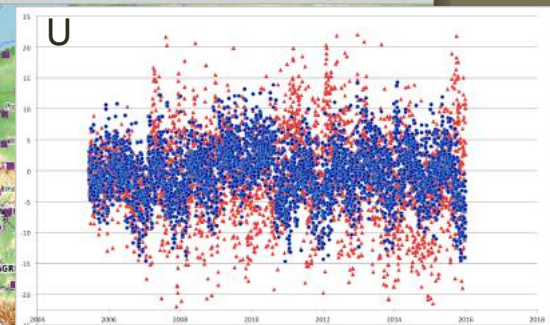
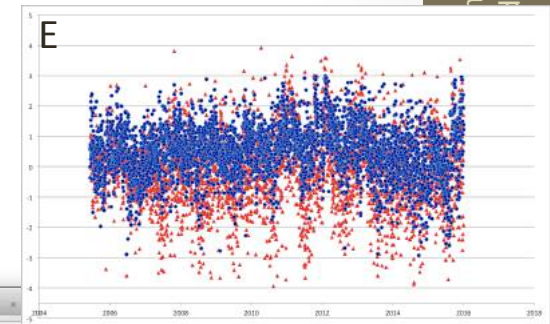
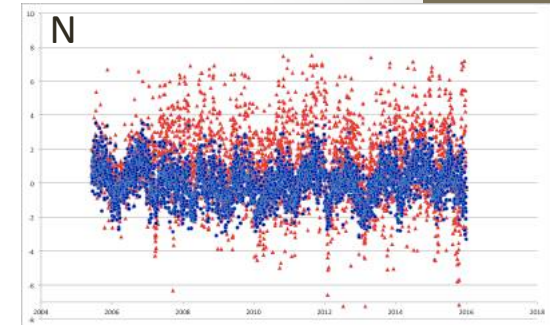
Products : Time series comparison, DD vs PPP: example, BORJ (NL)

EPOS-IP prototype solutions for the processing centers
UGA-CNRS and INGV

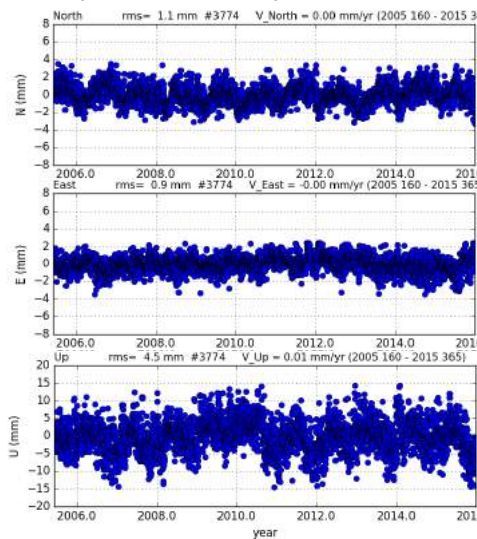
Time series generated with PYACS using the protocole described
before for both DD and PPP solutions (reduced SINEX files) :

- **Detrend it**
- Remove the **outliers**
- Estimate and correct for the **jumps** associated with material changes using the information contained in the meta-data

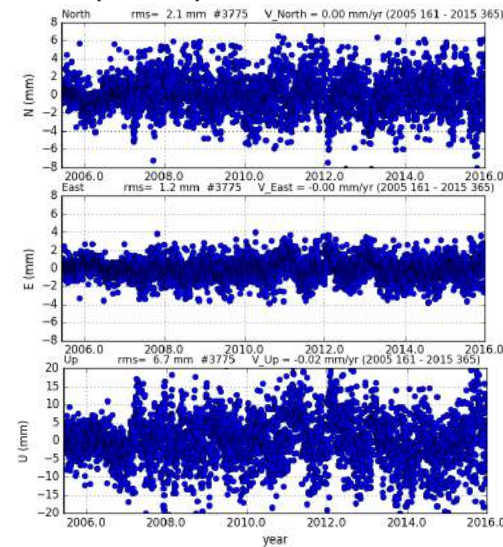
- DD (UGA-CNRS)
- ▲ INGV (PPP)



DD (UGA-CNRS)

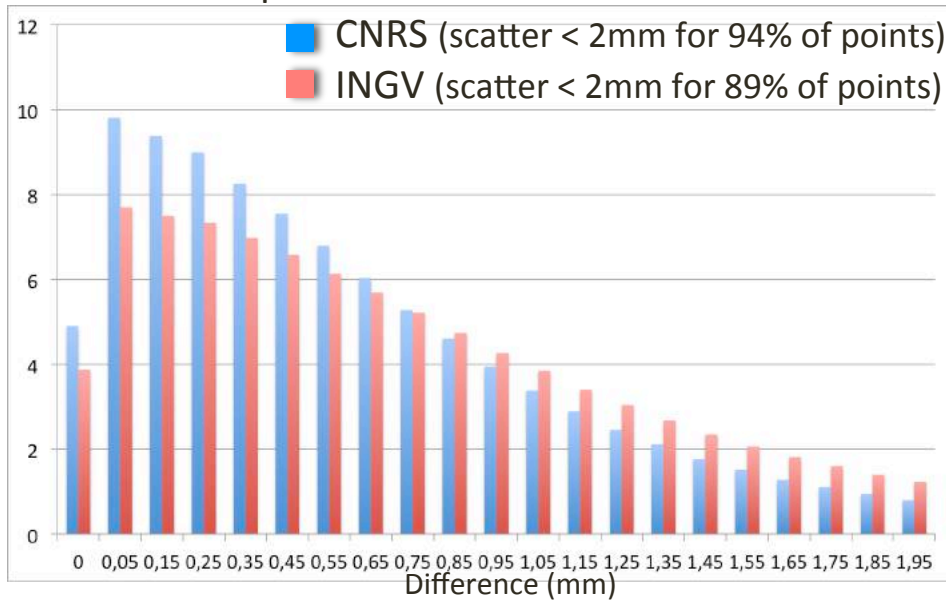


PPP (INGV)

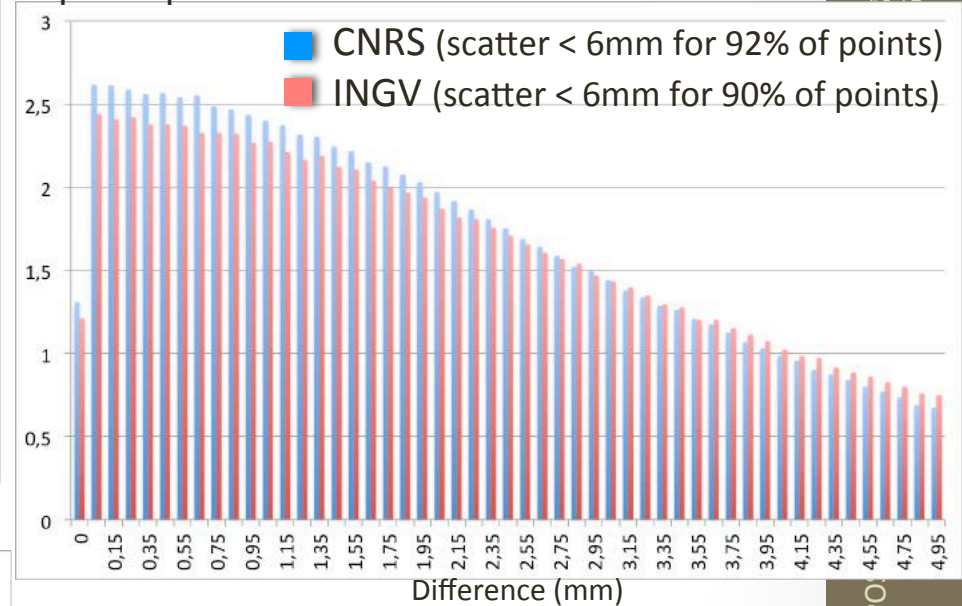


Products : Time series comparison, DD vs PPP: difference to a sliding mean value (in%)

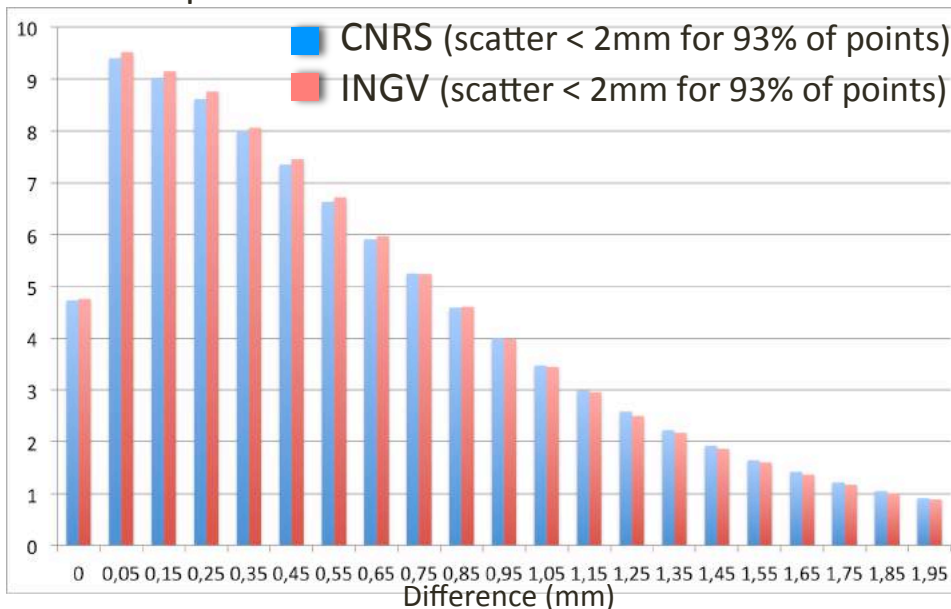
North component



Up component

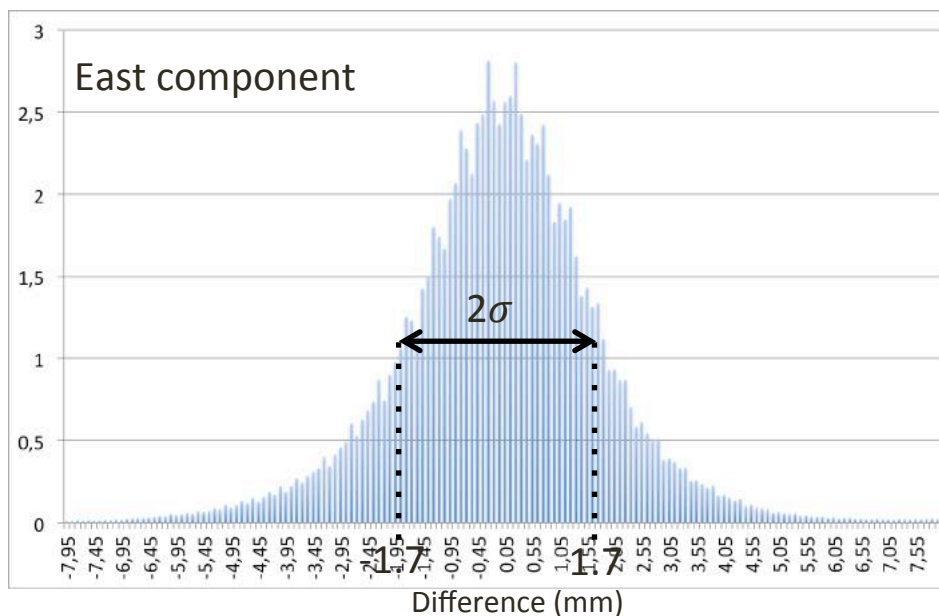
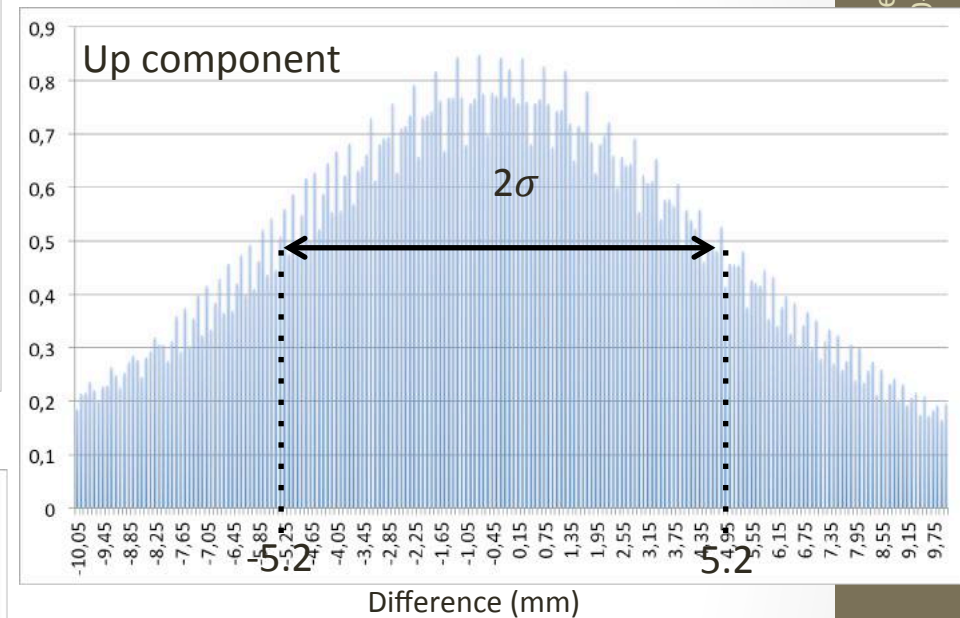
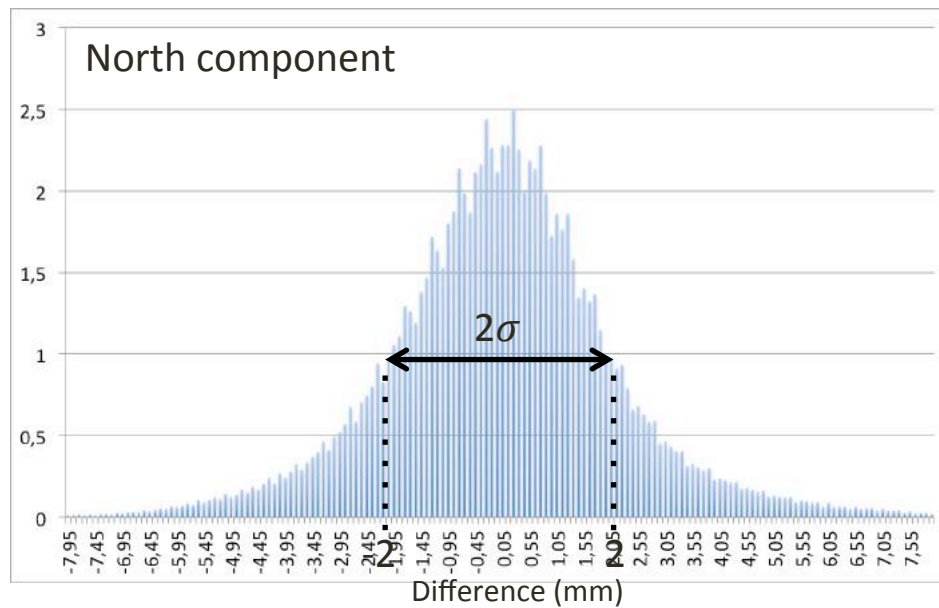


East component



- Average computed within a sliding window encompassing 15 values before and after the observed point
- Global statistics for 524 time series spanning the 2000-2005 period

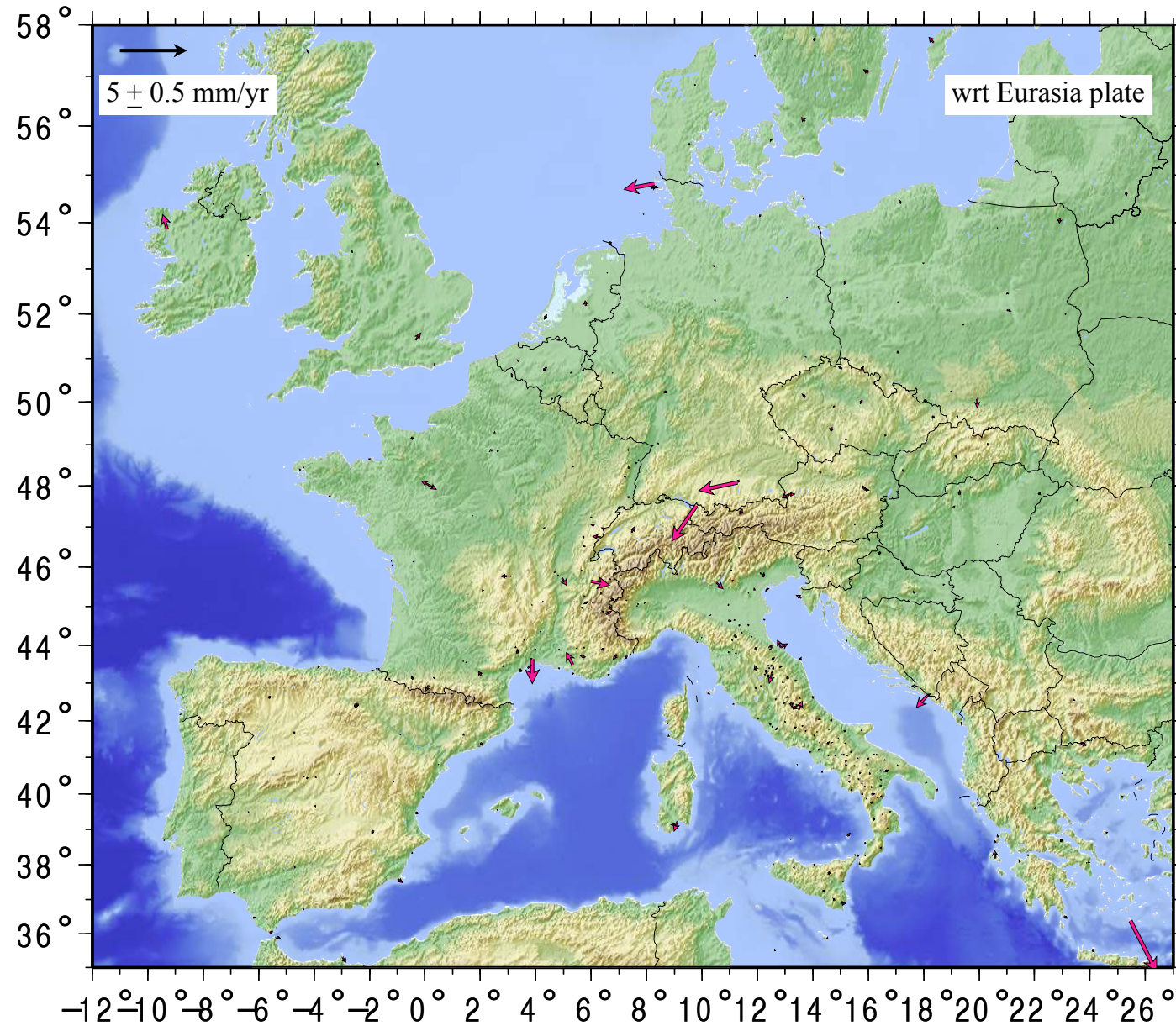
Products : Time series comparison, DD vs PPP: differences in daily positions (in%)



- Daily differences (DD-PPP)
- Global statistics for 524 time series spanning the 2000-2005 period

Products : Velocity fields comparison, DD vs PPP

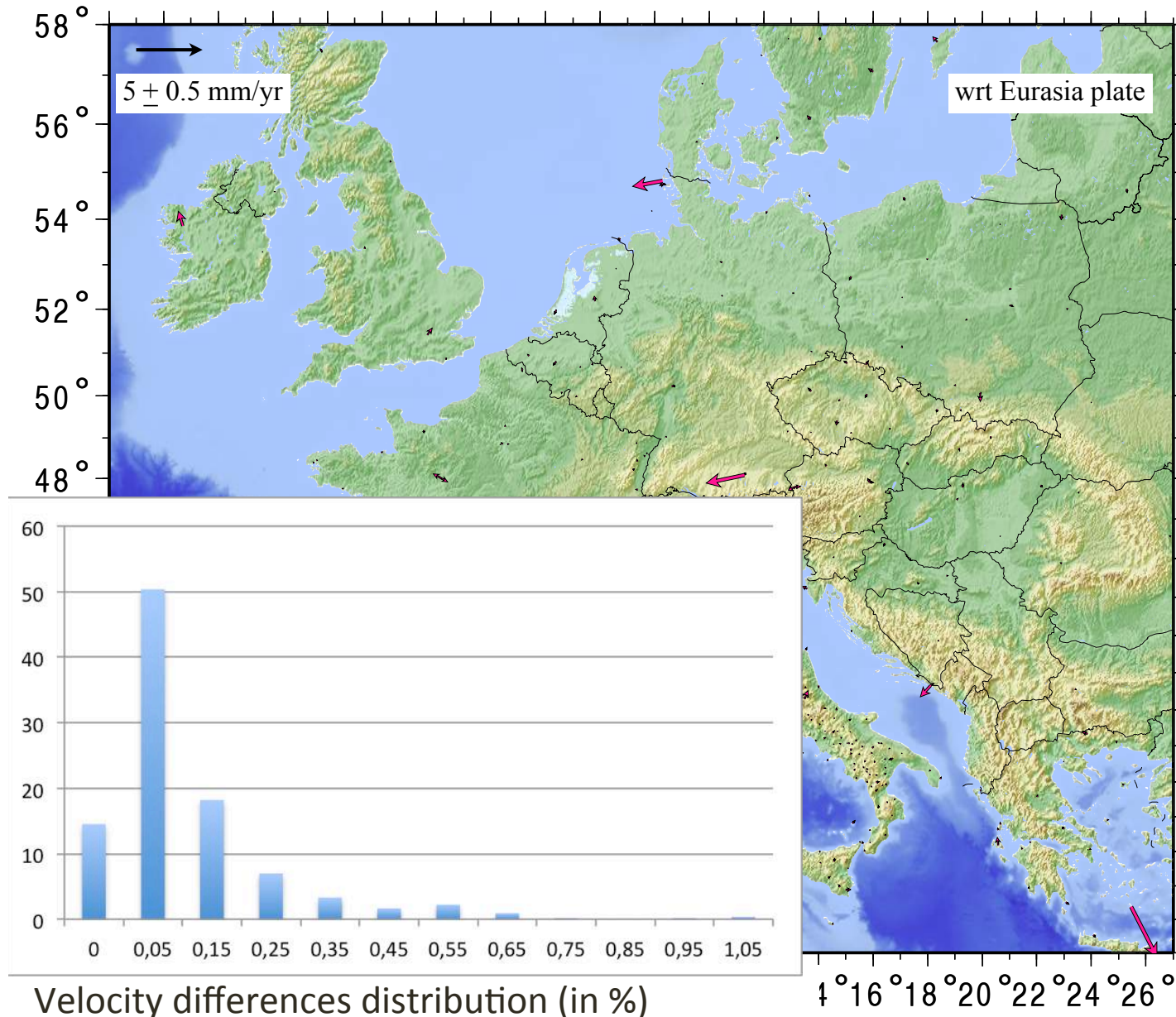
Velocity fields generated with MIDAS software from both DD and PPP raw time series :



- Difference of the velocity fields
- PPP and DD are very similar

Products : Velocity fields comparison, DD vs PPP

Velocity fields generated with MIDAS software from both DD and PPP raw time series :



- Difference of the velocity fields
- PPP and DD are very similar
- Large differences (9 stations with a difference > 1 mm/yr) are most of the time associated with very low amount of data

References:

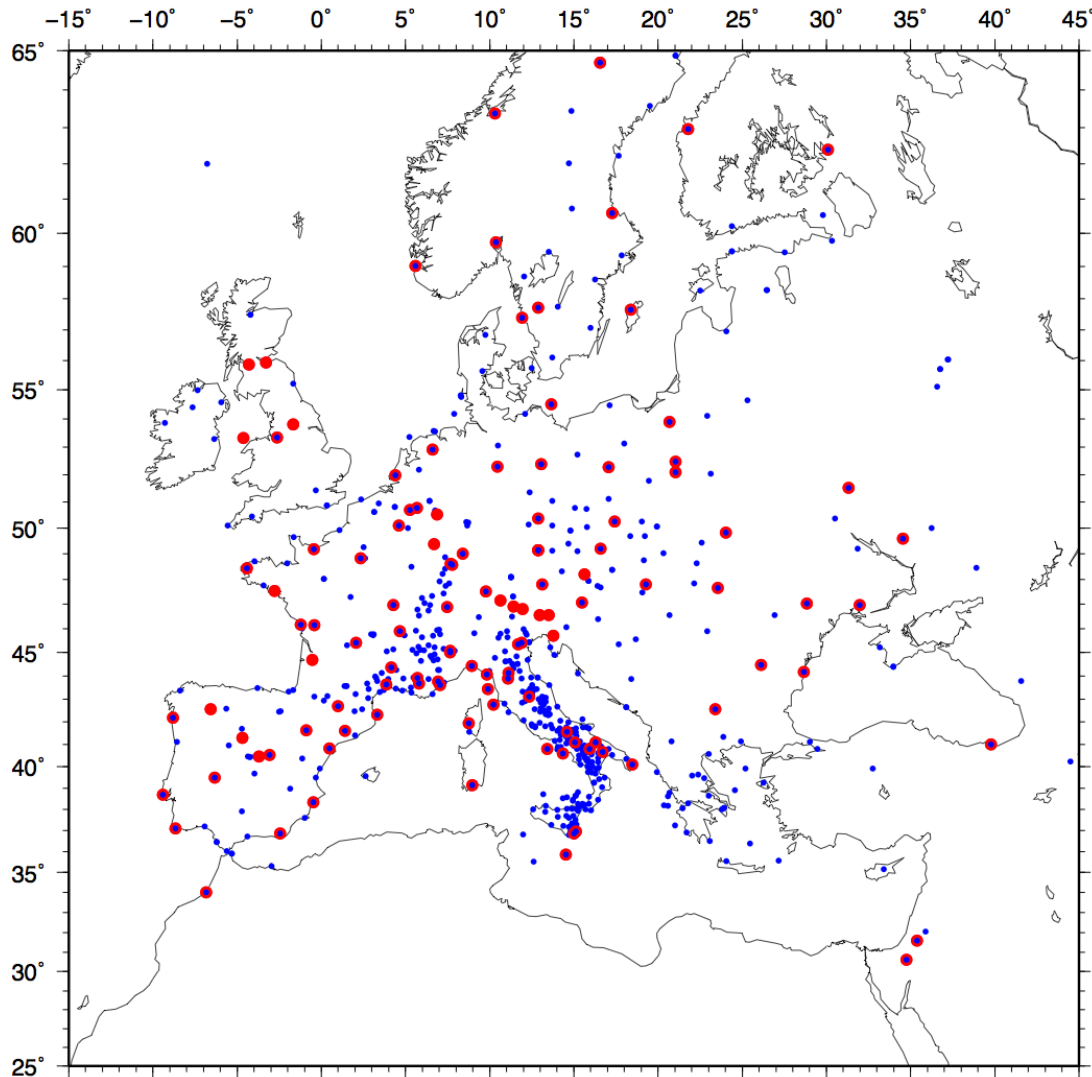
- Blewitt, G., C. Kreemer, W.C. Hammond, J. Gazeaux, 2016, MIDAS robust trend estimator for accurate GPS station velocities without step detection, accepted for publication in the Journal of Geophysical Research, doi: 10.1002/2015JB012552
- King, R. W. et Bock, Y. (2015). Documentation for the GAMIT/GLOBK GPS software analysis, release 10.06. Massachusetts Institute of Technology, Cambridge.
- PYACS : PhD thesis Dinh Trong Tran supervised by J. M. Nocquet. Analyse rapide et robuste des solutions GPS pour la tectonique. Autre. Université Nice Sophia Antipolis, 2013. Français.
- Masson, F., Lehujeur, M., Ziegler, Y., and Doubre, C. (2014). Strain rate tensor in Iran from a new GPS velocity field. Geophys. J. Int., 197(1) :10–21.
- Gipsy-Oasis, JPL : <https://gipsy-oasis.jpl.nasa.gov>

Annex 2.3 : INGV PPP solution for EPOS-IP

INGV PPP SOLUTIONS FOR EPOS-IP

CNT - INGV

EPOS Prototype Network (667 sites)



EUREF(331)

IGS(58)

RENAG(76)

RING(194)

NOA(18)

**STATIONS USED FOR FRAME
ALIGNMENT**

STATION INFO

EUREF:

<ftp://epncb.oma.be/pub/station/general/euref.snx>

IGS:

<ftp://igscb.jpl.nasa.gov/pub/station/general/igs.snx>

RENAG:

Sinex from RENAG GSAC

RING:

Log files from <http://ring.gm.ingv.it>

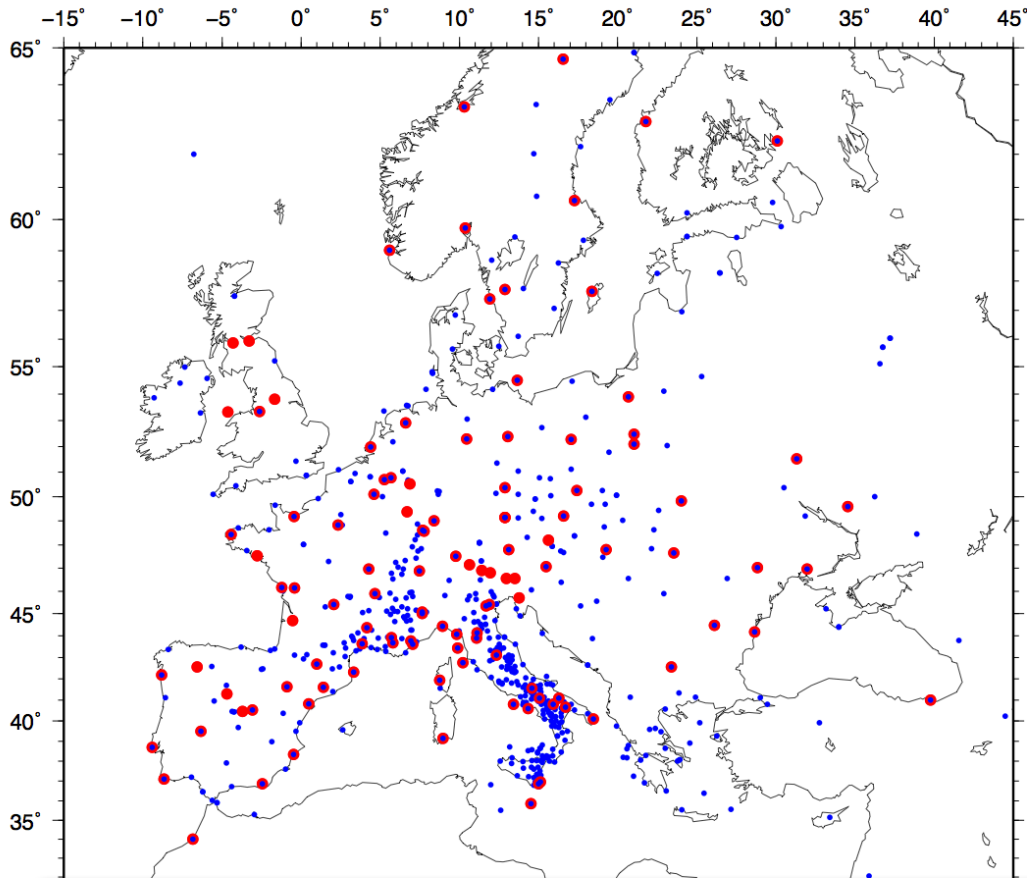
NOA:

Sinex from NOANET GSAC

Software/ Processing strategy

- GIPSY OASIS 6.4 (Jet Propulsion Laboratory)
- JPL free-network orbits, clocks and IGS08 x-files
- igs08_?????.atx, FES2004 OLM, No Atmospheric loading
- 3 processing steps:
 - Precise Point Positioning (IGS08 with JPL x-files)
 - Wide-Lane-Phase-Bias (Bertiger et al., 2010)
 - Final alignment to EU16 (IGS08 less Eurasia rotation)

EU16: A terrestrial frame for geodetic studies of crustal deformation near the Eurasian plate



Stations used to define EU16 (plus others out of map)

EU16 is a terrestrial frame for geodetic studies near Eurasian plate (approach follows Blewitt et al., 2013)

Based on GPS data 2000.0-2016.37

Position and velocity of 132 sites

Aligned to IGS08, no-net-rotation with respect “stable” Eurasia

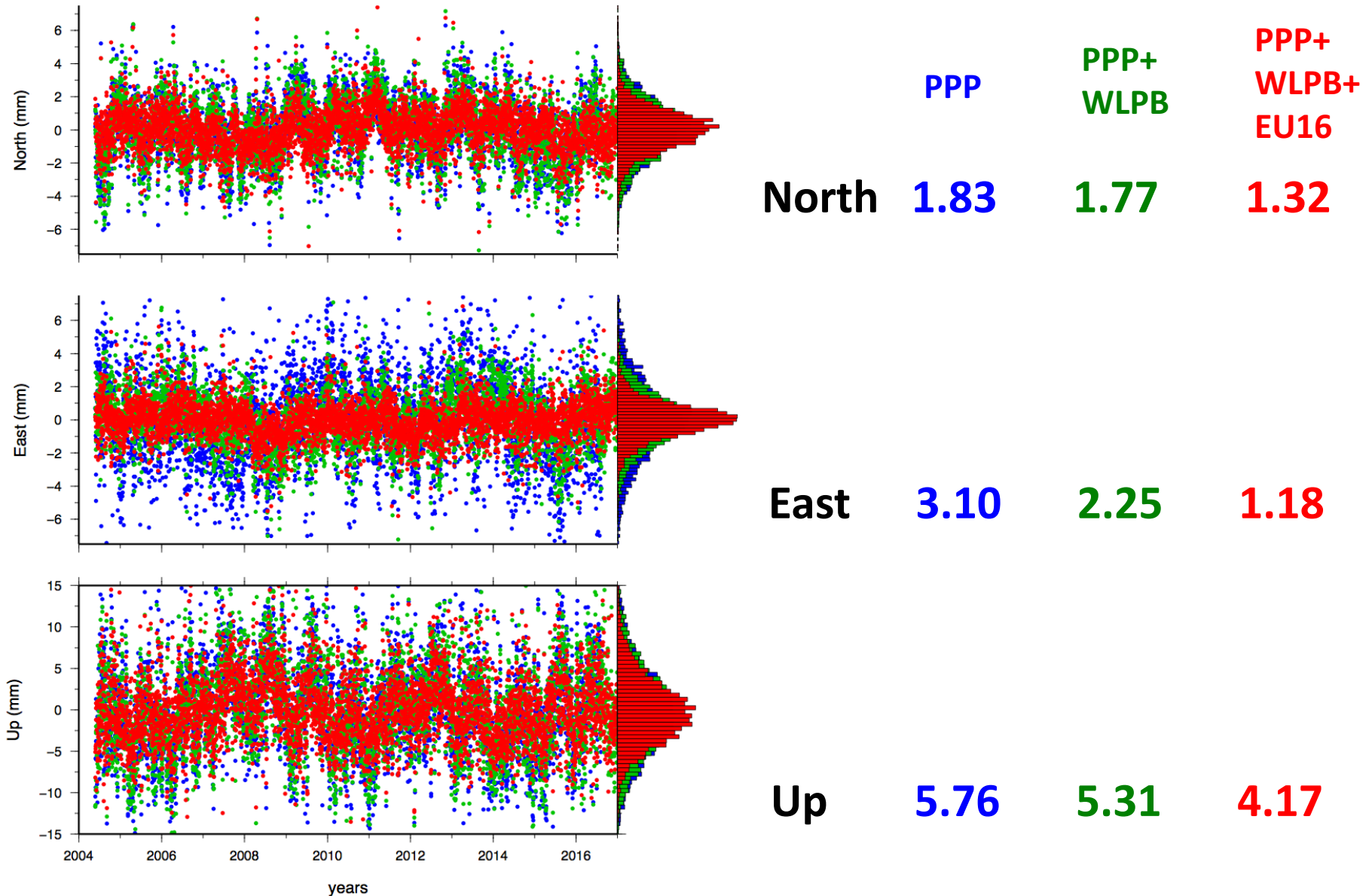
Daily RMS scatter (East, North, Up):
1.0, 1.3, 3.8 mm

27 sites used to define IGS08 Eulerian pole of Eurasian plate
(RMS horizontal: East 0.22 mm/yr,
North 0.21 mm/yr)

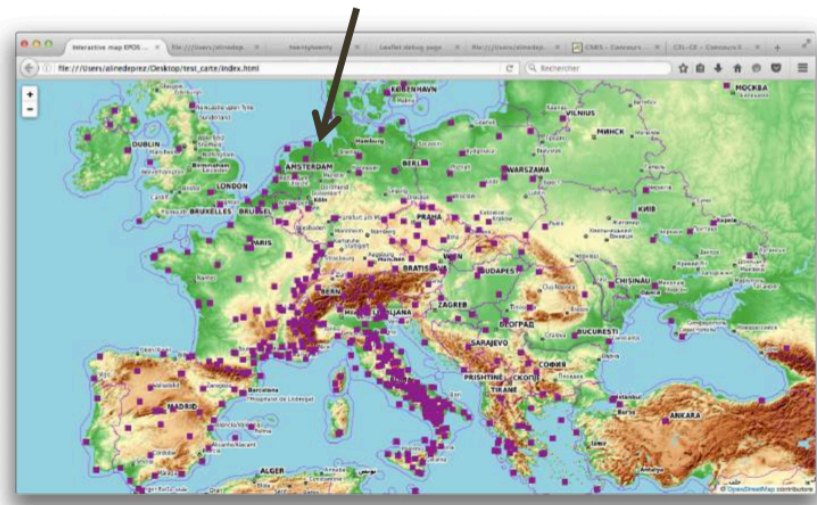
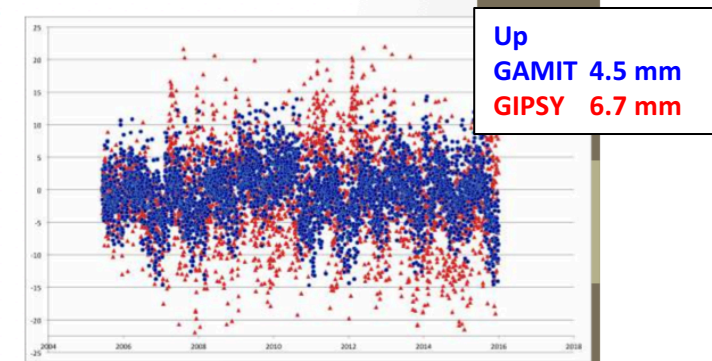
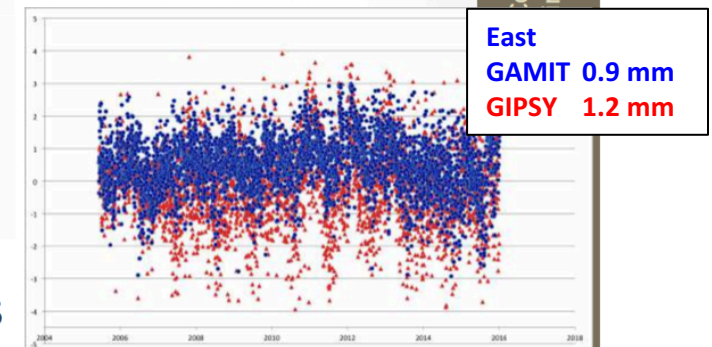
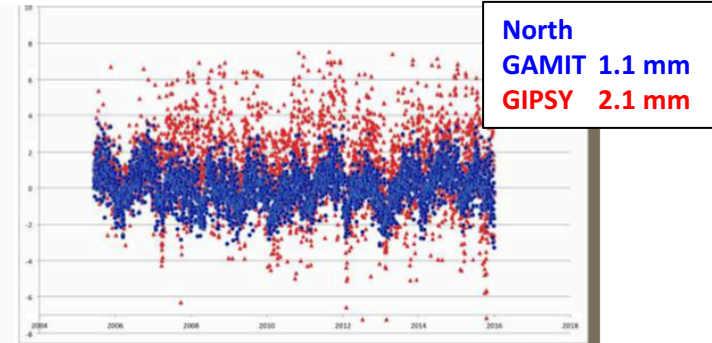
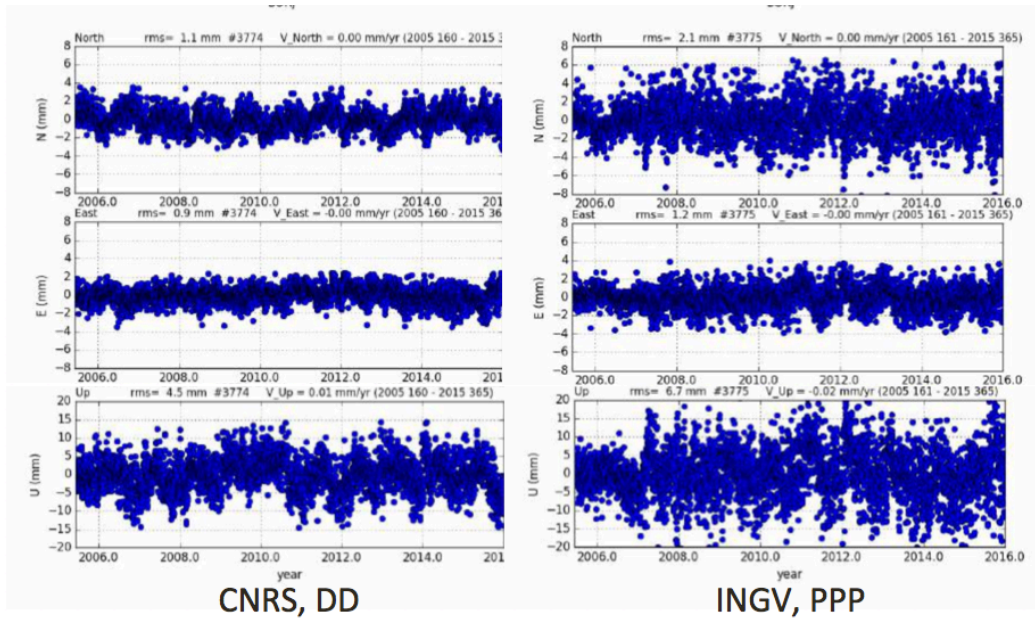
**x-files available:
can be used by GIPSY users to rotate their
free-network stacovs in Eurasia-fix frame**

Effects of GIPSY processing steps in time series precision

RMS of GROT (Grottaminarda RING station) time serie (mm)

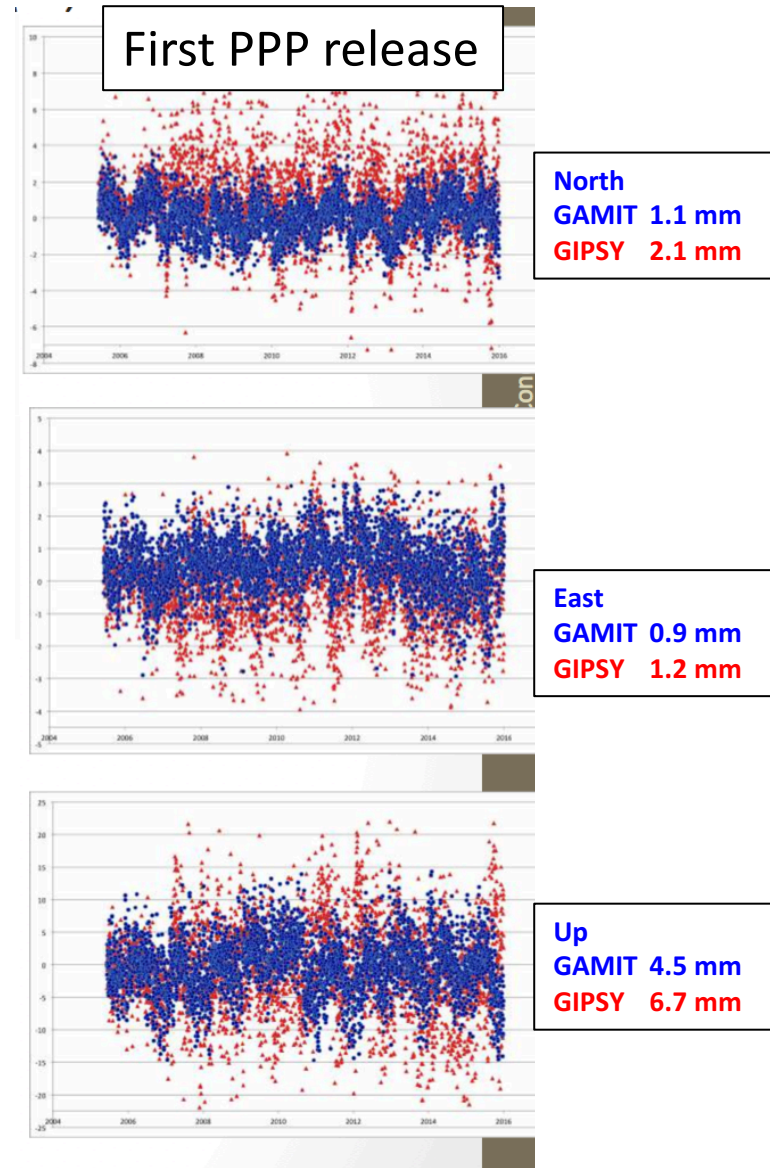
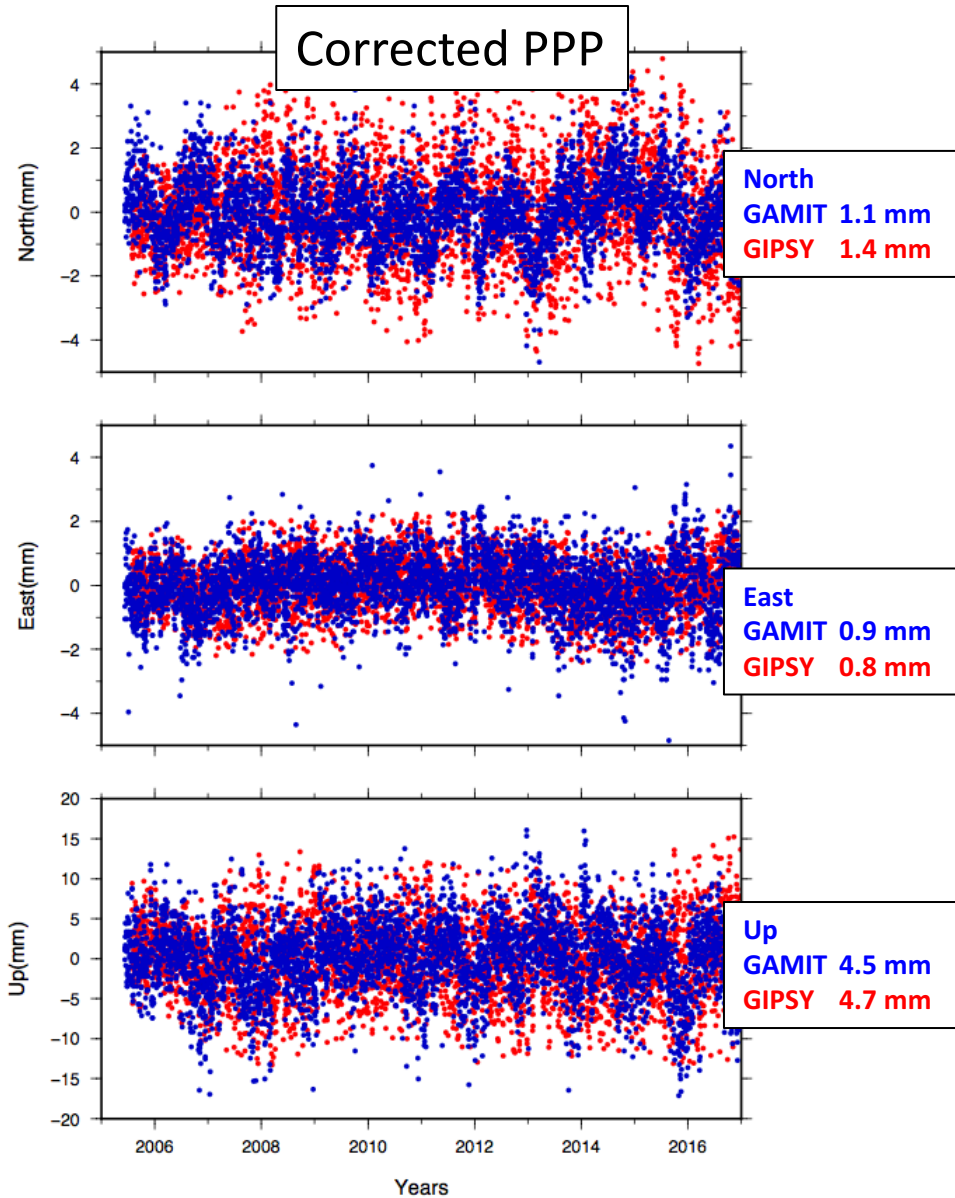


Discrepancy between GAMI/GIPSY in the first PPP release: Larger scatter in GIPSY for some EUREF sites



● CNRS
 ▲ INGV

Discrepancy between GAMI/GIPSY: Problem resolved GIPSY processing pointing to wrong ocnd tables for some sites

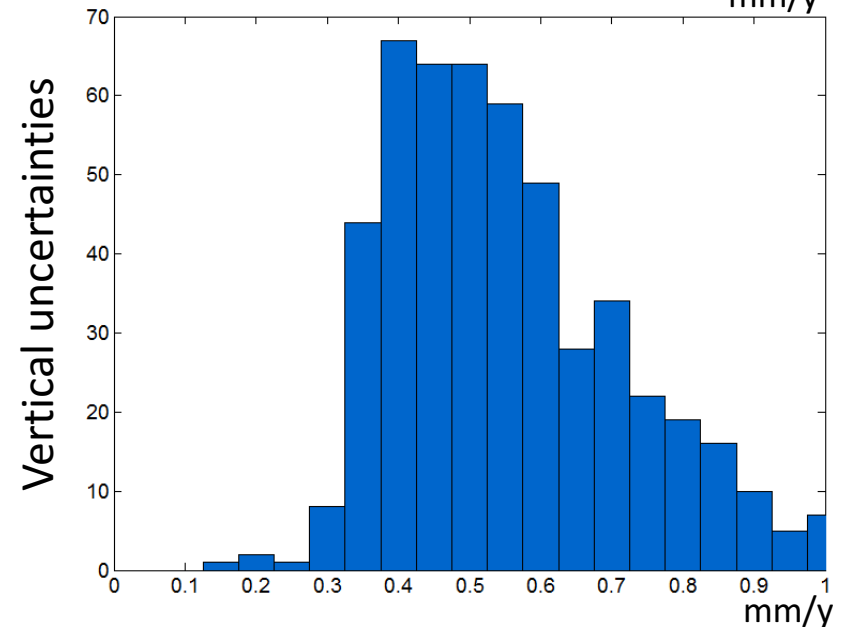
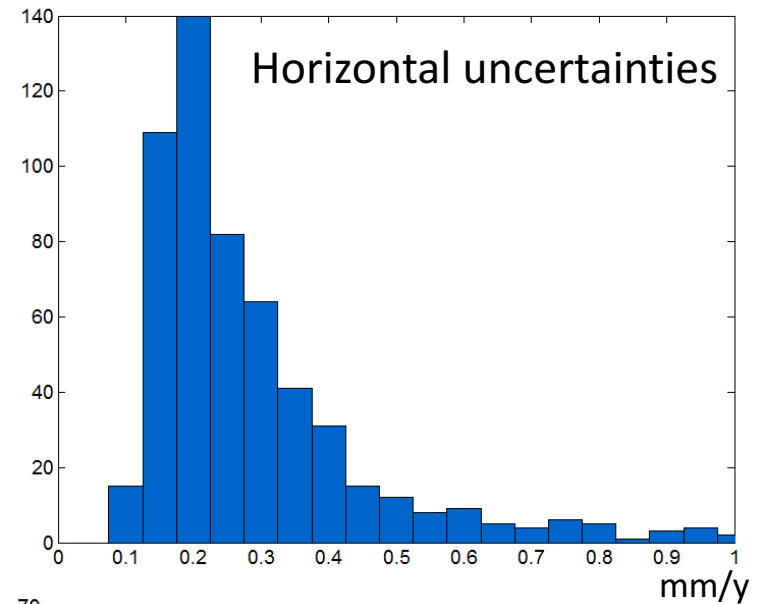


Annex 2.4 : INGV combination process

Summary of combination process

CNRS solution

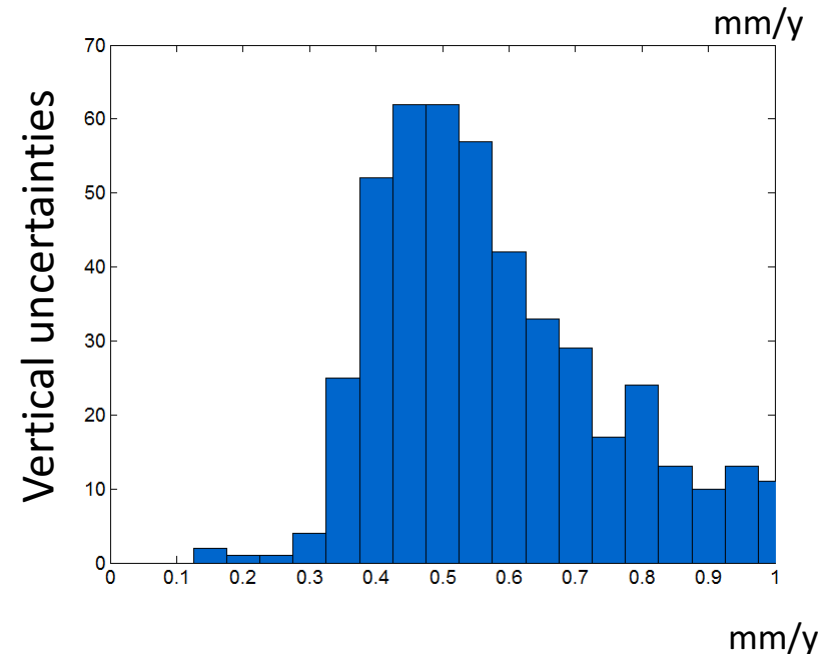
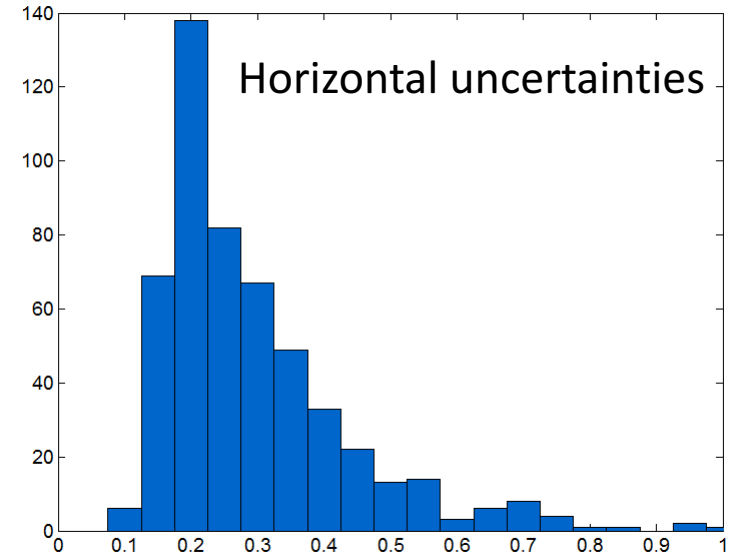
- n. of station velocities: 572
- N. of edited stations: 3
- Reference : ITRF2008
- Covariance matrix \rightarrow diagonal
- MEAN Horizontal- σ : 0.31 mm/y
- MEAN Vertical- σ : 0.66 mm/y



Summary of combination process

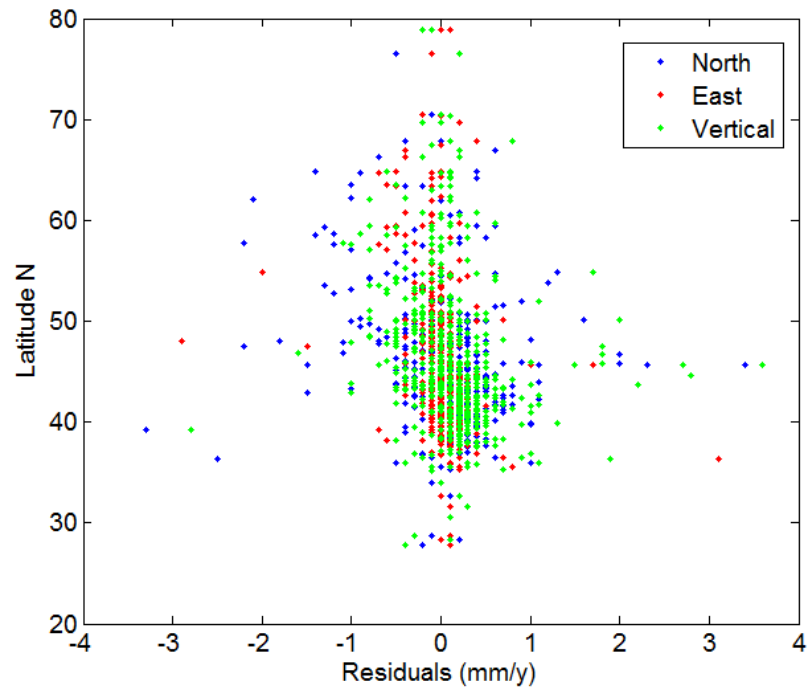
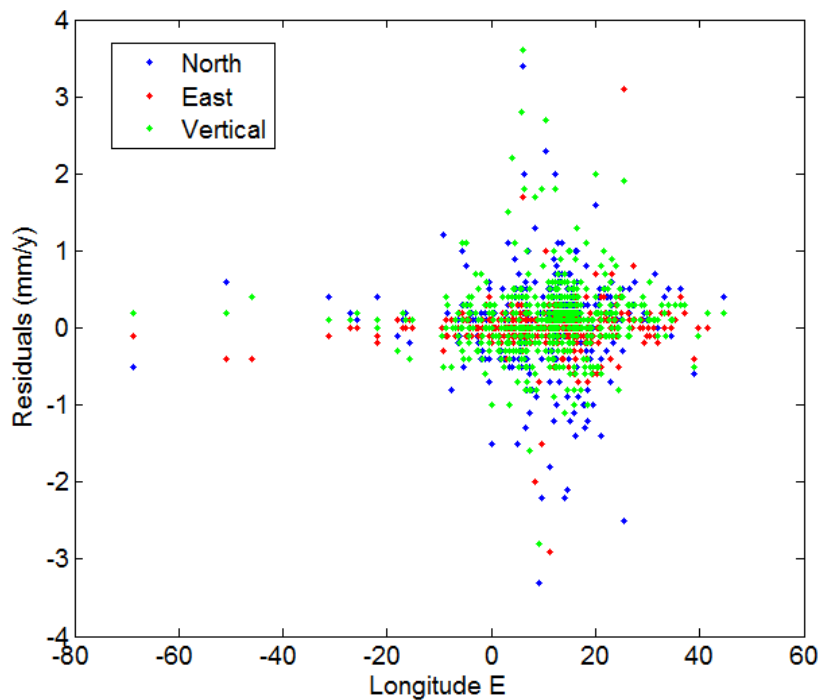
INGV solution

- n. of station velocities: 537
- N. of edited stations: 7
- Reference : ITRF2008
- Covariance matrix \rightarrow diagonal
- MEAN Horizontal- σ : 0.32 mm/y
- MEAN Vertical- σ : 0.69 mm/y

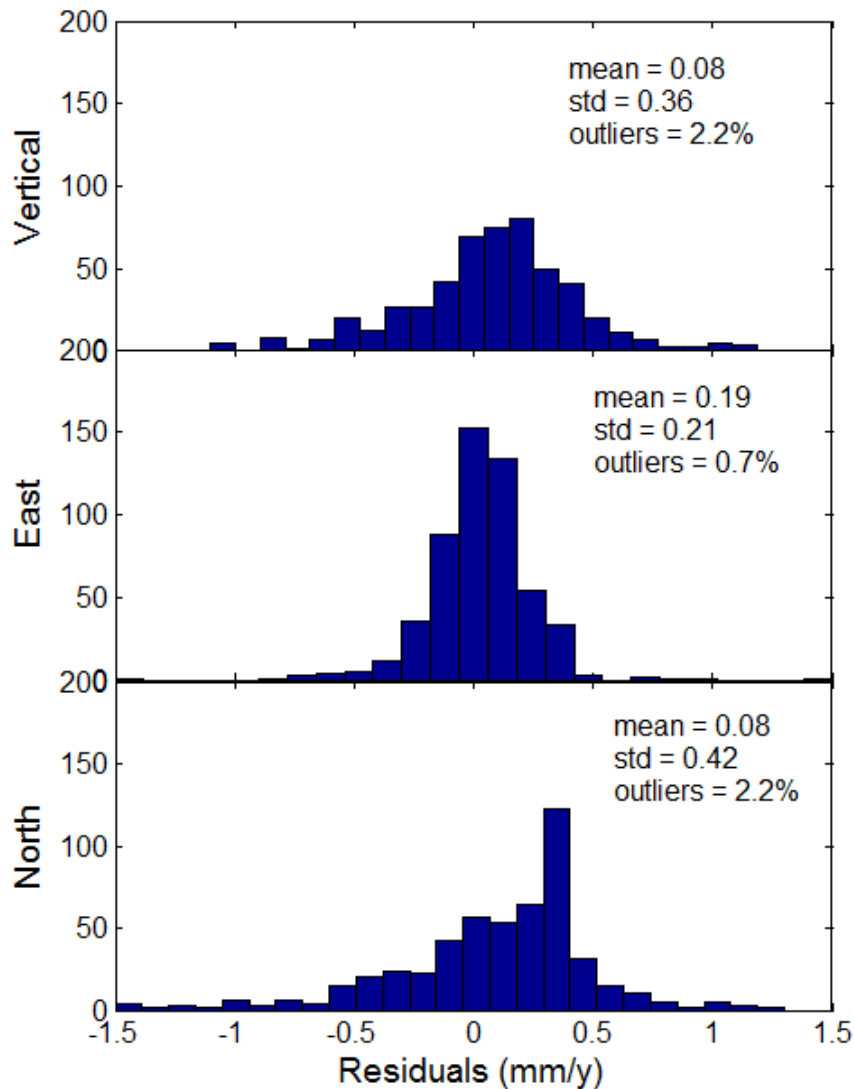


MIDAS Velocity differences: CNRS vs. INGV

Geographical distribution



MIDAS Velocity differences: CNRS vs. INGV statistics



INGV vs CNRS Rotation parameters:

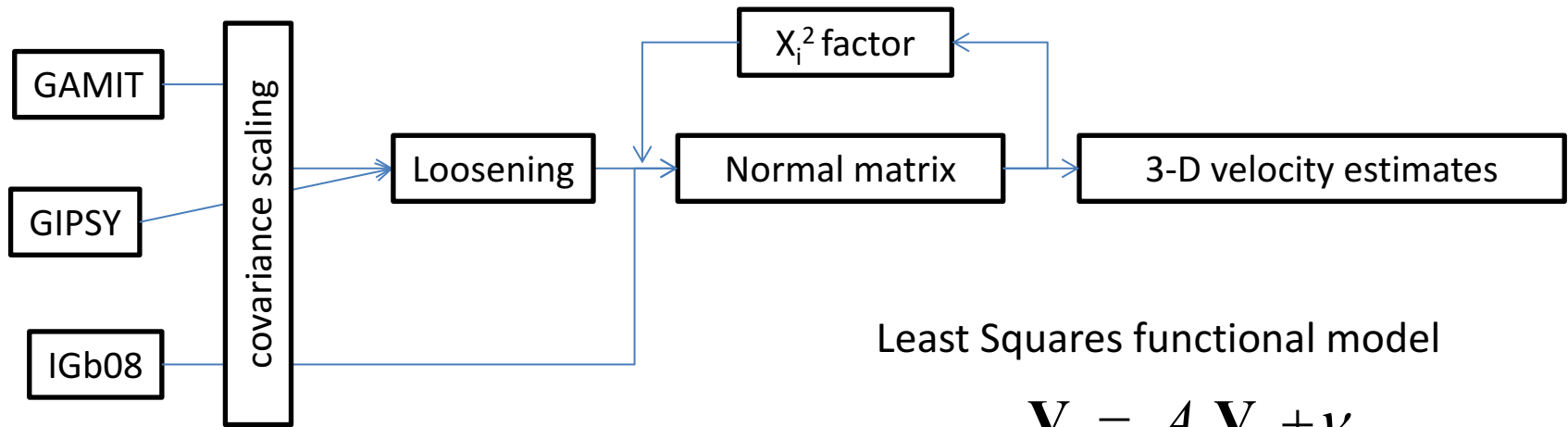
$$R_x = -0.09^\circ \pm 0.1^\circ$$

$$R_y = -0.14^\circ \pm 0.1^\circ$$

$$R_z = 0.09^\circ \pm 0.1^\circ$$

- No detectable systematics
- Velocity residuals < mean-uncertainties

Combination Method



Least Squares functional model

$$\mathbf{V}_s = \mathbf{A}_{c \rightarrow s} \mathbf{V}_c + \mathbf{v}$$

Covariance scaling: (initialization) the median of variances are set equal.

Loosening: rotation and scale relaxation.

Normal matrix: covariance scale factor estimated such as

$$\chi_i^2 = \mathbf{R}_i^T \mathbf{W} \mathbf{R}_i \text{ and } \chi^2 = \sum \chi_i^2 = 1.$$

\mathbf{V}_s : velocity of solution "s"

\mathbf{V}_c : velocity of combined solution

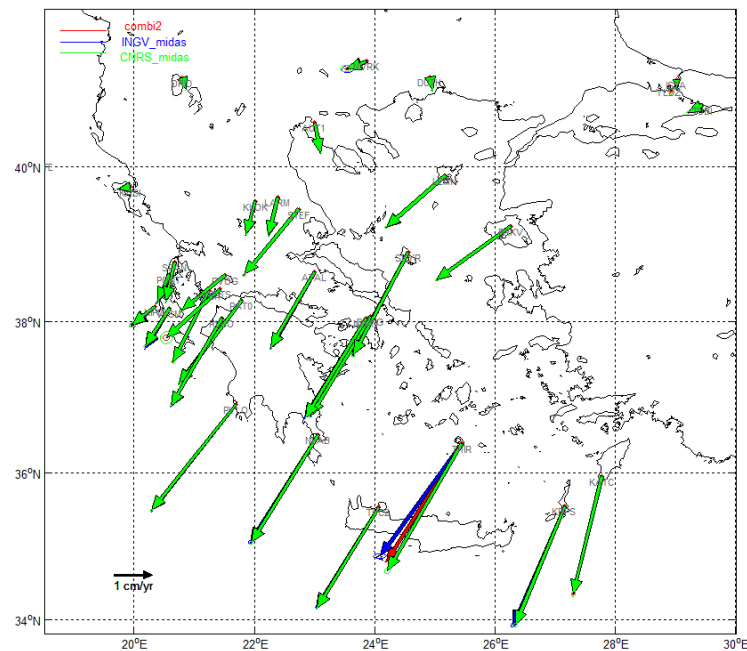
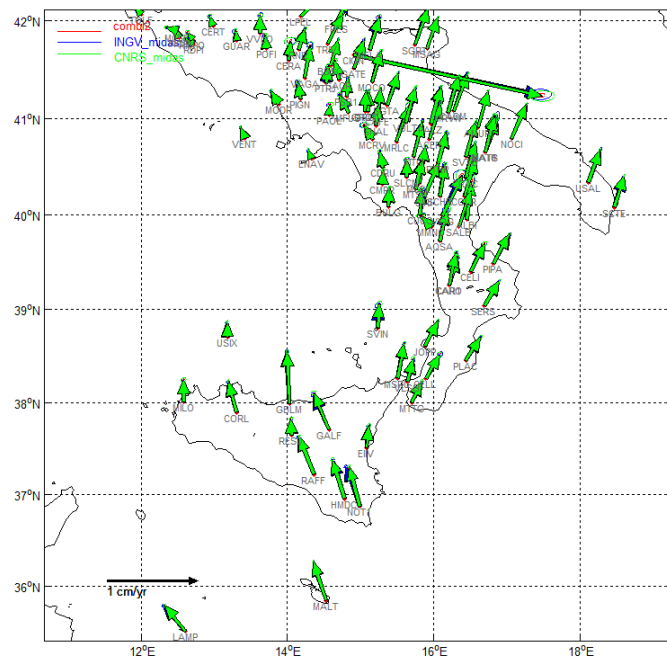
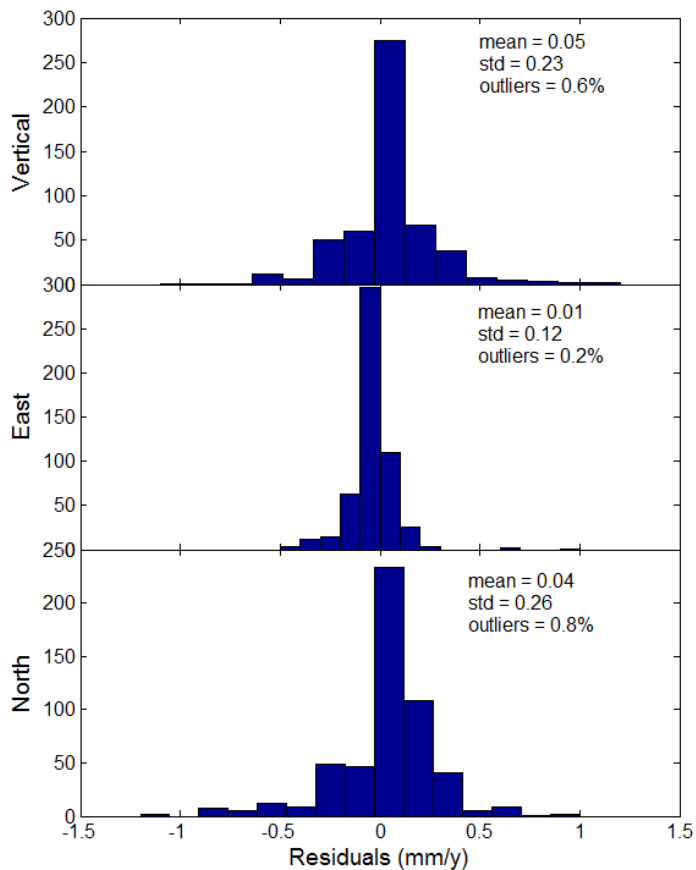
\mathbf{A} : reorder matrix

\mathbf{v} : noise

Due to scale and rotation loosening (relaxation), rigid rotations among velocity solutions should not be explicitly estimated !

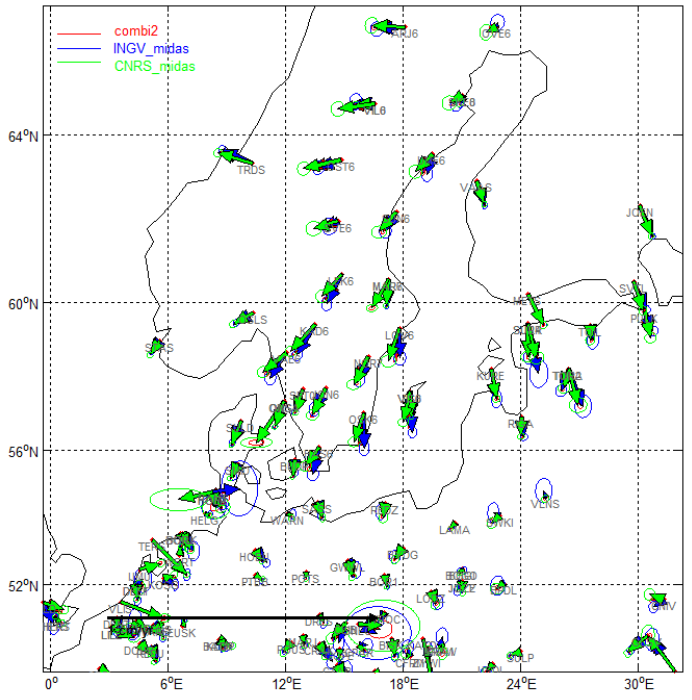
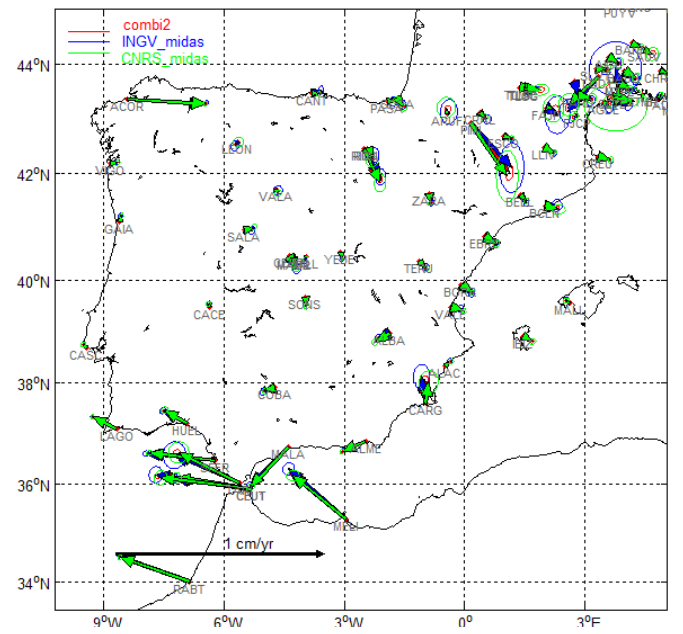
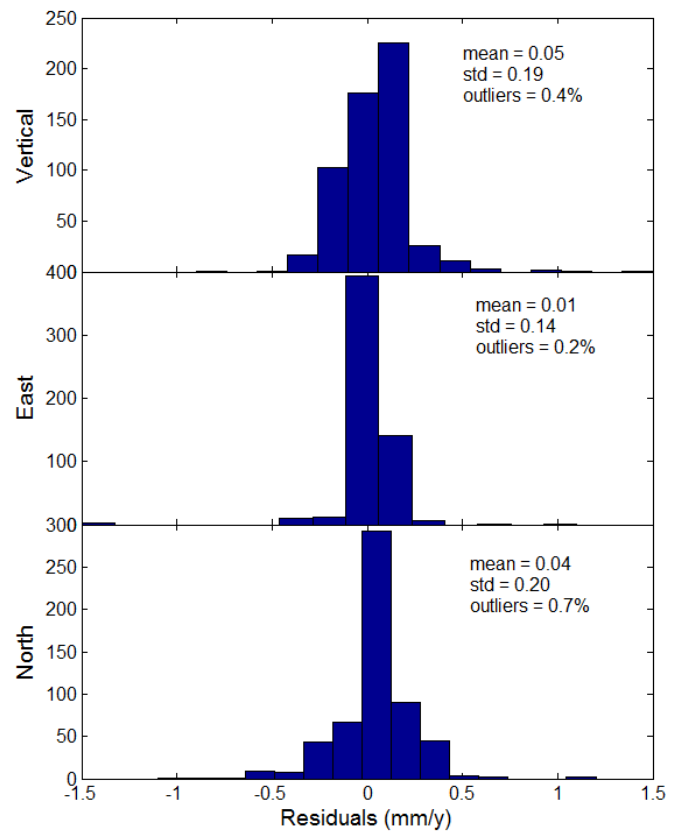
MIDAS: INGV velocity field

INGV vs COMBI residuals



MIDAS: CNRS velocity field

CNRS vs COMBI residuals



COMBI: Combined velocity field vs. IGb08

Residuals of only IGb08 station velocities

COMBI vs. IGb08 (mm/y)

Vertical: mean = 0.03

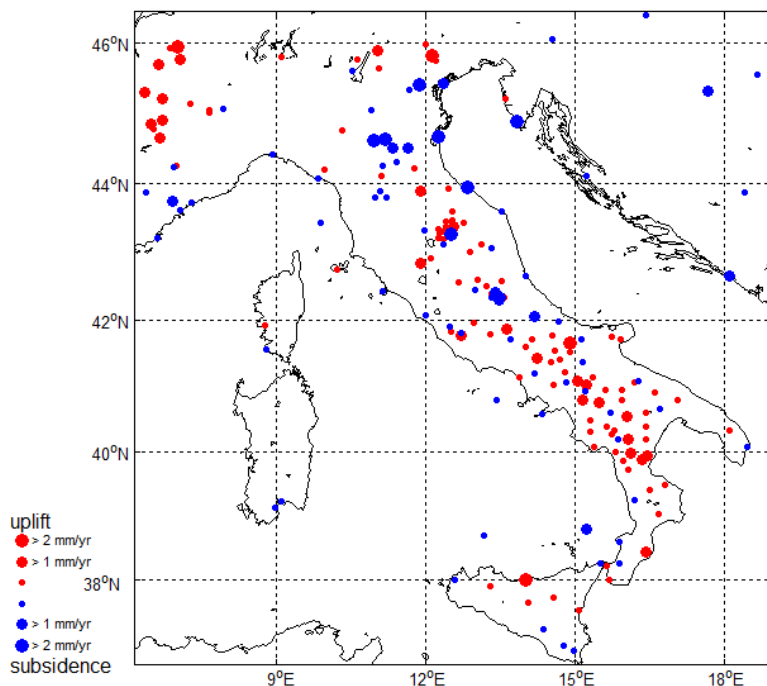
std = 0.31

East: mean = -0.02

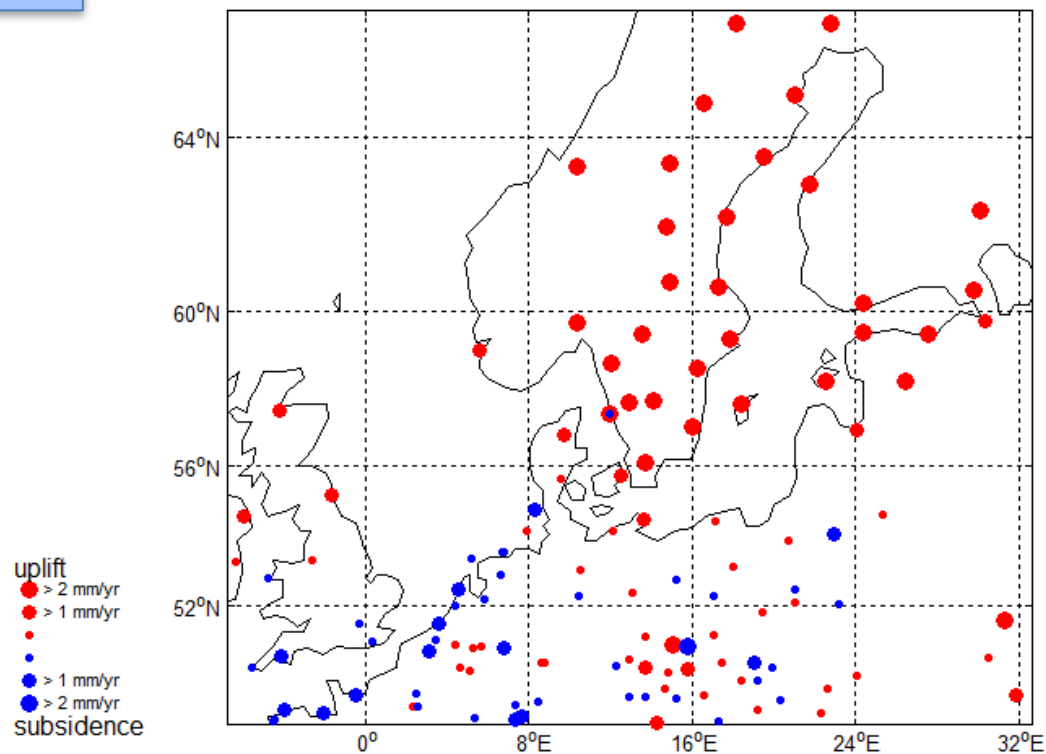
std = 0.30

North: mean = 0.10

std = 0.32



Vertical velocities



Annex 2.5 : Annals of Geophysics, Devoti et al. 2017 (INGV)

A Combined Velocity Field of the Mediterranean Region

Roberto Devoti¹, Nicola D'Agostino¹, Enrico Serpelloni¹, Grazia Pietrantonio¹, Federica Riguzzi¹, Antonio Avallone¹, Adriano Cavaliere¹, Daniele Cheloni¹, Gianpaolo Cecere¹, Ciriaco D'Ambrosio¹, Luigi Falco¹, Giulio Selvaggi¹, Marianne Métois¹, Alessandra Esposito¹, Vincenzo Sepe¹, Alessandro Galvani¹, Marco Anzidei¹

¹ Istituto Nazionale di Geofisica e Vulcanologia, Rome, Italy

Article history

Received May 20, 2016; accepted November 30, 2016.

Subject classification:

GPS, Velocity combination, Crustal motion, Mediterranean, INGV.

ABSTRACT

We present a full 3-D velocity field of the Earth's surface in the Euro-Mediterranean area obtained from a combination of three different velocity solutions computed at the Centro Nazionale Terremoti (CNT) of the Istituto Nazionale di Geofisica e Vulcanologia (INGV). All the publicly available GPS data since 1993, have been fully reprocessed by three different software tools and the final velocity field is estimated combining three independent velocity solutions in a least squares sense. The input velocity solutions are treated as stochastic samples of the true velocity field by loosening the reference frame constraints in the associated variance-covariance matrix. The proposed approach allows for a fast and efficient combination of multi velocity solutions, taking into account the full network covariance, if available. The velocity map for the Euro-Mediterranean region will be updated and released regularly on the web portal of the National GPS Network (<http://ring.gm.ingv.it>) and made available to the scientific community. Here we show and discuss the data analysis and the combination schemes, and the results of the combined velocity field.

1. Introduction

For Earth scientists the Mediterranean region represents a unique natural laboratory to test and assess geodynamical theories, being the place where three major continental plates, Eurasia, Africa and Arabia interact in a very complex way, displaying a wide range of crustal deformation patterns. Here several microplates have been described from geological, seismological and geodetic data, among which the major ones are the Anatolian, Aegean, Apulian and Adriatic sub-plates. Thus from a scientific perspective, this region represents a key area for understanding the basic processes of plate tectonics and specifically the interplay of different tectonic styles in a continental collision area. The advent of space geodesy, especially exploiting the increasing number and density of Global Navigation Satellite System (GNSS) networks, allows us to provide an accurate measurement of the 3D Earth's surface motion, revealing the details of the kinematics and strain accumulation rates at different spatial

scales. The EUREF permanent network (EPN), represents an important European infrastructure (<http://www.epncb.oma.be>) that operates and shares GNSS data over a continental scale. The EPN is a voluntary federation of self-funding agencies, research institutions and universities that maintain the Terrestrial Reference System in the European area, realizing and delivering fundamental geodetic products, such as Receiver INdependent EXchange (RINEX) data and position time series, used to build the global International Terrestrial Reference Frame (ITRF). On the other hand, the data provided on a local scale (national and regional) are currently not readily available to the scientific community. Several networks owned by private companies but also by local administrations do not contribute to the data disclosure policy that should sustain and motivate any scientific initiative. For this reason, the European Plate Observing System (EPOS; <http://www.epos-ip.org>) has initiated a long term project aiming at facilitating the use of integrated data and products in the field of geosciences. As in the past the Mediterranean was the locus of thorough cultural and economical exchanges between diverse peoples, we hope that it still represents a great opportunity for sharing knowledge and awareness.

At present-days, a few thousands of permanent GNSS stations provide unprecedented spatial and temporal coverage of the European deforming plate and its boundaries. This continuous monitoring effort, carried out by various public and private institutions is crucial to understand the large scale kinematics and to shed light on the physics that governs tectonic deformation and seismic, and aseismic faulting. The INGV is the primary Italian research center interested in the collection, management and analysis of GPS measurements. The INGV is archiving all the available GNSS data at national level. Three distinct analysis centers (AC) at INGV process and analyze routinely all the regional GPS data using respectively Bernese, GAMIT/

GLOBK and GIPSY-OASIS scientific software packages. They produce daily position solutions for up to 2000 stations located mostly along the African-Eurasian boundary and on the central and western European continent.

A large amount of work has been recently dedicated to study velocity fields from GNSS data at different geographic scales. In this study we are not willing to present an exhaustive list of such research effort, which is out of the scope of this work, but rather to propose a methodology to obtain rapid and reliable velocity fields on a wide continental scale. Recently, a number of authors published various deformation fields retrieved from GNSS data, on regional or even global scale (e.g. Caporali et al., 2009; Le Pichon and Kreemer, 2010; Pérouse et al., 2012; Nocquet, 2012; Kreemer et al., 2014, and references therein). Their efforts are partly directed to assemble all available geodetic solutions already published and to reduce systematic errors arising from different reference frame adoptions in order to obtain a velocity field as homogeneous as possible. These overviews of crustal deformation models over wide areas are of fundamental importance to test tectonic and geophysical models that govern the plate and plate boundary interplay. Here we present a cross-validated velocity field, based on a complete re-analysis of the whole GPS dataset, focusing on reference frame consistencies, homogeneous modeling over the whole data time-span and evaluating the repeatability of common stations. The purpose of this project is to generate a consistent, combined geodetic velocity model of the Mediterranean area on a regular basis, to offer high-quality geodetic products to a broad community of potential users. This action aims to increase data and products access to the scientific community and promote scientific studies on the deformation processes acting across the Mediterranean basin, but also informing engineers and public policy makers, who may use such results to plan for disaster mitigation and environmental monitoring.

2. GPS data collection and processing

Many GNSS permanent stations, managed by both scientific and commercial institutions, are available on the Eurasian plate and its boundaries. Although part of them are not specifically devoted for geophysical monitoring (cadastral, topographic, etc.) and may potentially be of lower quality in terms of monumentation and data flow, their integration has a large potential to improve the resolution of the kinematic patterns of the area. The complete knowledge of metadata is usually not at the level of scientific devoted GNSS stations and needs a distinct analysis and cross-check.

In this study we find that at least 40% of the stations fall in this subsidiary category in which the metadata has to be carefully reconstructed. The data collection rate used in the analysis by all the AC is one sample every 30 seconds. Most of the stations are also streaming data at 1 Hz or even higher sampling rates in real time, but these streams are not processed in this study.

The INGV institute also manages the RING network in Italy (<http://ring.gm.ingv.it>), a GPS network of about 200 stations that meet specific research criteria based on geographic location and instrumental standardization (monumentation, receiver and antenna type). INGV collects and processes also GPS data from networks not belonging to the International GNSS Service (IGS) or the EUREF Permanent Network (EPN) nor in partnership with the international scientific community, thus expanding and supplementing the GPS database with those regional data whose historical records are often not preserved. Figure 1 shows the distribution of the GPS stations (updated at January 1, 2016) for which INGV collects and archives raw RINEX data. At present, depending on the data availability, more than 1600 European stations are regularly stored every day. These data have been fully re-processed by three AC, in which different approaches and analysis software are adopted (see also Avalone et al., 2010). Figure 2 shows the relative contribution to the combined velocity of the three AC distinguished by different color codes, blue for Bernese, green for GIPSY-OASIS and red for GAMIT/GLOBK processing chain.

The different processing schemes adopted by the three AC, are summarized in Table 1. Essentially two of them (Bernese and GAMIT/GLOBK) are based on the relative positioning concept using phase observables double differencing techniques, whereas the third processing scheme is based on the Precise Point Positioning (PPP) approach using the GIPSY-OASIS software. Each AC estimates a variable number of station velocities, ranging from 900 to about 1500 values, with overlapping points. The availability of three independent solutions, in terms of daily stations positions and covariances, secular velocities, seasonal and transient signals, give us the possibility to internally compare and validate the results, with the main goal of assessing the repeatability of the independent velocity estimates. The combined velocity field has to be considered as a “consensus” (of cross-validated) geodetic product, that has been obtained after an iterative trial and error process and a final least squares combination of the overall velocity field. The validation procedure is also a key issue of the INGV effort in the EPOS project.

2.1 Details on the Bernese solution

The Bernese Analysis Center (BeAC) uses the Bernese software Ver. 5.0 (Beutler et al., 2007), following

A COMBINED VELOCITY FIELD OF THE MEDITERRANEAN REGION

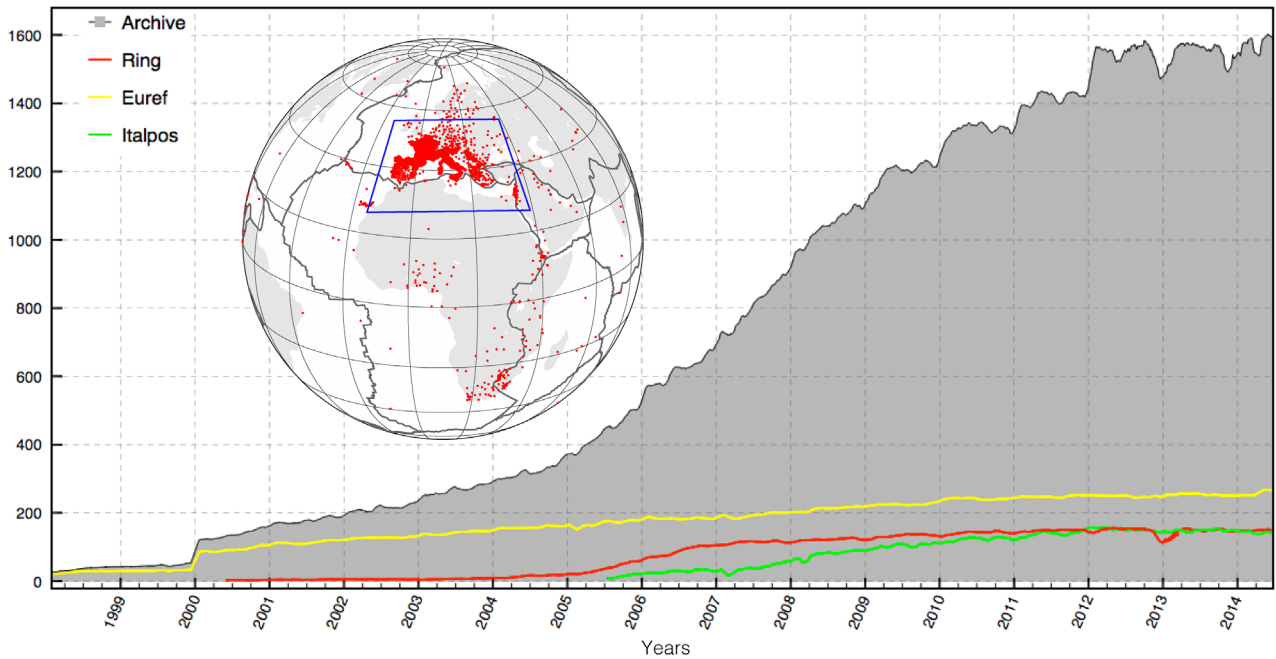


Figure 1. History of the number of GNSS stations archived at INGV. The yellow, red and green lines show the evolution of sites number for the Euref, RING and ItalPos networks, respectively. The blue box in the inset show the area for which we provide the combined solution in this work.

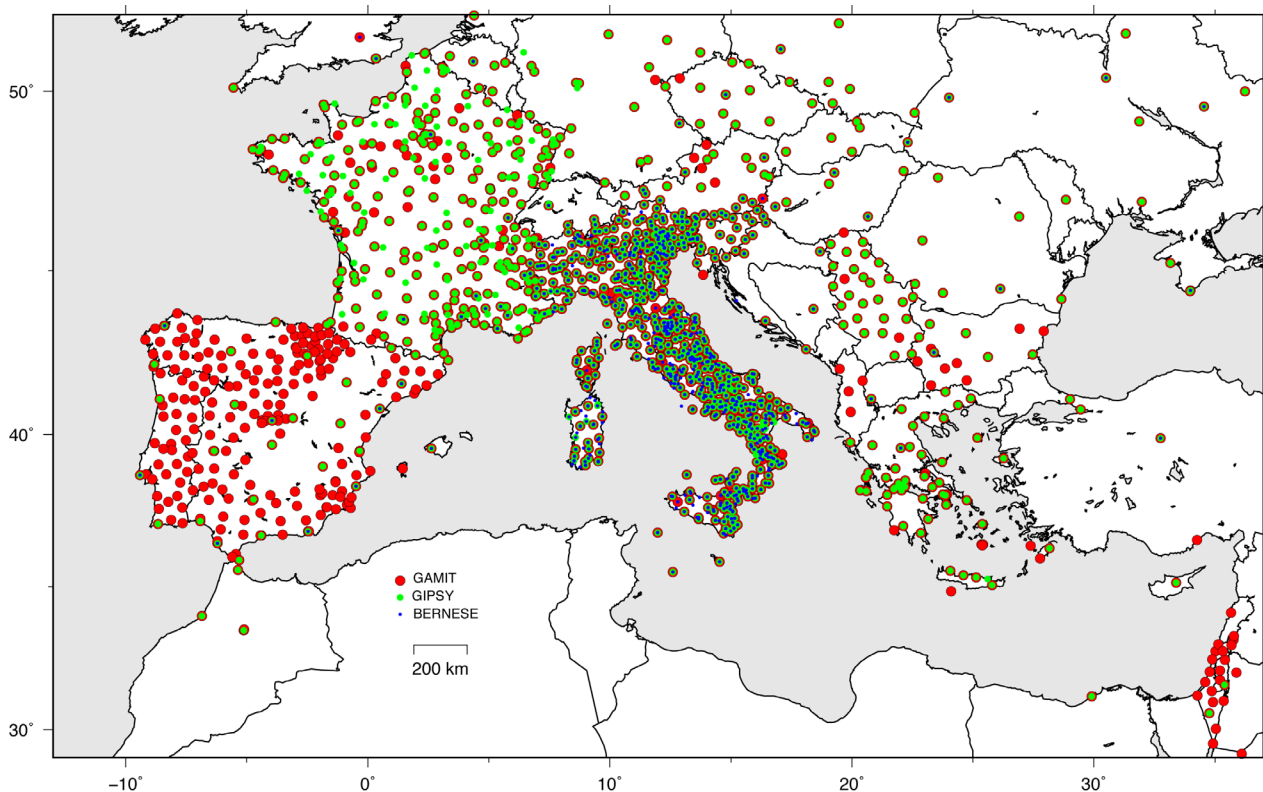


Figure 2. GPS network arrangement of the combined velocity solution. The following color code of the bullets has been used to highlight the contribution of the three AC: blue (Bernese), green (Gipsy) and red (Gमित).

the recommended guidelines for EUREF Analysis Centers (<http://www.epncb.oma.be>). Daily coordinate solutions of a network of stations are obtained by means of Ionosphere Free linear combinations of phase observables using the Quasi Ionosphere Free approach to properly solve phase ambiguities (Beutler et al., 2007).

For computational efficiency the full network is divided into sub-networks, each with about 50 or fewer stations. To allow the combination of the sub-networks into a full network daily solution, each sub-network contains a minimal of 11 tie stations. The troposphere modeling consists in the a-priori dry-Niell model fulfilled by the

	BERNESE	GAMIT	GIPSY
Solution type	Double Differences	Double Differences	Precise Point Positioning
Ionosphere	“Ionofree” combination	“Ionofree” combination	“Ionofree” combination
Troposphere	Niell Mapping	Global Mapping	Global Mapping
Orbits & EOP	IGS final products	IGS final products	JPL final products
Antenna PCV	IGS abs calibration	IGS abs calibration	IGS abs calibration
Ocean loading	FES2004	FES2004	FES2004

Table 1.

estimation of zenith delay corrections at 1-hour intervals at each station using the wet-Niell mapping function (Niell, 1996). In addition, one horizontal gradient parameter per day at each site is estimated. Ocean loading is computed using the FES2004 tidal model coefficients (Lyard et al., 2006) provided by the Ocean Tide Loading web service (<http://holt.oso.chalmers.se/loading>). The GPS orbits and the Earth’s orientation parameters are fixed to the combined IGS products (Dow et al., 2009) and an a-priori loose constraint of 10 m is assigned to all site coordinates. The IGS08 absolute antenna phase center correction has been applied to each station receiver antenna. The daily coordinates are thus estimated in a loosely constrained reference frame. In order to express the GPS time series in a unique reference frame, the daily solutions are first projected imposing tight internal constraints (at millimeter level), and then the coordinates are transformed into the IGS realization of the ITRF2008 frame (i.e., IGB08) by a 4-parameter Helmert transformation (translations and scale factor). The regional reference frame transformation uses 45 IGB08 anchor sites located in central Europe. To get rid of common translations of the entire network, the time series are readjusted through a common mode filtering procedure similar to that proposed by Wdowinski et al. (1997). Velocities at GPS stations are estimated by a linear weighted least squares fit of all the coordinate time series simultaneously, using the full daily covariance matrices and modeling secular drifts, episodic offsets and annual sinusoids (Devoti et al., 2014).

2.2 Details on the Gamit solution

The Gamit Analysis Center (GaAC) processes double-differenced ionosphere-free GPS carrier phase observations using the GAMIT/GLOBK (Ver. 10.4) software, developed by the Massachusetts Institute of Technology (Herring et al., 2015). The estimated daily parameters are site positions and time-variable, piecewise, linear zenith and horizontal gradient tropospheric delay parameters, loosely a-priori constraints are applied to geodetic parameters, and the GPS orbits are fixed to the SOPAC products (<http://sopac.ucsd.edu>). The whole GPS network is divided into in smaller sub-networks,

containing each less than 50 stations, sharing some high quality tie-sites. The ocean loading correction is applied using the FES2004 tidal model (Lyard et al., 2006). The Global Mapping Function (Boehm et al., 2006) is adopted to model both the dry and wet component of the tropospheric delay; pole tide correction is applied accounting for IERS data (pole.usno) (Petit and Luzum, 2010). The IGS08 absolute antenna phase center model for both satellite and ground-based antennas is used. Loosely constrained solutions, in the form of ASCII GAMIT H-files, are later combined, using the ST_FILTER program of the QOCA software (Dong et al., 1998) with the IGS network solutions available from SOPAC. A global reference frame is realized by minimizing coordinates and velocities of the IGS global core stations, estimating a 7-parameter Helmert transformation (translations, rotations and scale factor) with respect to the IGB08 reference frame. GPS velocities are obtained by fitting a linear trend, annual and semi-annual terms and site specific offsets, assuming a white plus flicker (power-law) noise model (see also Serpelloni et al., 2013). The Common Mode Error in the time series is estimated using the Principal Component Analysis (PCA) strategy, following the method proposed by Dong et al. (2006).

2.3 Details on the Gipsy solution

The GIPSY-OASIS II software, Ver. 6.2 (Zumberge et al., 1997), developed by the Jet Propulsion Laboratory (JPL) is used to produce Precise Point Positioning (PPP) solutions using ionosphere-free carrier phase and pseudorange observables and using JPL’s final fiducial-free GPS orbit products (Bertiger et al., 2010). Tropospheric wet zenith delay and horizontal gradients are estimated as stochastic random-walk parameters every 5 min using the Global Mapping Function (Boehm et al., 2006). Ocean loading is modeled using the FES2004 tidal model coefficients provided by the Ocean Tide Loading web service run by Chalmers University of Technology. The IGS08 absolute antenna phase center variations are used to model the azimuthal and elevation dependence. Station coordinates obtained in the loosely constrained frame of JPL fiducial-free GPS orbits are transformed into the IGS08 reference frame using daily 7-parameter

transformations delivered by JPL. In order to reduce the common mode signal, we have specifically developed a terrestrial reference frame (called EU14) suitable for crustal deformation studies in and around that plate following the approach of Blewitt et al. (2013). This frame is defined by 6 Cartesian coordinates and velocities of each of 174 stations selected by specific quality criteria. The EU14 frame is aligned in origin and scale with IGB08. GPS velocities are obtained by fitting a linear trend plus annual and semi-annual terms and site specific offsets at position time-series, assuming a white plus flicker noise stochastic model.

3. Velocity combination

Prior to the velocity combination phase, all nuisance parameters needed to build the velocity solutions, such as local eccentricities, seasonal variations and position offsets, are solved consistently by each analysis group, in accordance with the station data quality and metadata accuracy. Thus, eventual inconsistencies in the definitions of reference markers and station position eccentricities do not concern the combination process. We consider each velocity field as a sample of the true velocity field while the combined velocity, as the best estimate of the true velocity field. The availability of different samples of the station velocities allows a sort of validation in which the velocity repeatability can be truly assessed. Another important advantage of combining the velocity field follows from the averaging effect, i.e. the combination of velocities obtained with almost independent procedures reduces to a minimum the chance of including biased velocities.

The velocity combination procedure is a generalization of the loosely constraints approach, first proposed by Heflin et al., (1992) and subsequently developed by Davies and Blewitt (2000). Blewitt (1998) evidenced an important property of the standard least squares theory, in which a functional model is fitted to a set of observations affected by a Gaussian noise. He demonstrates that refining the functional model by adding extra unknowns is equivalent, in the limit of unknown a priori information, to an augmentation of the stochastic model i.e. a redefinition of the noise process. In our framework, the functional model is a trivial identity between velocities, but in order to account for reference frame systematic errors, the functional model could be augmented through the estimation of additional reference frame biases. This augmentation is equivalent to enhancing the stochastic model through a loosening transformation of the covariance matrix (*sensu* Blewitt, 1998), so that it can be consid-

ered as the implicit estimation of additional parameters but without computing their full covariance. Loosely constrained solutions assign large errors to the implicit parameters and allow treating the differences between the observations as stochastic variables without the need to explicitly estimate them. In our context, loosening the reference frame constraints allows to save computation complexity, by waiving to Helmert transformation parameters and its covariances.

The three dimensional Cartesian velocities are combined in a least squares scheme and by treating the reference frame differences as a stochastic process. For this reason it is important to establish which parameters describe the actual reference frame transformation of our regional network. In global geodetic problems, the transformation of Cartesian coordinates of any point (X) between two terrestrial reference frames (TRF1 and TRF2) is expressed by the well-known Helmert transformation that, in its linearized form, reads

$$X_2 = X_1 + T + sX_1 + RX_1 \quad (1)$$

where T is the translation vector, s is the scale factor and R is the infinitesimal rotation matrix. All these parameters, including the position coordinates, are time-varying quantities. Then the time derivative of the Helmert transformation is

$$\dot{X}_2 = \dot{X}_1 + \dot{T} + \dot{s}X_1 + s\dot{X}_1 + \dot{R}X_1 + R\dot{X}_1 \quad (2)$$

It relates the velocities \dot{X}_1 and \dot{X}_2 expressed in two different TRFs in the most general way. Depending on the problem we are facing, the two velocity fields are affected by different biases s , R , \dot{T} , \dot{s} and \dot{R} , some of which possibly negligible or even highly correlated (degenerate case). The selected GPS networks span a geographical region of approximately 30x50 degrees, which is less than 5% of the whole Earth surface, therefore the Mediterranean region could be rightly treated as a small-scale network. In this approximation some parameters may be considered fully correlated and consequently degenerate. For instance R and \dot{R} represent respectively the rotation of velocity vectors and the rotation rate of the reference frame (plate-like rotation), thereby their effects may locally be indistinguishable especially if the two rotation axes are orthogonal. The same remarks apply to the translation rate and scale rate factors (\dot{T} and \dot{s}), describing the addition of a constant velocity and a vertically directed velocity, respectively. Locally, the \dot{T} vector may mimic a velocity variation in any arbitrary direction. Hence

in a confined small region, only three parameters are really independent and are adequate to describe the reference similarity transformation between two velocity fields

$$\dot{X}_2 = \dot{X}_1 + \dot{T} + s\dot{X}_1 + R\dot{X}_1 \quad (3)$$

In this approximation the reference frame transformation is independent from the vector positions, confining the whole combination process in the velocity phase space. This consequence is of fundamental importance, since it makes the velocity combination independent from the knowledge of the station position coordinates. Thus the unknowns that transform the velocity field into different reference frames are three translation rates (\dot{T}), three rotation angles (R) and one scale factor (s). A further simplification arises if all velocity solutions are obtained using the same datum (IGb08), and if the time series of the stations used to materialize the TRF are sufficiently long (in our case >15 years) so that common differences in the velocities, induced by center of mass motion, are expected to be negligible. In this case the similarity transformation reduces to a four parameters transformation where the rotation matrix (R) and the scale factor (s) describe most of the reference frame biases.

The functional model for the velocity combination is trivial, since each input velocity v_s should match the combined velocity v_c

$$v_s = A_{c \rightarrow s} v_c + v \quad (4)$$

where $A_{c \rightarrow s}$ is the reorder matrix that translates the combined velocity vectors to the order of the solution velocity vectors and v is the noise vector. Since the velocity solutions are considered independent among each other, the least squares solution for the combined velocities may be recursively defined as follows

$$v_c = \sum_s (A^T W_s A)^{-1} A^T W_s v_s \quad (5)$$

where W_s is the weight matrix ($W_s = C_s^{-1}$) of the solution (S), i.e. the inverse of the solution covariance matrix (C_s) and the summation runs over all the solutions.

The combination process consists of two main steps: the stochastic model augmentation, in which rotations and scale uncertainties are increased (i.e. covariance loosening) adopting a diagonal (E) matrix with 10 arc-sec and 10^{-4} respectively as assumed loosening parameters. The loosening constraints are in principle arbitrary and should be on the order of the expected systematic differences in order to allow the solutions

to rotate and scale by the required amount. The covariance augmentation is provided by the external (E) a-priori covariance matrix that changes the solution covariance matrix (C_s) as follows

$$C_{loose} = C_s + BEB^T \quad (6)$$

where the matrix B specifies which linear combinations will be relaxed. As an example, the loosening of a rigid rotation is modeled as usual by the rotation matrix ($x' = x + R\theta$), where θ is the vector of the 3 unknown angles and R contains the partials of the vector rotation transformation. In this case the B matrix in eq. 6 takes the form of the rotation matrix R ($B \equiv R$). The resulting covariance matrix is termed as loosened covariance (Blewitt, 1998) and is associated to the corresponding (unchanged) velocity solution. The second step consists in the least squares estimation of the combined velocity field, where the observations are the velocity solutions with the associated loosened covariances together with a fourth IGS velocity solution, used to establish the ITRF frame. We choose the latest update to the IGS08 solution (<ftp://igs-rf.engg.eu/pub/IGb08/>), called IGb08, which contains the best performing IGS stations and through their covariances contribute to realize the ITRF2008 frame. The 59 IGb08 common stations, located on the Eurasian, African and Arabian plates, conveniently define the ITRF2008 reference frame and act as fiducial ‘‘anchor’’ stations providing the datum constraints in the least squares problem. The combination is iterated twice in order to estimate the corresponding solution weighting factors, balancing mutual weights according to each solution chi-squared (χ^2) (Devoti et al., 2010)

$$\chi^2 = \Delta W_s \Delta^T \quad (7)$$

where Δ are the velocity residuals ($v_s - v_c$) and W_s the weight matrix for each solution (S).

Finally we foresee the possibility of forcing two or more parameters to be estimated together (e.g. tying velocities together). This is achieved using the classical method of Lagrange multipliers (e.g. Arfken et al., 2013), where the least square problem is solved with the equality constraints.

The resulting velocity field includes 1729 stations in the Euro-Mediterranean area from west of the Straits of Gibraltar to east of the Levantine Sea (Fig. 2). The average (median) 1-sigma standard deviation for the combined velocities is respectively 0.3 mm/y for the horizontal components and 0.7 mm/y for the

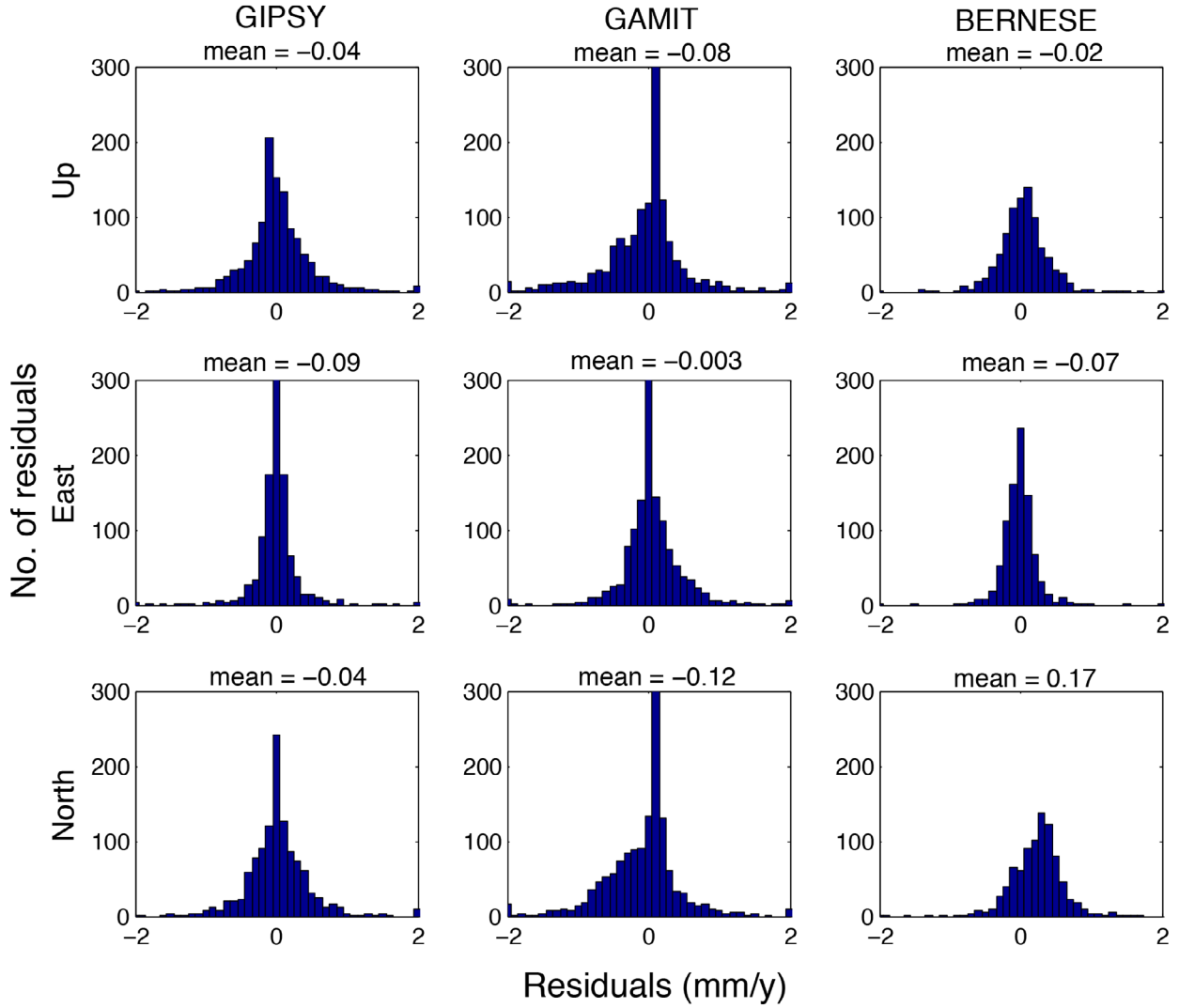


Figure 3. Histograms of velocity residuals with respect to the combined solution. Top, middle and lower rows are respectively the vertical, east and north components, columns from left to right refer to Gipsy, Gamit and Bernese residuals.

	# stations (edited)	Time Span Median, max, min(years)	Velocity residual Wrms (mm/Y)		Weighting factor
			Horiz.	3-D	
BERN	875 (3)	6.6 ^{17.3} _{2.5}	0.24	0.25	2.0
GIPSY	1107 (10)	7.6 ^{15.1} _{3.5}	0.20	0.22	0.7
GAMIT	1452 (20)	6.7 ^{21.5} _{2.5}	0.24	0.25	11.8
COMBI	1728	6.8 ^{21.5} _{2.5}	-	-	-

Table 3.

vertical component. The histograms of velocity residuals with respect to the combined solution, in the vertical, east and north components for each input solution, are shown in Figure 3. The weighted root mean square (WRMS) of the residuals ranges from 0.20 to 0.25 mm/y for the three input solutions (see Table 3), whereas the central tendencies (mean) are all within 0.1 mm in modulus except for the north com-

ponent of the GAMIT and BERNESE solutions (see Figure 3). The distributions do not differ significantly, although the GAMIT and BERNESE solutions show a slight skewness especially in the northern component showing a mean of -0.12 and 0.17 mm/y respectively. These values, although below the repeatability of the combined velocity, may suggest a slight misalignment of the three reference frames that cannot be accom-

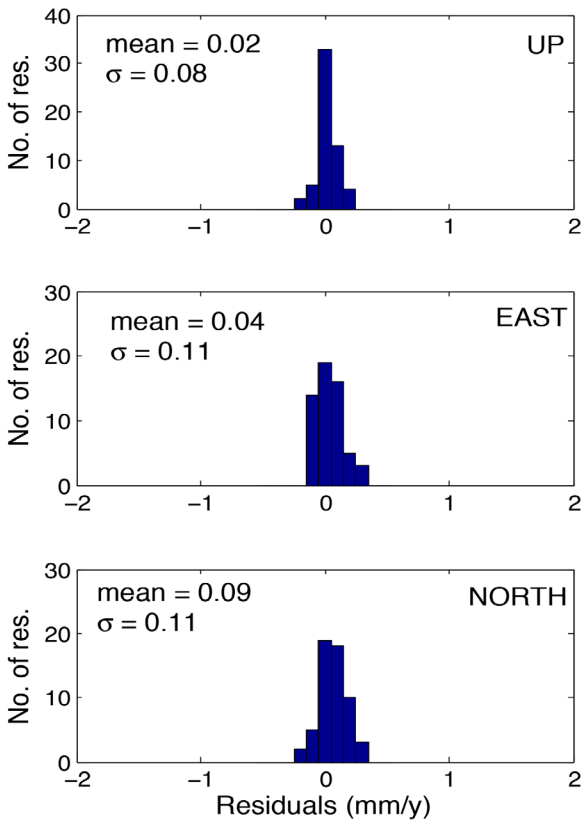


Figure 4. Histograms of velocity residuals of only the IGS stations with respect to the combined solution. Top, middle and lower panels show respectively the vertical, east and north components. Mean and standard deviations are indicated in units of mm/y.

modated by a rigid rotation and scale transformation, the only biases allowed to change in the combination process. At this time we were not able to isolate the input solution (or solutions) that causes such tiny effect, but we will track down the problem in the follow-on combination. The 59 European IGS stations used in this combination show a very little discrepancy with the IGB08 velocities, an overall WRMS of 0.12 mm/y indicates a robust repeatability of these long-lasting stations. Figure 4 shows the histogram of the IGS velocity residuals in the three spatial components. The IGS residuals in the north direction show again a modest bias (0.09 mm/y) with respect to the combined solution. Nevertheless the residuals and biases in the combined velocity field are well below and consistent with the given standard deviations (0.3 and 0.7 mm/y in the horizontal and vertical components respectively).

4. Technical issues and adopted conventions

A major problem in combining independent velocity solutions is the recognition of the station identity, since no naming convention is guaranteed in an open environment. Worldwide permanent GNSS stations are generally identified by a 4-character ID and,

eventually a IERS domes number (9 characters) univocally assigned by the Institut Géographique National (IGN), acting as a central authority to avoid overlays. This procedure has become standard in the IGS community. The GNSS stations must strictly comply to the IGS requirements and should be registered in the IGS data-base which, in turn, is not envisaged as a compelling procedure outside the IGS service. In Italy more than 50 networks contribute to the INGV data archive and are generally not involved in IGS activities. Therefore a thorough regulation of ID uniqueness is difficult to maintain. Instead of forcing an a-priori naming convention at the database or data archive level, we decide to adopt an a-posteriori approach based on the assignment of a unique label based on the station positions (i.e. geo-coding). In particular, we choose the GHAM code proposed by Agnew, (2005), to label each GPS station unambiguously. The GHAM code is composed of alternating letters and numbers, providing tags to geographic locations and defining addresses of equal-area cells with arbitrary precision. We choose a 12-character code that corresponds to a cell size of 1.9 m (square root of area), which is sufficiently small to identify a single GNSS antenna installation. The main advantage of this technique is the possibility to automate the site recognition process reducing the amount of knowledge to a minimum (only 12 characters). The geo-code has also an interesting hierarchical sorting property, in that alphabetically sorted codes group stations that would be nearby in space.

For simplicity and traceability of the GNSS stations in the combined solution, all the input 4-character IDs are preserved so that each station can be univocally identified by both the geo-code and the 4-character ID. Thus multiple velocities, referring to the same station (same geo-code) but different 4-character ID, will be estimated as tied velocities and appear independently in the combined solution but having the same velocities and covariances. Forcing two or more velocities to be estimated together (tied velocities) is achieved using the classical method of Lagrange multipliers (e.g. Arfken et al., 2013), where the least squares are solved with the constraints of having equal velocities.

The proposed combination approach provides a computationally efficient algorithm to combine a large number of station velocities in a region of limited size like the Euro-Mediterranean area. It completely neglects the station positions, which may be known only approximately (~ 1 m) and is able to combine velocities expressed also in different ITRF reference frames sin-

A COMBINED VELOCITY FIELD OF THE MEDITERRANEAN REGION

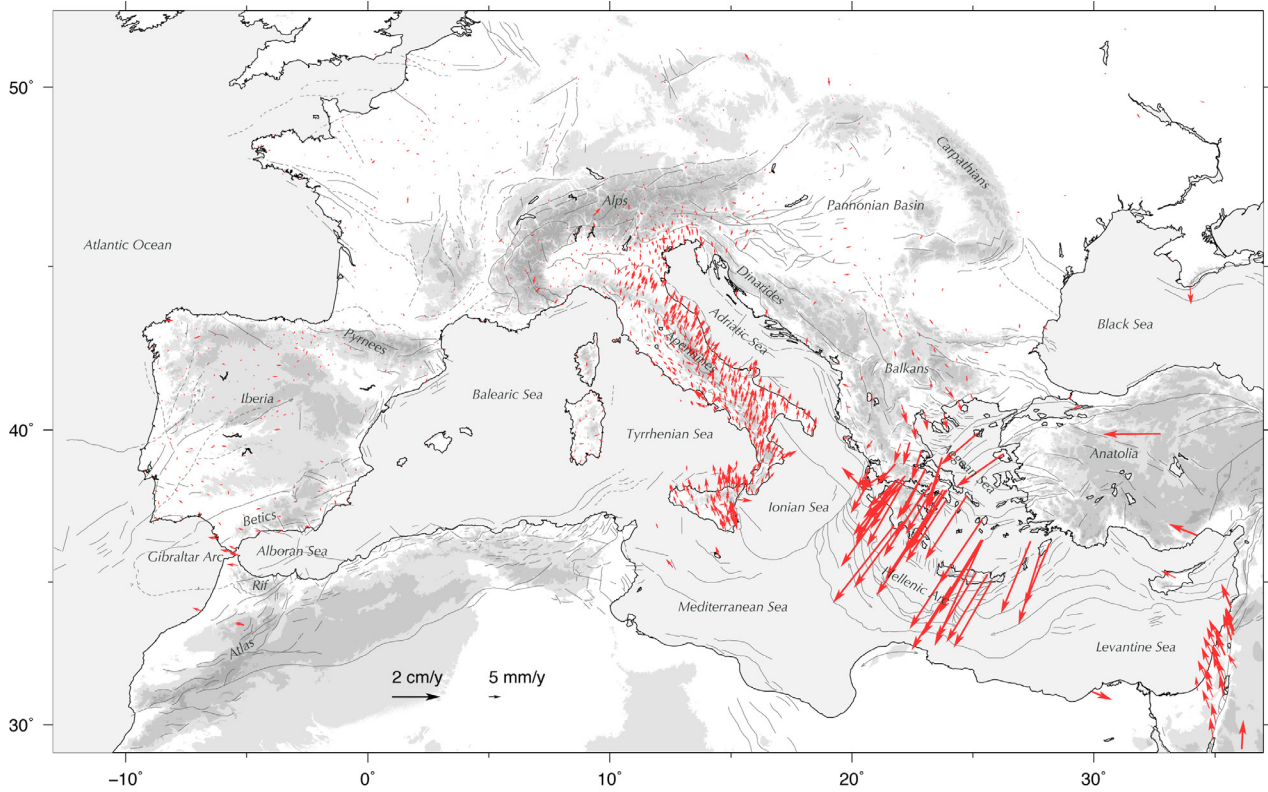


Figure 5. Map of the horizontal GPS velocities (in the Eurasian-fixed frame) from the combined solution. Error ellipses are not shown here for clarity of the figure.

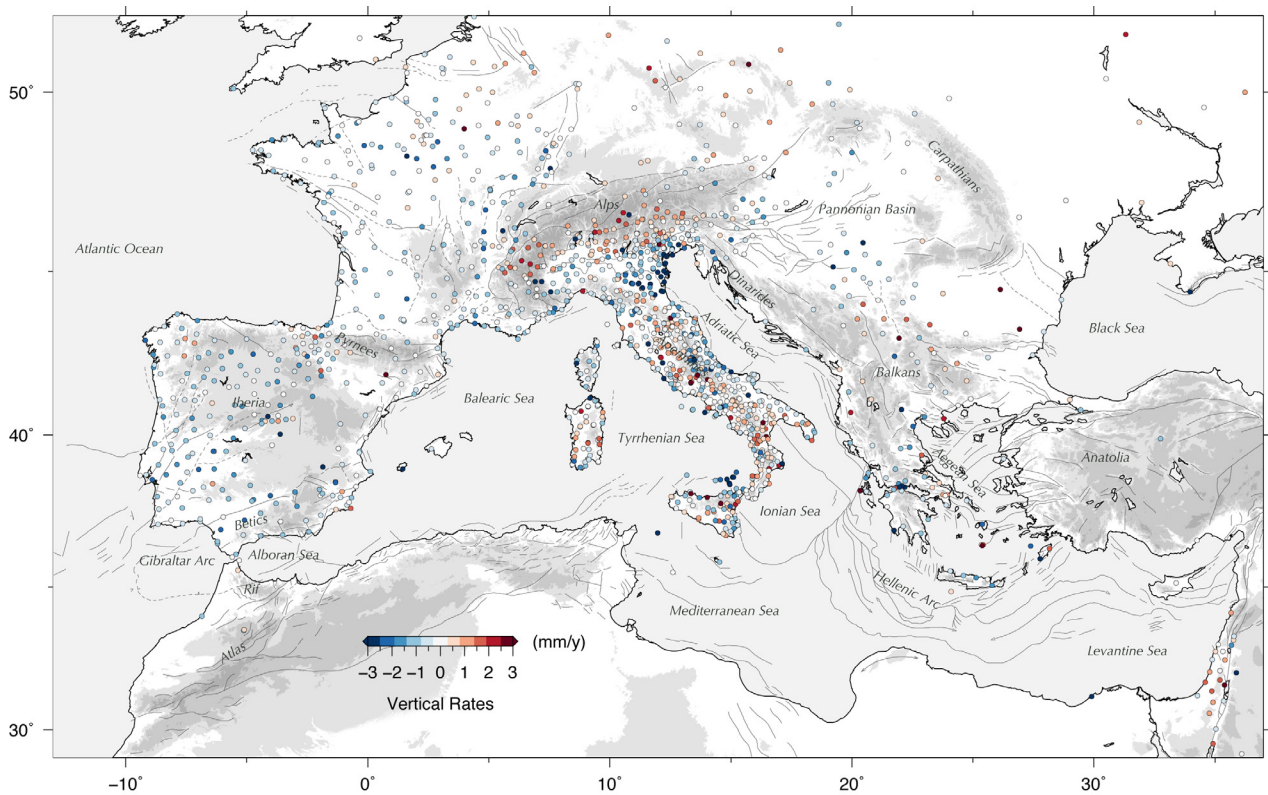


Figure 6. Map of the absolute (i.e. IGB08 frame) vertical GPS velocities of the combined solution.

ce the systematic differences are treated as stochastic variables Equation (6). The time series discontinuities, seasonal variations and local antenna eccentricities are treated in the earlier processing stage and could be sol-

ved for independently by each processing center. This may lose some modeling parameters, such as seasonal variations and position offsets, since each time series is processed independently but the main advantage is

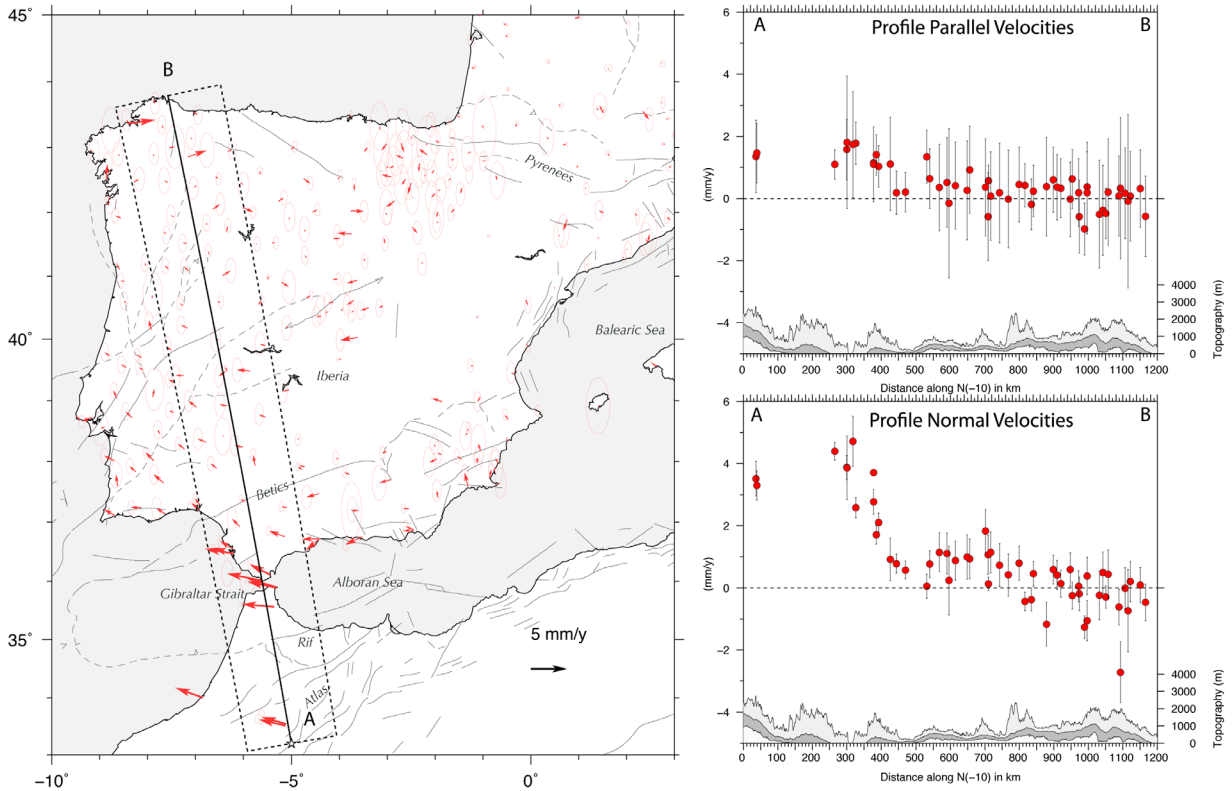


Figure 7. Left: combined Eurasian-fixed horizontal velocities (with 95% error ellipses) for the Iberian region. Right: profile parallel and profile normal velocity components (with error bars showing the 2σ uncertainties) projected along a $N10^\circ W$ cross section from northern Africa to northern Iberia (see the dashed black box in the left panel). The dark grey areas show the average (median) topography in the profile swath, with the light grey and white areas showing the maximum and minimum elevations, respectively.

a very quick and rather simple combination of GNSS networks addressed to assimilate a large number of a very quick and rather simple combination of GNSS networks addressed to assimilate a large number of crustal velocities in a common reference frame. The method uses the complete input covariances, if available, and definitely provides the complete covariance matrix of the combined velocity field.

5. Results: Europe-Africa boundary zone deformation

The combined horizontal velocity solution, estimated with respect to the stable Eurasian plate (Figure 5) and the vertical rates in the IGB08 frame (Figure 6), highlight with unprecedented details the 3D kinematics of a large portion of the Euro-Mediterranean region, with dense spatial sampling of crustal deformation across the Mediterranean plate boundary and the most important active fault systems. Although some of the station velocities have been already published elsewhere, and the overall surface kinematics is well known and discussed in several recent papers (e.g. Nocquet, 2012; Serpelloni et al., 2013; Kreemer et al., 2014; Métois et al., 2015; Palano et al., 2015), here the velocity field is represented for the first time at the Eurasian plate scale with homogeneous standards, best

available spatial resolution and special care for reference frame stability. Moreover the velocity field is obtained by re-processing the whole data set with different

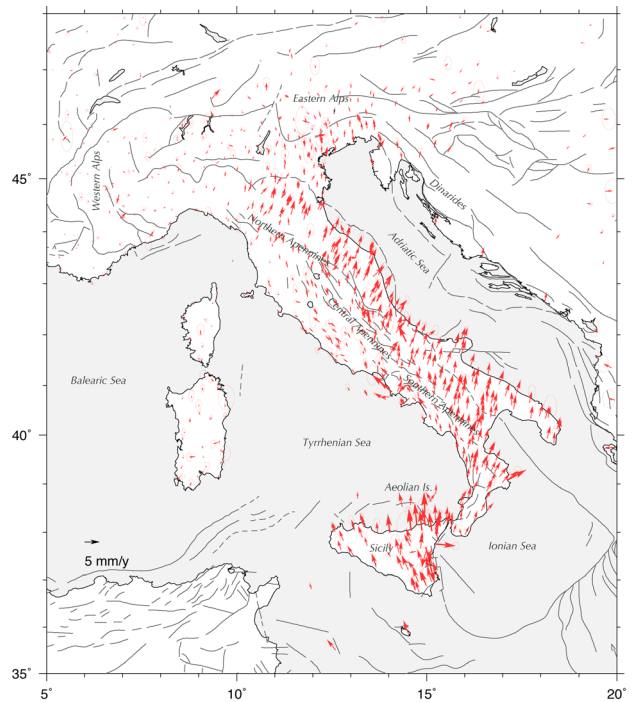


Figure 8. Combined Eurasian-fixed horizontal velocities (with 95% error ellipses) for the Italian region.

A COMBINED VELOCITY FIELD OF THE MEDITERRANEAN REGION

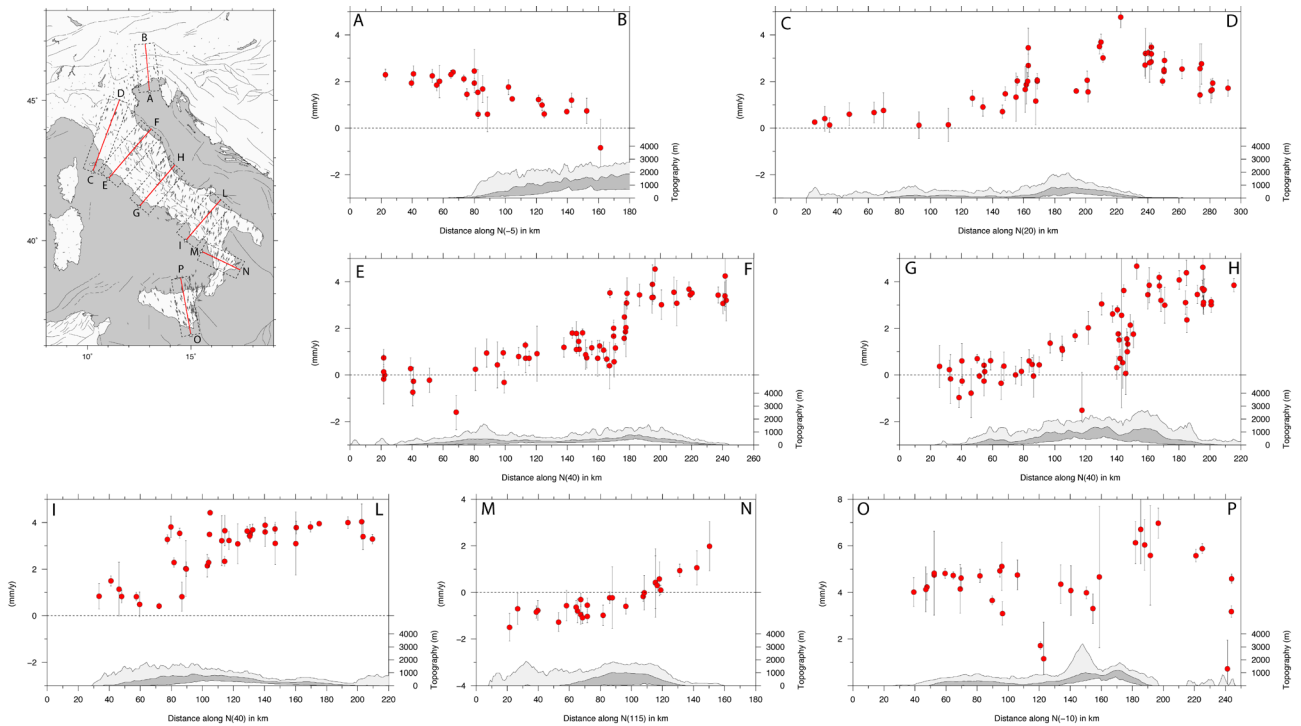


Figure 9. Selected velocity profiles (parallel projections) of the Italian peninsula. A-B profile across the Southeastern Alps, from C-D to P-O profiles along the Apennine chain, from northern Apennines to eastern Sicily. The dark grey areas show the average (median) topography in the profile swath, with the light grey and white areas showing the maximum and minimum elevations, respectively.

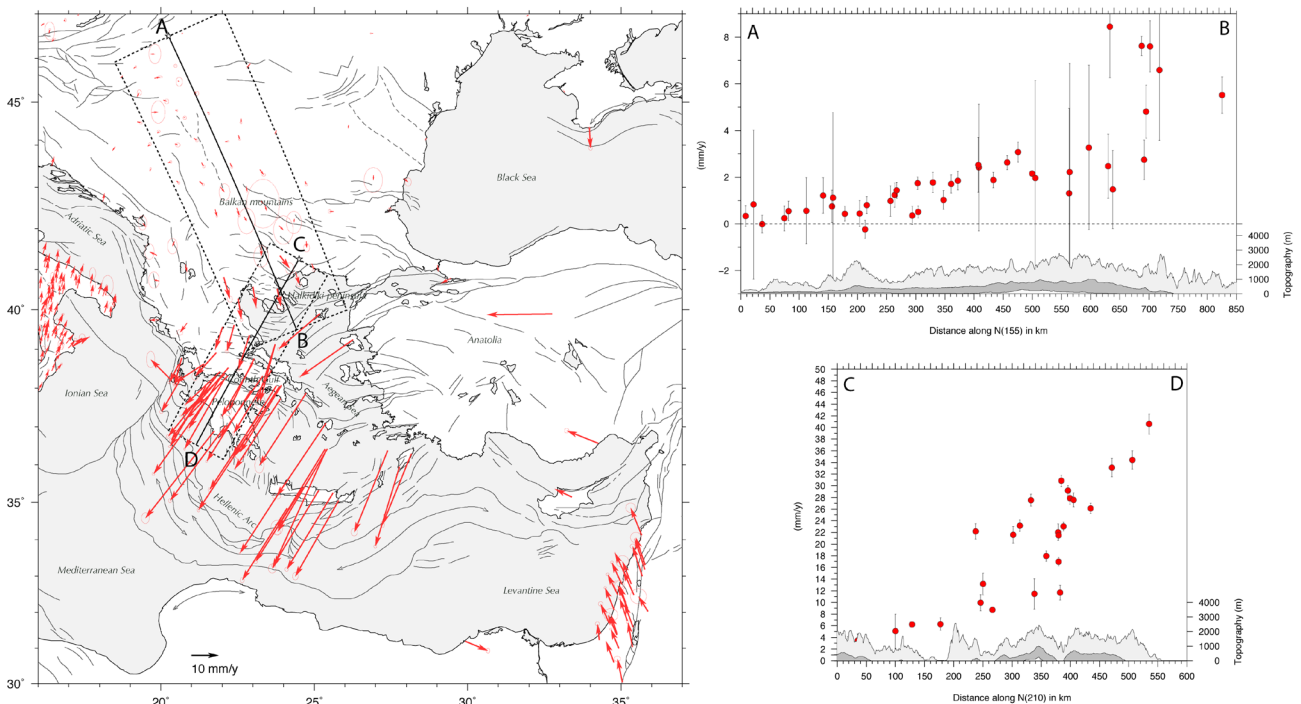


Figure 10. Left: combined Eurasian-fixed horizontal velocities (with 95% error ellipses) for the Balkans and Aegean region. Right: profile parallel velocity components (with error bars showing the 2σ uncertainties) projected along a $N155^\circ E$ (A-B) and $N210^\circ E$ (C-D) cross sections. The dark grey areas show the average (median) topography in the profile swath, with the light grey and white areas showing the maximum and minimum elevations, respectively.

approaches and combining the velocity fields with the aim of building on a regular basis a high level GPS pro-

duct for the scientific community. The combination ensures that solution specific biases, eventually indu-

Network	Location	Official-Owner	Provider	Sites
ABRUZZO	Central-Italy	Regione Abruzzo	http://gnssnet.regione.abruzzo.it/	20
AGROS	Serbia	Republic Geodetic Authority of Serbia	http://agros.rgz.gov.rs/	31
ALBANIA	Albania	GPScope, CNRS, France	https://gpscope.dt.insu.cnrs.fr/chantiers/albanie/	4
ASI	Italy	ASI-GEODAF, Matera	http://geodaf.mt.asi.it/	12
ASSOGEO	Central-Italy	ASSOGEO SpA	http://gnssnet.regione.abruzzo.it/	26
BASILICATA	Southern-Italy			4
CALABRIA	Southern-Italy	Protezione Civile, Regione Calabria	http://www.protezionecivilecalabria.it/	17
CAMPANIA	Southern-Italy	Regione Campania	http://gps.sit.regione.campania.it/	14
CARM	Murcia, Spain	Región de Murcia	http://147.84.216.57/	3
CATNET	Catalunya, Spain	Institut Cartogràfic y Geològic de Catalunya	http://www.icc.cat/Home-ICC/Geodesia	10
CORINTH	Gulf of Corinth	INSU-CNRS, France and NOA, Greece	https://gpscope.dt.insu.cnrs.fr/chantiers/corinthe/	10
CVN	Northern-Italy	Consorzio Venezia Nuova	https://gpscope.dt.insu.cnrs.fr/chantiers/corinthe/	10
EGYPT	Alexandria, Egypt	Centre d'Etudes Alexandrines	http://www.sonel.org/-GPS-.html	1
EMILIA	Northern-Italy	Fond. Geometri e G. Laureati	http://www.fondazionegeometrier.it/	13
ERVA	Valencia, Spain	Institut Cartogràfic Valencià	http://icverva.icv.gva.es:8080/	8
EUREF	Europe	EUREF Consortium	http://www.epncb.oma.be/	252
EUSKADI	Basque, Spain	Comunidad Autónoma de Euskadi	http://www.gps2.euskadi.net/	11
FREDNET	Northern-Italy	OGS-CRS, Centro di Ricerche	http://frednet.crs.inogs.it/	16
FVG	Northern-Italy	Regione Friuli-Venezia-Giulia	http://gnss.regione.fvg.it/dati-GPS/	10
GALNET	Galicia, Spain	TOPCAD INGENIERIA S.L.	http://cartogalicia.com/galnet2/	16
GNSSPIEMONTE	Northern-Italy	Regione Piemonte	http://gnss.regione.piemonte.it	13
GRAF	Germany	BKG, Bundesamt für Kartographie und Geodäsie	http://www.bkg.bund.de/geodIS/GREF/DE/01Home/	19
GNSSPIEMONTE	Northern-Italy	Regione Piemonte	http://gnss.regione.piemonte.it	13
ICM	Madrid, Spain	Comunidad de Madrid	www.madrid.org/cartografia/planea/cartografia/html/web/VisorGps.htm	7
IGNE	Spain	Instituto Geográfico Nacional	http://www.ign.es/ign/layoutIn/geodesiaEstacionesPermanentes.do	8
IGS	Eurasia	International GNSS Service	https://igs.cb.jpl.nasa.gov/	27
INFN	Central-Italy	LNGS-INFN		1
IREALP	Northern-Italy	IREALP, Lombardia		13
ITACYL	Castilla y Leon, Spain	Inst. Tecnológico Agrario de Castilla y León	http://gnss.itacyl.es/	32
ITALPOS	Italy	Leica Geosystems SpA	http://smartnet.leica-geosystems.it/SpiderWeb/frmIndex.aspx	181
LARIOJA	La Rioja, Spain	Government of La Rioja	http://www.iderioja.larioja.org/?id=20&lang=en	5
LAZIO	Central-Italy	Regione Lazio	http://gnsslazio.no-ip.org/Spiderweb/frmIndex.aspx	18
LIGURIA	Northern-Italy	Regione Liguria	http://www.gnssliguria.it/	7
METRICA	Greece	Metrica S.A.	http://www.metricanet.gr/	25
NETGEO	Italy	Topcon Positioning Italy	http://www.netgeo.it/	112
NOA	Greece	National Observatory of Athens	http://www.gein.noa.gr/services/GPS/noa_gps.html	15
OLGGPS	Austria	Austrian Academy of Sciences, Space Research Institute	ftp://olggps.oeaw.ac.at/pub/	26
PIEMONTE	Northern-Italy	ARPA Piemonte	http://webgis.arpa.piemonte.it/gpsquakenet/GPSQuakeNET.php	6
PUGLIA	Southern-Italy	Regione Puglia	http://gps.sit.puglia.it/SpiderWeb/frmIndex.aspx	12
RAP	Andalucía, Spain	Junta de Andalucía	http://www.ideandalucia.es/portal/web/portal-posicionamiento/rap	23

A COMBINED VELOCITY FIELD OF THE MEDITERRANEAN REGION

REGAM	Murcia, Spain	Region de Murcia	http://cartomur.imida.es/regam/index.htm	10
RENAG	S-E France	RENAG consortium	http://webrenag.unice.fr/	46
RENEP	Portugal	DGT, Direção-Geral do Território	http://www.dgterritorio.pt/cartografia_e_geodesia/geodesia/redes_geodesicas/renep/	35
REP	Extremadura, Spain	DGT, Direção-Geral do Território	http://www.rep-gnss.es/	11
RGAN	Navarra, Spain	Gobierno de Navarra	http://www.navarra.es/appsext/rgan/default.aspx	14
RGP	France	IGN, Inst. Nat. L'Information Géographique Forestière	http://rgp.ign.fr/	190
RING	Italy	INGV, Istituto Nazionale di Geofisica e Vulcanologia	http://ring.gm.ingvit/	172
SARNET	Sardinia, Italy	Geodesia e Technologie Srl	http://topografia.unica.it/index.php?option=com_wrapper&Itemid=82	12
SIGNAL	Slovenia	Geodetski inštitut Slovenije	http://www.gu-signal.si/	24
SOI	Israel	Survey of Israel		20
SPLIT	Split, Croatia	Hydrographic Institute	http://www.sonel.org/-GPS-.html	1
STPOS	Northern-Italy	Provincia autonoma di Bolzano	http://www.stpos.it/Spiderweb/	7
TPOS	Northern-Italy	Provincia autonoma di Trento	http://www.catasto.provincia.tn.it/TPOS	10
UMBRIA	Central-Italy	Regione Umbria, Università degli Studi di Perugia	http://labtopo.ing.unipg.it/labtopo/	15
UNAVCO	Southern-Italy	UNAVCO data archive	http://www.unavco.org/	20
VENETO	Northern-Italy	Regione Veneto	http://retegnssveneto.cisas.unipd.it/	15

Table 2.

ced by the actual analysis procedure, are averaged out and possibly minimized, in the sense that for a combined solution the chance of having biased velocities is minimized with respect to a single solution. From a user point of view, the availability of standardized regional solutions favors multi-disciplinary access to high-level geodetic products enabling scientific stakeholders unfamiliar with geodetic techniques to benefit of the updated maps of crustal motion in their studies. In particular the wealth of stations allows to accurately map the accumulation of strain and crustal motion over a ~4000 km long plate boundary.

The kinematic boundary conditions in the Mediterranean are represented by the ~N-S Africa-Eurasia convergence. The NE-ward to N-ward motion of the Adriatic domain and the W-ward to SW-ward motions of the Anatolian and Aegean plates highlight the kinematics of the most important microplates of the Mediterranean area (McKenzie, 1970). Plates and microplates relative motions are accommodated across the major plate boundary zones, well mapped by the release of seismicity. Deviation from the major plate motions in the Mediterranean implies that additional geodynamic processes are required to explain the observed velocity field. The goal of this work is not that of discussing the tectonic and geodynamic implications of the newly proposed velocity field. In the following we present regional and more detailed velocity maps, including some velocity cross-sections

through the major deformation belts of the Mediterranean area.

In the western Mediterranean (Figure 5 - 6) the transition from oceanic-oceanic to continent-continent boundary shows a gradual widening of the deformation zone. Around the Alboran Sea, in southern Spain, the western Betics and in northwestern Morocco, the Moroccan Rif show a wide deformation pattern that cannot reflect a simple plate boundary interaction (see e.g. Monna et al., 2014; Chalouan et al., 2014). North Iberia and across the Pyrenees including the Balearic islands show no detectable motion with respect to Eurasia plate, nor significant vertical deformation (Figure 6). Figure 7 displays the velocity projections along a N10°W profile across the Strait of Gibraltar and the western Iberian region. The profile parallel components from south to north show a gradual decrease of the velocity projections from 1.5-2 mm/y to ~0 at north of the Betics (about 200 km inland from the Strait) indicating active shortening tectonic process. The profile normal projections show the right-lateral shear between the African plate and the Iberian peninsula with about 4 mm/y accommodated across the Strait of Gibraltar and the Betics, with the velocity components reaching zero at about the same 200km distance. The horizontal velocities also show a clockwise rotation, especially visible in southern Iberia crossing the Strait of Gibraltar from east to west.

North of Sicily (Figure 8), most of the African motion is absorbed offshore in the southern Tyrrhenian thrust system. The Apennines show extension with a strain rate axis at $\sim 90^\circ$ from the plate convergence vector. The Eastern Alps and the Dinarides accommodate N-NE motion of the Adriatic Sea relative to Eurasia. The Alps and Apennines show present uplift at different rates (1-3 mm/y) whereas subsidence is dominating in the Aeolian islands, NE of Sicily and along the Po plain, in northern Italy (Figure 6). The velocity projections across the Italian peninsula (Figure 9) clearly show how the new combined velocity field well samples the velocity gradients across the major seismically active belts. Profile A-B shows the NS compression in the Southeastern Alps (A-B) and the extensional patterns across the Apennine chain from north (C-D) across the Ferrara Arc facing the Po plain. In particular, this profile shows the crustal extension at a rate of about 3 mm/y across the Apennine belt and the compression at about 2 mm/y towards the Adriatic foreland. Other profiles (E-F, G-H, I-L, M-N) show different rates of extension at 3-4 mm/y along the Apennines from north to south. The profile (O-P) that crosses Sicily from south to north shows a significant extension in correspondence of the Peloritani Mountains, NE of Sicily, and compression close to the northern edge in the Aeolian Islands.

In the eastern Mediterranean the subduction along the Hellenic Arc dominates the tectonic deformation of the whole area (Papazachos, 1988; Wortel et al., 1990). The region between the Dinaric and the Balkan mountains, shows an increasing velocity from the Pannonian basin to the southernmost Macedonia (Figure 10). The profile A-B along the SSE direction shows the progressive increasing of the displacement rate up to 4-6 mm/y in the Halkidiki peninsula. The C-D profile, SSW oriented, depicts the velocity increase across the Isthmus of Corinth and the Peloponnese gaining a rate of about 40 mm/y near the Hellenic trench.

The large number of available GPS stations scattered in different regions of the investigated area, meets spatial densities that allows detailed estimates of the strain rate field, providing important information to improve probabilistic seismic hazard models (e.g. Bird et al., 2015). Under appropriate assumptions that the strain rate can be converted into an estimate of the rate at which strain energy is accumulating, it becomes possible to identify areas where relative changes of strain may correspond to points where energy will be possibly released in future seismic events.

Acknowledgements. We thank all of the agencies that have made the GPS observations available for this study. A complete list of such agencies is available on table 2. The RING network was partially funded by the Italian Ministry of Education University and Research (MIUR) through the «Programma per la Sismologia e l'Ingegneria Sismica» (PROSIS) and partially funded by the Italian Civil Protection Department (DPC). The data processing was partially funded by the MIUR within the National Research Program 2011–2013 COFIN MIUR 2010–2011 research project 'Response of morphoclimatic system dynamics to global changes and related geomorphologic hazard' and the COASTSAT project, funded by the Italian Space Agency.

References

- Agnew, D. C. (2005). GHAM: a compact global geocode suitable for sorting, *Comput. Geosci.*, 31, 1042–1047, doi:10.1016/j.cageo.2005.02.007.
- Arfken, G. B., H. J. Weber, F. E. Harris (2013). *Mathematical Methods for Physicists, A comprehensive guide*, 7th ed., Academic Press, Elsevier Inc., Oxford, 2013.
- Avallone, A. et al. (2010). The RING network: improvements to a GPS velocity field in the central Mediterranean, *Ann. Geophys.*, 53(2), 39–54, doi:10.4401/ag-4549.
- Bertiger, W., S. D. Desai, B. Haines, N. Harvey, A. W. Moore, S. Owen, J. P. Weiss, (2010). Single receiver phase ambiguity resolution with GPS data, *J. Geod* 84:327–337, doi:10.1007/s00190-010-0371-9.
- Beutler, G., H. Bock, R. Dach, P. Fridez, A. Gäde, U. Hugentobler, A. Jäggi, M. Meindl, L. Mervart, L. Prange, S. Schaer, T. Springer, C. Urschl, P. Walser, (2007). *Bernese GPS Software Version 5.0*, Edited by R. Dach, U. Hugentobler, P. Fridez, M. Meindl, Astronomical Institute, University of Bern, January 2007.
- Bird, P., D.D. Jackson, Y.Y. Kagan, C. Kreemer, and R.S. Stein (2015). GEAR1: A Global Earthquake Activity Rate model constructed from geodetic strain rates and smoothed seismicity, *Bull. Seism. Soc. Am.*, 105, 2538-2554.
- Blewitt, G. (1998), *GPS Data Processing Methodology From Theory to Applications*. In *GPS for Geodesy*, p. 231-270, Eds. P.J.G. Teunissen and A. Kleusberg, Springer-Verlag, Berlin.
- Blewitt, G., C. Kreemer, W.C. Hammond, and J.M. Goldfarb, (2013). Terrestrial reference frame NA12 for crustal deformation studies in North America. *J. of Geodynamics*, 72, pp. 11-24, doi:10.1016/j.jog.2013.08.004.
- Boehm, J., A. Niell, P. Tregoning, H. Schuh, (2006). Global Mapping Function (GMF): a new empirical mapping function based on numerical weather model data. *Geophys. Res. Lett.*, vol. 33, L07304,

doi:10.1029/2005GL025546.

- Caporali, A., C. Aichhorn, M. Barlik, M. Becker, I. Fejes, L. Gerhatova, D. Ghitau, G. Grenerczy, J. Hefty, S. Krauss, D. Medak, G. Milev, M. Mojzes, M. Mulic, A. Nardo, P. Pesec, T. Rus, J. Simek, J. Slezinski, M. Solaric, G. Stangl, B. Stopar, F. Vespe, G. Virag (2009) Surface kinematics in the Alpine–Carpathian–Dinaric and Balkan region inferred from a new multi-network GPS combination solution, *Tectonophysics*, Vol. 474, 295–321, doi: 10.1016/j.tecto.2009.04.035.
- Chalouan, A., A.J. Gil, J. Galindo-Zaldívar, M. Ahmamu, P. Ruano, M.C. De Lacy, A.M. Ruiz-Armenteros, M. Benmakhlouf, F. Riguzzi, (2014). Active faulting in the frontal Rif Cordillera (Fes region, Morocco): Constraints from GPS data. *Journal of Geodynamics*, 77, 110–122. DOI: 10.1016/j.jog.2014.01.002
- Davies, P., and G. Blewitt, (2000). Methodology for global geodetic time series estimation: A new tool for geodynamics, *J. Geophys. Res.*, Vol. 105, No. B5, pp. 11,083–11,100.
- Devoti, R, G. Pietrantonio, A. R. Pisani, F. Riguzzi, E. Serpelloni, (2010). Present day kinematics of Italy. In: M. Beltrando, A. Peccerillo, M. Mattei, S. Conticelli, C. Doglioni (eds) *J. Virtual Explor.* 36(2), doi:10.3809/jvirtex.2009.00237.
- Devoti, R., G. Pietrantonio, F. Riguzzi (2014). GNSS networks for geodynamics in Italy. *Fisica de la Tierra*, vol. 26, pp. 11–24.
- Dong, D., T.A. Herring, R.W. King, (1998). Estimating Regional Deformation from a Combination of Space and Terrestrial Geodetic Data. *J. Geod.*, 72, 200–214, doi:10.1007/s001900050161.
- Dong, D., P. Fang, Y. Bock, F. Webb, L. Prawirodirdjo, S. Kedar, P. Jamason (2006), Spatiotemporal filtering using principal component analysis and Karhunen-Loeve expansion approaches for regional GPS network analysis, *J. Geophys. Res.*, 111, B03405, doi:10.1029/2005JB003806.
- Dow, J.M., R. E. Neilan, C. Rizos, (2009). The International GNSS Service in a changing landscape of Global Navigation Satellite Systems, *J. of Geodesy* vol. 83, 191–198, doi: 10.1007/s00190-008-0300-3.
- Heflin, M., W. Bertiger, G. Blewitt, A. Freedman, K. Hurst, S. Lichten, U. Lindqwister, Y. Vigue, F. Webb, T. Yunck, J. Zumberge, (1992). Global geodesy using GPS without fiducial sites. *Geophys. Res. Lett.* 19: doi: 10.1029/91GL02933.
- Herring, T. A., R. W. King, M. A. Floyd, S. C. McClusky (2015). Introduction to GAMIT/GLOBK, Release 10.6, Massachusetts Institute of Technology, Cambridge, MA.
- Kreemer, C., G. Blewitt, E.C. Klein (2014). A geodetic plate motion and Global Strain Rate Model, *Geochemistry, Geophysics, Geosystems*, 15, 3849–3889, doi:10.1002/2014GC005407.
- Le Pichon, X., C. Kreemer, (2010). The Miocene-to-Present Kinematic Evolution of the Eastern Mediterranean and Middle East and Its Implications for Dynamics, *Annu. Rev. Earth Planet. Sci.*, 38, 323–351.
- Lyard, F., F. Lefevre, T. Letellier, and O. Francis (2006). Modelling the global ocean tides: Modern insights from FES2004, *Ocean Dyn.*, 56(5–6), 394–415, doi:10.1007/s10236-006-0086-x.
- McKenzie, D.P., (1970). Plate tectonics of the Mediterranean region, *Nature*, 226, 239–243,
- Métois, M., N. D’Agostino, A. Avallone, N. Chamot-Rooke, A. Rabaute, L. Duni, N. Kuka, R. Koci, and I. Georgiev (2015). Insights on continental collisional processes from GPS data: Dynamics of the peri-Adriatic belts, *J. Geophys. Res. Solid Earth*, 120, 8701–8719, doi:10.1002/2015JB012023.
- Monna, S., A. Argnani, G.B. Cimini, F. Frugoni, C. Montuori (2014). Constraints on the geodynamic evolution of the Africa–Iberia plate margin across the Gibraltar Strait from seismic tomography. *Geoscience. Frontiers*, vol. 6(1), 39–48, doi:10.1016/j.gsf.2014.02.003.
- Niell, A.E., (1996). Global mapping functions for the atmosphere delay at radio wavelengths, *J. Geophys. Res.*, vol. 101, n. B2, 3227–3246, doi: 10.1029/95JB03048.
- Nocquet, J.M. (2012). Present-day kinematics of the Mediterranean: A comprehensive overview of GPS results, *Tectonophysics* 579, 220–242, doi:10.1016/j.tecto.2012.03.037.
- Palano, M., P. J. González, J. Fernández (2015). The Diffuse Plate boundary of Nubia and Iberia in the Western Mediterranean: Crustal deformation evidence for viscous coupling and fragmented lithosphere, *Earth Planet. Sci. Lett.*, 430, 439–447, doi:10.1016/j.epsl.2015.08.040.
- Papazachos, B.C., (1988). Active tectonics in the Aegean and surrounding area. In: *Seismic Hazard in Mediterranean Regions* (ed. by J. Bonnin, M. Cara, A. Cisternas and R. Fantechi), pp. 301–331. Kluwer Academic Publisher, Dordrecht.
- Pérouse, E., N. Chamot-Rooke, A. Rabaute, P. Briole, F. Jouanne, I. Georgiev, D. Dimitrov, (2012). Bridging onshore and offshore present-day kinematics of central and eastern Mediterranean: Implications

for crustal dynamics and mantle flow, *Geochem. Geophys. Geosyst.*, 13, Q09013, doi:10.1029/2012GC004289.

Petit, G., B. Luzum, (2010). IERS Conventions (2010). IERS Technical Note No. 36, ssn:1019-4568, pp.179.

Serpelloni, E., C. Faccenna, G. Spada, D. Dong, S. D. P. Williams, (2013). Vertical GPS ground motion rates in the Euro-Mediterranean region: New evidence of velocity gradients at different spatial scales along the Nubia-Eurasia plate boundary, *J. Geophys. Res.*, 118 (11), 6003-6024, doi:10.1002/2013JB010102.

Wdowinski, S., Y. Bock, J. Zhang, P. Fang and J. Genrich, (1997). Southern California permanent GPS geodetic array: Spatial filtering of daily positions for estimating coseismic and postseismic displacements induced by the 1992 Landers earthquake, *J. Geophys. Res.*, 102(B8), 18057-18070, doi:10.1029/97JB01378.

Wortel, M. J. R., S. D. B. Goes, W. Spakman, (1990). Structure and seismicity of the Aegean subduction zone, *Terra Nova*, 2, 554-562.

Zumberge, J. F., M. B. Heflin, D. C. Jefferson, M. M. Watkins, F. H. Webb, (1997). Precise Point Positioning for the Efficient and Robust Analysis of GPS data from Large Networks, *J. Geophys. Res.*, 102, 5005-5017, doi:10.1029/96JB03860.

*Corresponding author: Roberto Devoti
Istituto Nazionale di Geofisica e Vulcanologia, Rome, Italy.

e-mail: roberto.devoti@ingv.it

©2017 by Istituto Nazionale di Geofisica e Vulcanologia. All rights reserved

Annex 2.6 : Presentation of BFHK done for EPOS meeting in Prague, Fev. 2017

EPOS COMBINATION STATUS REPORT

AMBRUS KENYERES
FOMI → **BFKH**

EPOS WP10 meeting, 27-28 February 2017, Prague

FOMI → BFKH

- FOMI as of 01.01.2017 had been completely moved under BFKH
- BFKH stands for: Government Office of Capital City Budapest
- Rationale: NOTHING (political decision to “decrease” of bureaucracy, but it is significantly increased ...)
- NO direct effect on the work in EPOS-IP
- The legal handling of the change is being managed within EPOS GA

~~FOM~~ → BFKH DDSS LIST

- MULTI-YEAR POSITION AND VELOCITY PRODUCT BASED ON WEEKLY SINEX COMBINATION FROM ALL AVAILABLE QUALIFIED/APPROVED SOURCES
 - CONTENT NOW:
 - EPOS PAN-EUROPEAN SOLUTIONS – station selection!
 - LATER MAY EXTENDED WITH ***EPN DENSIFICATION***
- DAILY COMBINED SINEX SERIES
 - CONTENT NOW:
 - EPOS PAN-EUROPEAN SOLUTIONS + KAN
 - LATER MAY EXTENDED WITH ***EPOS REGIONAL SOLUTIONS***

INPUT SOURCES:

(1) ALL YOU CAN EAT ... (AS PRESENT)
OR

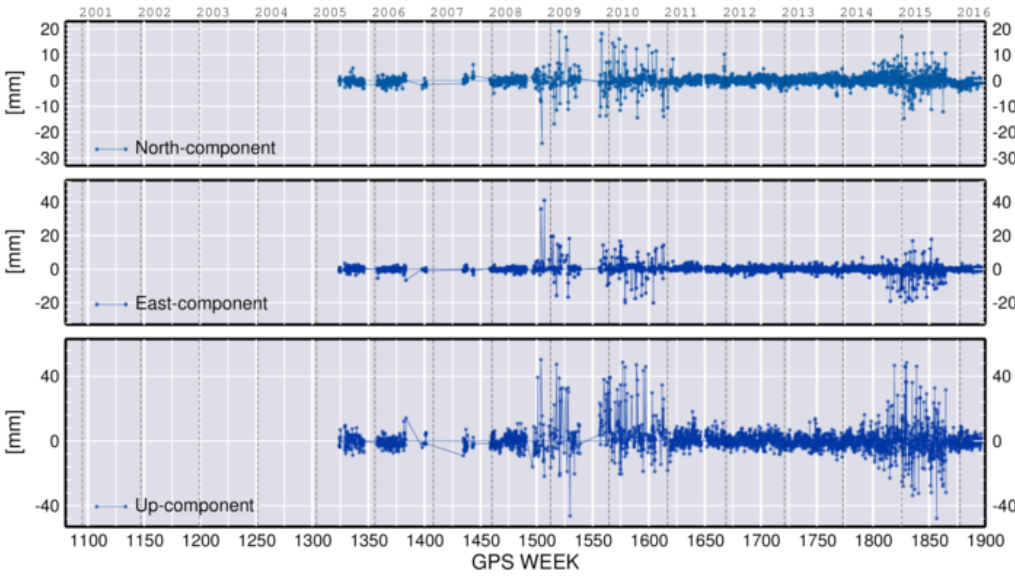
(2) SELECTION BASED ON VARIOUS CRITERIA
(! EPOS STANDARDS !)

- DATA (RINEX) AVAILABILTY
- META DATA AVAILABILITY
- DATA QUALITY – T3 (QC and time series scatter)
- STATION QUALITY (monumentation - “dancing” stations may excluded ...)

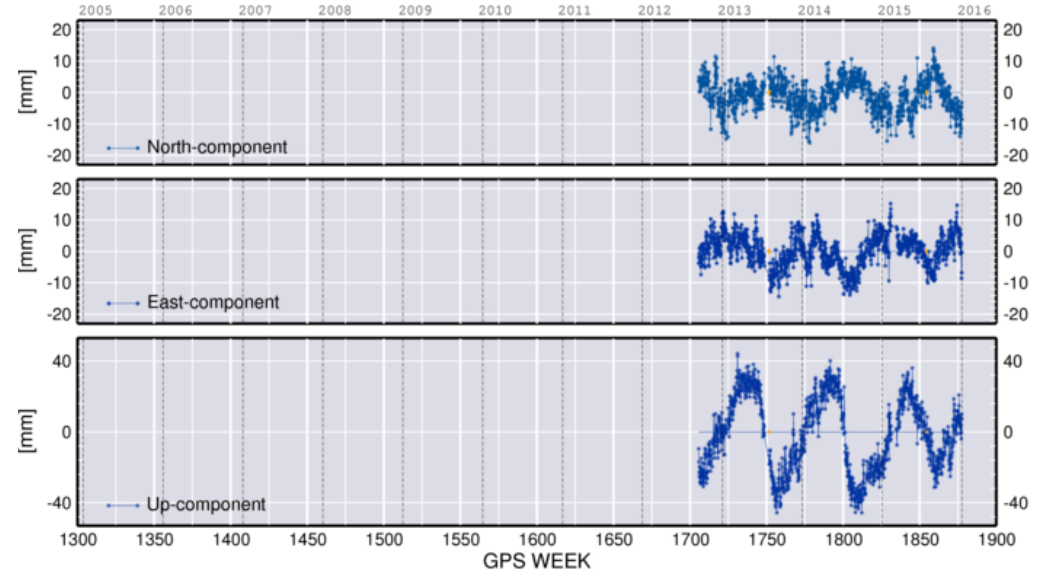
REVISION AND DECISION IS NEEDED NOW!

EXAMPLES

LEBE_10013V111

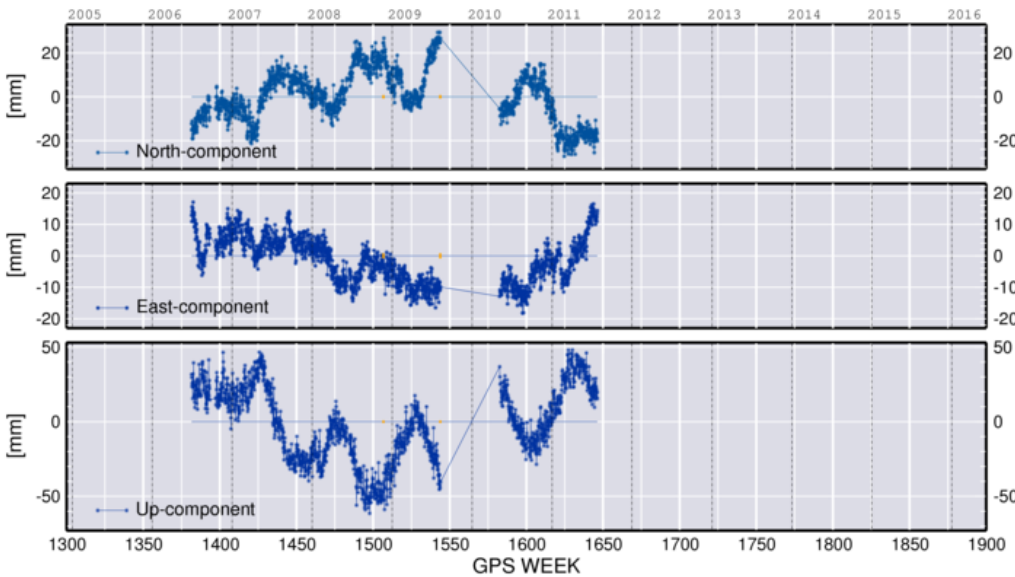


STEF_12646V111



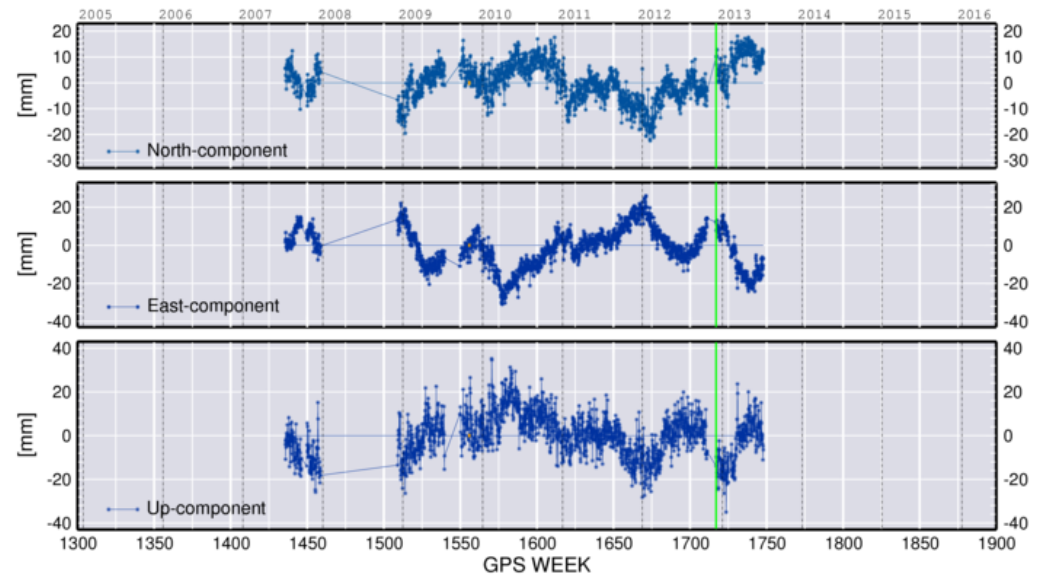
POS_ING00_daily

PES1_12790V222



A_UGA02_daily

NVRK_12630V111



UGA_UGA02_daily

UGA_UGA02_daily

COMBINED vs SINGLE AC

- ELIMINATION OF AC SPECIFIC ISSUES
 - SOFTWARE
 - PROCESSING STRATEGY
- HOMOGENEOUS REFERENCE FRAME REALIZATION
- HOMOGENEOUS OUTLIER HANDLING

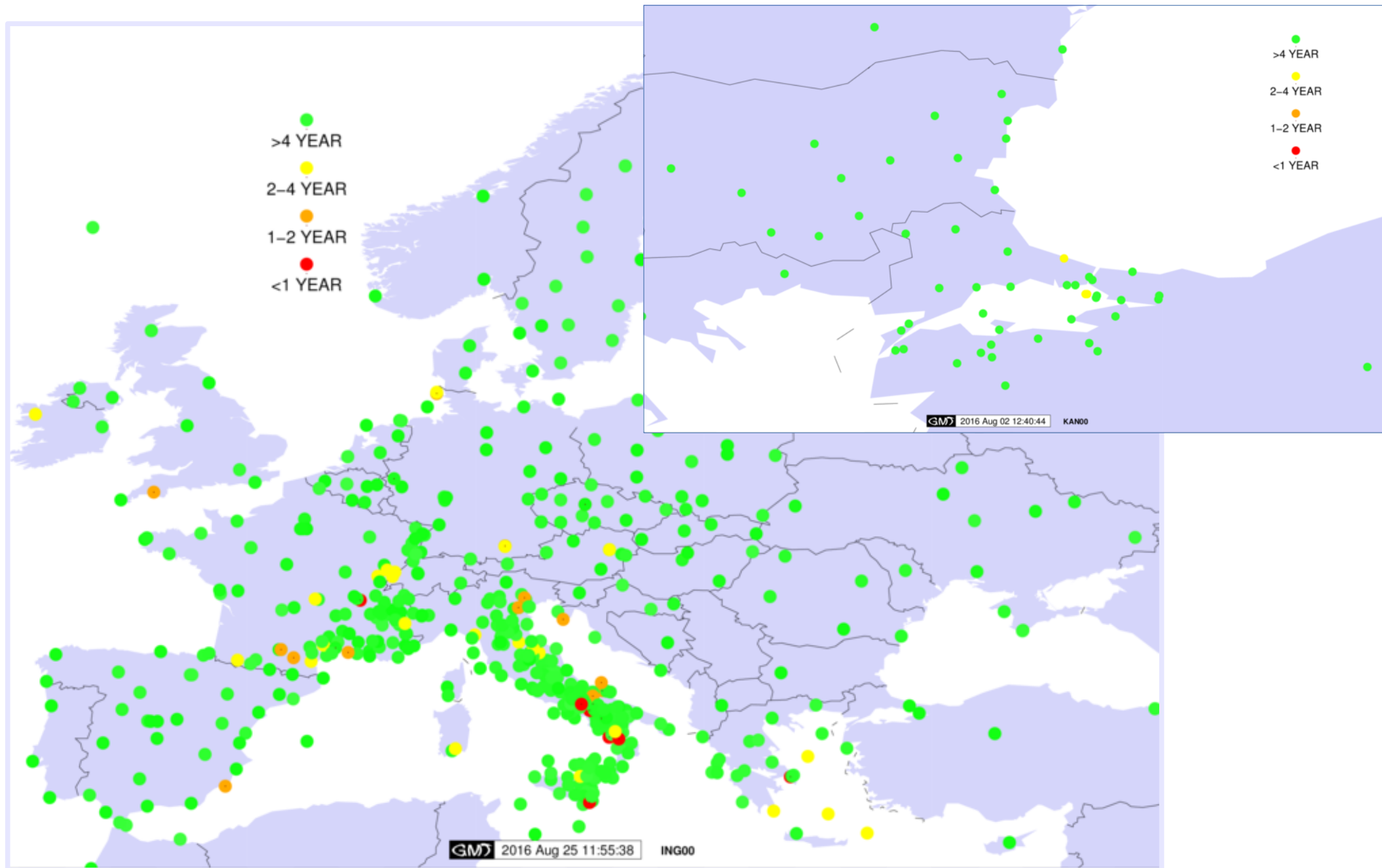
WEEKLY vs DAILY

- DAILY: MORE GEOPHYSICAL INFORMATION EXPECTED (DISREGARDING E.G. THE HIGH SCATTER AND RMS OF GIPSY SOLUTION?)
- FEASIBILITY OF LARGE SINEX HANDLING

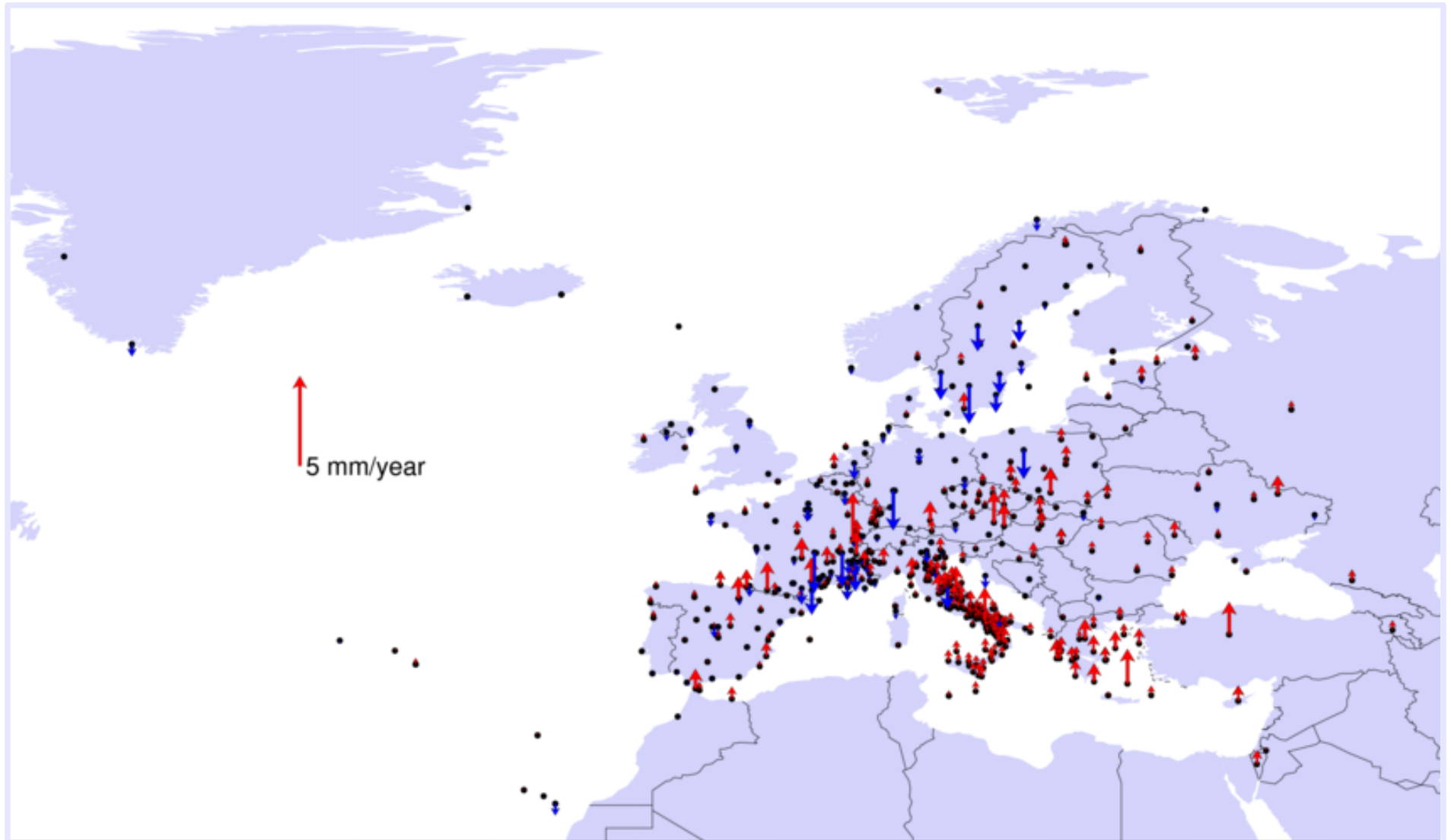
EPOS WEEKLY COMBINATION

- PAN-EUROPEAN SOLUTIONS (UGA-CNRS+INGV)
+ KANDILI UNIVERSITY (MARMARA REGION)
- COMPLETED:
 - SINEX CLEANING
 - = FEW CONCERNS ON DATA/STATION QUALITY =
(NOISE OR UNREALISTIC BEHAVIOR)**
 - WEEKLY LEVEL COMBINATION
 - MULTI-YEAR COMBINATION
 - RESULTS DELIVERY FOR TESTING
- NO OTHER SOLUTIONS ADDED YET, NEGOTIATIONS AND EXPECTED WP10 DECISION ON STATIONS WITHOUT META DATA

SINEX AVAILABILITY – EPOS PROTOTYPE



INGV & UGA/CNRS velocity differences

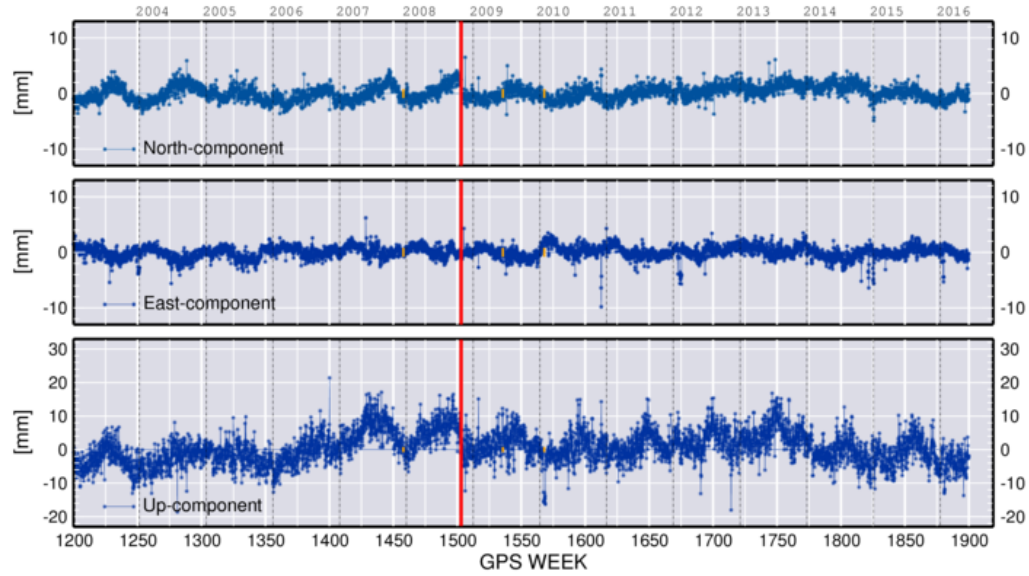


EPOS DAILY COMBINATION

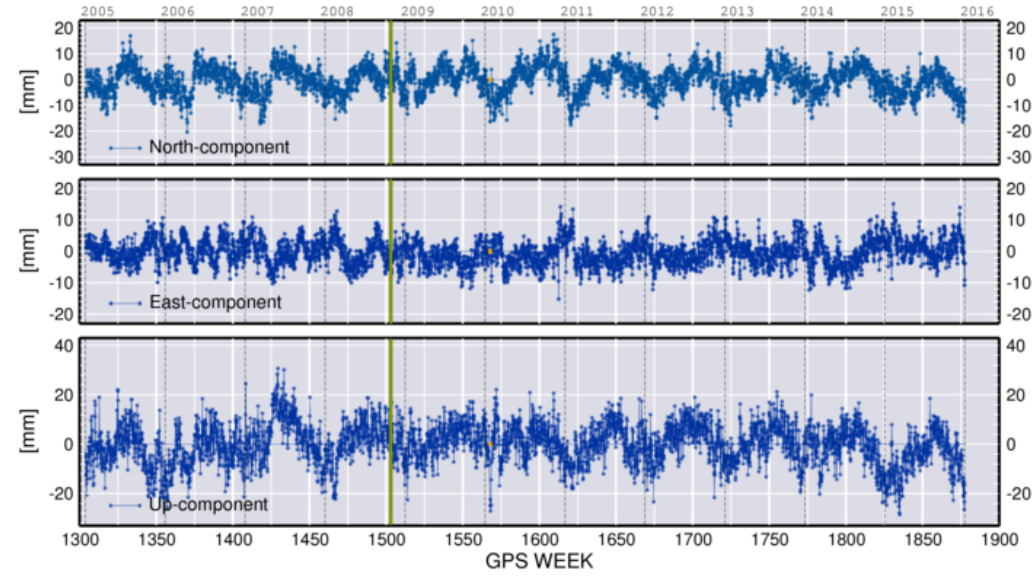
- PAN-EUROPEAN SOLUTIONS (UGA-CNRS+INGV)
+ KANDILI UNIVERSITY (MARMARA REGION)
- COMPLETED:
 - SINEX CLEANING
- DAILY LEVEL COMBINATION IN PROGRESS
- MULTI-YEAR COMBINATION IS NOT FEASIBLE DUE TO HANDLING LARGE MATRICES
- DAILY COMBINED SINEX FOR TIME SERIES DERIVATION AS DDSS

INDIVIDUAL INPUTS

BUCU_11401M001

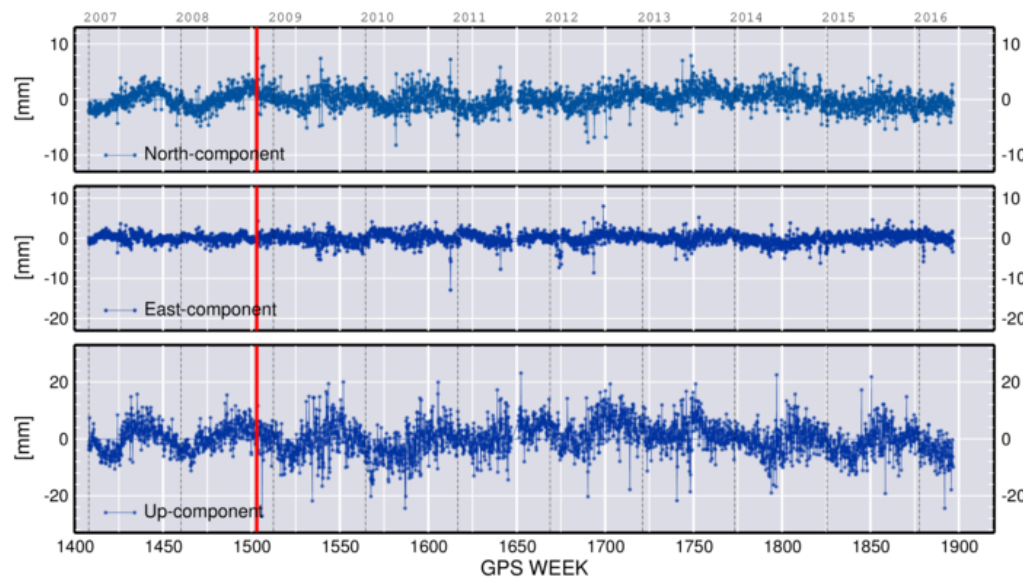


BUCU_11401M001

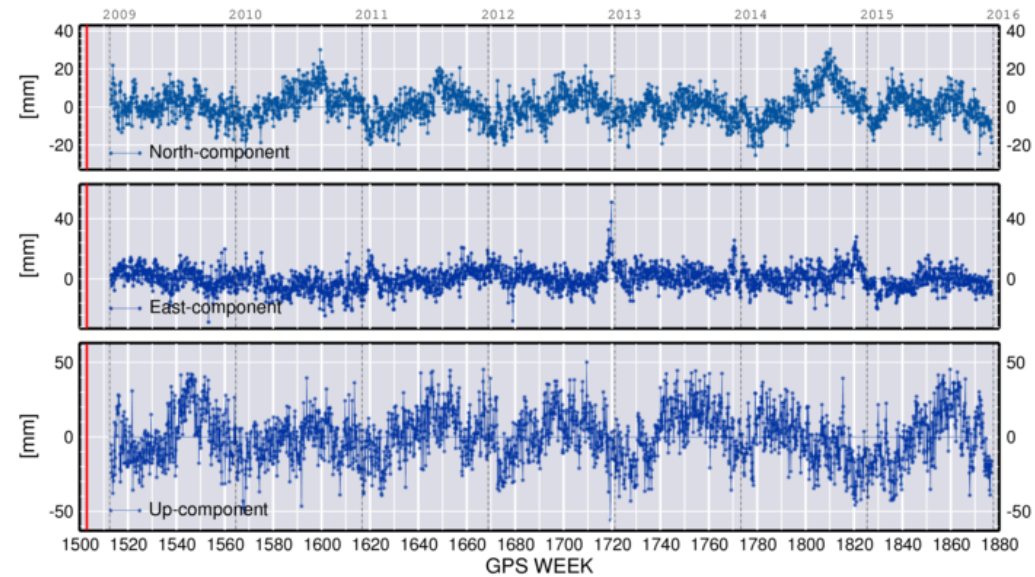


EPD_EPD02_daily

BUCU_11401M001



BUCU_11401M001



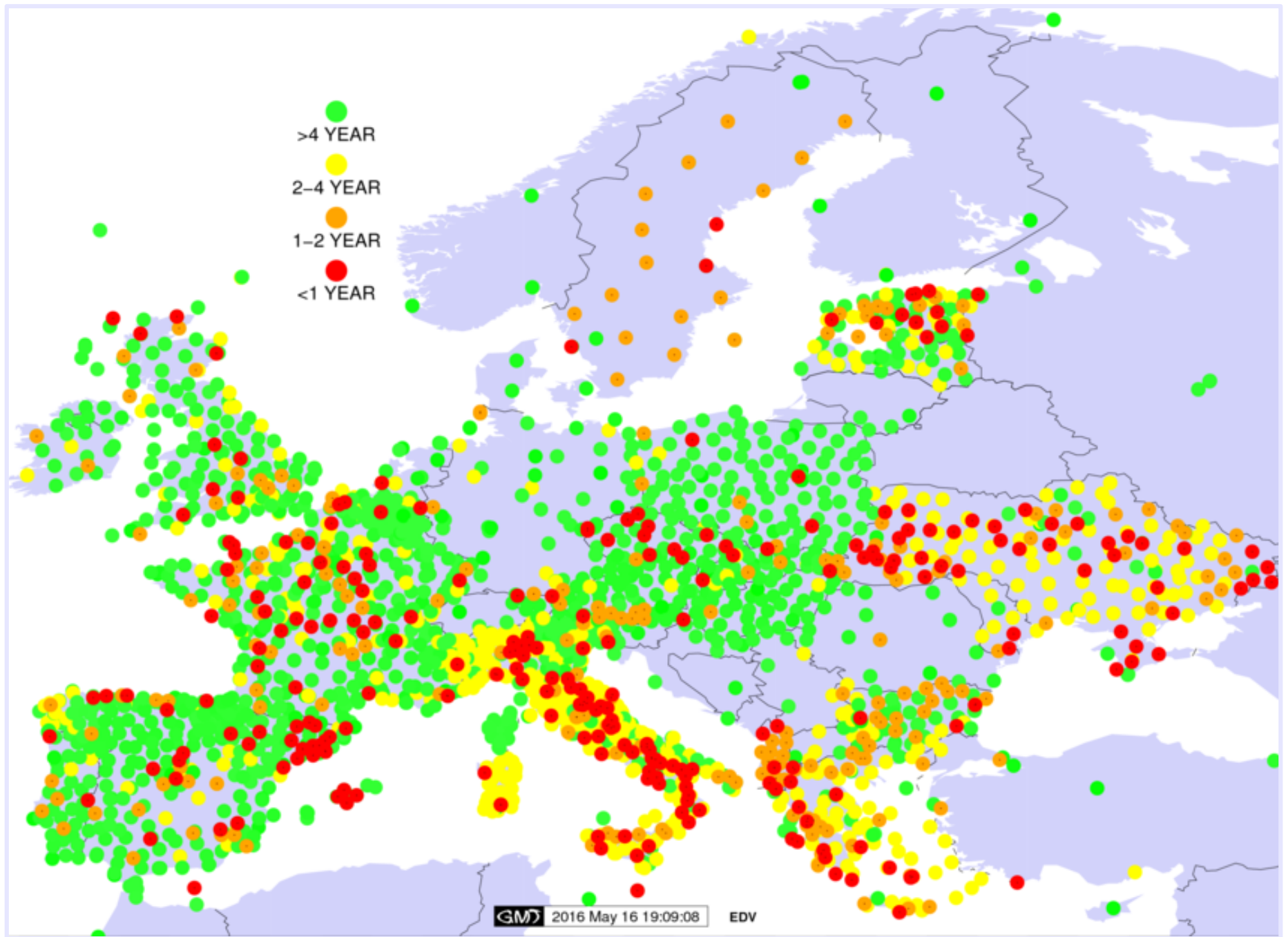
EPOS_ING00_daily

OS_KAN00_daily

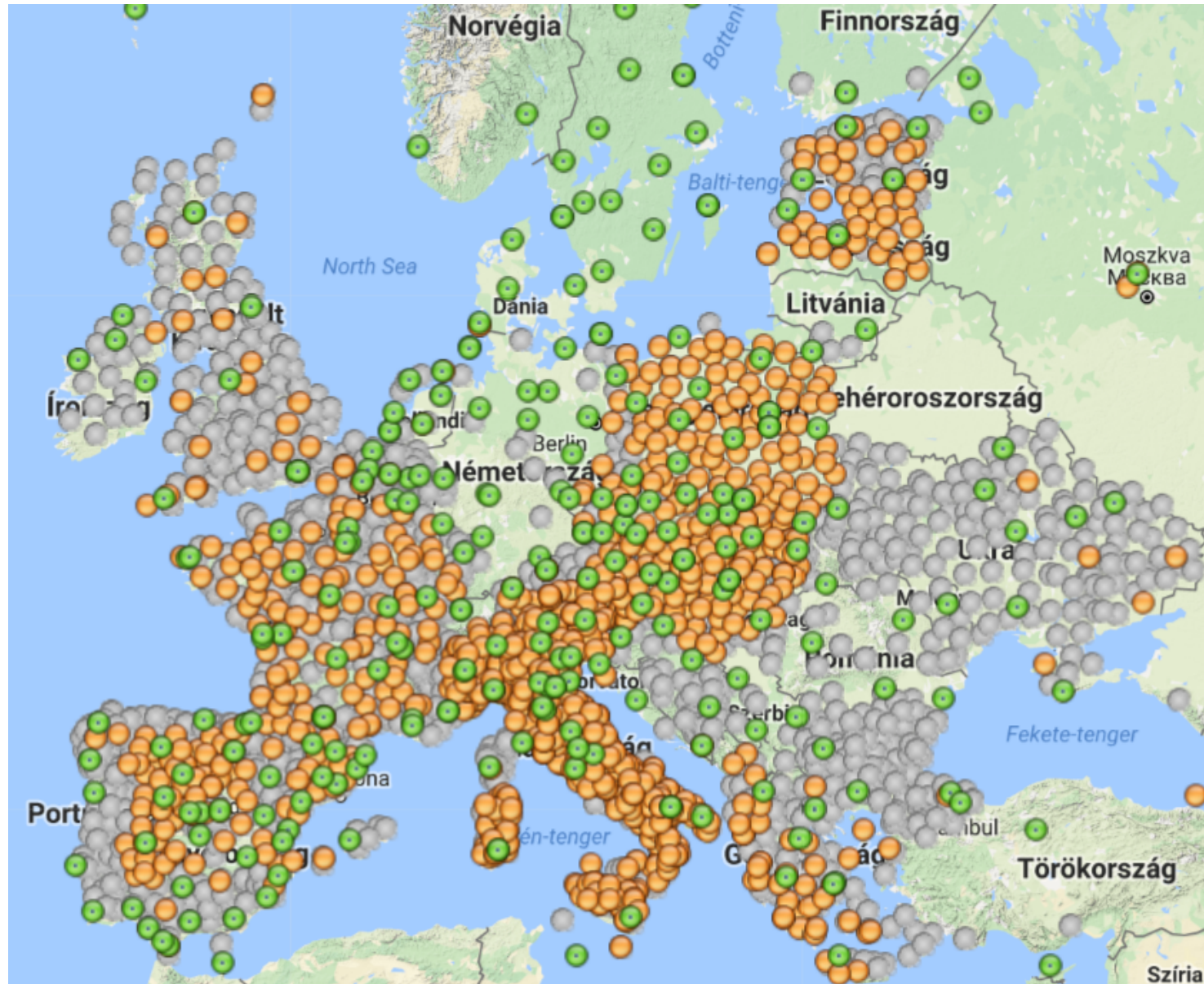
EPN DENSIFICATION

- 22 NETWORK SOLUTIONS
- MOSTLY WEEKLY SINEX, ONLY 4 DAILY SOLUTION
- MOSTLY FROM WEEK 1400 ON
- ACTIVE STATIONS: 3250
- MAINLY REFER TO IGb08 (STILL SOME IGS05 INPUT)
- NEXT MULTI-YEAR COMBINATION IS UP TO WEEK 1934
- COMBINATION WITH EPOS NEED TO BE DISCUSSED

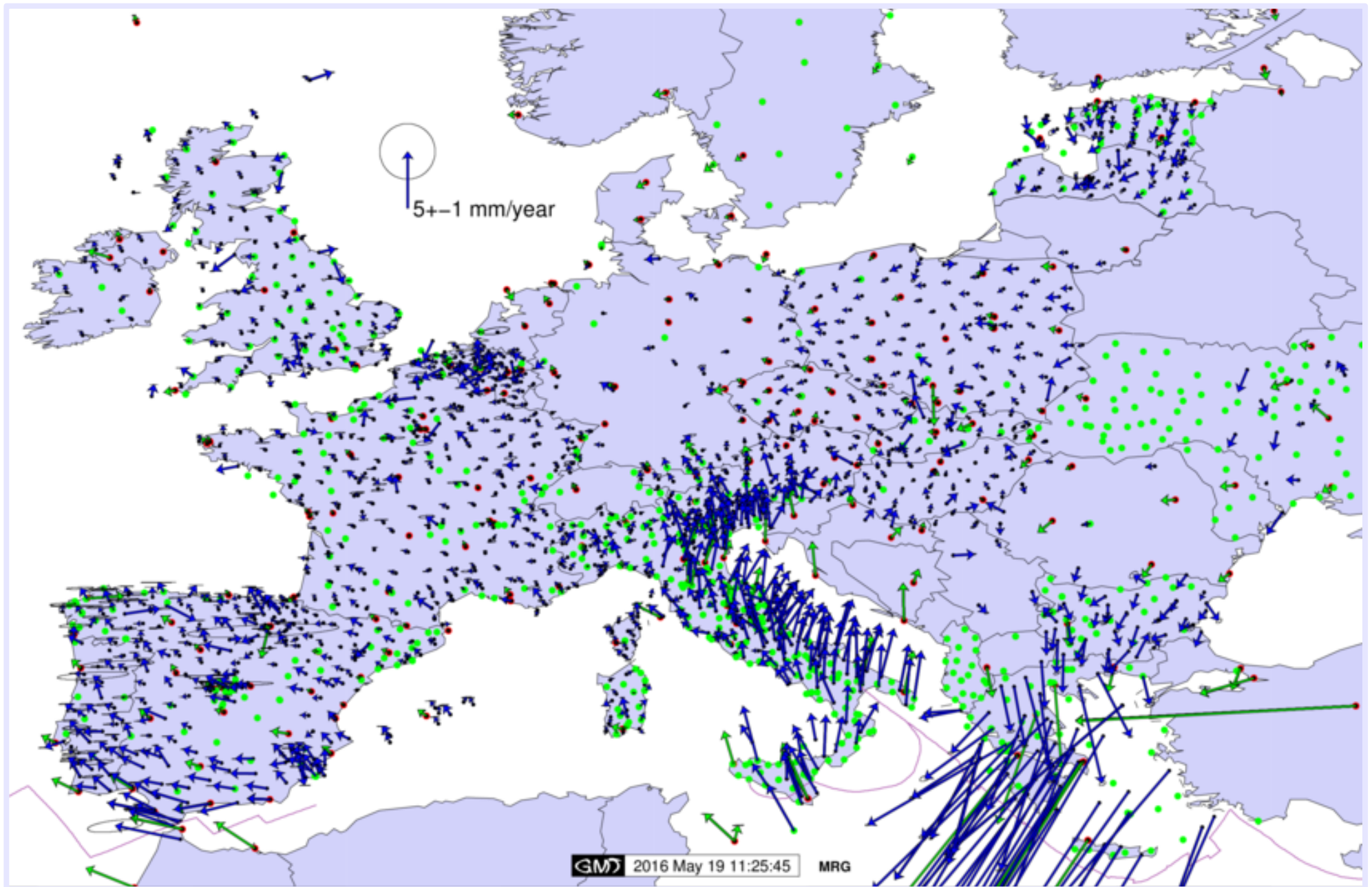
EPN DENSIFICATION NETWORK



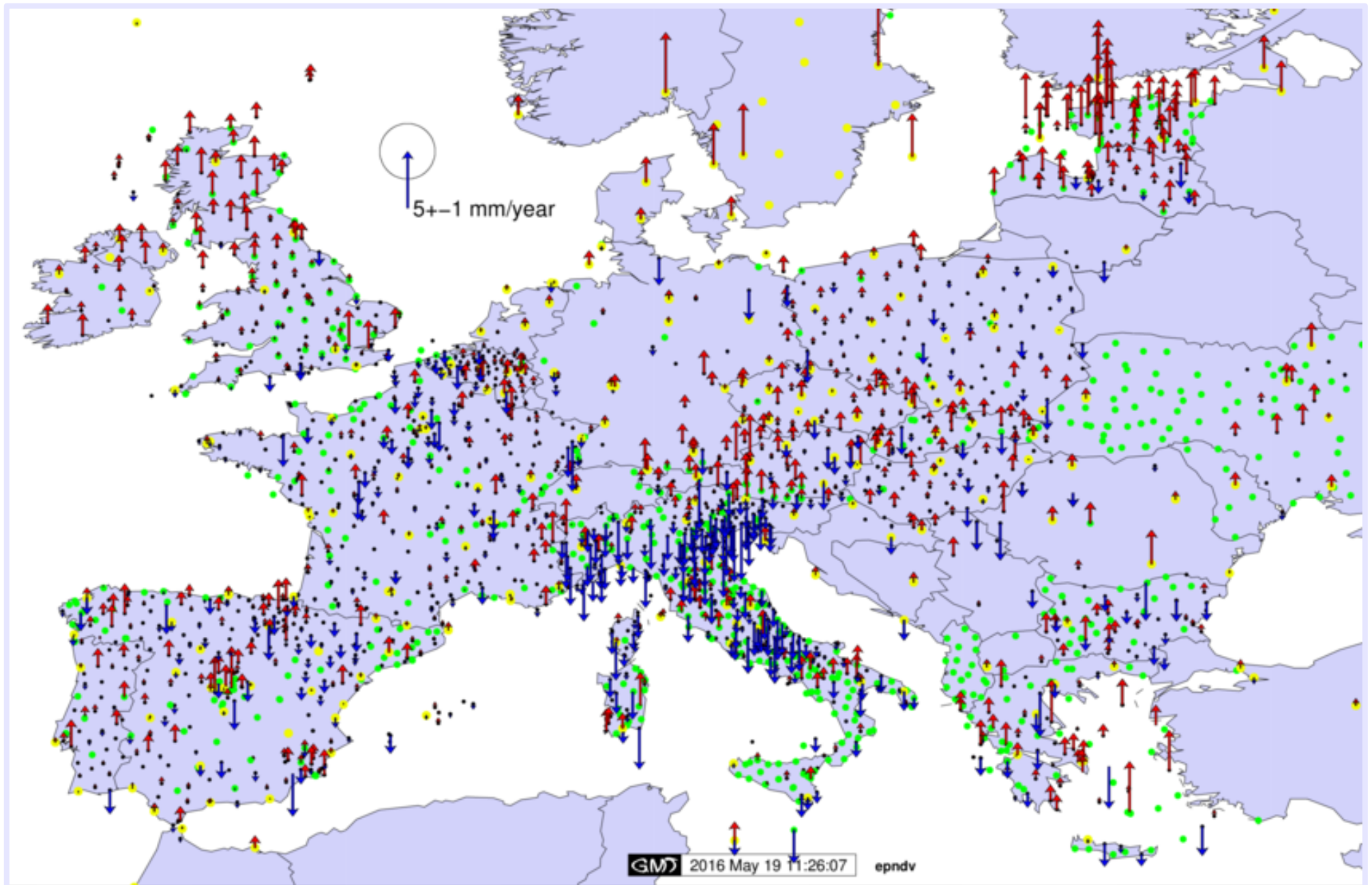
STATIONS WITH LOG AVAILABILITY



ETRF2000 VELOCITIES



UP VELOCITIES



Annex 2.7 : KOERI GAMIT Processing

MARMARA CONTINUOUS GPS NETWORK (MAGNET)

MAGNET is the Continuous GPS Network in Marmara Region. The establishment of the network was started in 1998 and now it reaches 22 continuous GPS stations (Error! Reference source not found. and Error! Reference source not found.). Besides MAGNET, complementary GPS surveys have been carried out since 1998 (Error! Reference source not found.).

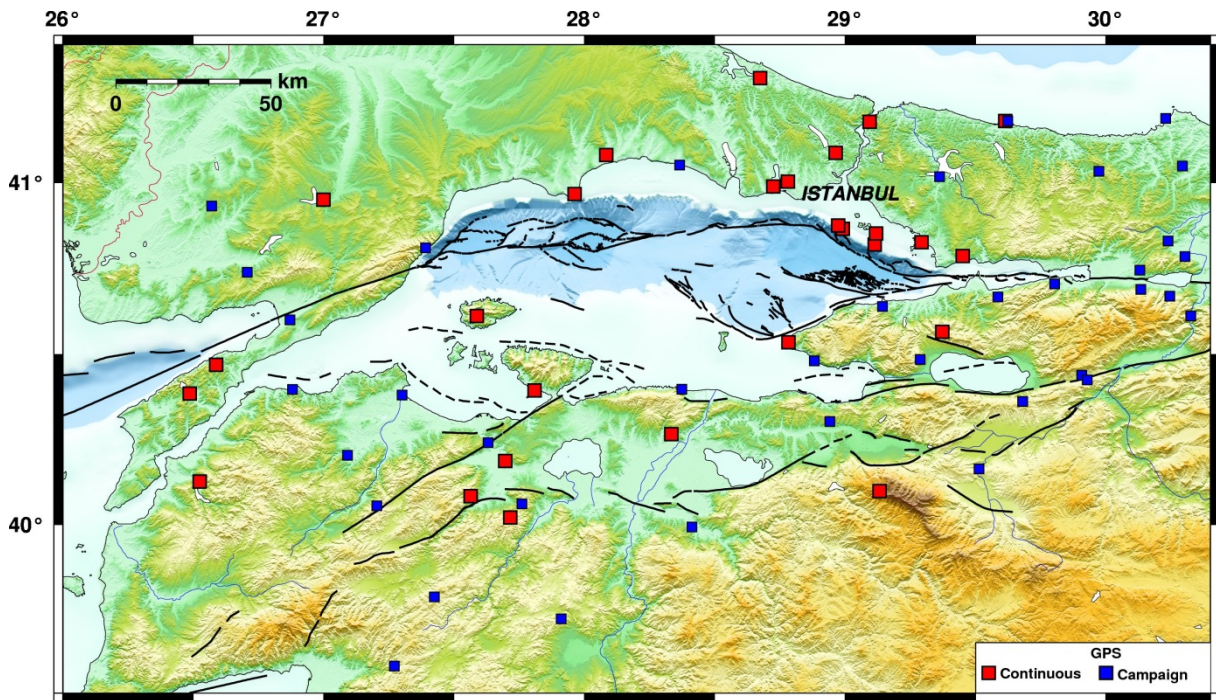


Figure 1. Continuous GPS stations (MAGNET) (red) and campaign survey GPS sites (blue) in the Marmara Region.

Table 1. Continuous GPS stations of MAGNET

Station ID	Station Name	Location	Coordinate (WGS84)		Up (m)
			Long °	Lat °	
TYF1	Tayfur	Çanakkale Gelibolu	26.48567790	40.38407251	200.5213
ATHT	Atikhisar	Çanakkale	26.52361322	40.12569083	106.5721
YENT	Yeniköy	Çanakkale Gelibolu	26.58727012	40.46833405	302.9550
KRDT	Karaıdemir	Tekirdağ Malkara	26.99850520	40.95072905	180.0202

ATCT	Atıcioba	Balıkesir Gönen	27.56330556	40.08302355	327.1198
MADT	Marmara Adası	Balıkesir	27.58694299	40.61135232	749.1330
ALAT	Alaattin	Balıkesir Gönen	27.69579844	40.18643674	104.4632
CHMT	Çobanhamidiye	Balıkesir Gönen	27.71496430	40.01985331	496.4170
ERDT	Erdek	Balıkesir	27.80794911	40.39322336	92.1755
MER1	Marmara Ereğlisi	Tekirdağ	27.96174890	40.96693379	91.7447
KART	Karacabey	Bursa	28.33256626	40.26525876	485.6161
AVCT	Avcılar	İstanbul	28.72386047	40.98866667	122.3623
BOZT	Bozburun	Yalova	28.78203580	40.53438555	115.5547
SVRT	Sivriada	İstanbul P. Islands	28.97351098	40.87471369	57.4326
YSST	Yassıada	İstanbul P. Islands	28.99086717	40.86577765	75.3325
KANT	Kandilli	İstanbul Üsküdar	29.06143119	41.06080795	155.0009
YANT	Yandros	İstanbul P. Islands	29.11271904	40.81972387	63.9704
BAD1	Büyükada	İstanbul P. Islands	29.11789697	40.85211710	239.1318
ULUT	Uludağ	Bursa	29.13144549	40.09754875	2088.8951
DUM2	Dumanlı	Bursa Orhangazi	29.37189633	40.56552512	930.3721
TUBI	TUBITAK	Kocaeli Gebze	29.45068361	40.78672512	221.6744
UCG2	Üçgaziler	Kocaeli	29.96240059	40.84551416	397.4312

3 DATA PROCESS

GAMIT / GLOBK software developed by the Massachusetts Institute of Technology Department of Atmospheric and Planetary Sciences (EAPs MIT, USA) was used for processing of data mentioned in the previous section. First of all, in data processing, continuous and survey GPS measurements have been converted into RINEX format and required information for evaluation are prepared (such as receiver and antenna types, antenna height and type of height measurement). The precise orbit information produced by International GPS Service (IGS) in SP3 (Standard Product 3) format is taken from SOPAC (Scrips Orbit and Permanent Array Center). Earth rotation parameters (ERP) taken from usno_bull_b (United States Naval Observatory_bulletin_b) values were used. 10-15 stations from IGS global monitoring network were included to the evaluation. To define the reference frame, ITRF2008 coordinate system was used. For Radiation-pressure effects, Berne 9 parameterized model (standard of the SOPAC) was used. For ocean loading effect, Scherneck model (IERS standards, 1992) was studied with. The zenith delays were calculated with the 2-hour intervals based on Saastamoinen precursor standard tropospheric model. In the evaluation, LC (L3), independent linear combination of the ionosphere of L1 and L2 carrier phases is used. For antenna phase center, the model depending on the height is used. Daily loosely constrained solutions from GAMIT were identified by transformation with 7 parameters (3 translations, 3 rotations and 1 scale factor) taking advantage of 12 IGS stations ¹ in ITRF2008 reference frame. Daily precise coordinates and repeated

¹ Now, we decided to use a new list, based on their long-term performances: NOT1, YEBE, MARSite (GA 308417) D3.1 GPS Time Series and Velocity Maps

measurements at each period were joined by Kalman analysis and time series containing position variations of these points are obtained. Also, with the help of the Kalman filtering using trend analysis from the time series velocities for sites are determined.

TIME SERIES AND VELOCITY FIELD

As mentioned in the previous section, time series of the stations and the velocity field respect to Eurasia (Figure 2) are produced for 2002-2013 time period. The velocities of the stations are also given in Table 2. In Annex, the time series of all GPS stations are shown.

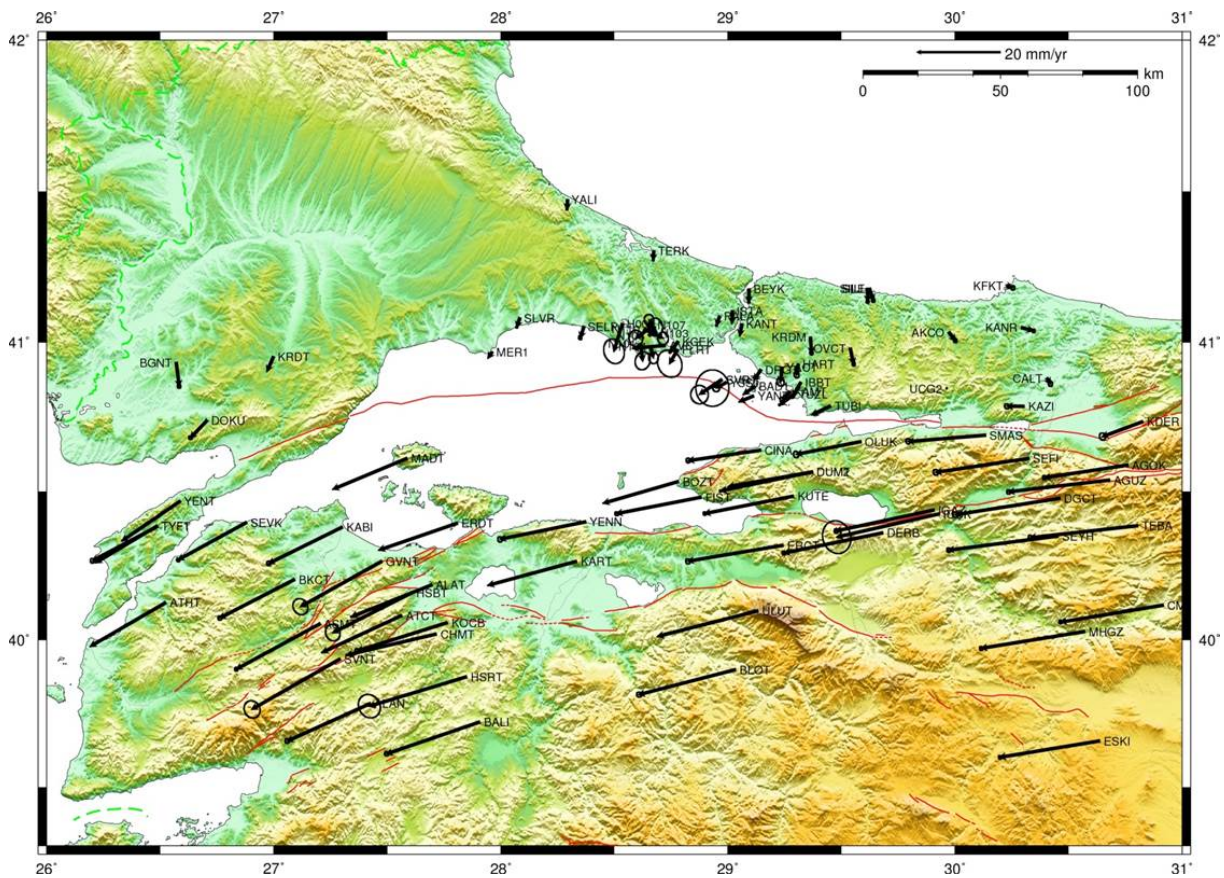


Figure 2. Velocity field for Marmara Region (respect to Eurasia and with %95 confidence ellipses) (2002-2013)

Table 2. Velocity field for Marmara Region (2002-2013)

Station ID	Long°	Lat°	Velocity (mm/yr)		Sig (mm/yr)		RHO
			East	North	East	North	
CMLN	30.91635	40.11795	-24.38	-4.02	0.15	0.18	-0.099
KDER	30.82663	40.73478	-9.57	-3.57	0.29	0.36	-0.175
TEBA	30.80449	40.38572	-25.55	-2.85	0.19	0.23	-0.111

BUCU, RAMO, NICO, GRAZ, WTZR, CRAO, ZECK, ISTA , GLSV , KABR
 MARSite (GA 308417) D3.1 GPS Time Series and Velocity Maps

AGOK	30.76109	40.58886	-19.84	-2.97	0.18	0.21	-0.074
AGUZ	30.68037	40.53834	-24.00	-2.78	0.18	0.22	-0.099
ESKI	30.63704	40.65758	-23.69	-3.89	0.15	0.17	-0.098
MHGZ	30.57041	40.02786	-24.60	-3.99	0.16	0.19	-0.103
DGCT	30.46175	40.47786	-24.89	-3.91	0.24	0.29	-0.087
SEYH	30.45336	40.35061	-25.99	-3.36	0.18	0.22	-0.134
CALT	30.40452	40.88000	0.85	-1.32	0.18	0.21	-0.078
SEFI	30.32520	40.61163	-22.16	-3.32	0.24	0.28	-0.135
KAZI	30.30341	40.78522	-4.06	0.05	0.22	0.25	-0.122
KANR	30.29356	41.04825	2.83	-0.72	0.15	0.18	-0.076
KFKT	30.22937	41.18680	1.39	-0.41	0.19	0.22	-0.053
SMAS	30.13402	40.68972	-18.39	-1.50	0.21	0.26	-0.086
AKCO	29.97311	41.03354	1.53	-2.02	0.16	0.19	-0.072
UCG2	29.96240	40.84551	0.13	0.07	0.02	0.02	-0.045
IUCK	29.92893	40.42473	-24.29	-5.49	1.38	1.59	-0.108
IGAZ	29.90799	40.43800	-23.31	-4.98	0.18	0.22	-0.078
DERB	29.68137	40.36165	-23.49	-4.82	0.17	0.19	-0.086
SILE	29.62324	41.17945	0.89	-2.90	0.16	0.18	-0.076
SILI	29.61332	41.17900	0.13	-3.08	0.14	0.16	-0.013
OLUK	29.58524	40.66713	-15.38	-3.02	0.26	0.31	-0.096
OVCT	29.53923	40.97974	0.76	-3.73	0.16	0.19	-0.080
TUBI	29.45068	40.78672	-4.34	-2.07	0.02	0.02	-0.047
DUMT	29.37189	40.56552	-21.82	-4.49	0.09	0.10	-0.047
DUM2	29.37189	40.56552	-20.82	-3.49	0.03	0.03	-0.041
KRDM	29.36246	41.01709	0.30	-3.77	0.16	0.19	-0.074
IBBT	29.32081	40.86602	-1.90	-3.23	0.16	0.19	-0.041
HART	29.31021	40.92680	-0.44	-2.55	0.25	0.29	-0.123
TUZL	29.29245	40.82650	-3.54	-2.55	0.07	0.08	-0.023
KUTE	29.28794	40.48473	-21.08	-4.14	0.15	0.16	-0.087
KAMT	29.27328	40.83435	-1.86	-1.88	0.21	0.25	-0.053
ERCT	29.24320	40.31874	-22.63	-3.77	0.22	0.25	-0.073
YACT	29.23786	40.91670	-0.33	-3.52	0.35	0.41	-0.141
DRGT	29.14526	40.90880	-1.56	-2.43	0.03	0.04	-0.053
CINA	29.14313	40.63947	-17.17	-2.49	0.20	0.23	-0.058
ULUT	29.13144	40.09755	-23.80	-6.07	0.02	0.02	-0.052
BAD1	29.11790	40.85212	-2.71	-1.90	0.02	0.02	-0.049
YANT	29.11272	40.81972	-3.36	-1.36	0.03	0.03	-0.045
BEYK	29.09352	41.17672	-0.09	-3.09	0.09	0.10	-0.005
KANT	29.06143	41.06081	-0.53	-2.76	0.02	0.02	-0.053
BLOT	29.03304	39.89917	-22.93	-5.93	0.23	0.25	-0.055
ISTA	29.01934	41.10445	-0.09	-2.94	0.02	0.02	-0.050
YSST	28.99087	40.86578	-2.29	-1.34	0.33	0.35	-0.017
SVRT	28.97351	40.87471	-5.32	-3.53	0.85	0.89	-0.013
SVR1	28.97351	40.87471	-2.26	-1.98	1.61	1.77	-0.004
PALA	28.96320	41.08632	-0.70	-2.15	0.08	0.08	-0.010
FIST	28.88184	40.48057	-20.08	-3.90	0.17	0.20	-0.081
BOZT	28.78203	40.53438	-17.81	-5.15	0.02	0.02	-0.047
KCEK	28.77975	41.00275	-1.85	-2.60	0.09	0.09	-0.005
FLRT	28.77893	40.97483	-1.90	-3.30	1.19	1.33	-0.142
AVCT	28.72386	40.98867	-7.69	-0.70	0.02	0.02	-0.048
N103	28.68388	41.03013	-1.68	3.16	0.46	0.52	-0.038
TERK	28.67358	41.30307	-0.13	-2.10	0.09	0.09	-0.010

N107	28.67184	41.05651	-4.16	-3.15	0.65	0.80	-0.024
N104	28.65969	40.98540	0.67	-2.69	0.47	0.56	-0.032
N108	28.65249	41.02162	1.50	2.04	0.71	0.88	-0.029
N110	28.63109	41.04333	4.52	-2.20	0.51	0.61	-0.013
N101	28.61528	40.99572	0.51	-4.13	0.73	0.87	-0.120
H009	28.53579	41.06188	-2.02	-6.56	1.00	1.20	-0.144
YENN	28.37327	40.39790	-20.36	-4.13	0.23	0.26	-0.107
SELP	28.36533	41.05183	-0.83	-2.63	0.16	0.18	-0.093
KART	28.33257	40.26526	-20.99	-5.69	0.02	0.02	-0.048
YALI	28.29320	41.47335	-0.12	-2.27	0.09	0.09	-0.006
SLVR	28.08340	41.08022	-0.70	-2.15	0.08	0.08	-0.016
MER1	27.96175	40.96693	-0.95	-1.38	0.02	0.02	-0.049
BALI	27.90643	39.72167	-22.14	-7.57	0.20	0.21	-0.047
HSRT	27.84810	39.87523	-23.06	-6.99	1.07	1.14	-0.143
ERDT	27.80795	40.39322	-18.60	-6.39	0.02	0.02	-0.046
KOCB	27.76345	40.05858	-21.43	-6.74	0.19	0.22	-0.054
CHMT	27.71496	40.01985	-21.29	-5.01	0.06	0.06	-0.026
ALAT	27.69580	40.18644	-19.14	-7.59	0.05	0.06	-0.020
HSBT	27.60821	40.15944	-18.78	-9.50	0.71	0.80	-0.118
MADT	27.58694	40.61135	-17.59	-7.34	0.02	0.02	-0.043
ATCT	27.56330	40.08302	-18.87	-8.77	0.05	0.05	-0.025
GVNT	27.47554	40.26550	-19.32	-10.78	0.73	0.78	-0.146
ALAN	27.42449	39.78469	-19.73	-8.93	0.21	0.23	-0.070
KABI	27.30123	40.38099	-17.46	-8.63	0.19	0.21	-0.073
SVNT	27.29249	39.93513	-20.94	-11.95	0.78	0.84	-0.119
ASMT	27.20352	40.05448	-19.89	-10.79	0.16	0.18	-0.063
BKCT	27.09140	40.20343	-17.76	-9.15	0.18	0.20	-0.116
KRDT	26.99851	40.95073	-1.52	-3.44	0.02	0.02	-0.043
SEVK	26.87973	40.39580	-16.20	-8.86	0.16	0.18	-0.068
DOKU	26.70644	40.73927	-3.95	-4.16	0.16	0.18	-0.063
YENT	26.58727	40.46833	-13.77	-9.42	0.03	0.03	-0.032
BGNT	26.57014	40.93244	0.72	-5.66	0.17	0.19	-0.076
ATHT	26.52361	40.12569	-17.89	-10.39	0.02	0.02	-0.041
TYFT	26.48698	40.38310	-15.43	-8.16	0.20	0.22	-0.051
TYF1	26.48568	40.38407	-14.51	-8.68	0.02	0.02	-0.037

TUSAGA-AKTIF NETWORK

TUSAGA Aktif network has been established for the RTK applications since 2009 by Photogrammetry and Geodesy Administration of the General Directorate of Land Registration and Cadastre of Turkey and the Auxiliary Control Station in headquarters of the General Command of Mapping of Turkey. In 2014, the 30-s data opened to scientific community in Turkey. Registered user can access the last 2-year data set.

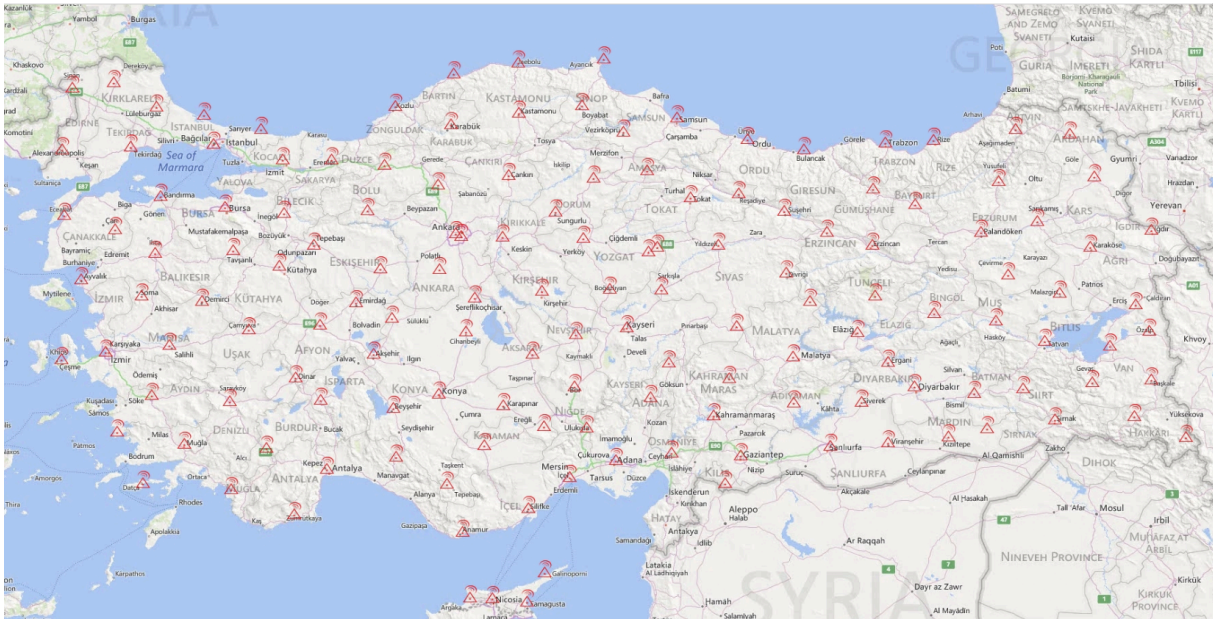


Figure 3. TUSAG-AKTIF network

A total of 146 TUSAGA Aktif reference stations are established in the field with baseline separation of 70-100 km (Figure 3). Now, in the network, Trimble NetRS systems run and all data processed by Trimble software. Now, we still organize its station logs. Unfortunately its station logs do not update, regularly. Also, we have no idea about their long term performance. I

GENERAL COMMENTS

-I will focus to MAGNET. I know their long-term history very well. Actually, I installed them when I was in TUBITAK.

-When we will decide to the common parameters, I will re-run GAMIT&GLOBK and I will share daily solutions.

-Remember, MAGNET affected by 1999 devastating earthquakes and we still observe the postseismic motions.

-When I will combine all information for TUSAGA-Aktif, I will start the processing but it is not possible within 2016 (may be, it can be ready for the end of 2016). My priority is MAGNET network.

Annex I: Time Series

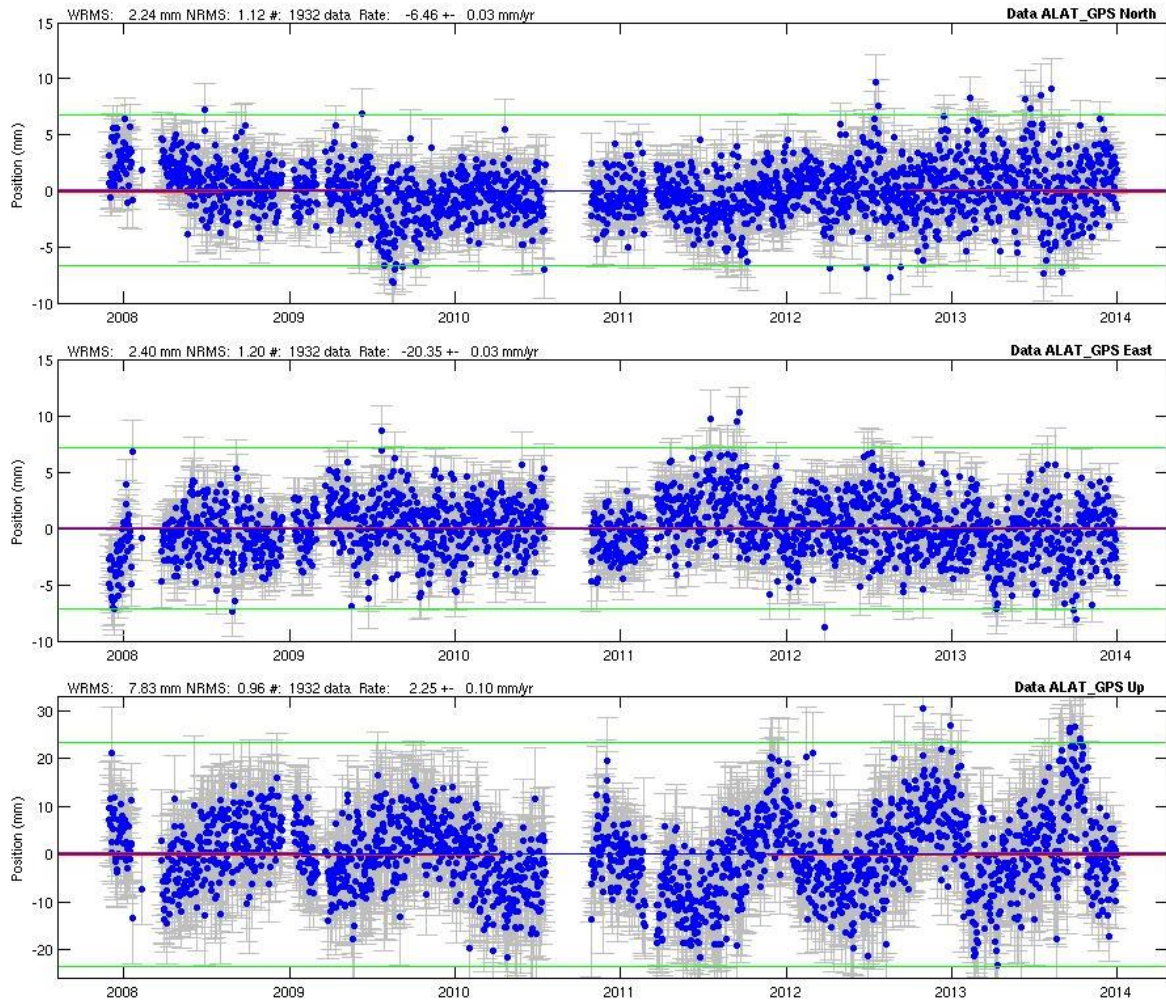


Figure 4. Time series for ALAT (in the graph, north-south, east-west and elevation components are shown respectively). The horizontal axis represents the GPS day, the vertical axis is representing the changes in the respective component coordinates are in mm scale.

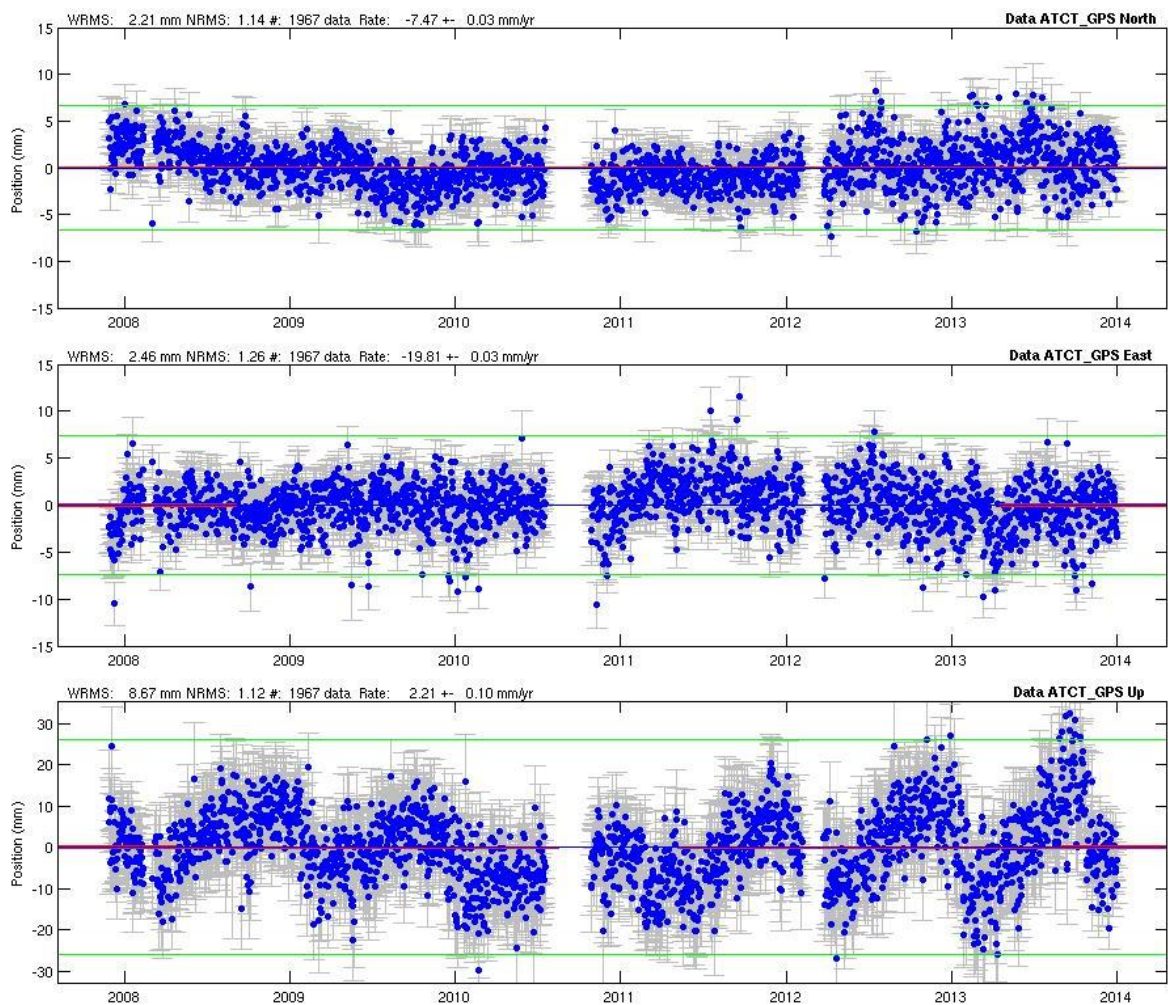


Figure 5. Time series for ATCT (in the graph, north-south, east-west and elevation components are shown respectively). The horizontal axis represents the GPS day, the vertical axis is representing the changes in the respective component coordinates are in mm scale.

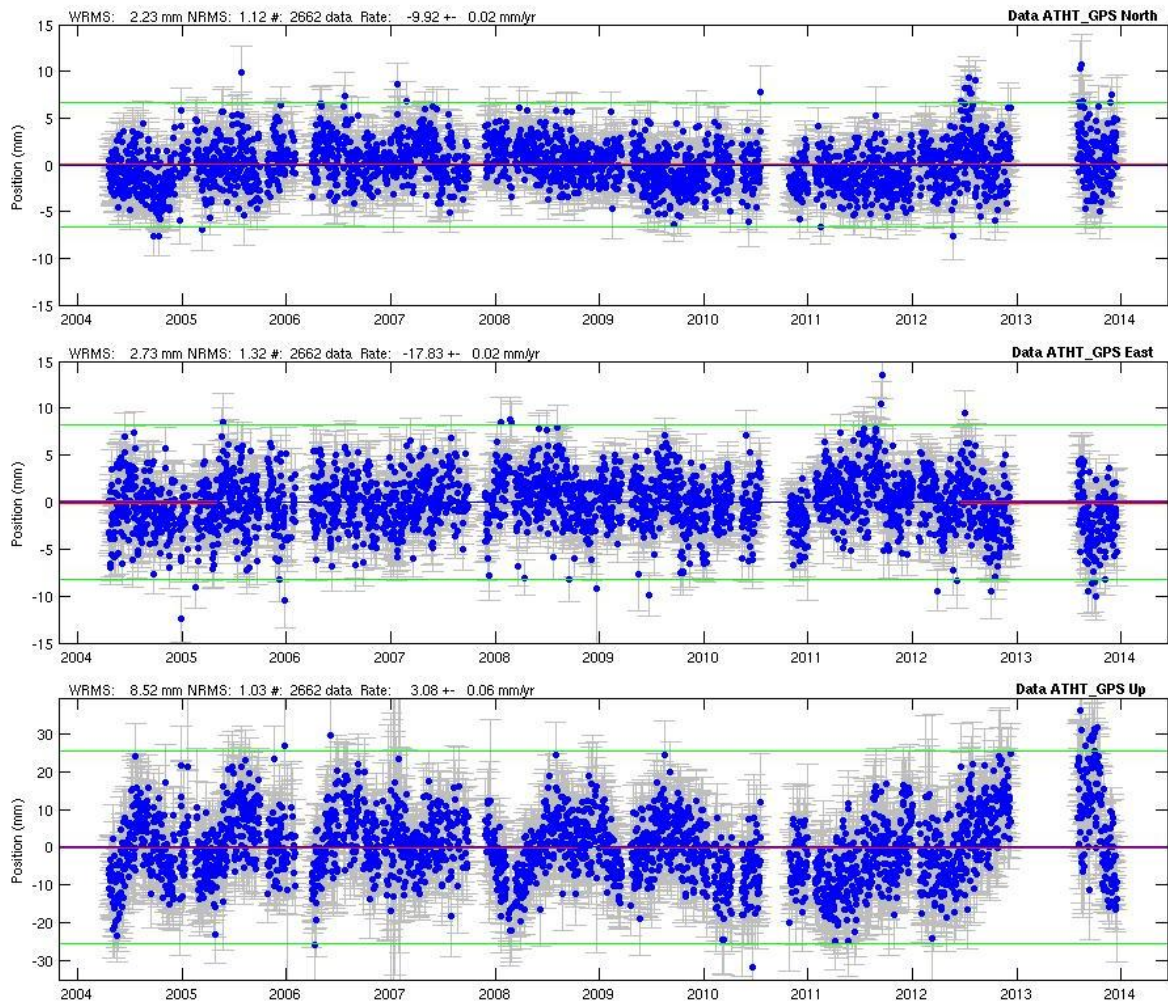


Figure 6. Time series for ATHT (in the graph, north-south, east-west and elevation components are shown respectively). The horizontal axis represents the GPS day, the vertical axis is representing the changes in the respective component coordinates are in mm scale.

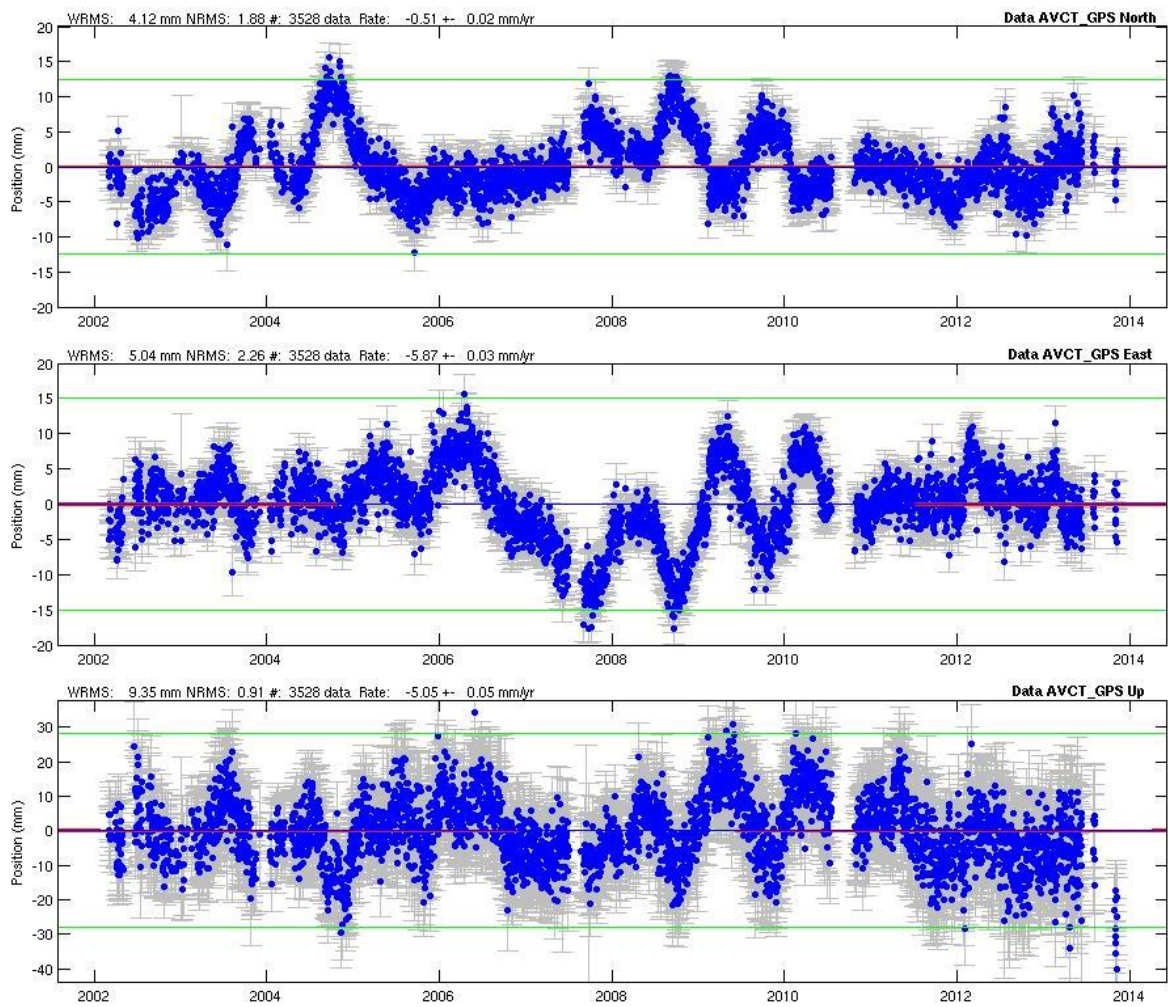


Figure 7. Time series for AVCT (in the graph, north-south, east-west and elevation components are shown respectively). The horizontal axis represents the GPS day, the vertical axis is representing the changes in the respective component coordinates are in mm scale.

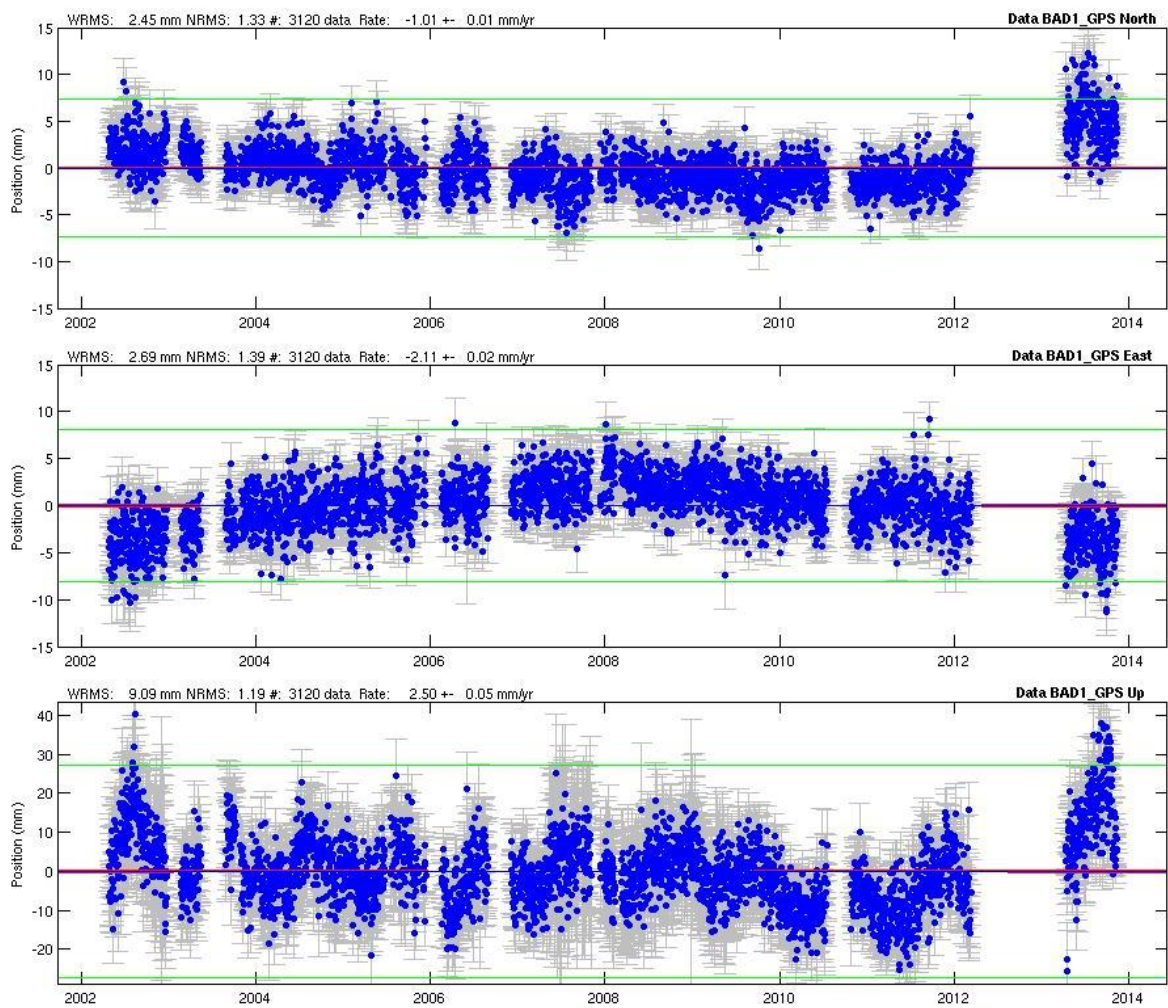


Figure 8. Time series for BAD1 (in the graph, north-south, east-west and elevation components are shown respectively). The horizontal axis represents the GPS day, the vertical axis is representing the changes in the respective component coordinates are in mm scale.

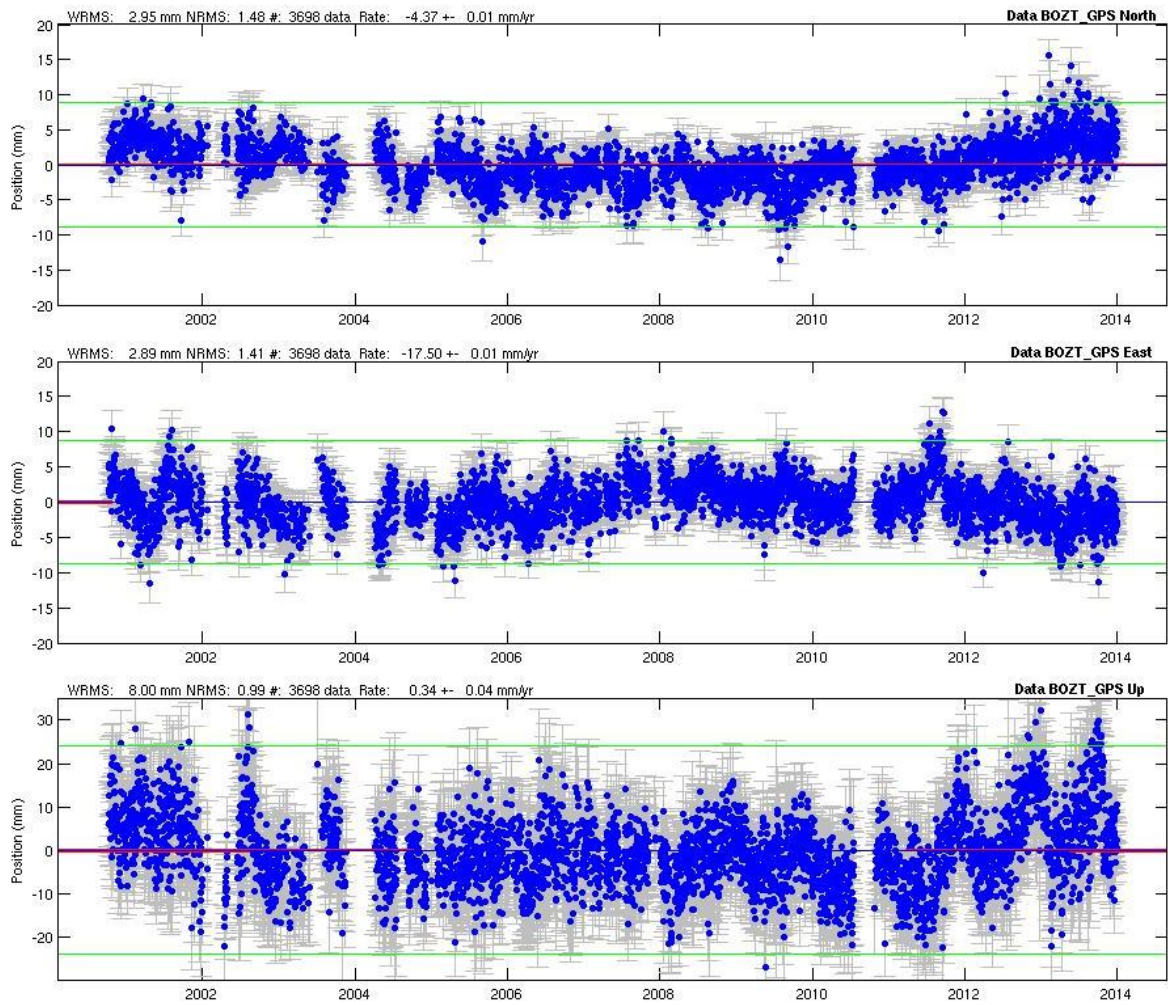


Figure 9. Time series for BOZT (in the graph, north-south, east-west and elevation components are shown respectively). The horizontal axis represents the GPS day, the vertical axis is representing the changes in the respective component coordinates are in mm scale.

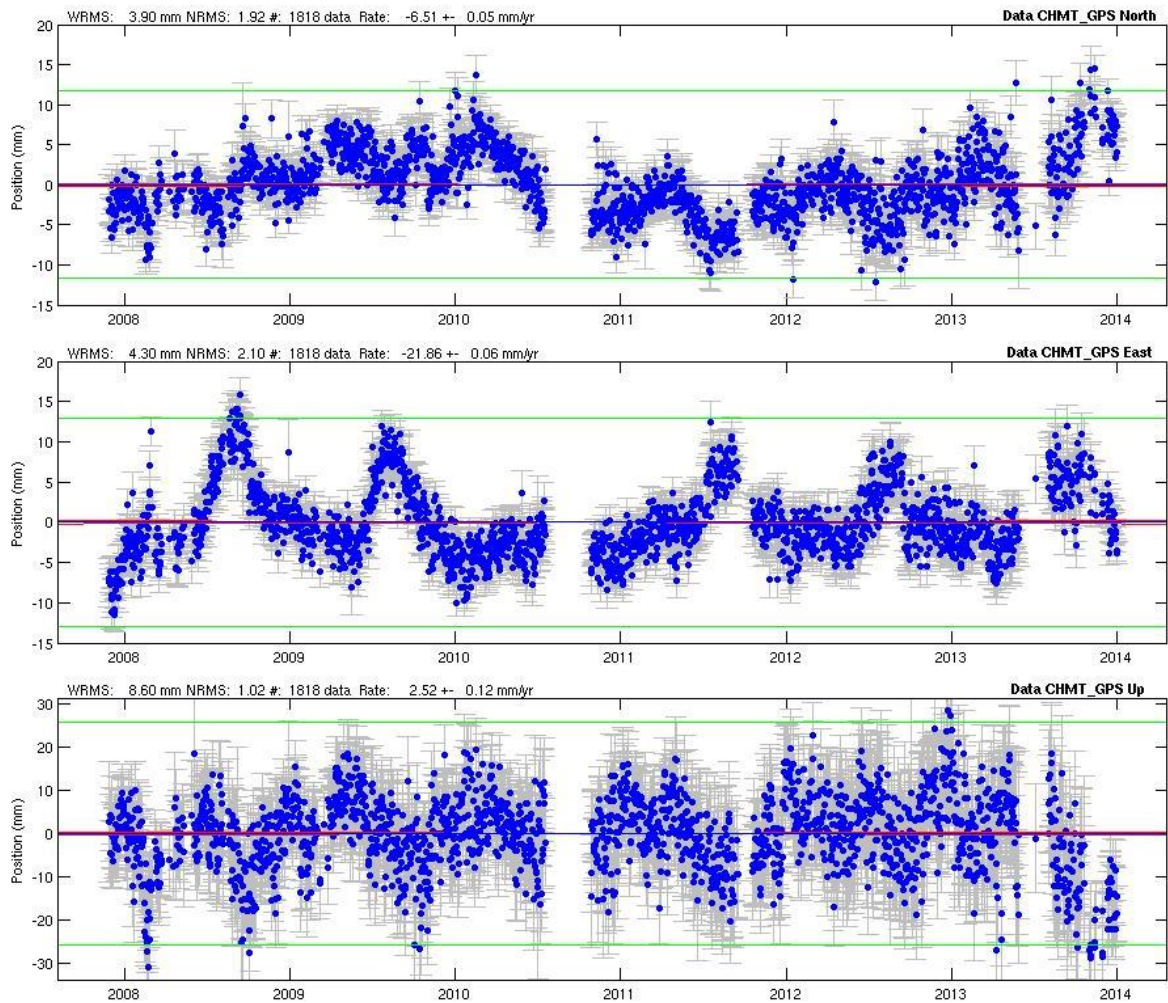


Figure 10. Time series for CHMT (in the graph, north-south, east-west and elevation components are shown respectively). The horizontal axis represents the GPS day, the vertical axis is representing the changes in the respective component coordinates are in mm scale.

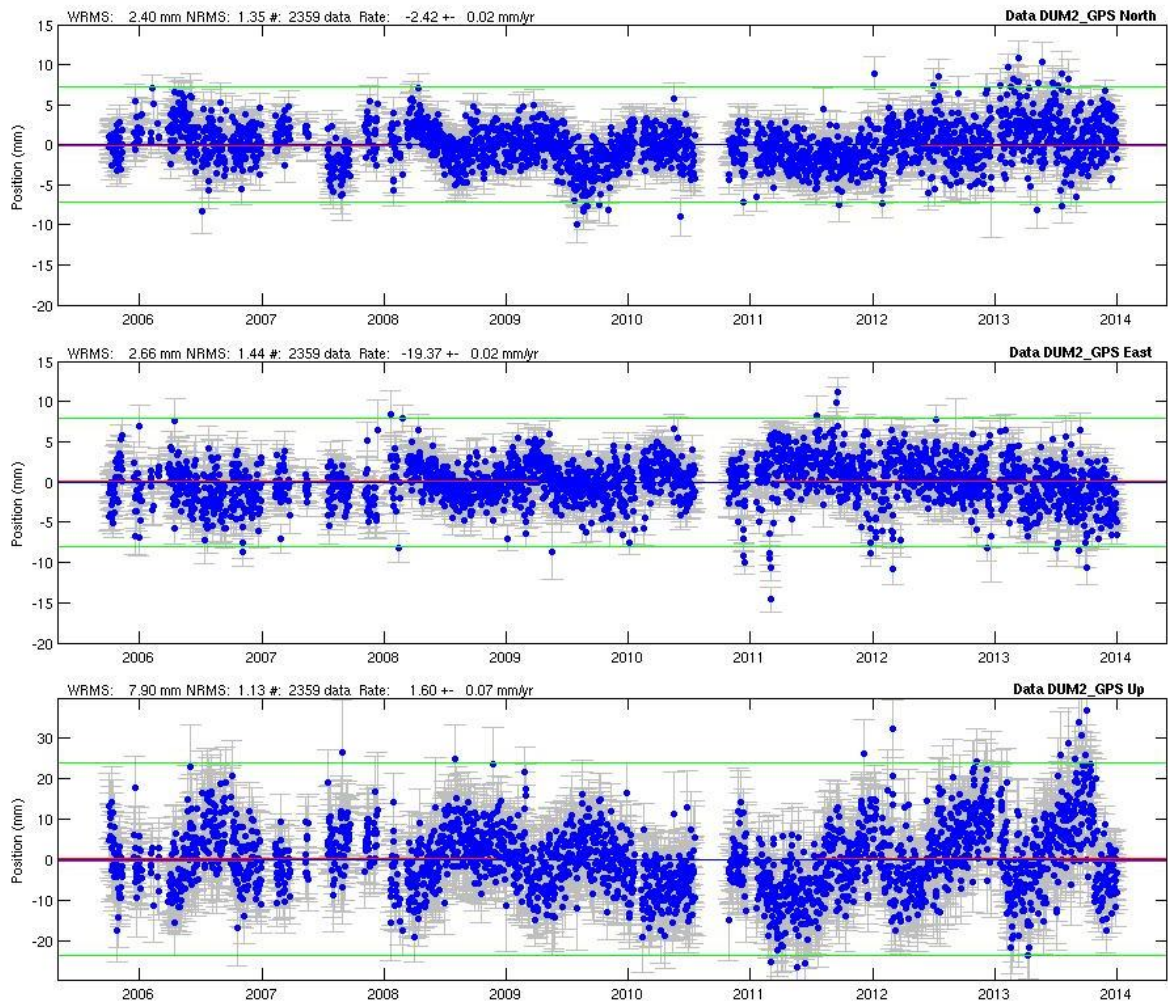


Figure 11. Time series for DUM2 (in the graph, north-south, east-west and elevation components are shown respectively). The horizontal axis represents the GPS day, the vertical axis is representing the changes in the respective component coordinates are in mm scale.

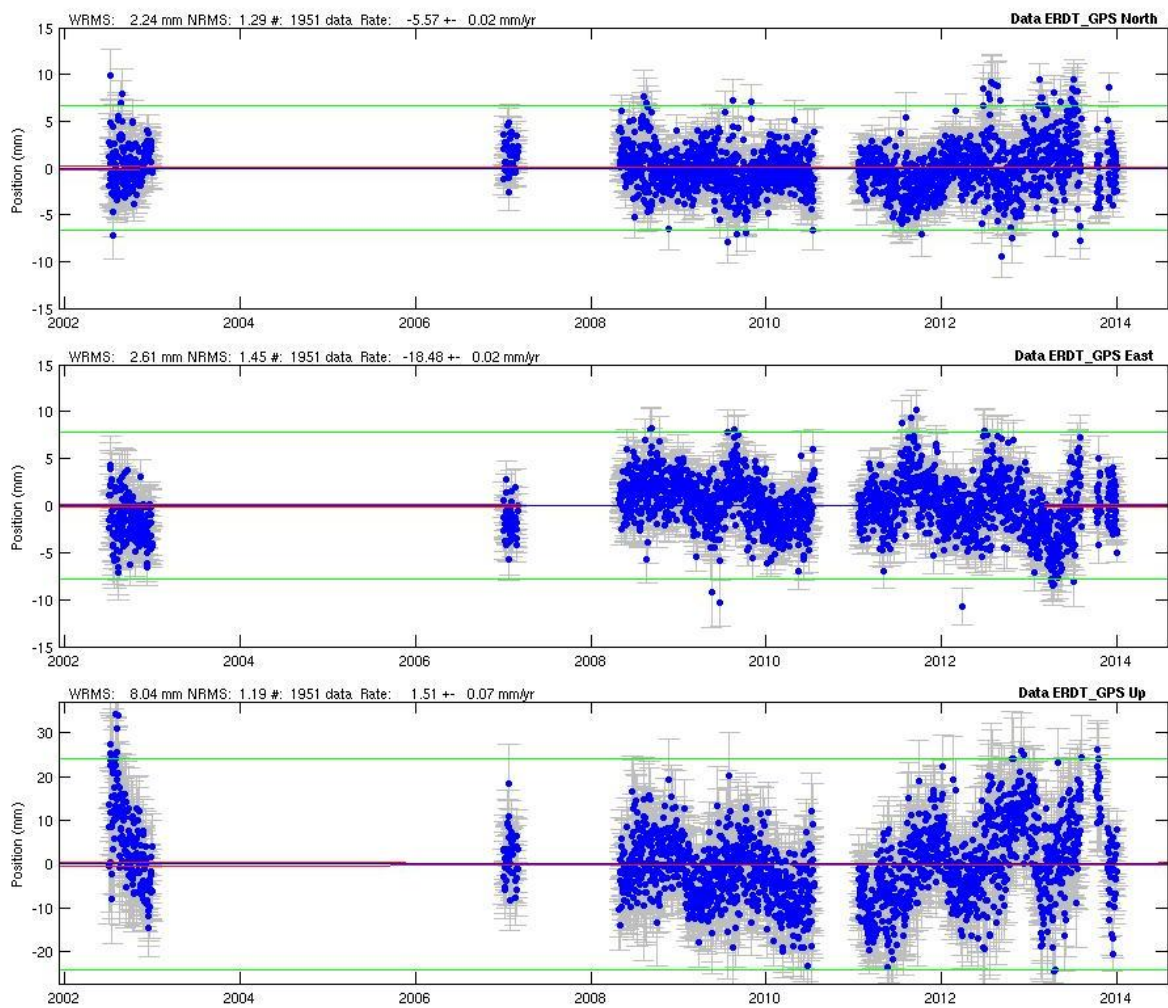


Figure 12. Time series for ERDT (in the graph, north-south, east-west and elevation components are shown respectively). The horizontal axis represents the GPS day, the vertical axis is representing the changes in the respective component coordinates are in mm scale.

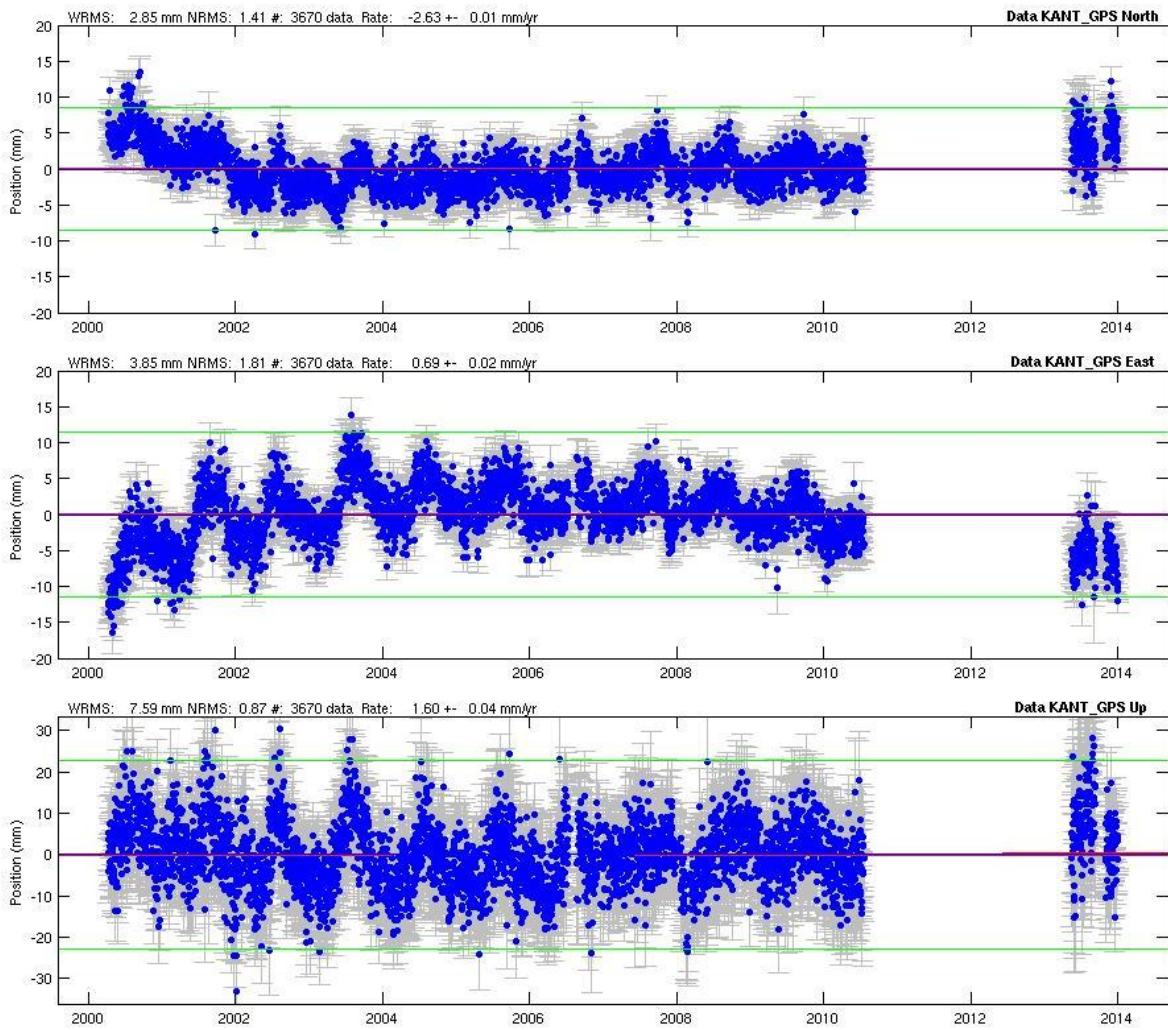


Figure 13. Time series for KANT (in the graph, north-south, east-west and elevation components are shown respectively). The horizontal axis represents the GPS day, the vertical axis is representing the changes in the respective component coordinates are in mm scale.

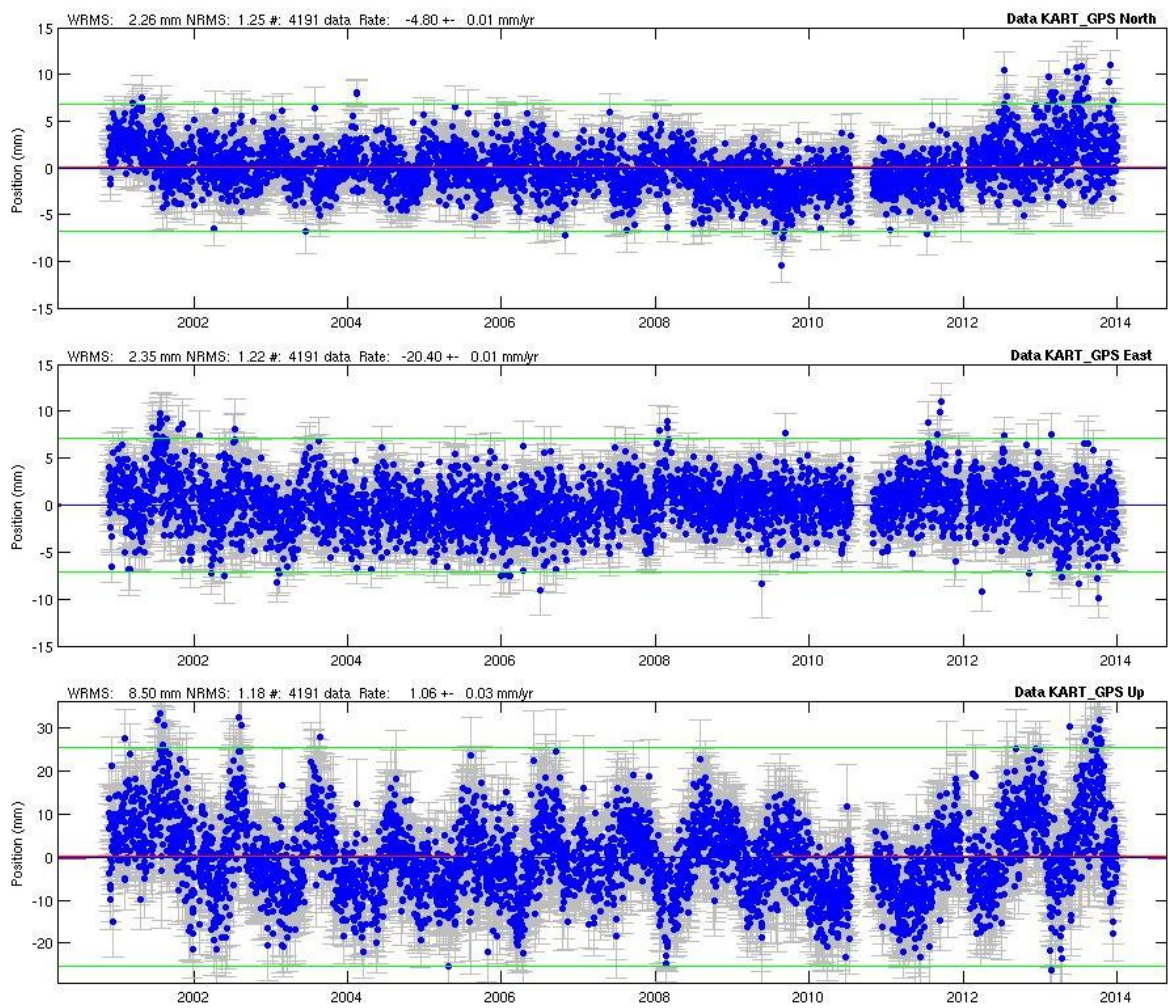


Figure 14. Time series for KART (in the graph, north-south, east-west and elevation components are shown respectively). The horizontal axis represents the GPS day, the vertical axis is representing the changes in the respective component coordinates are in mm scale.

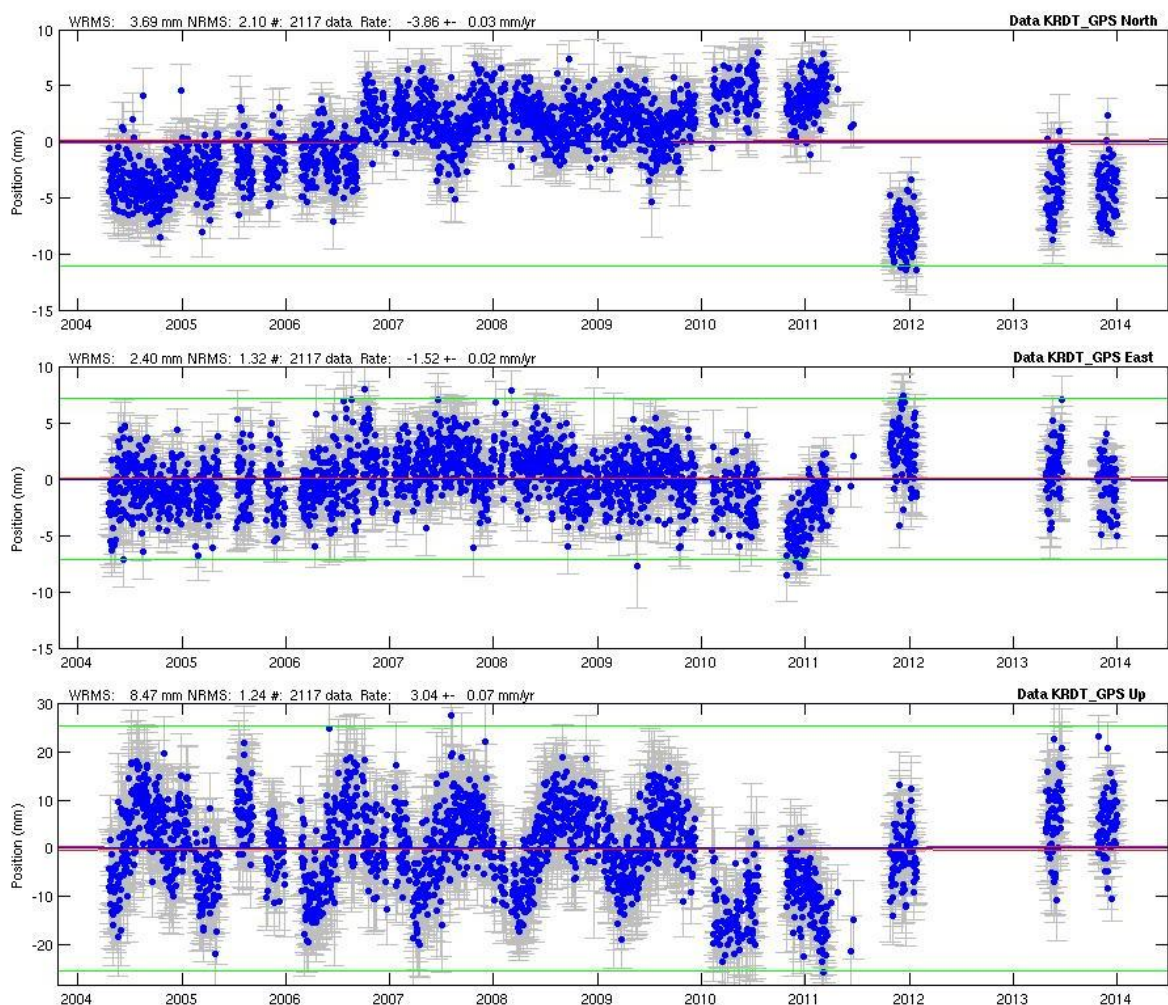


Figure 15. Time series for KRDT (in the graph, north-south, east-west and elevation components are shown respectively). The horizontal axis represents the GPS day, the vertical axis is representing the changes in the respective component coordinates are in mm scale.

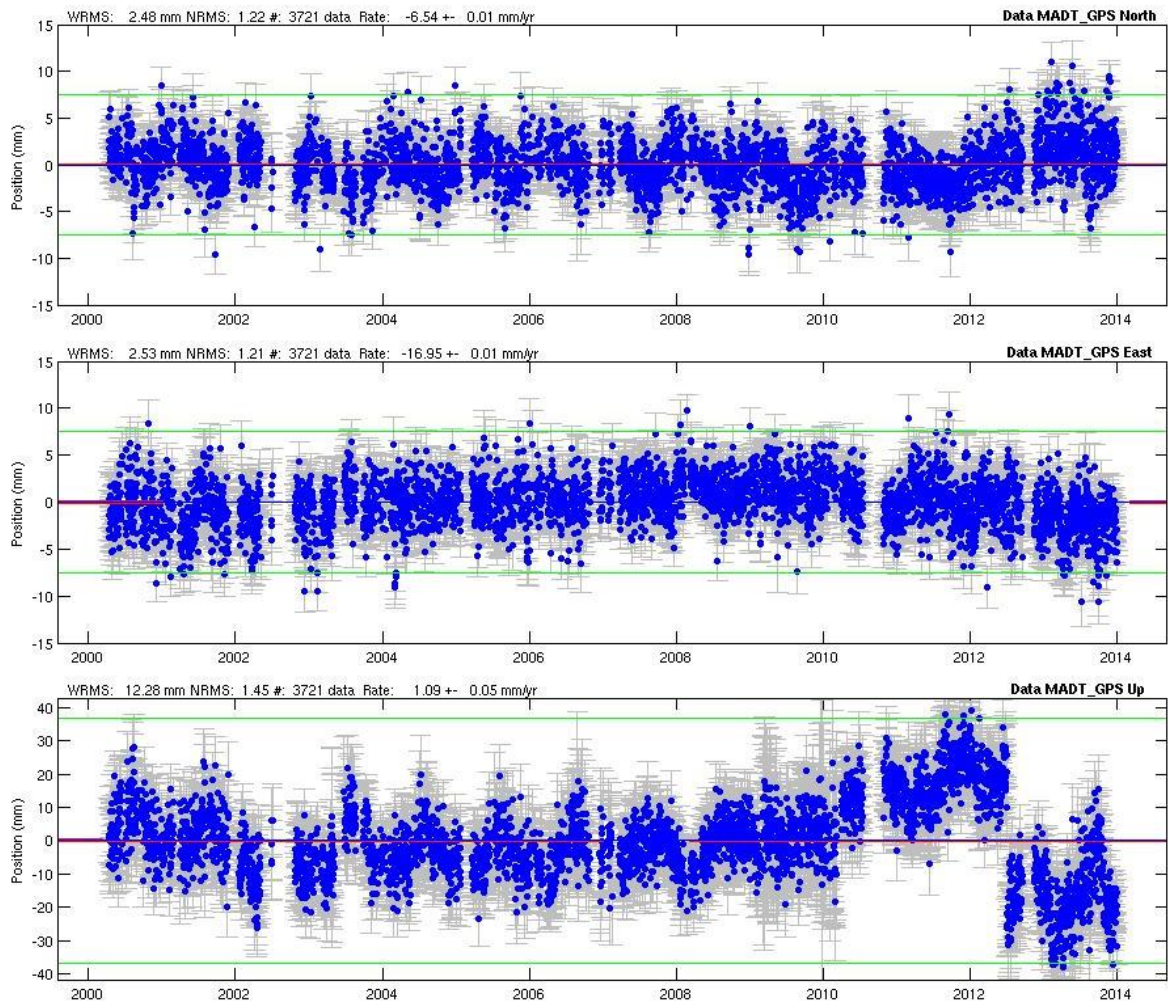


Figure 16. Time series for MADT (in the graph, north-south, east-west and elevation components are shown respectively). The horizontal axis represents the GPS day, the vertical axis is representing the changes in the respective component coordinates are in mm scale.

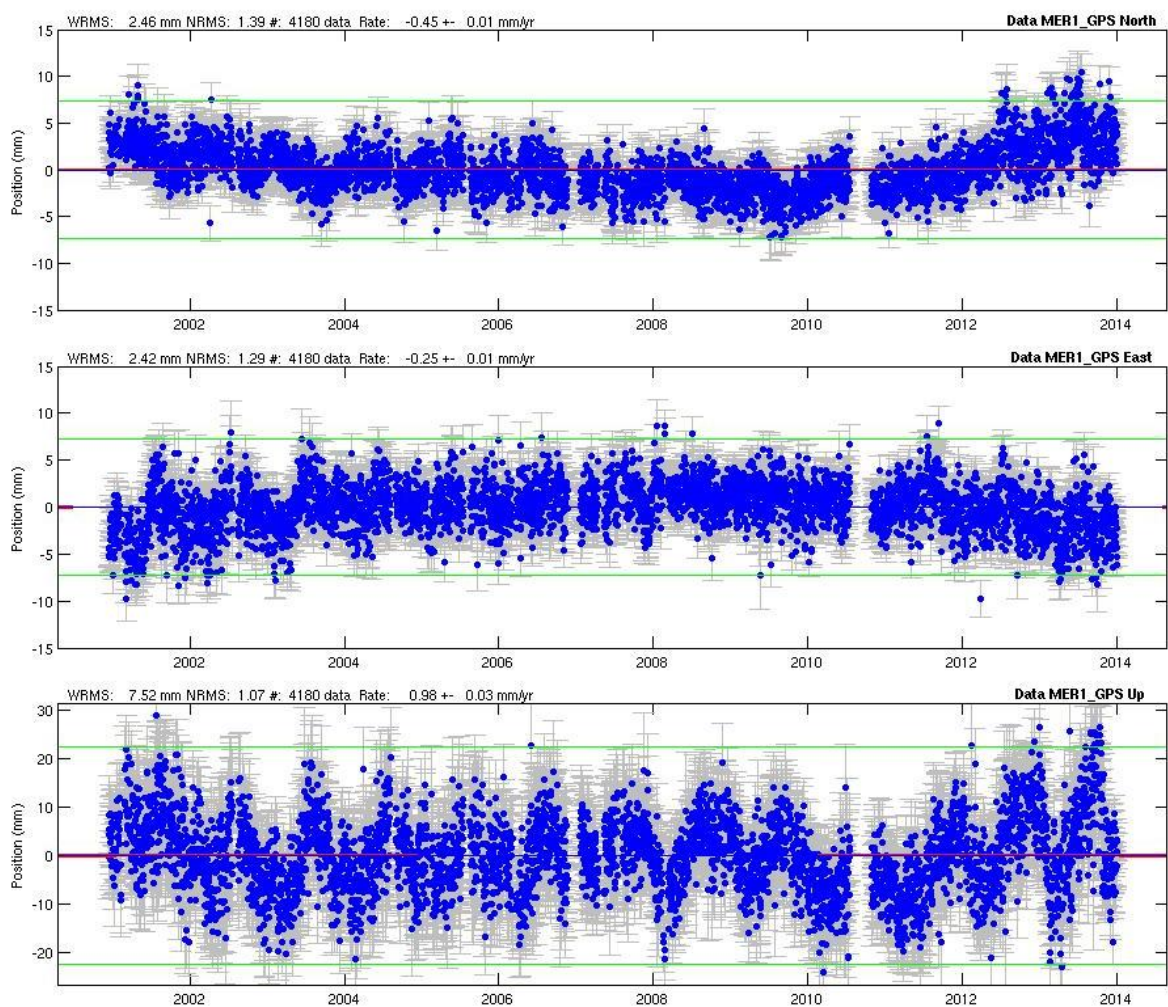


Figure 17. Time series for MER1 (in the graph, north-south, east-west and elevation components are shown respectively). The horizontal axis represents the GPS day, the vertical axis is representing the changes in the respective component coordinates are in mm scale.

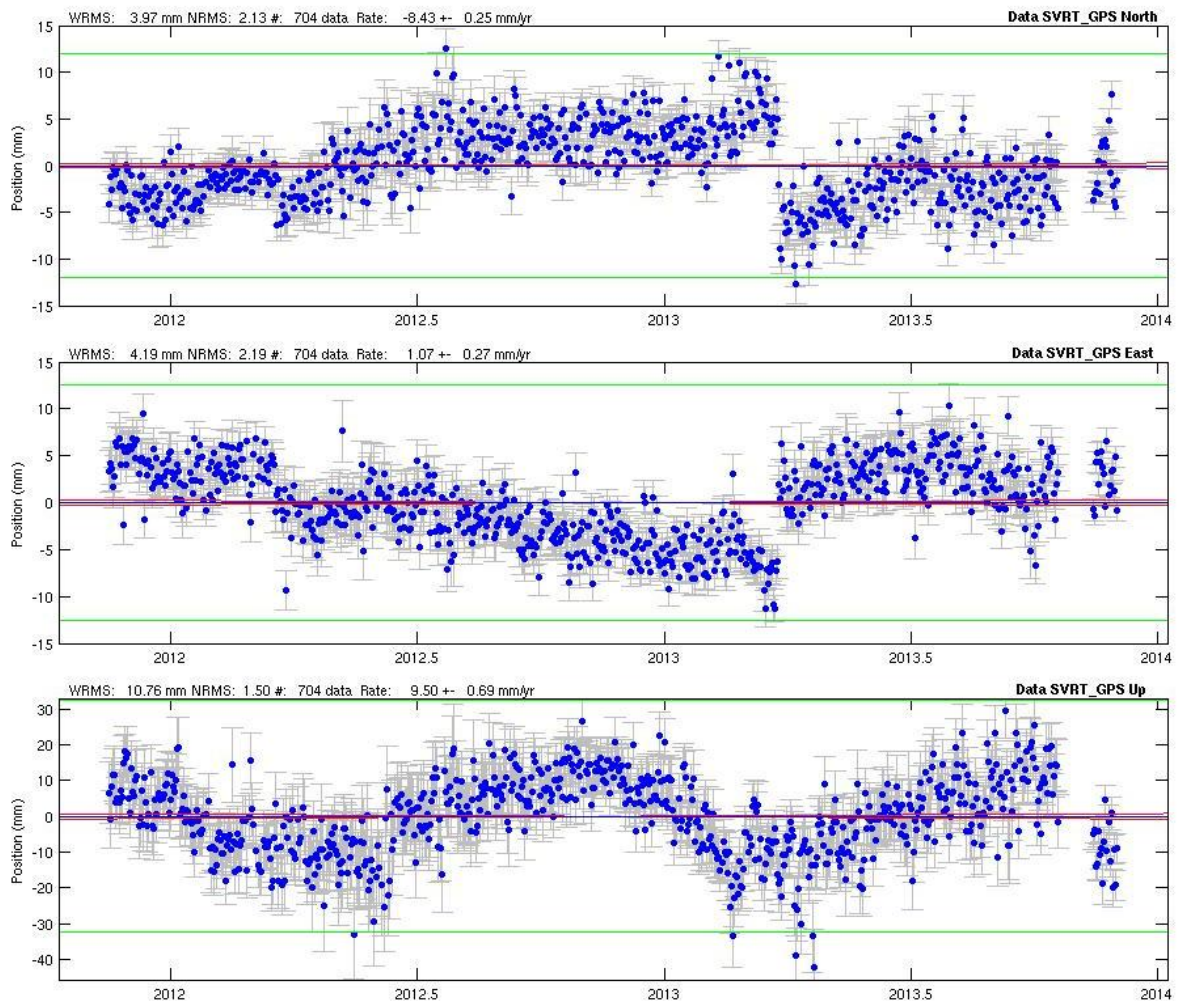


Figure 18. Time series for SVRT (in the graph, north-south, east-west and elevation components are shown respectively). The horizontal axis represents the GPS day, the vertical axis is representing the changes in the respective component coordinates are in mm scale.

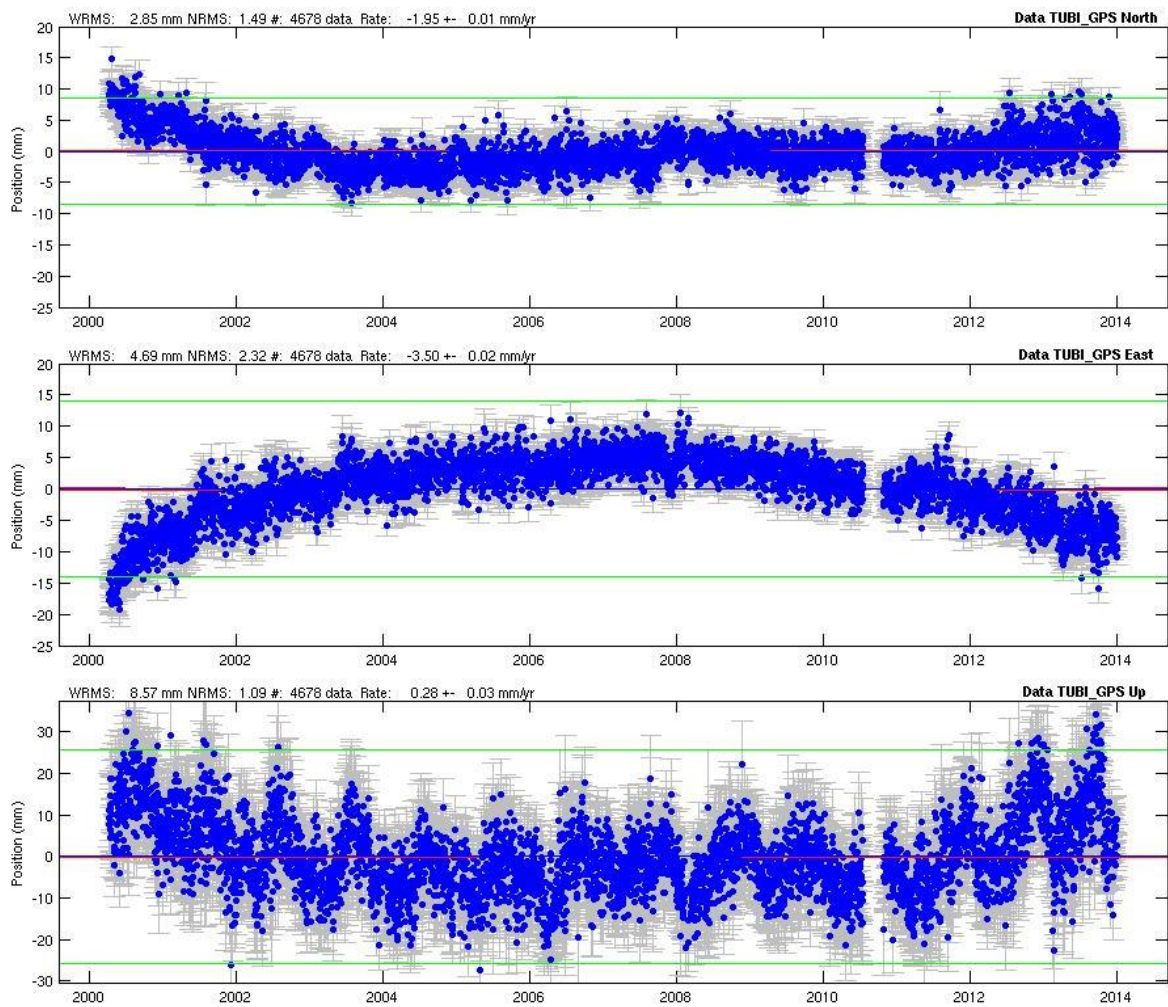


Figure 19. Time series for TUBI (in the graph, north-south, east-west and elevation components are shown respectively). The horizontal axis represents the GPS day, the vertical axis is representing the changes in the respective component coordinates are in mm scale.

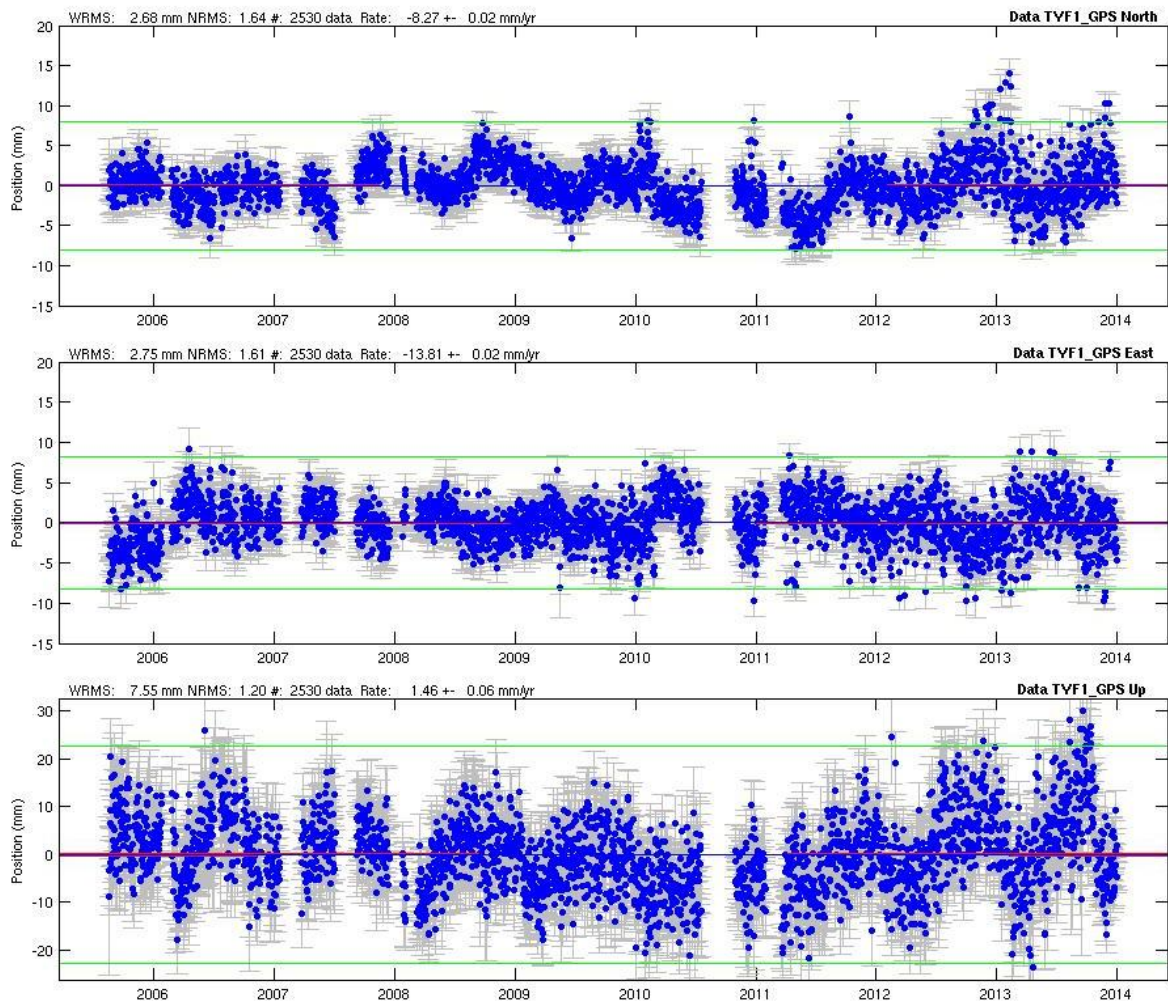


Figure 20. Time series for TYF1 (in the graph, north-south, east-west and elevation components are shown respectively). The horizontal axis represents the GPS day, the vertical axis is representing the changes in the respective component coordinates are in mm scale.

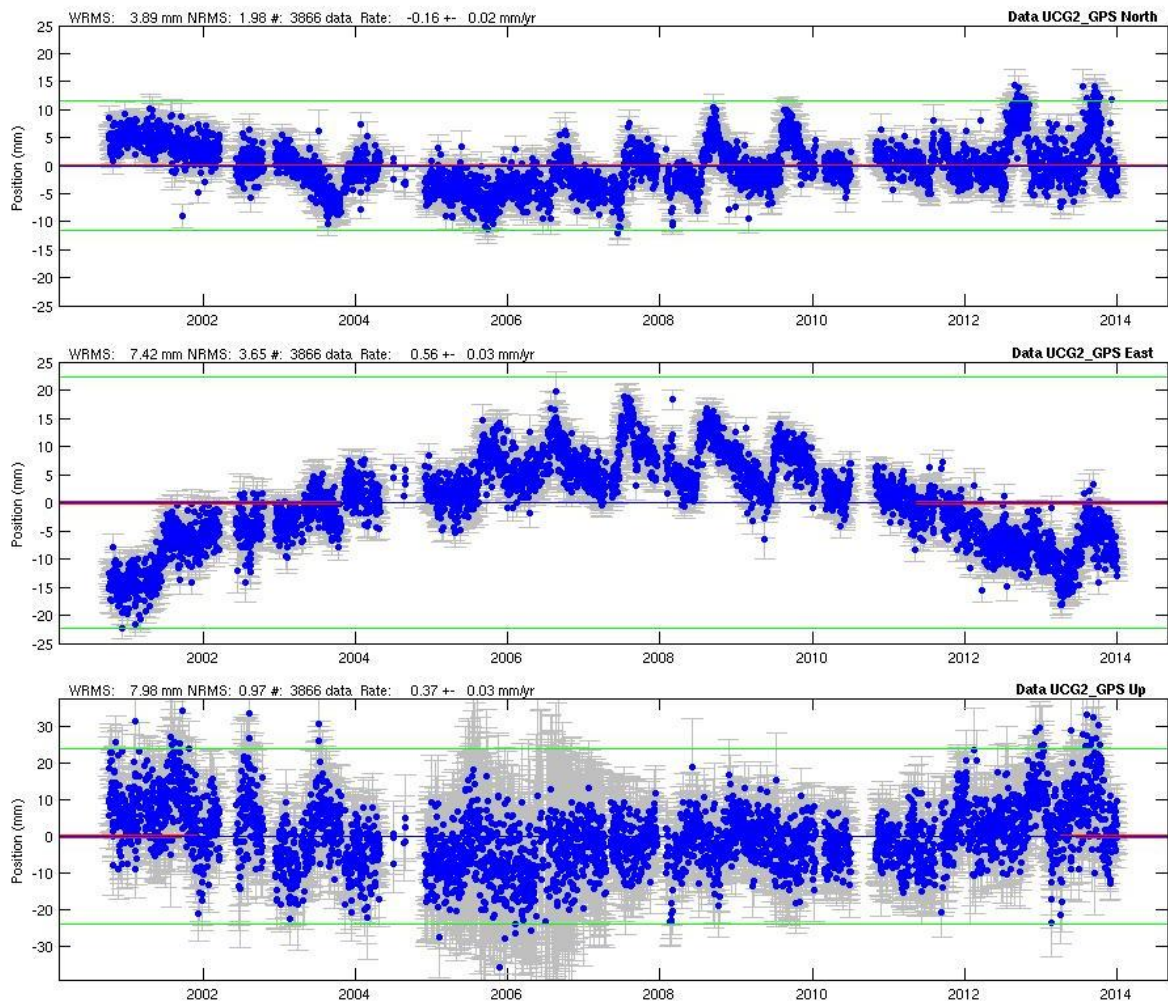


Figure 21. Time series for UCG2 (in the graph, north-south, east-west and elevation components are shown respectively). The horizontal axis represents the GPS day, the vertical axis is representing the changes in the respective component coordinates are in mm scale.

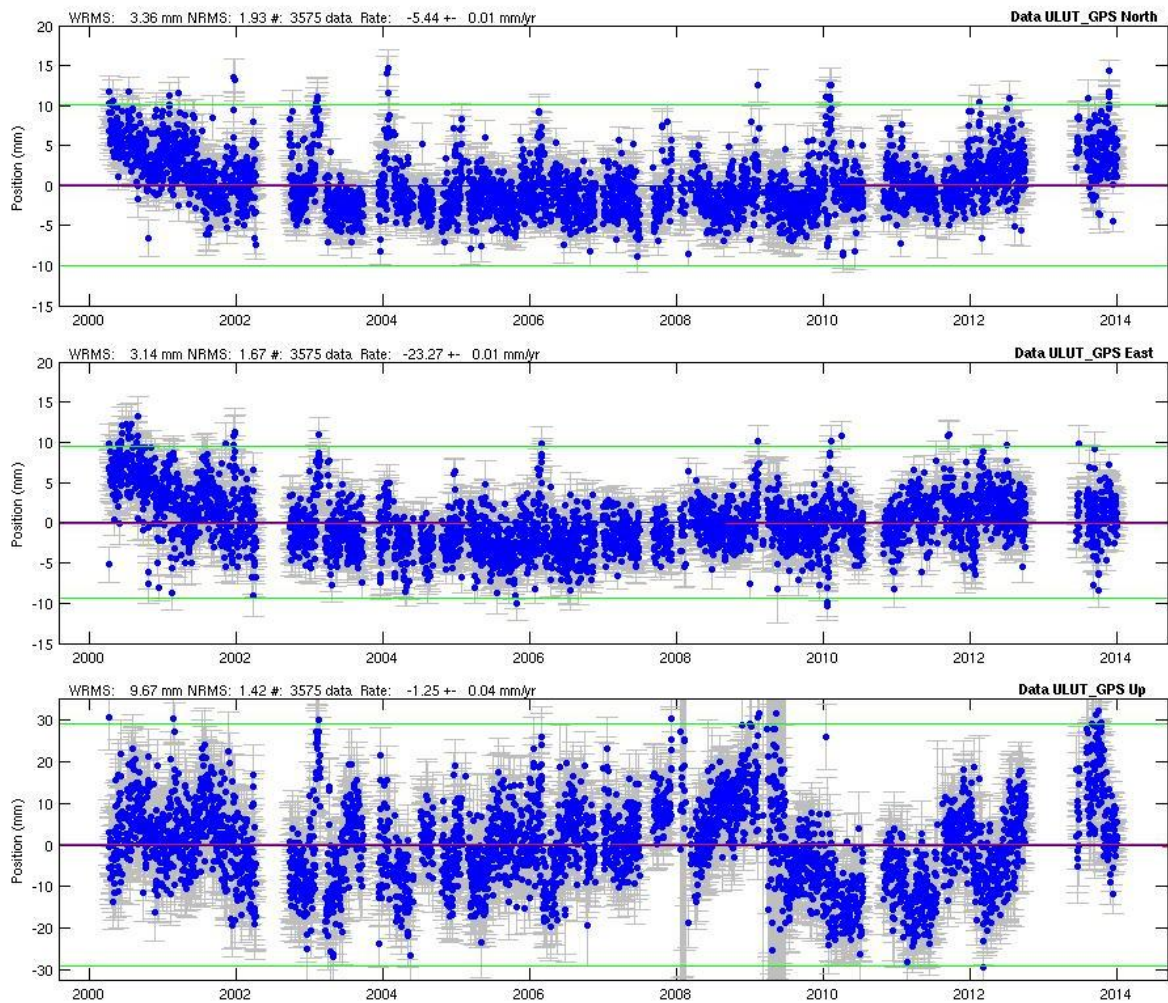


Figure 22. Time series for ULUT (in the graph, north-south, east-west and elevation components are shown respectively). The horizontal axis represents the GPS day, the vertical axis is representing the changes in the respective component coordinates are in mm scale.

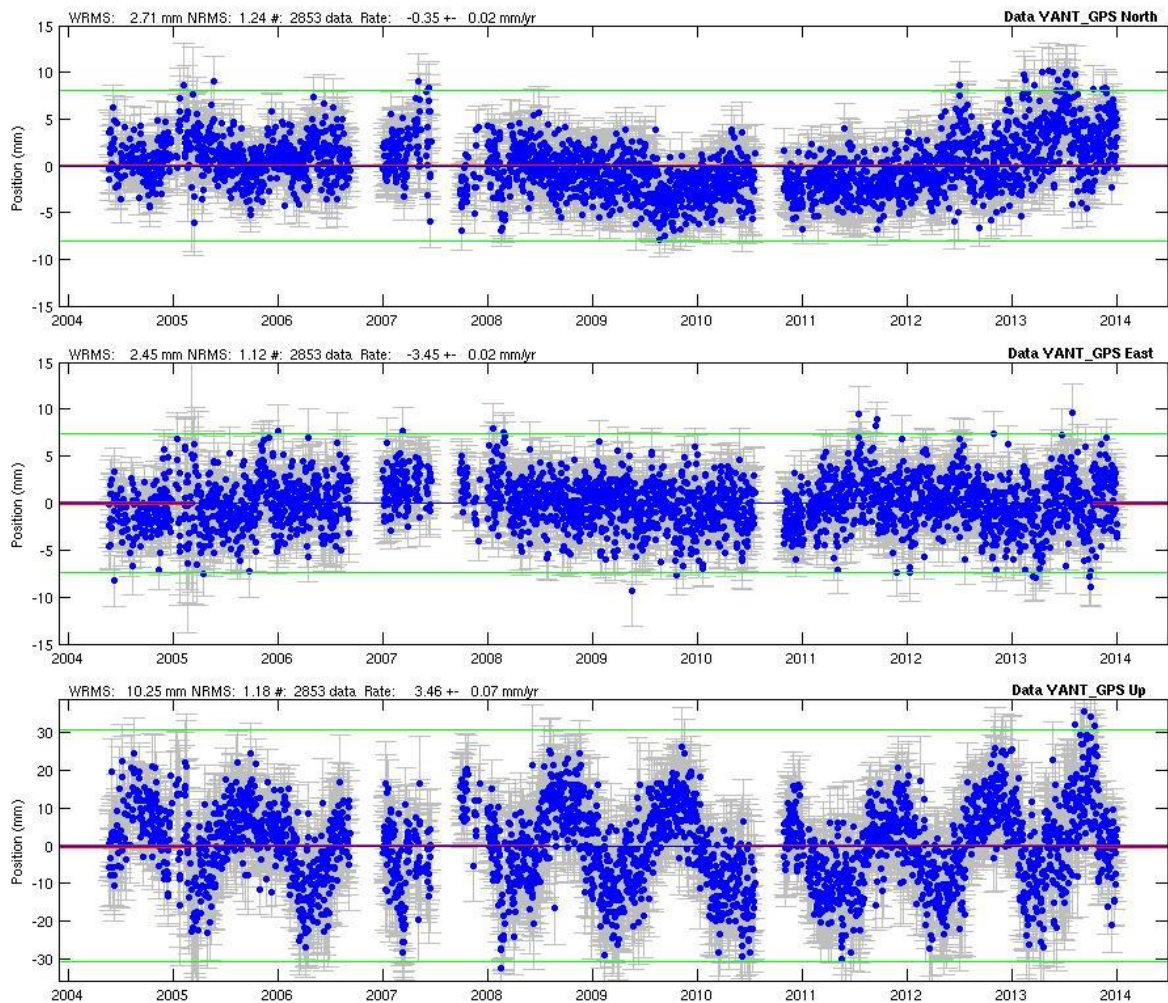


Figure 23. Time series for YANT (in the graph, north-south, east-west and elevation components are shown respectively). The horizontal axis represents the GPS day, the vertical axis is representing the changes in the respective component coordinates are in mm scale.

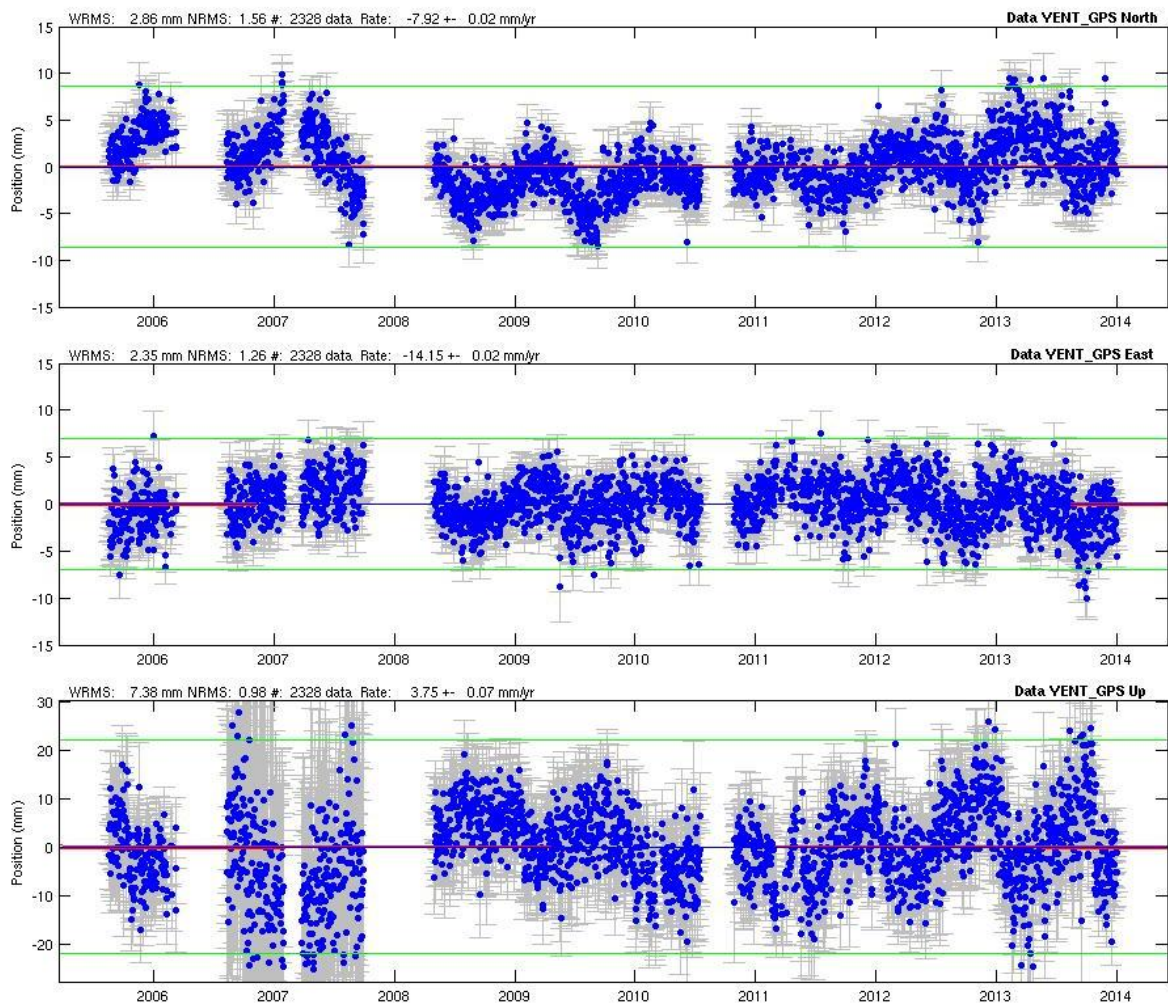


Figure 24. Time series for YENT (in the graph, north-south, east-west and elevation components are shown respectively). The horizontal axis represents the GPS day, the vertical axis is representing the changes in the respective component coordinates are in mm scale.

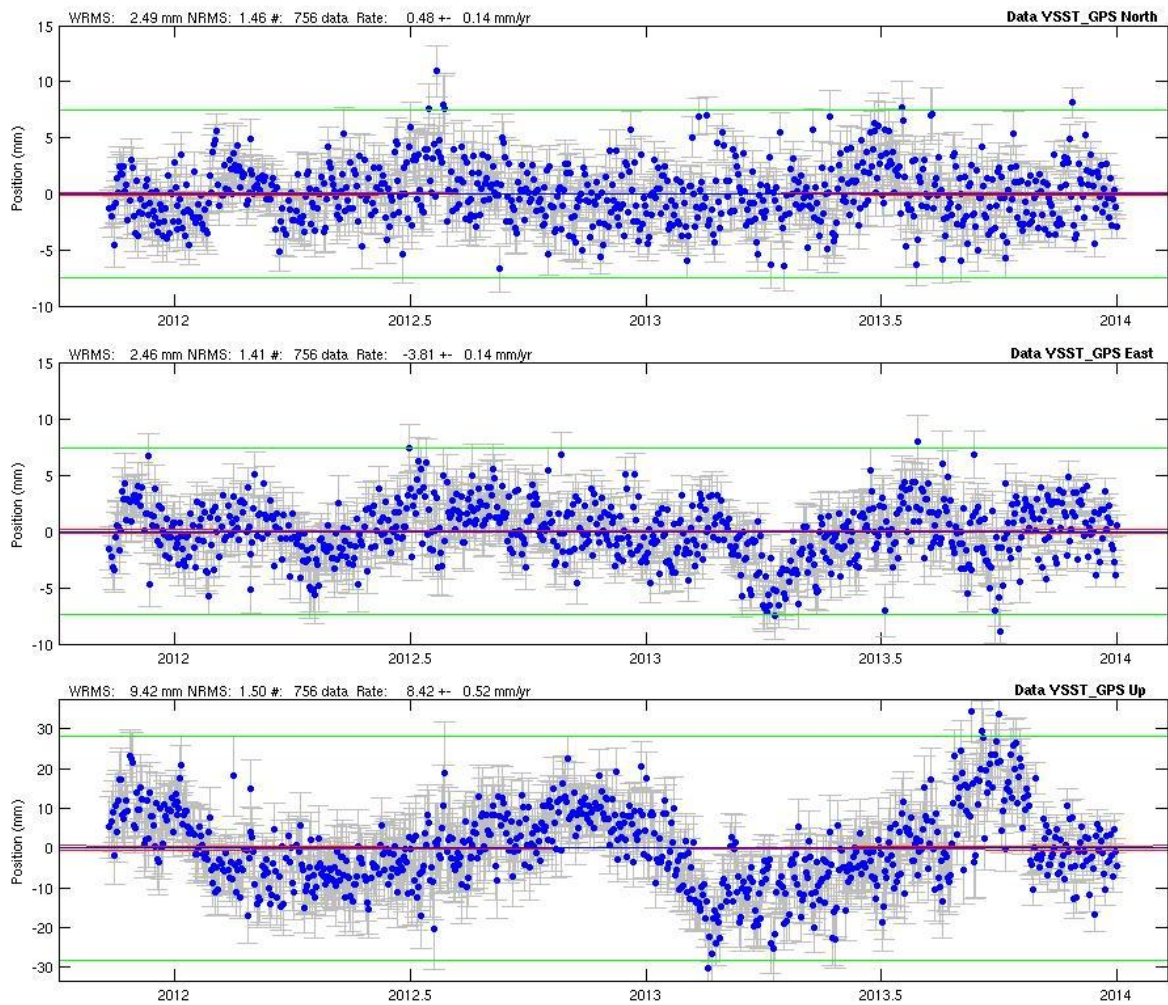


Figure 25. Time series for YSST (in the graph, north-south, east-west and elevation components are shown respectively). The horizontal axis represents the GPS day, the vertical axis is representing the changes in the respective component coordinates are in mm scale.